Flood Prediction and Mitigation in Data-Sparse Environments

JOY SANYAL

Abstract

In the last three decades many sophisticated tools have been developed that can accurately predict the dynamics of flooding. However, due to the paucity of adequate infrastructure, this technological advancement did not benefit ungauged flood-prone regions in the developing countries in a major way. The overall research theme of this dissertation is to explore the improvement in methodology that is essential for utilising recently developed flood prediction and management tools in the developing world, where ideal model inputs and validation datasets do not exist.

This research addresses important issues related to undertaking inundation modelling at different scales, particularly in data-sparse environments. The results indicate that in order to predict dynamics of high magnitude stream flow in data-sparse regions, special attention is required on the choice of the model in relation to the available data and hydraulic characteristics of the event. Adaptations are necessary to create inputs for the models that have been primarily designed for areas with better availability of data. Freely available geospatial information of moderate resolution can often meet the minimum data requirements of hydrological and hydrodynamic models if they are supplemented carefully with limited surveyed/measured information. This thesis also explores the issue of flood mitigation through rainfall-runoff modelling. The purpose of this investigation is to assess the impact of land-use changes at the sub-catchment scale on the overall downstream flood risk.

A key component of this study is also quantifying predictive uncertainty in hydrodynamic models based on the Generalised Likelihood Uncertainty Estimation (GLUE) framework. Detailed uncertainty assessment of the model outputs indicates that, in spite of using sparse inputs, the model outputs perform at reasonably low levels of uncertainty both spatially and temporally. These findings have the potential to encourage the flood managers and hydrologists in the developing world to use similar data sets for flood management.

Flood Prediction and Mitigation in Data-Sparse Environments

Joy Sanyal

Thesis submitted for the degree of Doctor of Philosophy

Department of Geography

Durham University

2013

Table of contents

List of Figures

List of Tables

Declaration

I confirm that no part of the material presented in this thesis has previously been submitted for a degree in this or any other university. In all cases the work of others, where relevant, has been fully acknowledged.

Chapter 3 of this thesis has been published in an international journal. Chapter 4 , 5 and 6 have been submitted to scientific journals for publication. The work presented in these papers is purely part of my PhD research. I declare that the contributions of the co-authors in these papers are limited to editorial advice.

The details of these publications are provided below.

Chapter 3

Sanyal J, Carbonneau P, Densmore A. L. (2013) Hydraulic routing of extreme floods in a large ungauged river and the estimation of associated uncertainties: A case study of the Damodar River, India. *Natural Hazards* 66(2), 1153-1177.

Chapter 4

Sanyal J, Carbonneau P, Densmore A.L. (*Accepted subject to minor corrections*) Low-cost flood inundation modelling at a reach scale with sparse data in the Damodar river basin, India, *Hydrological Sciences Journal*

Chapter 5

Sanyal J, Densmore A. L., Carbonneau P (Submitted) 2D finite element inundation modelling in anabranching channels with sparse data: examination of uncertainties, *Water Resources Management.*

Chapter 6

Sanyal J, Densmore A. L., Carbonneau P (Submitted) Analysing the effect of land use/cover changes at sub-catchment levels on the downstream flood peak: a semi-distributed modelling approach with sparse data. *Catena*

Statement of Copyright

Acknowledgement

I would like to express my deep appreciation and gratitude to my supervisors Dr. Patrice Carbonneau and Professor Alexander L. Densmore for their patient guidance and mentorship during the entire course of my doctoral research. I could not have imagined having better supervisors for my Ph. D study.

I would also like to convey my gratitude to Durham University for funding my PhD research including the generous support provided for covering the research expenses. I am also indebted to Dr. Charles Moulinec of Science and Technology Facilities Council, UK and Dr. Henk Slim of Computing and Information Services (CIS), Durham University for their active assistance in installing TELEMAC2D modelling suite in the high performance computing cluster based in Durham University. Miss Samantha Waugh of Department of Geography, Durham University provided very useful insights regarding the use of field instruments.

I would also like to thank the Irrigation and Waterways Department of Government of West Bengal, India and Damodar Valley Corporation, India for providing access to the hydrological data for the study site. Professor Ashis Sarkar of Presidency University, Kolkata, India provided invaluable assistance for conducting the fieldwork in India and his assistance is gratefully acknowledged.

My parents and in-laws provided me full moral support during my research while my baby daughter Gangotri has been my constant source of happiness. Finally, I'd be remiss if I didn't acknowledge the innumerable sacrifices made by my wife, Sagar, in shouldering far more than her fair share of the parenting and household burdens while I pursued this degree. Without her love and constant encouragement I would not be able to produce this piece of scientific work.

Dedication

For my mother

Chapter 1

Introduction

1.1 Background

1.1.1 Flood as a global natural hazard

Floods account for approximately one third of global natural hazards and more people are adversely affected by flooding than any other geophysical phenomenon (Smith and Ward, 1998). On average, 20,000 people lose their lives due to flooding each year and it affects 75 million people globally, most of whom become homeless (Smith, 2001). These global figures mask much regional variation in the occurrence of floods, the causes and the consequences on the populations. Recently, Adhikari et al. (2010) compiled a digitised global flood inventory for the period of 1998 to 2008 that reveals some important facts about different causes of flooding, the spatial variation and frequency of occurrences. According to this database, heavy rain, monsoon rain and tropical cyclones were reported as the causative factors for 64 %, 11 % and 6 % floods respectively. These types of meteorological phenomena occur only in the tropical and sub-tropical regions where most of the developing countries are located. This database further reported that seven of the top ten countries with most flooding events reported between 1998 and 2008 were outside the industrialised world and that Asia and Africa have the highest percentage of reported flood events each year. Jonkman (2005) pointed out that the floods caused by Asian rivers claim the most lives and affect more people than any other region in the world. Flood-affected population in the developed world have the means to combat the extreme natural events through better infrastructure, health care and functional flood warning systems (Allenby and Fink, 2005) while in the developing countries vulnerable populations lack the capital resource to develop sustainable protection mechanisms or rebuilt their damaged infrastructure after a major flood event.

`All the above information demonstrates that the developing countries in the low latitudes are more prone to flood hazards and the population is more vulnerable, particularly in Asia due to the high population density near the flood-prone rivers and low spending capacity for creating an early warning system and flood protections. Thus, the developing countries urgently need to develop a flood-prediction capability at an affordable cost for creating an early warning system and adopting structural (such as

building embankments) and non-structural (such as floodplain zoning) measures for flood management.

1.1.2. The issue of limited data in flood-prone regions

Hydraulic models are the standard tools for predicting fluvial inundation. Streamflow data and topography of channels and floodplains are the two most significant model inputs that influence the flow hydraulics and modelled flood extents. Bates (2012) commented that the science of inundation modelling has transformed rapidly in the past few years from a 'data-poor' to a 'data-rich' discipline. He was referring to the increasing availability and constant improvement of very high resolution terrain data form of LiDAR survey and all-weather capable Synthetic Aperture Radar (SAR) images for calibrating and validating distributed performances of flood-inundation models.

The study by Bates et al. (2006) in a 16 km reach of the River Severn in the UK is a typical example of the data intensive inundation modelling approach. This study used LiDAR-generated DEMs in combination with a series of airborne synthetic aperture radar (ASAR) images captured opportunistically during the peak and recession limb of the flood hydrograph in order to calibrate and validate flood models. The LiDAR DEM used was of <1 m horizontal resolution with a vertical root mean square error (RMSE) of 0.079 m. Elevation is measured by differential GPS points of approximately 0.01 m vertical accuracy was used as reference spot heights for obtaining the RMSE value of the DEM while the ASAR images were of 1.2 m resolution. This dataset was further supplemented with space-borne RADARSAT images, upstream and downstream gauging records at 15 minute intervals and extensive field data collected during the actual flood event.

The quality of LiDAR data has improved further in recent years. Inundation modelling has been performed successfully at 10 cm grid size for a small piece of urban land by using very high resolution LiDAR data captured with vehicle mounted terrestrial laser scanner (Fewtrell et al., 2011; Sampson et al., 2012). High resolution SAR data are typically available at ~25 m ground resolution but recently Mason et al. (2010a) utilized TerraSAR-X images with 3 m resolution for detecting flood water in the urban

environment. The availability of fine resolution inputs, particularly the fine resolution validation data from SAR imageries help reduce the equifinality arising from the difficulty in differentiating between different model physics and parameters and provided a more controlled environment for comparing the effect of including individual hydraulic process in the code (Bates, 2012). Thus, it is clear that a steady trend of advancement in the quality and coverage of the required data has led to marked improvement in the science of inundation modelling. Nevertheless, the major flood-prone areas in the world are not able to benefit much from this development of state-of-the-art inundation models given that LiDAR derived terrain data and SAR images are almost always unavailable in the developing countries due to the prohibitive cost of acquiring them (Sanyal et al., 2004). This scenario leaves us with the option of using freely available DEMs such as the Shuttle Radar Topography Mission (SRTM) DEM or the Advanced Spaceborne Thermal Emission and Reflection Radiometer (ASTER) Global Digital Elevation Model (GDEM) for defining the model geometry and the cloud-free optical imagery of flood water as the primary source of distributed observed data for model calibration and validation.

Although Sanders (2007) demonstrated the potential of employing the SRTM DEM in inundation modelling and Manfreda et al. (2011) highlighted the reliability of this data to identify flood-prone regions with a modified topographic index, it is well known that these terrain data contains considerable noise (Bhang et al., 2007). A global performance assessment study of the SRTM data by Rodriguez et al. (2006) revealed an absolute height error of 6.2 m, 5.6 m and 6.2 m for Eurasia, Africa and South America respectively. Since, the X and C band radars used in the SRTM instrument do not penetrate the canopy the SRTM DEM captured the tree top elevation rather than the surface at any place with dense foliage. The ASTER GDEM, in spite of having a higher spatial resolution of 30 m is reported to have significant anomalies and much higher RMSE than the SRTM DEM when compared with LiDAR derived elevation data derived from ICESat (Reuter et al., 2009). While evaluating the recently available 2nd version of the ASTER GDEM Slater et al. (2011) commented that the data have an effective resolution which is lower than 30 m and contain systematic bias in comparison to the other reference DEMs and ground control points. Hence, both the SRTM and GDEM products are not quite suitable for inundation modelling, at least in the forms

which are available for download. Bates (2012) did in fact note that the purpose of creating these global data sets most probably did not include inundation modelling.

Due to the high cost of acquiring radar imagery there are very few requests for data acquisition over the developing nations to capture flooding on the ground. Consequently, for any flood-prone river basin outside the industrialised countries there is very limited chance of finding a flood scene in the archive of radar data providers. In the absence of radar imagery optical imagery has been successfully used in many occasions for delineating the flood extent (Wang et al., 2002; Sanyal and Lu, 2005; Jain et al., 2005; Ip et al., 2006). The Landsat archive, which is accessible at no cost, contains numerous cloud-free scenes of inundated surface which can be quite valuable for inundation modelling in the developing world.

In spite of all the constraints mentioned above there is an increasing trend of utilising freely available terrain data for hydraulic modelling of streamflow. Due to the coarse nature of the available terrain data (e.g. SRTM DEM), the majority of these studies has been undertaken at continental scale. For example, Yamazaki et al. (2012a) applied a global river model: CaMa-Flood (Yamazaki et al., 2011) to model the seasonal cycles of water level elevations in the Amazon River using the SRTM DEM as the terrain input and the simulated water surface elevations were compared with Envisat altimetry. Development and application of flow routing and inundation models in the data sparse regions of the world is mostly confined in the very large continental river basins such as the Amazon (da Paz et al., 2011), Congo (Jung et al., 2010), Niger (Neal et al., 2012a) and Ob (Biancamaria et al., 2009). The abovementioned studies are primarily engaged in simulating seasonal or annual cycle of river discharge and water level or even water budget and flooding pattern of large wetlands of the Niger River (Zahera et al., 2011) and the Nile Basin (Petersen and Fohrer, 2010). A number of novel attempts have been reported to deal with the low resolution of the freely available DEMs that were used in these investigations. Paiva et al. (2011) developed a GIS-based algorithm that includes extraction of river cross-sections, delineation of river networks and catchments from the SRTM DEM and used geomorphic principles to estimate the river width and depth. Yamazaki et al. (2012b) proposed a pit removal strategy to reduce the anomalies in the SRTM data arising from vegetation canopy and sub-pixel structure and reported an improvement in the simulated water surface elevation with the adjusted DEM in terms

of agreement with the observed records. Neal et al. (2012a) demonstrated how a sub-grid scale representation of a channelized portion of the flow can help to simulate streamflow in narrow channels that cannot be captured in the low resolution global DEMs. However, this model still needs measurements about channel depth and width to derive the empirical relationship for estimating channel-bed elevation from bank elevation and channel width.

1.1.3 Inundation modelling at different scales with limited data

In general, there is a lack of focus on flooding as a natural hazard when it comes to hydraulic modelling in data sparse regions. When we develop a tool for a flood prediction and warning system it is conventionally focussed on modelling extreme flow events with an accuracy that is acceptable in flood management and planning practices. There are very few case studies at regional scales outside the industrialised countries for river basins that are fairly large (length > 500 km) but not of continental scale such as the Amazon and of cases that regularly inundate densely populated floodplains. Use of the global DEMs for routing high magnitude floods at a regional scale is likely to require some additional reference data in order to correct the systematic bias and noise present in them and increase the details of topographic representations where it is absolutely necessary. Few attempts were made to simulate river flows in regional scales with the SRTM DEM using 1D models such as MIKE11 in sparsely gauged parts of the Mahanadi (Patro et al., 2009) and the Brahmani Rivers (Pramanik et al., 2009) in India. In the absence of a measured river cross section, the SRTM DEM has been used in both studies to extract river cross sections. The cross-section heights were modified using available spot heights from topographic maps.

Apart from the SRTM DEM, recently there has been some interest in utilising relatively recent ASTER GDEM data in hydraulic modelling, probably due to their higher spatial resolution. One such study undertaken by Wang et al. (2012) to model the possible outcome of a glacial lake outburst flood in southeast Tibet has shown that the simulated extent of inundation and the depth of water resulting from the use of ASTER GDEM is only 2.2 % larger than the predictions derived from a much more accurate DEM provided by the National Geomatics Centre of China at 1:50,000 scale. However, this study reported a depth of the simulated flood water which was 2.3 m deeper than what

was achieved using the reference DEM. An overestimation of 2.3 m in the flood depth may be reasonable in mountainous regions like Tibet and results in a small overestimation in the areal extent of flooding but such error in the modelled depth can make a huge difference in the predicted flood extent in the lower course of river basins which are typically most flood-prone and associated with very low relief. The 2nd generation of ASTER GDEM, known as GDEM2 which was released in the public domain in October, 2011 has also been tested for inundation-area analysis by means of delineating the impoundment area that is likely to be under water for a proposed dam in Indonesia and an improvement in the maximum contour level has been noted as compared to the GDEM2 (Suwandana et al., 2012). However, the vertical accuracy of the ASTER GDEM was found to deteriorate in the recent version and recorded to be 5.68 m as compared to 4.04 m in the GDEM1 for the area investigated by Suwandana et al. (2012).

Casas et al. (2006) evaluated the effect of quality of input terrain data on the accuracy of predicted water surfaces using HEC-RAS model. Although this study reported poor performance of contour maps with 5 m intervals in comparison with high resolution LiDAR DEMs, it is interesting that the observed error in predicted water surface reduced quite dramatically as the flow crosses the bank limit and lack of river channel bathymetry becomes less significant. Adding GPS control points to the less accurate contour-derived TIN model improved the predicted water-surface elevation by 4.5 m. This finding is particularly encouraging with a view to employing relatively low resolution DEMs for large flood prediction which can be supplemented with GPS surveyed control data to improve accuracy. Although both studies on the Mahanadi and the Brahammani River in India achieved good agreement with the observed downstream hydrograph the models were focussed on modelling the river regime during the period of Indian monsoon rather than extreme floods.

The majority of the inundation modelling that is focussed on analyzing flood risk is conducted at the reach scale (< 20km). Generally, a major flood is considered for which detailed topographic data for the flood-prone reach is available. There is an acute lack of literature that deals with this kind of study outside the industrialised countries because the globally available DEMs are normally too noisy to accurately simulate floodplain flow at this scale. Detailed configuration of the channel bed is also an

essential prerequisite to perform reasonably accurate inundation modelling at the reach scale. One such attempt has been made by Masood and Takeuchi (2012) for creating a flood risk map for part of Dhaka City in Bangladesh where the SRTM data was resampled into 30 m resolution. The area which experienced significant land filling since the time of the SRTM mission were identified and the corresponding grid cells were raised to match the current topography. A more rigorous validation of the results in the reach scale derived from freely available DEMs is necessary. It is evident that the SRTM or ASTER DEMs in their available form are not suitable for modelling widespread floodplain flow at reach scale. Even for applications in regional scale such as Patro et al. (2009) or Pramanik et al. (2009) the SRTM DEM was modified with reference ground control points before employing in 1D hydraulic models. For undertaking hydraulic modelling at the reach scale without access to very high resolution terrain data some researchers have tried to combine elevation information from a variety of sources to increase the detail of channel and floodplain representation. For example, Tate et al. (2002) exported the ground surveyed XYZ data from HEC-RAS model into real world coordinates and merged them with a relatively low resolution DEM to get more detailed representation of the channel and embankments. The assumption of straight-line cross-sections are one of the limitations of this approach as the cross-sections are generally doglegged in shape. Shapiro and Nelson (2004) edited and merged terrain data from various sources and created a TIN with higher density of elevation points at or near the channel and less resolution further away.

The most significant determinant of the performance of a hydraulic model is the accuracy in the representation of channel geometry (French and Clifford 2000; Pappenberger et al., 2005). Creating a continuous and detailed terrain data for the channel is a requirement for 2D hydrodynamic models. Even for the 1D models a continuous DEM including the channel is often required to derive the extent of inundation where the terrain height is subtracted from the simulated water level at each cross-section to identify the wet cells. While undertaking inundation modelling at the reach scale in data sparse regions creating a reasonably accurate river terrain model can be quite challenging because of the narrow width of the channel in comparison with the coarse resolution of the freely available DEMs. Particularly, for the SRTM DEM the problem is aggravated by voids in the wet part of the channel arising from specular reflection of radar backscatter from calm water. In the ‘finished’ versions of the SRTM

DEM, that has less void and noise any river with more than 183 m of width was monotonically stepped down at the direction of flow (Slater et al., 2006). This processing led to step like appearance in channels along their longitudinal profiles and made them difficult to use, at least in the reach scale.

Merwade et al. (2008a) pointed out that linear interpolation of the available surveyed cross-sections for creating a continuous river terrain model is not straight forward due to various facts including bends in the river, imperfect location of the cross-sections. In addition, the existence of channel islands not captured by enough number of cross-sections and failure to capture the river thalweg by the bathymetric surveys also makes the interpolation a challenging task. Merwade et al. (2006) reported that in a flow-oriented coordinate system the performance of anisotropic spatial interpolation techniques resulted in significant reduction in RMSE as compared to the conventional interpolation techniques such as nearest neighbour or kriging. This study proposed elliptical inverse distance weighting, a modified version of conventional inverse distance weighting (IDW), to take advantage of the flow oriented coordinate system as the channel bed morphology is essentially anisotropic due to greater variability of bed elevation perpendicular to the flow direction than along it. However, the investigation used spatially irregular bathymetry data collected by boat-mounted acoustic depth sounders rather than linear channel cross-sections. Even the isotropic techniques of interpolation were reported to perform well if the surveyed bathymetry data are de-trended and transformed into a flow oriented coordinate system (Merwade, 2009). However, after experimenting with various interpolation techniques in a flow-oriented coordinate system, Legleiter and Kyriakidis (2008) commented that the density of surveyed points exerts primary control over the accuracy of interpolated surface and the RMSE of the interpolated surface has a strong relation with the spacing of the cross-sections.

All the abovementioned interpolation techniques are likely to create accurate interpolated surfaces of the channel if there is adequate data in the form of irregular elevation points or linear surveyed cross-sections. In the case of anabranching and anastomosing rivers with a number of flow bifurcations and large river islands the above mentioned methods may not perform well (Merwade et al., 2008a). For a successful implementation of the aforesaid interpolation techniques to capture the flow diversion near the river bifurcations very high density of surveyed points will be

required and therefore these methods may not be suitable for use in a complex fluvial system, especially in the developing countries where acquisition of expensive surveyed data at a very high density is not possible due to resource constraints.

Recently, there have been few attempts to generate terrain data from relatively affordable stereo satellite imagery sources for reach scale inundation modelling in the developing world where generally the SRTM DEM is the best available option. For example, Tarekegn et al. (2010) generated a DEM of 15 m resolution from ASTER imagery using ERDAS LPS digital photogrammetry software for 2D hydrodynamic simulation of flooding in the Ribb River in Ethiopia but reported only 30.5 % match between the simulated flooded extent and observed flood extent derived from a MODIS image. Considering the previous studies regarding the accuracy of the ASTER DEM data this result is not surprising.

High resolution (2.5 m) IRS Cartosat-1 stereo images were found to produce more accurate DEMs than the SRTM or ASTER data when compared against surveyed GCPS (Rawat et al., 2012). Sarhadi et al. (2012) used Cartosat-1 images to create high resolution DEM of 2.5 m grid spacing in order to perform inundation modelling in the mountainous region of Iran and reported a high accuracy in the modelled flood extent. Nevertheless, the nature of the reach scale studies performed with no access to LiDAR DEMs or other comparable sources in the developing countries such as Bangladesh (Masood and Takeuchi, 2012), Iran (Sarhadi et al., 2012) or Thailand (Keokhumcheng et al., 2012) were probabilistic in nature. The flood events considered were only designed events with a high return period, not the actual ones and the modelled flood extents were compared with the observed flood extent of a typically larger event rather than the actual satellite overpass. It is worth noting that in the mountain areas small vertical error in the DEM is not likely to have a huge impact on the extent of flooded area as illustrated by the study by Wang et al. (2012) in Tibet. Both Tarekegn et al., (2010) and Sarhadi et al. (2012) produced a DEM with identical resolution of its source stereo images which is difficult to achieve using digital photogrammetric techniques. A moving window is used to calculate some form of statistics for the ‘fore’ and ‘aft’ images to find the location of the same feature on both images. If a very small window size is chosen it is unlikely to find enough matching points on the fore and aft images to create a uniform distribution of elevation points. A slightly larger window size (e.g. 3 ×

3), which is often used, means that the elevation for each point is derived from a much larger area of the source image than its individual pixel size. Therefore, a DEM grid size of at least double the size of the spatial resolution of the source stereo imageries is recommended. Otherwise, the effective resolution of a DEM becomes less than its nominal resolution.

1.1.4 Choice of the model and the required level of complexity

1D hydrodynamic models are computationally efficient and can produce accurate water surface elevations without very high resolution terrain data. However, high resolution terrain data are required for modelling extensive floodplain inundation as mentioned in the previous section of this chapter. Although 1D models were found to perform equally well as the 2D models in certain cases (Horritt and Bates., 2002; Alho and Aaltonen 2008), generally 1D models are less efficient in simulating the lateral diffusion of flood waves in the floodplain because of the discrete representation of the topography in the form of cross-sections (Hunter et al., 2008). It is also not technically sound for modelling backflow in floodplains (Merwade et al., 2008b). In addition, the roughness coefficients, which are required to account for the energy loss from a variety of sources depends on the dimensionality of coding and level of process representation (Lane and Hardy, 2002). The roughness parameters estimated from field data are more likely to work well in physically consistent 2D models such TELEMAC2D (Hervouet and Van Haren, 1996) than simpler models (Hunter et al., 2007).

Physically based more complex finite element codes were also found to be less sensitive to the resolution of the terrain model and therefore are effective in containing the uncertainty in the model outcomes (Cook and Merwade, 2009). There is an element of non-stationarity of the friction parameter arising from the variation in the magnitude of the flood under consideration and physically-based fully 2D models can keep the effect of this factor low (Horritt et al., 2007). Hunter et al. (2008) compared the performance of a number of diffusive and shallow water codes in an urban setting in Glasgow and noticed variations in the modelled depth and flooded extent depending on the hydraulic process representations and types of numeric solvers in use. Process representation was not always found to influence the model outcome decisively. Neal et al. (2012b) observed that often the subtle modelling decision such as methods of

downgrading the resolution of a DEM from 10m to 50m can have more effect on model outputs than selecting models with different degree of complexity. A number of benchmarking studies depending on the 1D versus 2D code (Horritt and Bates, 2001b), scale of the model domain (Fewtrell et al., 2008), the nature of the numerical solution of 2D hydrodynamic models (Horritt et al., 2007), and ways of setting up the parallel computing environment (Neal et al., 2010) have been carried out in the past but there is no literature that focusses on comparing the performance of 2D hydrodynamic models with varying degree of complexity with very limited data in an anabranching river with a number of smaller distributaries.

1.1.5 Treatment of uncertainties

A systematic estimation of the predictive uncertainty in a hydrodynamic modelling experiment is an essential component of any flood prediction mechanism. Uncertainty analysis in inundation modelling and flood risk analysis is important because it improves the evaluation of risk by identifying the sources of variation in model predictions, and even can influence decision-making on flood mitigation (Merz et al., 2008). It can also result in serious error in hazard assessment (Di Baldassarre et al., 2010). Merz, et al. (2008) further pointed out that if the uncertainty component of a particular prediction is found to be too large for a reasonable decision-making process it may highlight the necessity of further research to understand the physical process of inundation in that study area. Uncertainty assessment is more essential in the context of data-sparse situations in order to know the level of confidence we can attach to a particular prediction that was derived from model inputs of coarse quality and approximate measurements. The proportion of area in a model domain affected by the uncertain flood prediction increases with increasing uncertainties in the model inputs and choice of techniques and *vice versa* (Merwade et al., 2008b). An uncertainty assessment is important in order to know the extent to which the modelled flood extents are affected by 1) each of the uncertain inputs and modelling considerations; 2) the spatial dimension of the effect of changes in each of the uncertain variables; and 3) the nature of propagation of each uncertain variable in the inundation process and its effect over the combined state of uncertainty of a prediction (Jung and Merwade, 2012).

The uncertainties in the upstream and downstream boundary conditions mostly arise from the uncertainty in deriving river discharge from measured stages and rating curves and is well documented in literature (Di Baldassarre and Claps, 2011; Di Baldassarre and Montanari, 2009a). Channel cross-sections are sometimes difficult to measure in some locations (Sefe, 1996), sometimes they are not stationary (Callede et al., 2000), and particularly prone to modification after major floods. Uncertainty in the inflow of water in the model domain is considered as the most potent source of uncertainty in inundation modelling (Pappenberger et al., 2006). The effect of uncertain parameterization such as Manning's roughness coefficients (Pappenberger et al., 2005) and varying levels of confidence in the boundary-condition information (Pappenberger et al., 2006) on flood prediction were analysed in detail using Generalised Uncertainty Likelihood Estimation (GLUE) (Beven and Binley, 1992). The impact of possible land-use change in urban areas, modelled by means of changing roughness values, on the distributed uncertainty estimation was attempted by Weichel et al., (2007) but met with limited success. Uncertainty in the topographic data, especially if a continuous surface interpolated from spot heights and contours, can have significant impact over hydraulic variables such as velocity and depth of inundation in small scale (Wilson and Atkinson, 2005a; Wilson and Atkinson, 2005b).

The GLUE methodology has been widely used in inundation modelling in the past decade by using time series of river stages from gauging sites (Hunter et al., 2005) as well as distributed observed inundation patterns derived from satellite images (Horritt and Bates, 2001) and aerial photographs (Romanowicz and Beven, 2003). The choice of a performance measure of an inundation model is an important consideration in GLUE technique and can significantly influence the computed predicted uncertainty scenario. However, Jung and Merwade (2012) reported that the using different performance measures resulted in only 2% change in the uncertainty quantification.

Uncertainty in the measurements of observed data such as time series of stage/discharge records or flood-extent maps derived from airborne or spaceborne platforms may affect the computation of predictive uncertainty. Such error may also add a significant amount of uncertainty in estimating design flood events (Di Baldassarre et al., 2012). As the reference vertical datum for the river gauges are often based on local datum and not related to a global geoid model it is difficult to make a direct comparison between

simulated river stages and an observed one (Hall et al., 2011; Hall et al., 2012). For data-sparse regions we commonly use freely available global DEMs such SRTM or ASTER GDEM that are generated from global geoid models such as EGM96. Survey authorities in developing countries generally do not follow a geoid model for preparing large scale topographic maps and geodetic control networks. For example, in India no geoid model is used for determining the vertical datum and there is no straightforward way of converting the local mean sea-level information into an established geoid (Agrawal, 2005). This factor introduces uncertainty in the observed river-stage information when global DEMs and surveyed data collected through differential GPS is used in models to predict water-surface elevations.

Previously, distributed predictive uncertainty was quantified by using deterministic binary pattern flood extent maps that were generated from remotely sensed data (Horritt and Bates, 2001; Pappenberger et al., 2007). Although the scientific community acknowledged the inherent uncertainty in the satellite derived flood extent maps, Di Baldassarre et al. (2009) first illustrated a methodology of quantifying the uncertainty in satellite derived flood extent maps and incorporating this factor in the uncertainty analysis of the modelled flood extent. Stephens et al. (2012) used the distributed water-surface elevation derived from ERS-2 SAR as the observed data for conditioning the computation of distributed predictive uncertainty of an inundation model. They pointed out the impact of noisiness and strong spatial autocorrelation in the error of water surface elevation on the computed values of the predictive uncertainty. In addition, this paper also highlighted that using observed data corresponding to different parts of the model domain have varying degree of influence on the consequent computation of the distributed uncertainty pattern.

Although the literature is replete with studies regarding distributed and point-based uncertainties in simulated outputs of inundation models there is a general lack of attention in the scenarios where the study was undertaken in 1) developing countries with no access to high resolution topographic data / surveyed cross-sections, rating curves and radar images of flooding; 2) with complex and computationally demanding finite element models (e.g. TELEMAC2D) with a robust mechanism to account for hydraulic processes; and (3) in study sites with anabranching fluvial system associated

with a number of river bifurcations, large river islands and distributaries rather than a single channel.

1.1.6 Recent trends in inundation modelling

Recent advances have been made in improving the computational efficiency of raster-based 2D models using an inertial formulation (Bates et al., 2010) or graphic processing unit-based methodologies (Kalyanapu et al., 2012) to use Monte Carlo techniques for producing probabilistic flood hazard maps at a very fine resolution. In terms of distributed observed data, now we have high spatial resolution SAR images from sensors like TerraSAR-X (3 m) for successfully demarcating the flooded area in heavily built up environments (Mason et al., 2010). Stephens et al. (2012) delineated flood extents from SAR data using the method developed by Mason et al. (2009) and derived the distributed water-surface elevation by intersecting the shoreline with LiDAR DEM in order to assess the distributed uncertainty of modelled flood depth. For applications at continental scale involving large wide rivers such as the Amazon the modelled water surface was validated using the RA-2 altimeter on board Envisat (Yamazaki et al., 2012a). However, the majority of the new developments is geared towards making better use of ever increasing quality of distributed data that are available for only a very small portion of the flood-prone regions of the world.

1.1.7 Causal link between land use/cover and downstream flood risk

With changes in the climate, the frequency and magnitude of extreme hydrological events are increasing around the world (Huntington, 2006). Although it is quite evident that the impact of land use/land cover (LULC) change at plot or small catchment scale has a clear-cut effect on the flood peak (Wan and Yang, 2007) the causal relationship between the two becomes less clear as the size of the catchment and the number of LULC, increases (Andréassian, 2004). Exploring the nature of the relationship between the local LULC changes at the sub-catchment level and its impact on the hydrograph at the basin outlet is important because most of the watershed management planning is perceived and implemented at the sub-catchment level. Without a clear understanding of the scale-dependent processes responsible for propagating the effect of local LULC

changes into the basin hydrograph it is difficult to implement remedial land management measures to reduce flood peak (Pattison et al., 2008).

Lane et al. (2007) pointed out four potential ways by which land-management practices in a rural catchment might affect a storm hydrograph as 1) the influence in determining the share of rainfall following the rapid surface route and the slower subsurface one; 2) the efficacy of the process of transferring the rainwater from the hillslope to the channel; 3) the ease of passage of the flow within the riparian zone; and 4) the effect on existing catchment storage during heavy rainfall events. Pattison and Lane (2012) envisaged that the effect of LULC might have a different impact of different scale because a particular land-management practice may have an impact over more than one of the processes mentioned above. The effect of the intensity and duration of the precipitation and the type of soil is also very important in controlling the way in which changes in LULC can lead to alteration in the downstream flood hydrograph. The processes that lead to runoff generation are sensitive to the type of precipitation, therefore the effect of LULC change and land management has to be event specific (Bronstert et al., 2002). The reduction of surface runoff due to alteration in the soil infiltration capacity is restricted only in the initial phase of the rainfall event so that for events of longer duration the soil infiltration capacity is not at all found sensitive to existing LULC (Quast et al., 2012). Pattison and Lane (2012) came to the conclusion that due to the difficulty in upscaling the straightforward relationship between LULC changes and storm runoff, the linkage between LULC and the rate of flow to the downstream outlet of a large basin is rather unique and should not be generalised. Nevertheless, there have been efforts to explore the causal relationship between LULC changes and the downstream flood hydrograph through modelling. Ewen et al. (2012) focussed on the sensitivity of the peak flow rate on the factors that control runoff generation and analysed different scenarios based on ‘impact mosaic maps’ created by an algorithmic differentiation method. Quast et al. (2012) combined the use of infiltration and erosion models in a schematised approach for achieving a similar goal and concluded that the flood-causing amount of rainfall varies with reference to the combination of soil types and land use.

In data-sparse conditions, where detailed soil maps and other measurements of soil parameters such as hydraulic conductivity is not available, the NRCS Curve Number

(Natural Resources Conservation Service, 1986) approach can be a good proxy for capturing the combined effect of LULC and soil on the downstream flood hydrograph. Widely used hydrologic models like HEC-HMS (US Army Corps of Engineers, 2012) has been used with limited data to identify the sub-catchments that have high runoff generating potential and relative contribution to the storm hydrograph at the basin outlet (Saghafian and Khosroshahi 2005; Roughani et al., 2007; Saghafian et al. 2008). However, these investigations stopped short of evaluating the effect of changing LULC at the sub-catchment level on the downstream flow rates. Further research in this direction that make use of a modelling suite available in the public domain and inputs that can be derived from freely available satellite images and soil maps would be particularly beneficial for a wider community.

1.1.8 Summary

The scale of the fluvial system under investigation, the model output of interest (river stage vs extent of flooding) and the nature of extreme streamflow events (within bankfull level or floodplain flow) are significant considerations in the context of modelling flood without any access to the high quality model inputs and observed data for calibration and validation. Numerous studies have been successful in accurately predicting floods in a single channel fluvial environment where the extent of flooding takes place in more or less contiguous manner and the spatial extent of uncertainty is confined to a narrow strip of land at a distance from the channel. However, in an anabranching channel associated with multiple river islands and distributaries the occurrence of flooding does not take place in a spatially contiguous manner as it results from the overtopping of the levees at various points along the main channel as well as the smaller branches. The fluvial morphology of low lying areas in the tropics and sub-tropics frequently consists of multiple channel bifurcations due to frequent avulsion and they suffer major flooding such the Kosi flood in India in 2008 (Kaur and Das, 2011; Sinha, 2011). This kind of drainage pattern is also frequently observed in the flat deltaic landscape of large rivers which are inherently flood-prone. Hence, there is a need to understand to what extent inundation models of different complexities can simulate flooding in this kind of common flood-prone environment with coarse quality inputs found in the developing countries. With the development of methodologies for predicting inundation with limited data it is also required to investigate how we can

precisely prioritise our land use planning effort to mitigate the intensity of flood waves. The success of any land management strategy depends on our understanding of the causal linkages between local LULC changes and its impact on the flood hydrograph downstream.

An assessment of the uncertainty of the model outputs is crucial in the context of data sparse modelling environment. Incorporating the element of uncertainty in flood inundation modelling will help the transition from deterministic to probabilistic modelling. A deterministic prediction of river stage or flood extents that are based on optimum choice of parameters may mask the uncertainties in the modelling process and provide spuriously precise results (Bates et al., 2004; Beven, 2006). A probabilistic approach prevents incorrect planning decisions about future development in the areas adjacent to the rivers by having an understanding of the confidence level in the modelled outcomes (Di Baldassarre et al., 2010).

1.2 The thesis outline

It is evident from the background given earlier that we need varying kinds of flood prediction capabilities depending on the nature of flooding along with the morphology of the river basin. The required process for creating the inputs or for modifying the freely available data into an acceptable form, particularly the terrain data, will be different depending on the scale of the problem as well as the morphology of the river basin. Chapter 2 provides a general description of the study sites that have been selected for the four empirical experiments. The main content of this thesis is presented in the form of four articles in Chapter 3 to 6. Chapter 3 has been already published. Chapter 4 is in the final stages of preparation before submission. Chapters 5 and 6 are under review in reputed international journals. Each manuscript addresses a combination of the major issues highlighted in the background section. Due to the article format of the thesis, there is some element of overlap between the chapters, especially in the description of study sites and field methods. My intention is to demonstrate the challenges of modelling streamflow in data sparse situations and the effect of scale and channel morphology on the success of the modelling process.

The main focus of Chapter 3 is to develop a flood routing system in a regional scale using a 110 km reach in the middle course of the Damodar River as the study area. As the length of the river reach is too big for undertaking any computationally demanding and complex fully 2D hydraulic model, a simple and computationally efficient model is more suitable. Due to the large scale of this study only modifying the existing terrain data will be considered rather than creating a new one. In addition, this investigation will demonstrate how very limited ground survey can provide complementary terrain information for accurate routing of extremely high magnitude flood waves. The impact of uncertainty arising from inputs such as terrain, boundary conditions, channel configurations as well as modelling parameters like the selection of roughness coefficients will also be evaluated as part of this section of this thesis.

The issue of modelling inundation at the reach scale with limited data is addressed in Chapter 4. As mentioned earlier that a lot of flood-prone areas around the world are located in deltaic lowlands that are associated with numerous river bifurcations and channel islands. Chapter 4 tackles the challenge of simulating widespread floodplain inundation in anabranching channels without the access to a high resolution input terrain and SAR images for calibration and validation. The lower Damodar Basin has been chosen as the study area which is frequently flooded and associated with river bifurcations and river islands. Since the scale of this study is relatively small but with a complex morphology and high severity of hazards it demands more detailed treatment of both inputs as well as the physical process representation. Hence, I demonstrate a novel approach for creating an improved terrain data by combining elevation information extracted from low-cost stereo satellite imageries, modified SRTM DEM and limited surveyed cross-sections. The emphasis is on generating a hybrid terrain data that represent topographic features with greater influence on the inundation process such as channels, embankments and roads in finer details than the homogeneous farmlands. The other focus-point of this chapter will be evaluating how inundation models with varying levels of hydraulic process representation such as simple 1D-2D coupled LISFLOOD-FP or complex TELEMAC2D perform with the improved terrain data for simulating flood extents in an anabranching river system. The spatial distribution of inundated area in an anabranching river is often patchy and sometimes can be observed at considerable distance from the main channel. This is caused by the overtopping of the levees at the main channel as well as various smaller distributaries.

This chapter argues that the performance of any hydrodynamic code in this kind of fluvial system primarily depends on its ability to divert high velocity flows in the smaller distributaries from the main channel. The level of process representation and the suitability of the code for a terrain data of varying details are likely to affect this ability.

Chapter 5 examines the issue of uncertainty arising in the study conducted in Chapter 4. Uncertainty estimation is carried out under the GLUE framework. The salient features of this chapter are 1) distributed uncertainty assessment of a complex and computationally demanding finite element inundation model such as TELEMAC2D at high resolution for a model domain of ~ 300 km^2, 2) special emphasis on the spatial nature of uncertainty arising at the different stages of the considered flood event from the use of a terrain data with limited resolution and accuracy in a complex channel network, and 3) assessing the impact of incorporating the element of error in the observed flood extent map on the computation of uncertainty vis-a-vis the use of deterministic flood maps. In general, this chapter explores whether the element of uncertainty in the distributed observed records can make a significant impact in the overall uncertainty scenario when the inputs like inflow hydrograph and terrain have a high degree of uncertainty and the parameter space of the model has a higher dimension.

Chapter 6 investigates whether degrading land use/cover in steep hillslopes is intensifying the downstream flood risk. The event-scale rainfall-runoff modelling setup in this chapter is created primarily from a mitigation perspective. Mitigation measures such as remedial land use planning for reducing runoff coefficient of high runoff producing areas can be implemented only on local scale which generally corresponds with a sub-catchment of a river system. This chapter illustrates a systematic approach of investigating the causal relationship of sub-catchment-wise land-use change on the flood hydrograph at the basin outlet.

Chapter 7 is a general discussion chapter for the whole thesis. This chapter summarises the key findings of Chapter 3 to 6 and indicates where they fit into the broader perspective of predicting flooding at different scale and over varying physiography of land surface with limited data, typically available in the developing countries. Chapter 8

provides the conclusion and the scope and potential of further research under the broad theme of this thesis.

The overall purpose of this thesis is to demonstrate how the existing datasets available in developing countries can be adapted and modified to model flooding with number of freely available hydrological and hydrodynamic models. This study addresses the challenge of predicting flooding and its causes with the sparse datasets at different scale. The aim of this research work is to illustrate a holistic approach that deals with the necessary prediction capability of flooding for providing early warning system, developing flood defences, creating flood risk maps, as well as planning remedial measures to mitigate its effect in a controlled river basin.

Chapter 2

Study Area

The basin of the Damodar River, one of the important tributaries of the River Ganga (Ganges) in India has been selected as the study site for this thesis. India is a classic example of a vast flood-prone country in the global south with very limited availability of the type data that are ideally required in inundation modelling. In terms of their magnitude of flood and mean annual discharge the South Asian rivers are among the most important in the world (Kale, 2002). Profuse rainfall as a result of the combined effect of low-pressure systems and active monsoon conditions is the most frequent cause of large and extensive floods in the Indian sub-continent (Panchawagh and Vaidya 2011). Extreme floods in South Asia in the last two centuries have had a statistically significant link with excess monsoon epochs (Kale, 2012). The frequency of high magnitude floods in the large South Asian Rivers such as the Ganga, the Brahmaputra and the Indus is generally very high and is a common occurrence in almost every year (Kale, 2003). The annual average area affected by floods in India is 7.563 million ha with a minimum of 1.46 million ha in 1965 to a maximum of 17.5 million ha in 1978. On average, these floods affect 33 million people every year (Mohapatra and Singh, 2003).

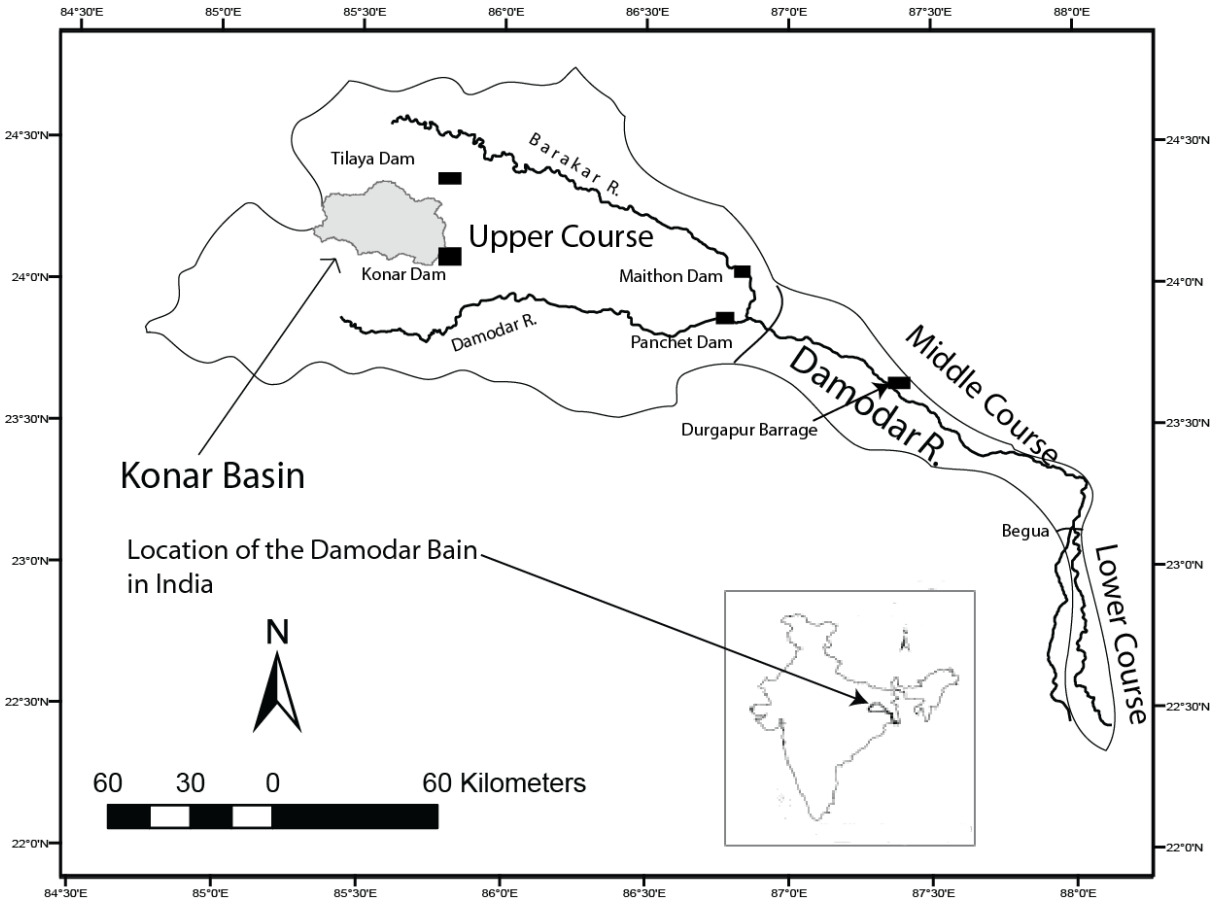

Figure 2.1 Description of the study area.

The Damodar River has 24,235 km^2 of basin area spreading over the Indian states of Jharkhand and West Bengal (Figure 2.1). The river originates in the Palamau Hills of Chotanagpur Plateau and flows in an east and southeasterly direction for 540 km before joining the Hoogly River which a major branch of the Ganga. A distinguishing feature of the Damodar Basin is that approximately 80 % of its area falls in the hilly and forested upper catchment while the remaining 20 % constitutes the flat and fertile floodplain where all the discharge from the upper catchment concentrates. This particular basin shape is mainly responsible for frequent inundation in the lower Damodar Basin (Choudhury, 2011).

This basin is heavily regulated with four major dams in the upper catchment, namely, the Maithon, Panchet, Tilaya and the Konar. Furthermore, Durgapur dams, is situated in the middle course of the river. The dams were built as part of India's first multipurpose river valley project called the Damodar Valley Corporation (DVC) in the early 1950s. Prior to dam construction, flooding had been a common natural process in the Damodar River Basin and historical records indicate occurrence major floods 19 times between 1770 and 1943. In the post-dam era from 1950 onwards, the lower valley experienced major floods 14 times between 1958 and 2000 (Chandra, 2003) and this trend still continues and probably the construction of the dams have made floods more frequent. During heavy monsoon storms when lot of discharge from the upper catchment converges to the reservoirs upstream , the DVC managers are left with little alternative but to release the water downstream at a very high rate to avert catastrophic dam breaks. All this water travels downstream to Durgapur Barrage which does not have a big enough reservoir to moderate this flood wave and the water flows almost unhindered downstream. While flowing downstream the flood water mostly remains within its bankfull level from Durgapur Barrage to Begua where the river bifurcates into two branches and the main flow diverts towards a branch known as Mundeswari River (Figure 2.1). The stretch from the border of West Bengal State to Begua will be referred as the middle course of the river henceforth in this thesis. Here the width of the river ranges from 2.5 km to 800 m with an approximately average depth of 10 m from the bankfull level.

Figure 2.2 Wide channel in the middle course of the Damodar River

From Begua further downstream (this stretch will be henceforth described as the lower reach of the Damodar River) both the Mundeswari and the minor branch of the Damodar River (also known as Damodar) experience frequent and widespread overbank flow, breaching and overtopping of levees that lead to major inundation of the adjacent floodplain. Inadequate capacity of the channels in the lower course due to heavy siltation is primarily responsible for frequent flooding (Basu, 1996). In the post-dam era numerous distributaries in the lower valley got cutoff from the main channel as the natural discharge reduced dramatically for filling up the reservoirs in the post-monsoon period. These smaller branches of the main river turned into moribund condition and no longer act as an effective conduit of water during a flood situation (Ghosh, 2011).

Figure 2.3 Relatively narrow channel of the Mundeswari River, the major branch of the main channel of the Damodar River in its lower course

The upper catchment has been subject to indiscriminate deforestation since the colonial period due to mining and agricultural activities (Saha, 1979). It is characterised by hilly terrain with high relative relief (Gupta, 2004) and therefore the deforestation is likely to have quickened the flood peak at the reservoir entry points and filled the reservoirs with an increased supply of sediment load from accelerated rate of erosion on the bare soil. These factors might have a combined effect on reducing the effectiveness of the dams to moderate the flood wave that rush down the steep slope during heavy monsoon rainfall events. The catchment of Konar River, one of the important tributaries of the Damodar River in its upper course is selected as a typical example for understanding the interaction of land use change and flood peak in the river headwaters. The existence of the Konar Reservoir at the outlet of the Konar Basin provides the ideal setting for examining whether land degradation in the past few decades has had an impact over the flood peak at the basin outlet that flows directly into the reservoir.

The Damodar basin is a perfect example of a river basin where flooding can be studied at different scales and over different type of channel patterns. In addition, the nature of high magnitude streamflow also varies from one course of this river to another. In the middle course the flood water is mostly confined within its bankfull level with occasional overtopping of its low right hand embankments. Predicting the timing and magnitude of flow from the Durgapur Barrage to the flood-prone lower course is of interest here. However, the widespread inundation across the anabranching channels in the relatively smaller lower valley makes it an ideal reach-scale study site for comparing the performance of 2D flood inundation models with varying levels of complexity. The distinct topographic and associated fluvial features of the upper, middle and lower course of the Damodar Basin help to identify the typical challenges of flood management in data sparse regions. These issues include developing design flood events in terms of river stages, vulnerability assessment of the flood-prone communities, and effectiveness of non-structural mitigation strategies. The middle and lower basins of the Damodar River provide us the experimental natural setting for the first and second issues while the Konar Basin in the upper catchment is used to test the third proposition.

Chapter 3

Hydraulic routing of extreme floods in a large ungauged river and the estimation of associated uncertainties: a case study of the Damodar River, India.

Abstract

Many developing countries are very vulnerable to flood risk since they are located in climatic zones characterized by extreme precipitation events, such as cyclones and heavy monsoon rainfall. Adequate flood mitigation requires a routing mechanism that can predict the dynamics of flood waves as they travel from source to flood-prone areas, and thus allow for early warning and adequate flood defenses. A number of cutting edge hydrodynamic models have been developed in industrialized countries that can predict the advance of flood waves efficiently. These models are not readily applicable to flood prediction in developing countries in Asia, Africa and Latin America, however, due to lack of data, particularly terrain and hydrological data. This paper explores the adaptations and adjustments that are essential to employ hydrodynamic models like LISFLOOD-FP to route very high magnitude floods by utilizing freely available Shuttle Radar Topographic Mission (SRTM) digital elevation model (DEM), available topographic maps and sparse network of river gauging stations. A 110 km reach of the lower Damodar River in eastern India was taken as the study area since it suffers from chronic floods caused by water release from upstream dams during intense monsoon storm events. The uncertainty in model outputs, which is likely to increase with coarse data inputs, were quantified in a generalised likelihood uncertainty estimation (GLUE) framework to demonstrate the level of confidence that one can have on such flood routing approaches. Validation results with an extreme flood event of 2009 reveal an encouraging index of agreement of 0.77 with observed records while most of the observed time series records of a 2007 major flood were found to be within 95% upper and lower uncertainty bounds of the modeled outcomes.

Keywords: Hydrodynamic Model, Developing Country, LISFLOOD-FP, SRTM DEM, GLUE, India

3.1 Introduction

The developing world, particularly Asia and Latin America, shares the highest concentration of flood occurrences due to high-magnitude storm events such as tropical cyclones and intense monsoon downpours. According to the EM-DAT database maintained by the Office of US Foreign Disaster Assistance and the Centre for Research on the Epidemiology of Disasters (OFDA/CRED), between 1900 and 2012, 3151 out of 3927 (more than 80 percent) of major floods occurred in Asia, Africa and Latin America. The impact of these disasters is more pronounced in developing economies as the cost of a partial or full recovery in relation to GDP may be very high (Alcantara-Ayala 2002). The technological capability to predict the dynamics of flood waves from upper catchments to low lying flood-prone areas downstream is essential for developing flood warning and flood management strategies, and thus mitigating the effects of these disasters. The last three decades have seen the development of many advanced tools for flood modelling and prediction. However, these technologies are typically not applied in developing countries due to lack of appropriate data. The aim of this study is thus to explore a methodology for utilising advanced flood routing tools in data-sparse settings in the developing world.

Hydrodynamic models have been widely used to route floods with remarkable accuracy. However, they require very high resolution terrain data as well as hydrological inputs from numerous gauging stations. The terrain data that are used for this purpose are typically derived from LiDAR survey, IFSAR such as NEXTMap in the UK at a horizontal resolution of 5 m and vertical accuracy of 0.5 to 1 m (Sanders et al., 2005; Mason et al. 2010b) or densely spaced surveyed cross-sections (Pappenberger et al., 2006). Gauging stations are commonly available at the inlet and outlet of the reach being modelled and these stations frequently record water discharge at high temporal resolution (e.g. 15 minute intervals). As an example, Bates et al. (2006) used LiDAR-generated DEMs, in combination with a series of airborne synthetic aperture radar (ASAR) images captured opportunistically during the peak and recession limbs of a flood hydrograph, in order to calibrate and validate a simple raster-based hydrodynamic model (LISFLOOD-FP). The LiDAR DEM used had <1 m horizontal resolution with a vertical root mean square error of

0.079 m. However, it is well documented that the lack of these data sets for the vast majority of developing countries is a major obstacle for employing hydrodynamic models there (Sanyal and Lu, 2004). In addition, the near-absence of an established network of permanent GPS base stations in many areas means that undertaking ground surveys with differential GPS in order to supplement the paucity of terrain data is also challenging. Hydrologic modelling techniques such as the Muskingum method could be an alternative as they are less dependent on accurate terrain as a model input. Nevertheless, the efficiency of these approaches are not very high due to their inability to account for the hydrodynamic processes associated with extreme floods, particularly backwater and the floodplain storage effects (Garbrecht and Brunner, 1991). The rarity of gauging stations at the downstream end of a flood-prone reach of interest, however, makes even these relatively simple flood routing techniques often unsuitable in large parts of Asia, Africa and Latin America.

India is a good example of this general issue, because it suffers frequently from large scale to localised flooding during the monsoon season and is characterised by a dearth of available data for flood routing that is typical in developing countries in general. During heavy monsoon storms, large dams in India are sometimes forced to release large amounts of water in a short time in order to prevent catastrophic dam breaks, and this release can lead to devastating floods downstream. This situation urgently demands the development of flood routing systems. As limited availability of suitable terrain data is the most significant obstacle for developing a flood routing model in developing nations in general and India in particular, we need to consider the available options carefully. Apart from the freely available Shuttle Radar Topography Mission (SRTM) digital elevation model (DEM) of 3 arc second (approximately 90 m) resolution, the other possible source of terrain data in India are Survey of India (SOI) topographic maps at 1:50,000 scale and 20 m contour interval, and the ASTER Global Digital Elevation Model (GDEM) of 30 m resolution. The large contour intervals and hence the low horizontal resolution and vertical accuracy of the SOI maps make them unsuitable for hydrodynamic models in flat areas that are coincidentally also the most flood-prone. The ASTER GDEM, although of moderately high horizontal resolution of 30 m, is reported to have a vertical RMSE of 18

to 29 m (Reuter et al. 2009) and is not considered as a suitable terrain input for hydrodynamic modelling. In contrast, Sanders (2007) compared the performance of the SRTM DEM with a very accurate LiDAR DEM for hydrodynamic modelling, and pointed out the value of the SRTM DEM as a global source of terrain data. Paiva et al. (2011) employed some generic rules of fluvial geomorphology in a GIS-based algorithm to derive simplified channel geometries from the SRTM DEM for 1D hydrodynamic modelling of a major tributary of the Amazon River. Modified SRTM DEMs have also been employed with the MIKE21 2D hydrodynamic model for simulating the seasonal dynamics of the Nile swamps of in southern Sudan (Petersen and Fohrer 2010). However, undertaking a fully 2D hydrodynamic modelling for a reach length of more than 100 km is likely to be associated with quite high computational cost.

Other studies have used river cross-sections derived from the SRTM DEM in order to route river flow in the Mahanadi River delta (Patro et al. 2009a; Patro et al. 2009b) and the Brahmani River basin (Pramanik et al. 2010) in India with the MIKE11 1D hydrodynamic model. Although these studies have showed that the SRTM DEM or its modified forms can be used to extract cross-sections for large-scale 1D flow routing, such an approach may not perform equally well where the accuracy of the DEM, especially over the river channel, is not consistent. The accuracy of flood routing can be very sensitive to DEM accuracies in the channel when dealing with extreme events (Casas et al., 2006). Some of the afore-mentioned studies such as Patro et al. (2009) had access to significant secondary information, like surveyed embankment heights, which may not be available in all flood-prone reaches. More broadly, employing sparse data inherently increases the uncertainties of the model predictions, but studies in the literature have rarely reported formal uncertainty analysis of model outputs that are derived from coarse terrain and hydrological inputs. A notable exception to this was the study reported by Pappenberger et al. (2006) that dealt with the influence of uncertain boundary conditions on HEC-RAS model output. To address this gap, the main objectives of this paper are 1) to find a suitable technique to route high magnitude and low frequency floods with the SRTM DEM, making use of limited cross-section surveys and no gauging record at the outlet and 2) to assess the uncertainty in model outputs that are induced by poor quality hydrologic and terrain inputs.

3.2 Study Area

The Damodar River Basin, with an area of 24,235 km^2, spreads across the Indian states of Jharkhand and West Bengal. The source of the river lies in the dissected Chotanagpur Plateau at a height of approximately 610 m above mean sea level. The river flows for 540 km, initially eastwards before turning southwards to join the Hoogly River (one of the main distributaries of the Ganges). As the river is heavily silted, the lower valley does not have the capacity to cope with a peak discharge of more than 2300 m^3/s (Central Technical Power Board India 1948). The lower Damodar Basin suffers from chronic flooding. There were 16 major floods recorded between 1823 to 1943, with a peak discharge of 18,500 m^3/s recorded at Durgapur in 1913 and 1935 (Saha 1979). The devastating flood of 1943 led to the establishment of the Damodar Valley Corporation, a multipurpose river valley project that built a network of dams to moderate flood waves and provide irrigation during the dry post-monsoon season. Although building the dams arguably achieved its objective of moderating flood waves, the lower Damodar Basin was still subject to flooding 14 times in the post-dam era of 1958 to 2000 (Chandra 2003). More recently, this area witnessed major floods in the years 2006, 2007, 2009 and 2011. The study area for the present investigation extends from the Durgapur Barrage to the point where the main channel bifurcates into two distributaries (Figure 3.1). The length of the study reach is approximately 110 km with an average width of 1.5 km. The flow of water during high magnitude floods in our study reach is primarily confined within the bankfull level, with occasional overtopping of the levees on the right bank. The floodplain flow,

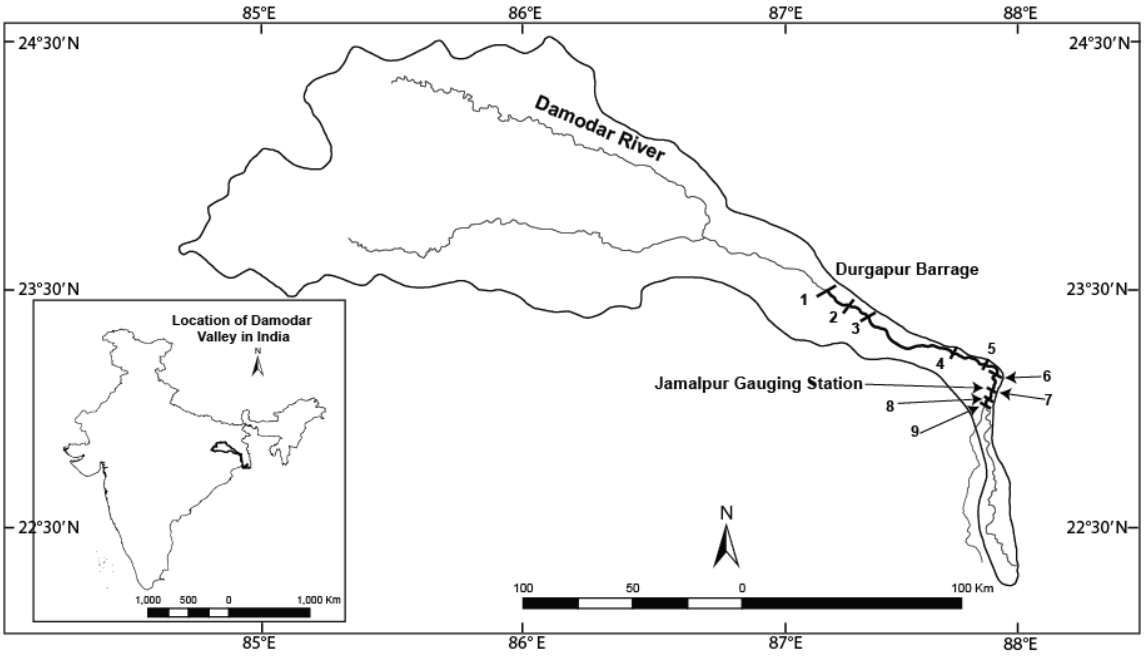

Figure 3.1 Overview of the Damodar Basin. The study reach is shown by heavy lines, and the surveyed cross-sections are indicated by numbers.

whenever it takes place, is intermittent in nature. There are some reasons for selecting this reach for the present study. First, predicting the travel time of flood waves from Durgapur Barrage to the downstream end of this reach and forecasting the river stage at this point is of primary interest because the areas situated further downstream of our study reach in West Bengal experience widespread floodplain flow. Secondly, Durgapur Barrage is the most downstream dam on the Damodar River and the flooding in the lower Damodar Basin is the direct result of the water release from this dam. Thirdly, there is no major structure downstream of the Durgapur Barrage that may affect the natural flow of water. Lastly, regular availability of discharge records at 1 to 3 hour intervals from the barrage and records of river stages at the Jamalpur gauging station at an intermediate location in the study reach (Figure 3.1) made it possible to procure the necessary hydrological input, calibration and validation data.

3.3 Data Used

Version 4 of the SRTM DEM (90 m horizontal resolution) was downloaded from http://srtm.csi.cgiar.org/. This version of the SRTM DEM is the most reliable and has been supplemented with auxiliary DEMs to fill the data voids. The vertical accuracy of this dataset was reported to be 7.58 m for Phuket Island of Thailand and 4.7 m in the Catskills Mountains in the USA (Gorokhovich and Voustianiouk 2006), while global validation studies of the SRTM DEM have reported an absolute vertical error of 6.2 m for Eurasia (Farr et al, 2007). Hofton et al. (2006) observed that the presence of large plots of dense canopy exaggerates the SRTM DEM elevation. As the floodplain and the river banks of our study reach have frequent clusters of trees and rural hamlets, a positive error in the SRTM DEM can be expected, and the methodology section addresses this issue by correcting the obvious inaccuracies in our terrain data. Apart from the DEMs, spot heights from the Survey of India (SOI) topographic maps were also collected as a source of elevation data in order to estimate errors of the SRTM DEMs in our study area. The maps were mostly at 1:50,000 scale with a few at 1:25,000 scale. A spheroid transformation was done in order to project the SOI maps from the Modified Everest to WGS84 spheroids so that the maps and SRTM DEM remain in the same coordinate system. There is also a potential degree of nonconformity between the SRTM DEM and the SOI spot heights due to the difference in the vertical datum used by these two datasets. SOI spot heights are elevation from local mean sea levels while SRTM DEM uses the EGM96 geoid model (Lemoine et al, 1996) as the vertical datum (Jarvis et al. 2008). A number of ad-hoc measurements were taken across our study area at known SOI spot height measurement sites with a differential GPS, and the difference was never found to be more than 50 cm. Since the SRTM DEM has a precision of 1 m we decided that SOI spot height and SRTM DEM pixel values are comparable.

The discharge records from the Durgapur Barrage were used at the inlet of the modelled river reach. Specifically, discharge records at 3 hour intervals for a flood event on 25-30 September 2007 and at 1 hour intervals for an event on 7-13 September 2009 were used as model inputs (Figure 3.2).

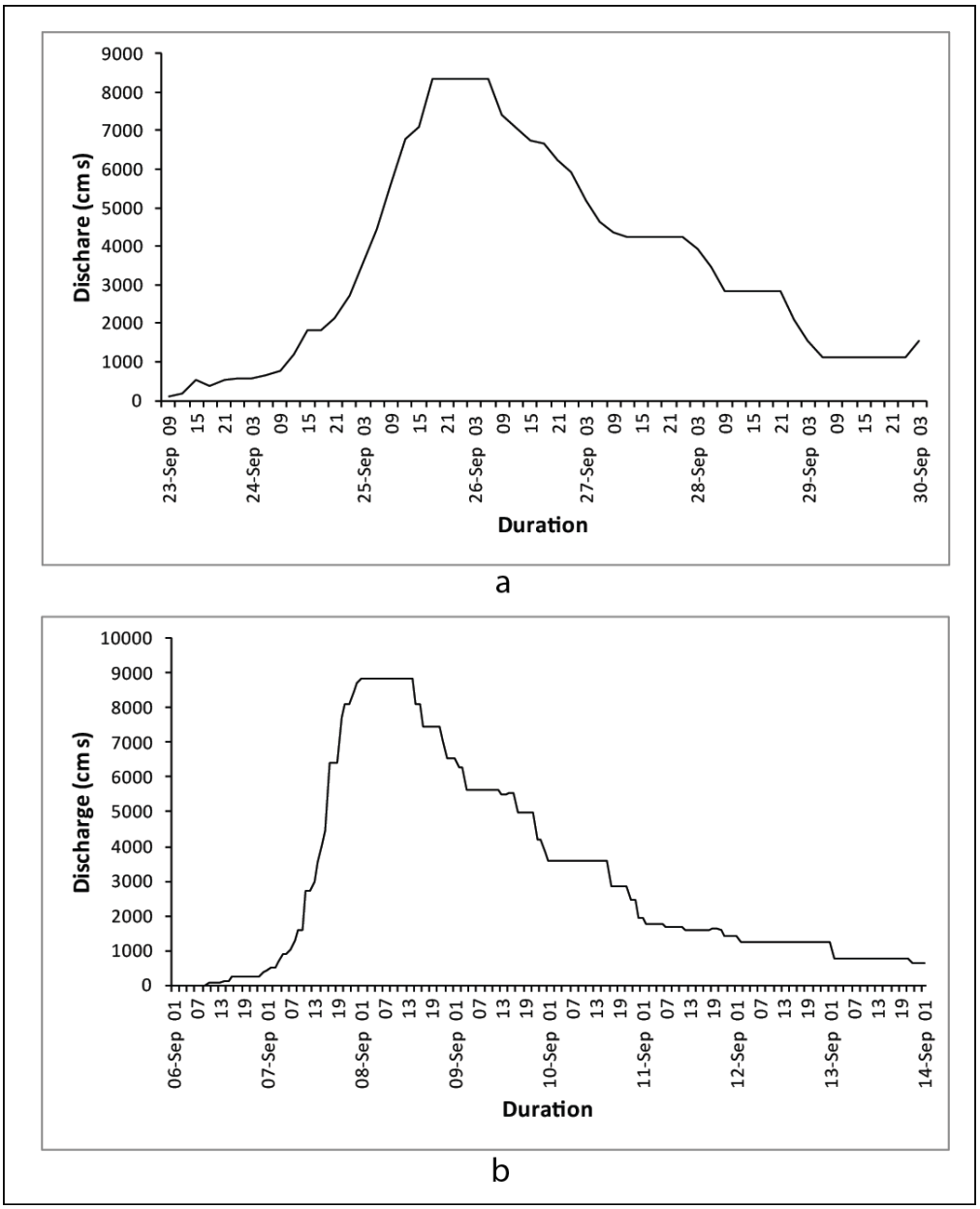

Figure 3.2 Hydrographs at Durgapur Barrage of the 2007 (a) and 2009 (b) flood events. Data were obtained at 3 hour and 1 hour intervals for the 2007 and 2009 events respectively.

In addition, a time series of annual maximum discharge from 1978 to 2010 was also obtained to compute the return periods/exceedance probability of the 2007 and 2009 events, assuming a log Pearson Type III distribution (Figure 3.3).

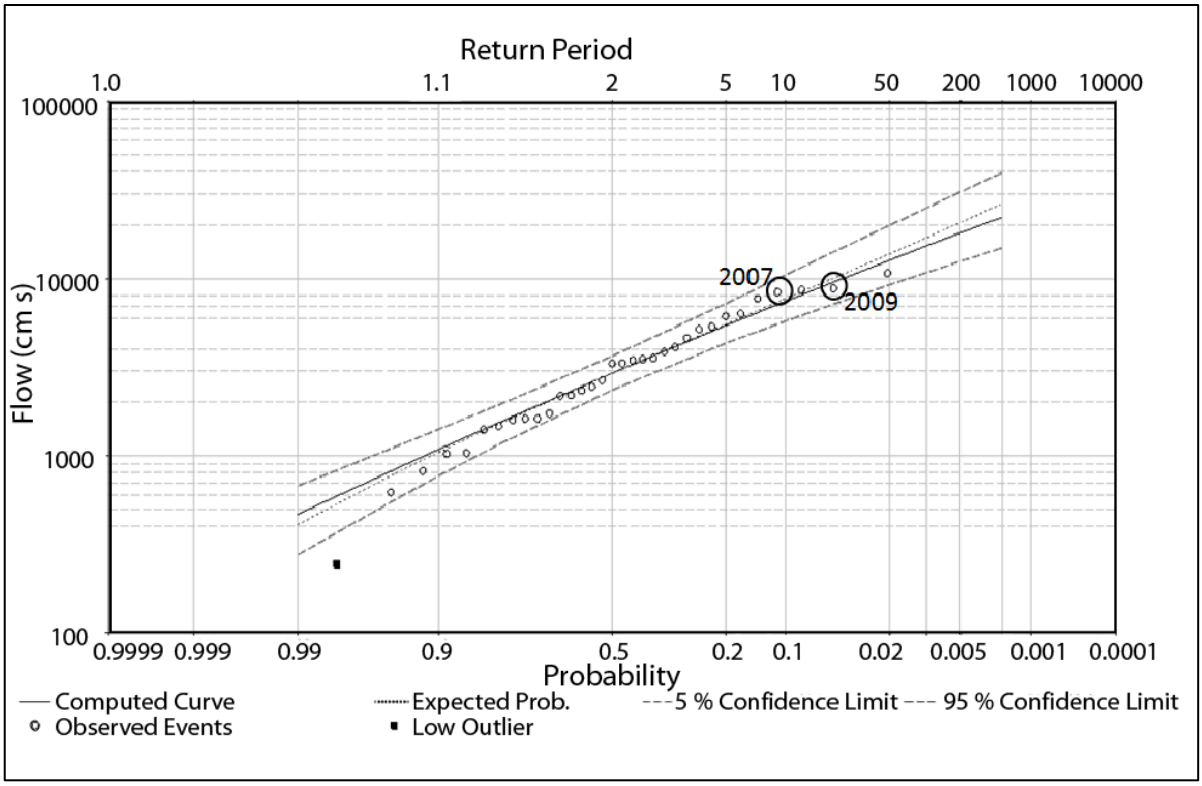

Figure 3.3 Flood frequency analysis of the annual peak discharge from the Durgapur Barrage. The 2007 and 2009 events, which are highlighted with circles, were used for calibration and validation respectively.

The hydrographs of the 2007 event, with an exceedance probability of 0.11, and the 2009 event, with an exceedance probability of 0.05, were used as the calibration and validation data. Here, a flood with an exceedance probability of 0.05 means that at any given year there is 5 percent chance of experiencing a flood of 2009 magnitude or more. These floods, with peak discharge values having a return period of approximately 10 years or more, were selected for this study because we are not aware of any previous attempts at estimating hydraulic routing of such damaging events with the SRTM DEM as the only available terrain input. The 2007 and 2009 events were also preferred for this study against other high magnitude events, such as 1978 and 1995, as they occurred quite recently in relation to the time of our field survey which was conducted in 2010. Water levels measured at 1 hour intervals at the Jamalpur gauging station (located approximately 100 km downstream of Durgapur Barrage) were used for the purpose of calibration, validation and uncertainty estimation of the modelled stages for both the 2007 and 2009 flood events. These stage

data were only available for high flow period during the floods, and the model performance was measured only against those data. There was no gauging station at the downstream end of the study reach, which is located 20 km downstream of Jamalpur station. All hydrological records were obtained from the Irrigation and Waterways Department of West Bengal, India.

3.4 Methods

3.4.1 Cross-section Surveys

Due to limited resources, we were able to survey only 9 cross-sections, shown with numbers in Figure 3.1, along the 110 km study reach. Cross-sections were surveyed at the inlet and outlet of the reach and at the Jamalpur gauging station. The rest of the 6 cross-sections were surveyed at places that represent the typical channel conditions regarding the width, depth, and bed material in that part of the study reach. Easy road access to the river bank was also an important factor that influenced the selection of survey sites. The Damodar River is fed by rainwater and during the dry post-monsoon season only about 10 percent of the channel width is generally occupied by the flowing water. Here we define channel width by the bankfull width normally filled with water during the peak of the monsoon season. The left bank of the study reach has a continuous artificial embankment which is more than 5 m higher than the river bank and very rarely breached during floods. Occasionally there are natural levees and short local artificial embankments on the right bank of the river.

The fieldwork was conducted during November-December, 2010, using a combination of differential GPS (dGPS) to survey the dry river bed and the water surface elevations, and a hand-held portable depth sounder to measure depths below the water surface. Special care was taken to measure the elevation of the water surface at the time of surveying (Figure 3.4). The measured depths were then subtracted from the water surface elevation to obtain the bottom elevation of the wet part of the channel. As the water level is expected to be at

approximately same elevation at the two banks of the wet channel it gave us a very useful indirect measure of the relative accuracy of the DGPS survey.

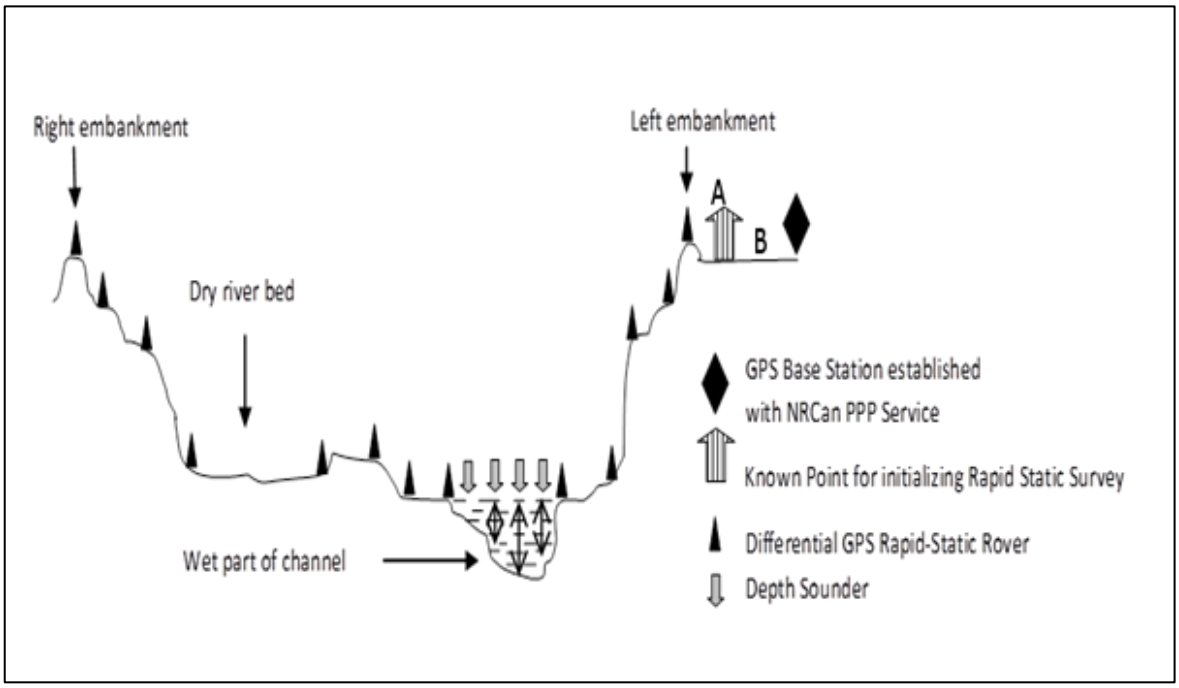

Figure 3.4 Schematic diagram illustrating the cross-section survey geometry along the Damodar River with differential GPS and depth sounder. NRCan PPP is the abbreviated form of Natural Resources Canada Precise Point Positioning.

The presence of a GPS base station within 20 km of the rover location is an essential prerequisite for conducting any dGPS survey with relatively inexpensive single frequency (L1) GPS receivers. No real-time observations of permanent GPS stations are available in the public domain in India, and the nearest International GNSS Service (IGS) base station was more than 2000 km from our study area. A base station with known coordinates in the International Terrestrial Reference Frame (ITRF)/WGS84 was essential for this survey in order to make the observations consistent with the global datasets such as the SRTM DEM. Many web-based free services can, however, correct a sufficiently long observation (more than 4 hours) of a dual frequency (L1 and L2) GPS receiver from decimetre to centimetre accuracy. A comprehensive review of these services can be found in Tsakiri (2008). We used the Natural Resources Canada's Precise Point Positioning (PPP) service, also known as CSRS-PPP, which uses very precise GPS orbit or clock estimates from IGS to correct user-supplied observations. CSRS-PPP has reported that only 2 hours of continuous

observation in dual frequency receivers are capable of achieving a vertical accuracy of approximately 4 cm and with more than 2 days of continuous observation it can achieve a vertical error of 11.8 mm (Ebner and Featherstone 2008). Other services that use the nearest available IGS base station data to apply a differential correction to the user-supplied observation were not used, because differential corrections that are based on distant (e.g. more than 300 km) IGS stations are likely to be of lower positioning accuracy (El-Mowafy 2011).

At each survey site, a ~4 hour dual frequency GPS observation provided the base station observation, as this duration was sufficient to achieve 5-8 cm errors for the base station position. After the survey, the GPS data were converted into Receiver Independent EXchange (RINEX) format and uploaded to the CSRS-PPP service. A single frequency PROMARK3 GPS was used as the rover for collecting points over the channel. We took static observations at two points by occupying the points for more than 20 minutes. These two points are depicted as point A and B in Figure 3.4. The actual survey was done in a rapid-static mode. The rover was initialised by occupying point A for 30 seconds and thereafter each surveyed point was occupied for 30 seconds. Special care was taken not to lose the satellite lock once the rover was initialised over a known point (here point A). After the survey was completed an additional observation was taken at point B without losing the satellite lock which was used as the measure of accuracy for the rapid-static survey. It was assumed that static points are likely to have higher accuracy than the rapid-static points and therefore can be used as the reference for measuring the accuracy of the rapid-static measurements. The rover data were post-processed in the Thales GNSS Solution software as described below:

i) The CSRS-PPP output was used as the known coordinates for the base station. The Z coordinate, supplied in ITRF/WGS84 ellipsoid height, was converted into orthometric height using the EGM96 geoid model available freely for download from http://cddis.nasa.gov/926/egm96/new_improved.html#geoidgrid. The orthometric height (OH) was calculated as OH = WGS84 Ellipsoid Height - EGM96 Height

ii) The L1 observations of the static points, A and B were differentially corrected with reference to the base station established in step i.

iii) The corrected coordinates of point A were used as a known point and the rapid-static observations were corrected with the base station observation to get the final cross-section data with the planimetric coordinates in latitudes and longitudes and elevation as orthometric heights.

3.4.2 Error analysis and modification of the SRTM DEM

A total of 218 spot heights were obtained from SOI topographical maps and were compared with the corresponding pixel values of the SRTM DEM. Figure 3.5a depicts the location of SOI spot heights and shows a bias in their concentration towards the upstream portion of our study area. This was primarily because of the availability of more detailed topographic maps at 1:25,000 scale in that area. There is no systematic correlation between elevation values from the SRTM and SOI maps (Figure 3.5b, 2.5c), indicating that there is no relationship between error and increasing elevation, in contrast to the results of Pramanik et al. (2010) in an area approximately 350 km southwest of our study area. A histogram of differences between the spot heights and the SRTM DEM (Figure 3.5d) shows that 28.4 percent of errors lie within a value of ±2 m (that is, the SRTM DEM is 2 m higher than the observed SOI spot heights).

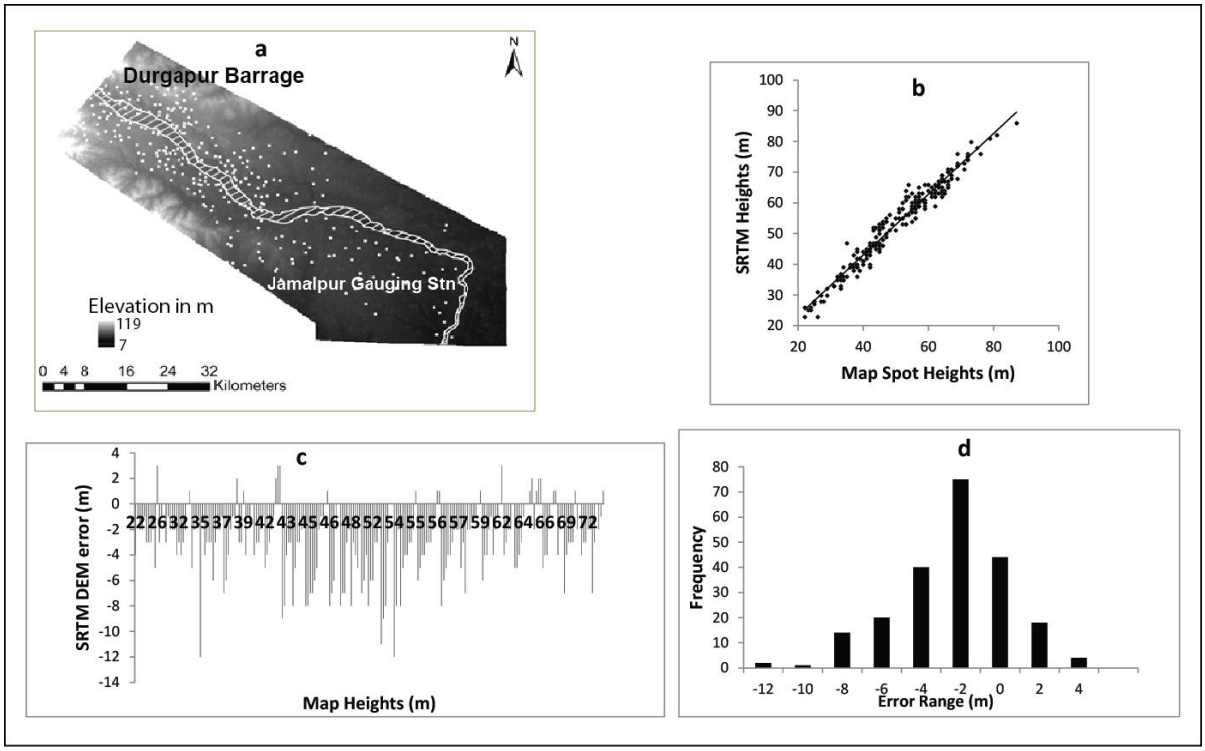

Figure 3.5 Distribution of error in the SRTM DEM. a, location of the Survey of India spot heights for computing the SRTM DEM errors. b, scatter plot of the SRTM DEM and Survey of India spot heights. c, occurrence of error, calculated as the difference between the SRTM DEM and the spot heights, in different elevation ranges (negative values signify that SRTM DEM is higher than SOI spot heights). d, Histogram of the errors in showing their distribution; 28.4 % of the points are within 2 m of error.

Because of the lack of trends in the distribution of error, the SOI median error value (2 m) was subtracted from the entire SRTM DEM dataset of our study area. Also, in order to reduce local spikes in elevation caused by the presence of trees or settlements, we manually digitised all such features in the floodplain from GoogleEarth. Those polygons were imported in the ERDAS Imagine software and the SRTM DEM was modified by replacing the pixels under the polygons with a smooth surface created by fitting a spline interpolated plane with the pixel values located at the edge of the polygons. To evaluate the effect of these modifications, we compared the modified SRTM DEM with the independent GPS data collected from the channel. The modifications produced a substantial increase in accuracy for the SRTM DEM when compared with the GPS data (see Table 3.1).

No. of Observation	Mean	Median	Mode
218 (SOI)	-2.13	-2	-2
210 (GPS)	-3.26	-3.17	-3.86
After modification of the raw SRTM DEM			
210 (GPS)	-1.47	-1.2	-0.5
RMSE calculated with 260 SOI spot heights = 2.05			

Table 3.1 Computed central tendency figures of the SRTM DEM error before and after the modification. All figures are in metres. –ve figures signify that the SRTM DEM cell values are higher than the known elevation values of the same location. GPS surveyed points for the channel recorded a decline in error from -3.17 to -1.2 m after the median error derived with respect to the SOI spot heights was subtracted from the SRTM DEM.

Finally, we noted that the left river embankment was not clearly visible in its correct alignment in the original SRTM data, probably because its width is less than the pixel dimension (< 90 m) of the DEM. Therefore we created an artificial 15 m high embankment on the modified SRTM DEM, following the actual alignment of the left embankment, in order to prevent the modelled flood water from extending beyond the left embankment.

3.4.3 Hydrodynamic modelling

Encouraged by the success of previous studies such as Patro et al. (2009a) and Pramanik et al. (2010) in routing flows with SRTM DEM-based cross-sections, we set up a similar 1D hydrodynamic simulation using the HEC-RAS model. However, preliminary experiments gave unstable results at peak flow and it was therefore decided that a simpler modelling framework would be used. 2D hydrodynamic models are more robust in their treatment of flood waves, particularly for the floodplain component of the flow. As a full 2D model for a 110 km river reach involves a high computational cost, we used the simple LISFLOOD-FP model (Bates and De Roo 2000). LISFLOOD-FP combines the virtues of both 1D and 2D approaches, where an implicit Newton-Raphson scheme is used for

kinematic approximation to the full 1D St Venant's equation for channel flow and a raster-based storage cell approach is used in order to give an approximation to a 2D diffusive wave for floodplain flow. The current version also includes a diffusive wave formulation of 1D channel flow. Although LISFLOOD-FP has been successfully used in various small to medium size rivers, mainly in Europe where the required terrain input is available at very high spatial resolution and hydrologic input at very high temporal resolution (Horritt and Bates, 2002; Bates et al., 2010; Neal et al., 2011), its application to wide rivers such as the Damodar has been limited. One such study was conducted by Wilson et al. (2007), who aggregated the SRTM DEM to 270 m resolution to reduce the overall error and increase the precision of the data and fed these data into LISFLOOD-FP in order to analyse the seasonal flooding pattern of the Amazon River. Although this study did not focus on routing discrete high magnitude flood events, they reported a 0.99 m RMSE in river stages at high water.

The primary preference for selecting LISFLOOD-FP came from its simple requirements of terrain input, particularly for the channel. In LISFLOOD-FP the channel is represented by a series of points, each having one value for the bed elevation and another for the channel width. The channel is assumed to be rectangular for computational efficiency. Since we need a single value for the bed elevation at each point of the 1D channel vector instead of a series of points captured by the cross-sections the water surface elevation was used to obtain it. Figure 3.6 and 3.7 show that, at very low flow when the survey was conducted, the elevation of the water level is a very good approximation of the channel bottom of a roughly rectangular channel. The water surface elevation at the cross-sections, when connected along the longitudinal profile of the river, also provides a good approximation of the energy gradient of the river which is important information for any hydrodynamic model.

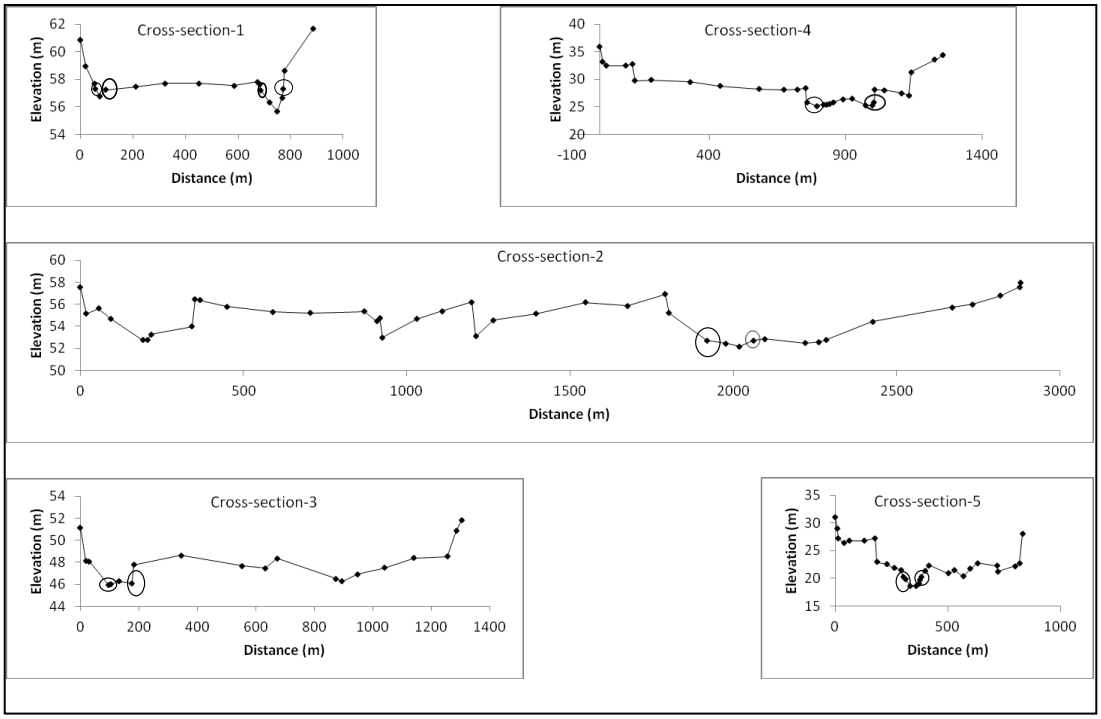

Figure 3.6 Surveyed cross-sections (1-5). See Fig. 3.1 for locations. Surveyed points that are marked with circles show the water level during the survey.

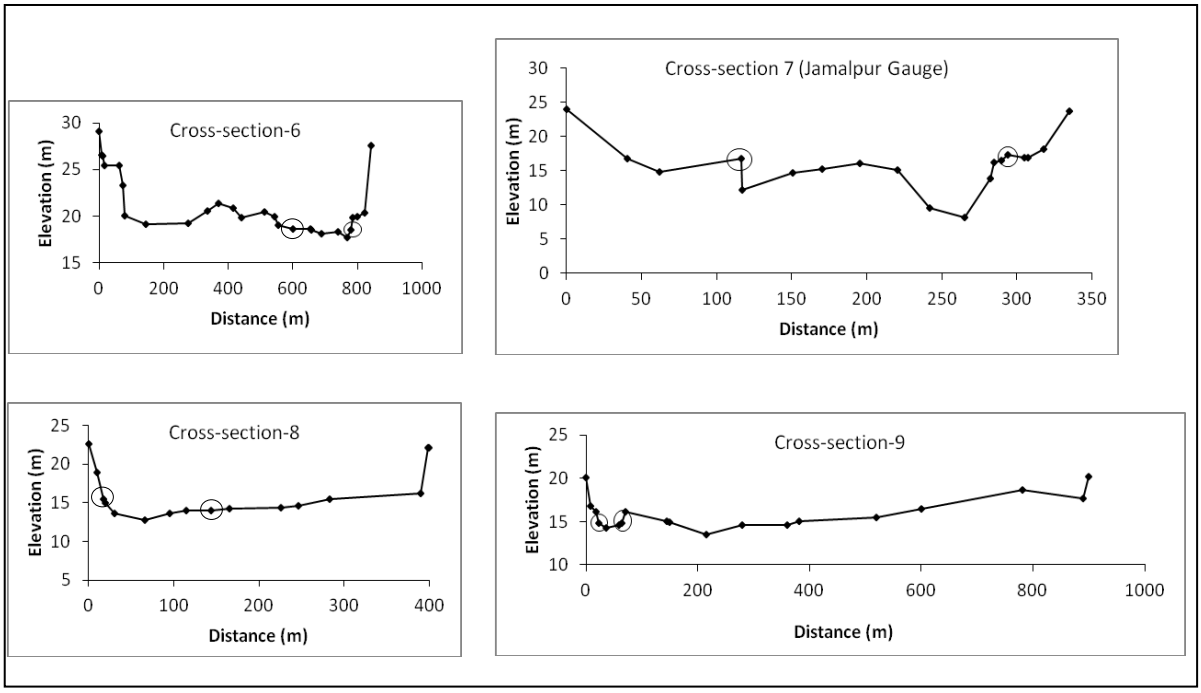

Figure 3.7 Surveyed cross-sections (6-9). Surveyed points that are marked with circles show the water level during the survey. A smaller horizontal scale was used for cross-sections 7 and 8 to properly depict the configuration of the channel in these two locations, where the channel is narrow and deep.

The bankfull channel width was estimated from high resolution images in GoogleEarth and the bed elevation was derived at each point by linearly interpolating between the surveyed elevations of the water surface along the longitudinal profile of the river (Figure 3.8a). As the channel component in the LISFLOOD-FP model is unable to handle a flow split or channel bifurcation in the 1D framework, routing the flood became less efficient near the river islands that are occasionally present in our study reach. Only the primary channel as identified from GoogleEarth was represented in 1D, and the secondary channels around islands were simply considered as part of the floodplain and handled by the 2D storage cell framework (Figure 3.9). The study reach was represented with 129 points which were carefully chosen to represent the varying width of the channel. There was no gauging station available at the downstream boundary of the study reach, and hence there were no data for imposing a water level at the model outlet. In order to minimise the effect of an uncertain downstream boundary condition, we artificially extended the channel vector for few hundred metres with an artificially steep slope. Our intention was to create an artificial

torrent at the downstream boundary and to use a fixed water surface elevation corresponding to very low flow as the downstream boundary condition for the model. The Manning's roughness coefficient (*n*) of the channel was taken as the calibration parameter. As the entire study reach is characterised by a relatively uniform sand based channel bed, a global *n* value for the channel was used for the calibration runs. Initial estimates for the channel *n* values were taken from Chow (1959). It is well known that LISFLOOD-FP is less sensitive to the floodplain roughness coefficient and this was kept at 0.035 which is the normal value for farmlands given by Chow (1959).

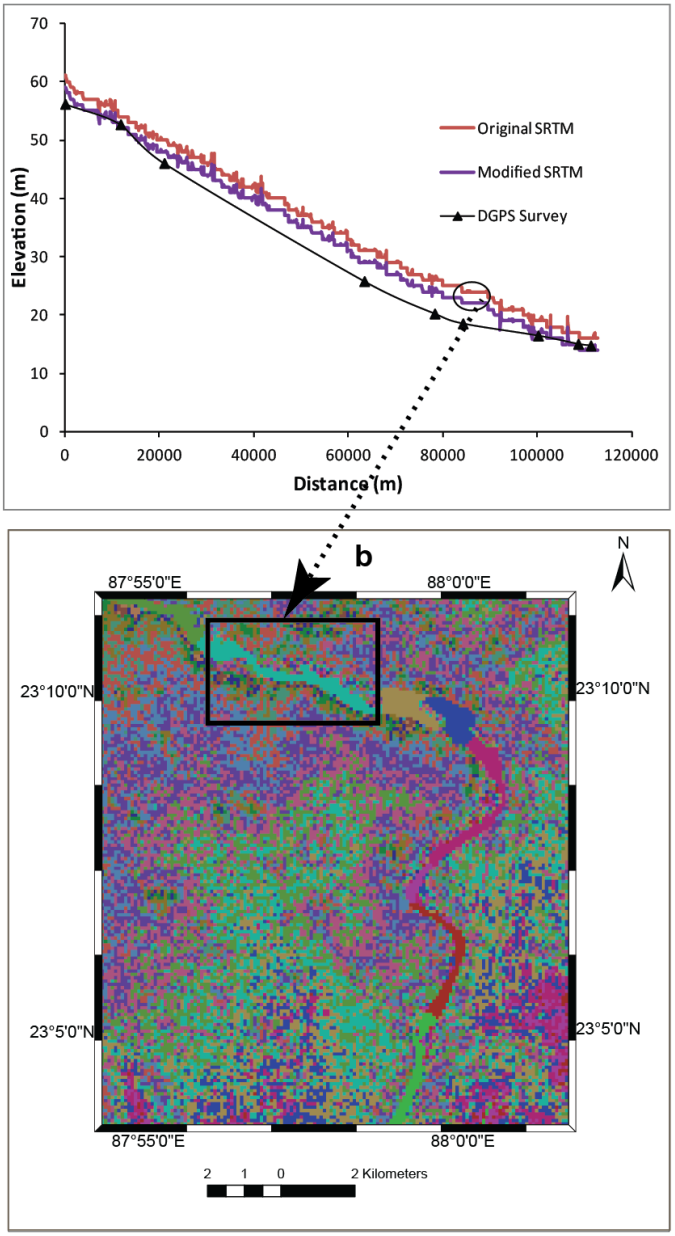

Figure 3.8 Long profile of the study reach. a, comparison between the profiles derived from the original SRTM DEM, modified DEM and field survey. The slopes of the surveyed profile at the extreme upstream and downstream of the study reach are distinctly different from those derived from the SRTM DEM or its modified form . b, example of the extensive flat surface in the channel portion of the original SRTM DEM. Unique elevation values are represented in unique colours to show homogeneous values over the channel, depicting spurious flat surfaces.

Figure 3.9 Representation of an island in the Damodar River within LISFLOOD-FP. Red arrows show the 1D configuration of the main channel. The shallower secondary channel and the floodplain, depicted with shading, are handled by the 2D component of the model.

A high magnitude flood event of September, 2007 was used to calibrate the model and validation was performed with the extreme event of September, 2009. The diffusive wave formulation for the 1D channel component was used, as Trigg et al (2009) reported that this method is suitable for subcritical flow for channels with shallow bed slope and is able to capture downstream propagation of flood waves along with the response of flow to free surface slope. The model performance was measured using hourly river stage data at the Jamalpur gauging station. Various efficiency criteria have been used in hydrology to quantify how accurately observed records are reproduced by numerical simulations. These measures include but are not limited to the Nash-Sutcliffe efficiency (E), the coefficient of determination (r^2), and the index of agreement (d). In this study, the index of agreement (d) proposed by Wilmot (1984) was used for judging the efficiency of the LISFLOOD-FP model. Here, d is defined as

$$d = 1 - \frac{\sum_1^n (O_i - P_i)^2}{\sum_1^n (|P_i - \bar{O}| + |O_i - \bar{O}|)^2} \quad (1)$$

where O_i and P_i are observed and modelled data respectively, $\bar{O}$ is the mean of the observed series, n is the number of observations in the time series and i is the number of data points. Legates and McCabe (1999) argued that d is a better performance measure than E and r^2 because it is more sensitive to the differences in the modelled and observed means and variances.

3.4.4 Quantifying uncertainty

Use of sparse data inputs inevitably increases the degree of uncertainties in the model output. When we are dealing with a disaster warning model, a quantitative estimate of the uncertainty is an essential prerequisite for this kind of system before they qualify for the forecasting of a severe natural hazard. In this paper, the uncertainty of our model predictions was quantified in generalised likelihood uncertainty estimation (GLUE) framework as proposed by Beven and Binley (1992). Uncertainty estimation of LISFLOOD-FP within a GLUE framework has been previously carried out by using synthetic aperture radar images of the extent of flooding as the observed data (Aronica et al. 2002; Hall et al. 2005; Stephens et al. 2012). However, utilising observed stage records for analysing uncertainty of LISFLOOD-FP output is relatively rare (see Hunter et al. 2005 for an exception).

In the GLUE framework, a set of behavioural models, that is, a set of inputs and model parameters that reasonably replicate an observed phenomenon, are weighted according to a likelihood measure. The likelihood measure is commonly an objective function that reflects the performance of each set of models during calibration (Beven 2010). Beven (2001) pointed out that a number of decisions, some of which are subjective, have to be made for implementing the GLUE methodology in order to obtain an uncertainty estimation for a hydrological model. These decisions include the range of uncertain parameters, a sampling method for drawing the parameters from the chosen range, an

appropriate likelihood measure, and classification of a model as non-behavioural based on the chosen measure. We identified four types of uncertain inputs in our study: 1) the Manning's roughness coefficient (*n*) for the channel, 2) the fixed water level at the downstream boundary of the model, 3) the channel width and 4) error in the modified SRTM DEM. In the absence of any information to the contrary, we assumed that the uncertainty is uniformly distributed for all four input types. The values of *n* were decided from preliminary calibration of the 2007 flood event with observed river stages at Jamalpur gauging station, and were set to be from 0.020 to 0.030. The range of the somewhat arbitrary fixed water level at the downstream boundary was chosen to be between 12.25 to 14 m. The low end of this range was set to be just greater than the bed elevation of the last point of the river vector, 12.20 m, to ensure that at the initial state the entire study reach remained wet. This measure provided some degree of stability to the model in the initial spin-up period. The high end estimate of 14 m was chosen because this is the water surface elevation during very low flow conditions, as were sampled in our survey. Any higher value of fixed water surface elevation at the outlet would function as a wall and artificially impede efficient drainage of water from the model domain. Channel width was derived from high resolution Geoeye-1 imagery (1 m spatial resolution) available in GoogleEarth. At the majority of points along the channel vector, the river bank was clearly distinguishable from the channel by the permanent vegetation line and it was decided that the maximum possible error in measuring the channel width would not be more than ± 20 m. However, we identified 8 points in the channel vector where clear demarcation of the river banks were difficult due to the absence of a clear vegetation line, evidence of channel shifting, or agricultural practice on the channel bed. After careful consideration the channel width at each of these points was allowed to vary in a random fashion. The amount of this variation depended on the degree of uncertainty present in the measurement of bankfull width from GoogleEarth at each of the 8 identified locations and ranges from ± 80 m to ±150 m.

Finally, the range of error for the modified SRTM DEM was determined from a semivariogram model of error distribution (Figure 3.10). The error was computed by

subtracting the SOI spot heights from the modified SRTM DEM. Some of the SOI spot heights that were located at the periphery of the model domain or over very high ground, not likely to be inundated in any flood event, were omitted from the semivariance calculation. A lag of 1000 m, which was very close to the average nearest neighbour distance, and a total of 30 lags were used. The range of the semivariogram of error (Figure 3.10) revealed that the error is spatially autocorrelated for a distance of ~ 3000 m. An unconditional Gaussian Sequential Simulation (GSS) was performed with the derived semivariogram of error using the Geostatistical Analyst extension of ArcGIS 10.0 to produce 3000 realisations of error surfaces for the entire model domain. These error surfaces were added with the modified SRTM DEM to produce the input for the uncertainty analysis. Comparison between semivariograms for the DEM before (Figure 3.11a) and after the addition of error surface (Figure 3.11b) did not reveal any significant change in the spatial autocorrelation pattern of the elevation values. However, for similar lag values the DEM with added error component showed a slight increase in the semivariance values compared to the modified SRTM DEM.

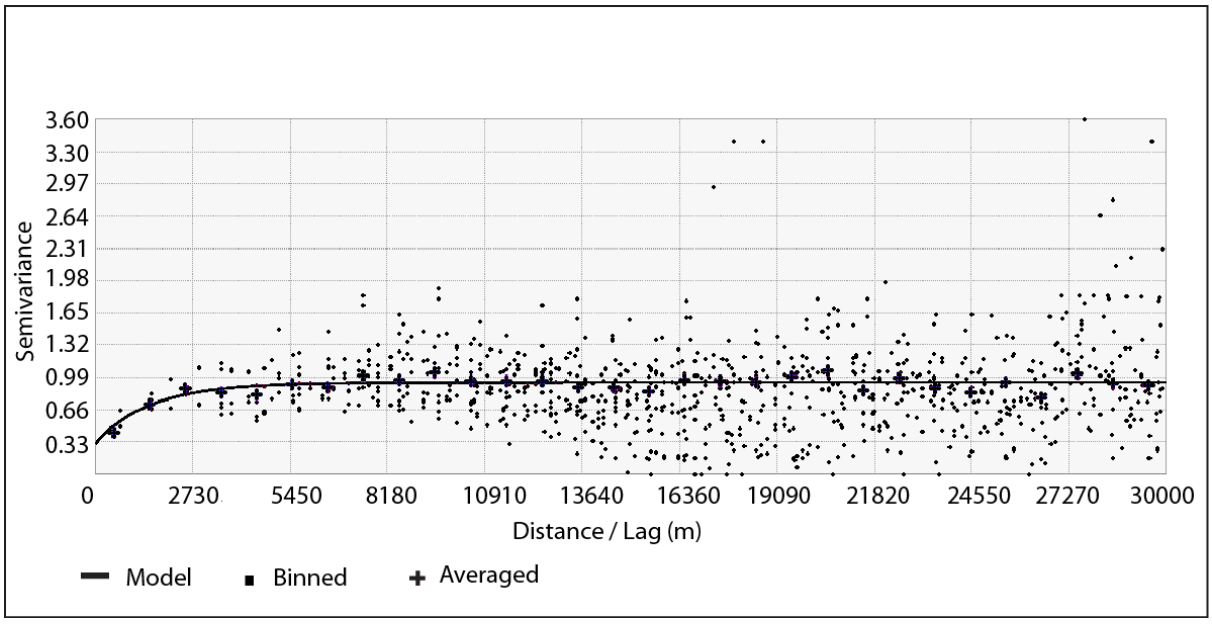

Figure 3.10 Semivariogram model derived from the error of the modified SRTM DEM measured at the location of available spot heights from Survey of India topographic maps.

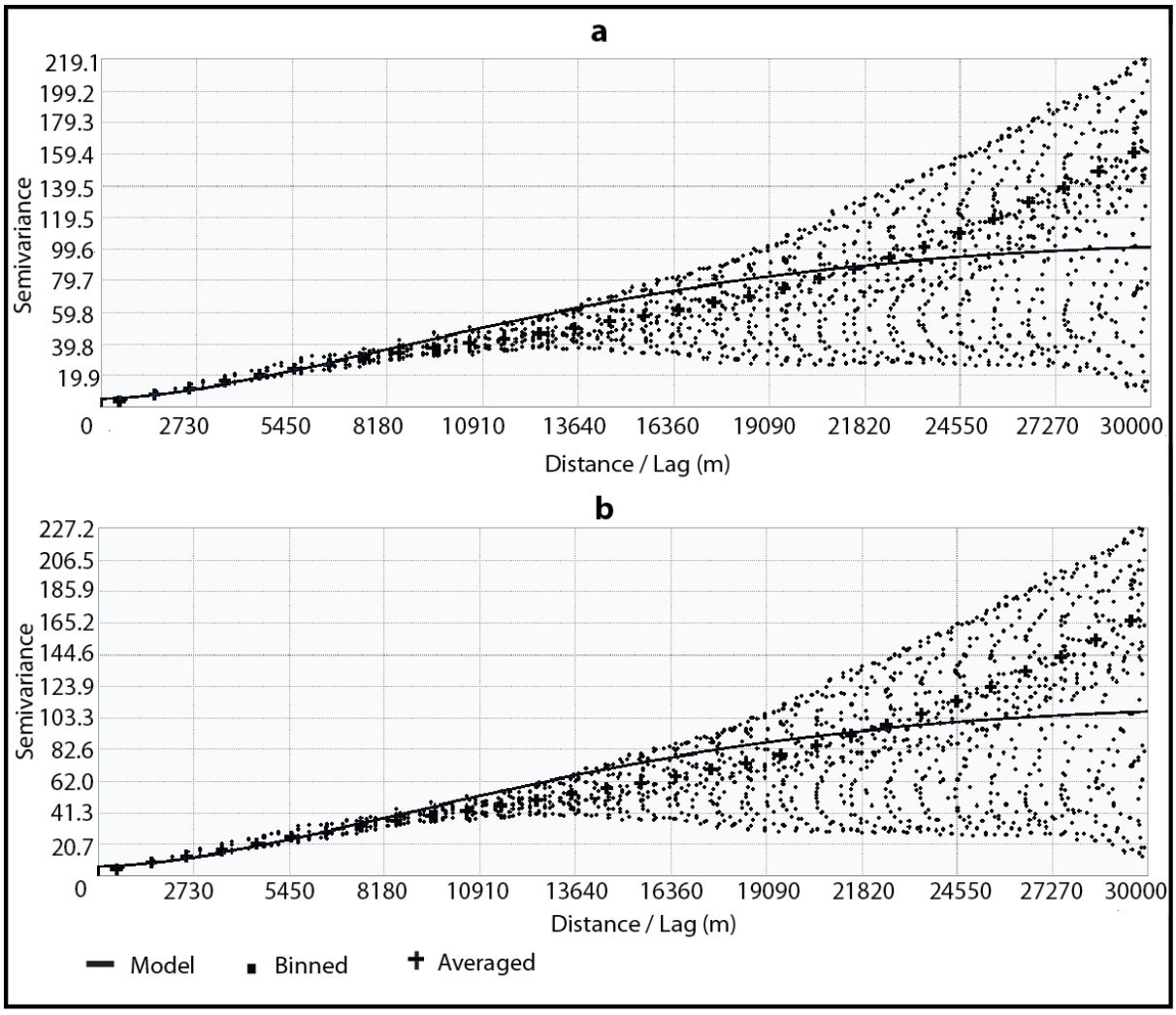

Figure 3.11 Semivariograms of the input DEMs for LISFLOOD-FP model. a, semivariogram of the modified SRTM DEM. b, semivariogram of a DEM where the error surface derived from Gaussian Sequential Simulation was added with the modified SRTM data.

The index of agreement (d) was selected as the objective function for computing the likelihood weights. The values of d range from 0 to 1 and increases monotonically with better model performance, and hence is appropriate for use as a likelihood measure in the GLUE environment.

The GLUE methodology was implemented in the following steps:

1) The LISFLOOD-FP model was run 3000 times with randomly chosen values for *n*, river stage at the model outlet and variation in the terrain as described above, following a Monte Carlo approach.

2) The values of d were computed for all model runs by comparing the modelled stage output at the Jamalpur gauging station with the observed record. After consulting the model sensitivity graph (Figure 3.12) a d value of 0.75 was used as the cut-off to distinguish between behavioural and non-behavioural models. According to this criterion 1918 out of 3000 runs qualified as behavioural models.

3) The d values were rescaled using the following formula so that the models with higher performance are assigned very high likelihood weight:

$$L_i = d_i - \text{Min}(d) / \text{Max}(d) - \text{Min}(d) \quad (3)$$

where L_i is the likelihood measure of realization i, d_i is the d value for realization i and Max (d) and Min (d) are the maximum and minimum value of the computed index of agreement for the 1918 behavioural model runs.

4) Each of these L_i values was divided by the sum of all 1918 computed L values so that the series adds up to 1. The resulting series constituted the final likelihood weights.

5) For each time step, the modelled stage values at the Jamalpur gauging station were put together with their final likelihood weights and sorted in ascending order according to the simulated stage values. Then, the cumulative sum of the likelihood weights was computed and upper and lower 95 % uncertainty bounds were obtained by deriving the stages that corresponds to the 5^{th} and 95^{th} percentiles of the cumulative likelihoods. This process was repeated for each 1-hour time step for which the observed data was available. The entire process was automated using MATLAB. We used the readstage.m code (Wilson, 2012) in order to read the stage outputs of the LISFLOOD-FP model.

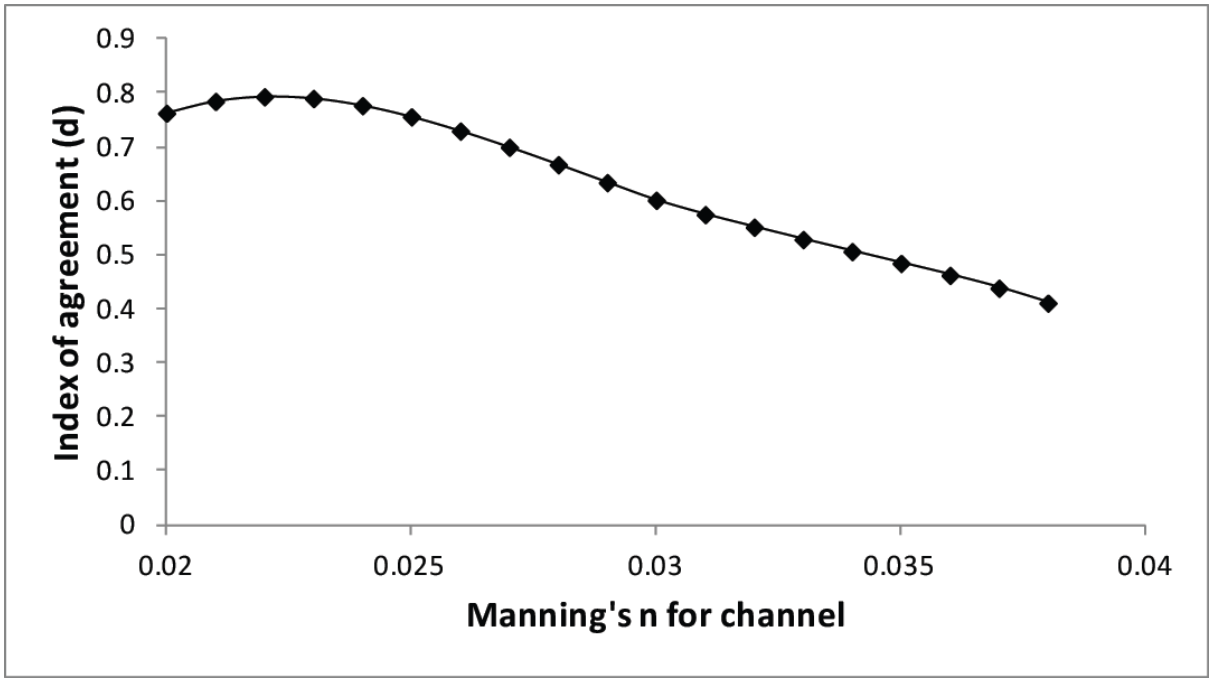

Figure 3.12 Performance of LISFLOOD-FP with different channel roughness coefficients during calibration with the 2007 flood event. The performance of the model peaked at a channel Manning's *n* of 0.022 but declined with further reduction in roughness.

3.5 Results

3.5.1 Flood routing

We took the channel Manning's *n* as the calibration parameter. Figure 3.12 shows how the model performance steadily declined with increasing values of *n*. The model performed best at a relatively low *n* value of 0.022. The best calibrated result for the 2007 flood event, with a channel *n* value of 0.022 and an index of agreement (d) of 0.79, is shown in Figure 3.13. The September 2009 flood event was then simulated in a similar model setup using the calibrated channel *n* value of 0.022, yielding a d value of 0.77 (Figure 3.14) .

Variability of the discharge at the model downstream boundary for the 3000 MonteCarlo simulations is shown against the figures from the best calibrated output for the 2007 event

in Figure 3.15. There is some attenuation in the flood hydrograph over the 110 km study reach (see Figure 3.2a). We did not have any measured discharge data at the model downstream boundary.

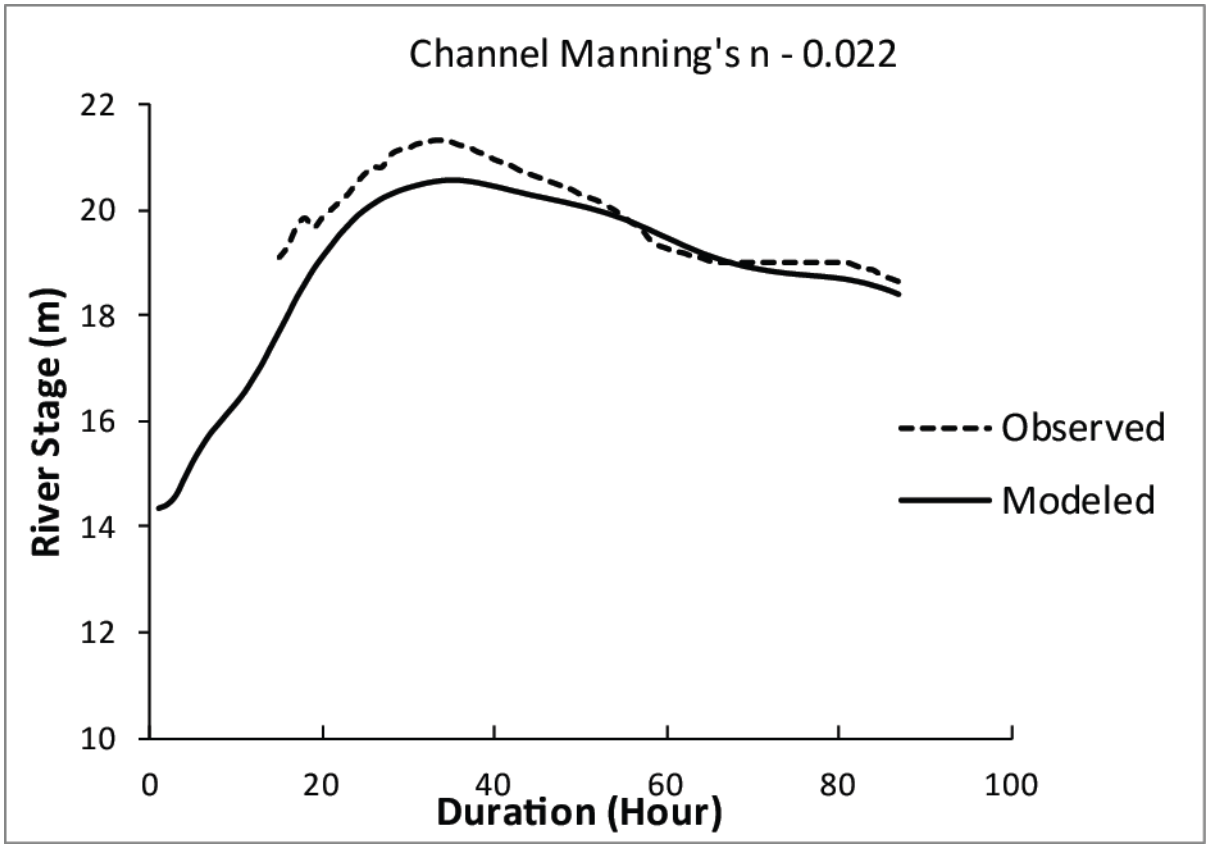

Figure 3.13 Best calibrated output of modelled stages from LISFLOOD-FP at Jamalpur gauging station for a global channel Manning's *n* of 0.022.

Assuming a similar pattern of difference between the modelled and observed records as found in the case of river stage at Jamalpur gauge (Figure 3.13), situated ~20 km upstream of the model downstream boundary, we realise that the best calibrated simulation of the outflow discharge at the model downstream boundary is likely to underestimate the actual discharge consistently. Level of this underestimation is expected to be more pronounced during the rising limb of the flood while during the descending limb the simulated figures possibly lie just below the actual ones. The 3rd quartile of all simulated flow at each time

step was found to be very close to the rising limb of the best calibrated hydrograph. It indicates that during the rising limb of the hydrograph majority of the simulation runs could not produce a pattern of outflow discharge that is even close to the best calibrated level which is likely to be quite lower than the actual. However, we find that the descending limb of the best calibrated outflow discharge curve lies slightly below the median of the simulated figures at each time step. It illustrates that a substantial portion of the MonteCarlo simulations performed comparatively well after the flood peak was attained.

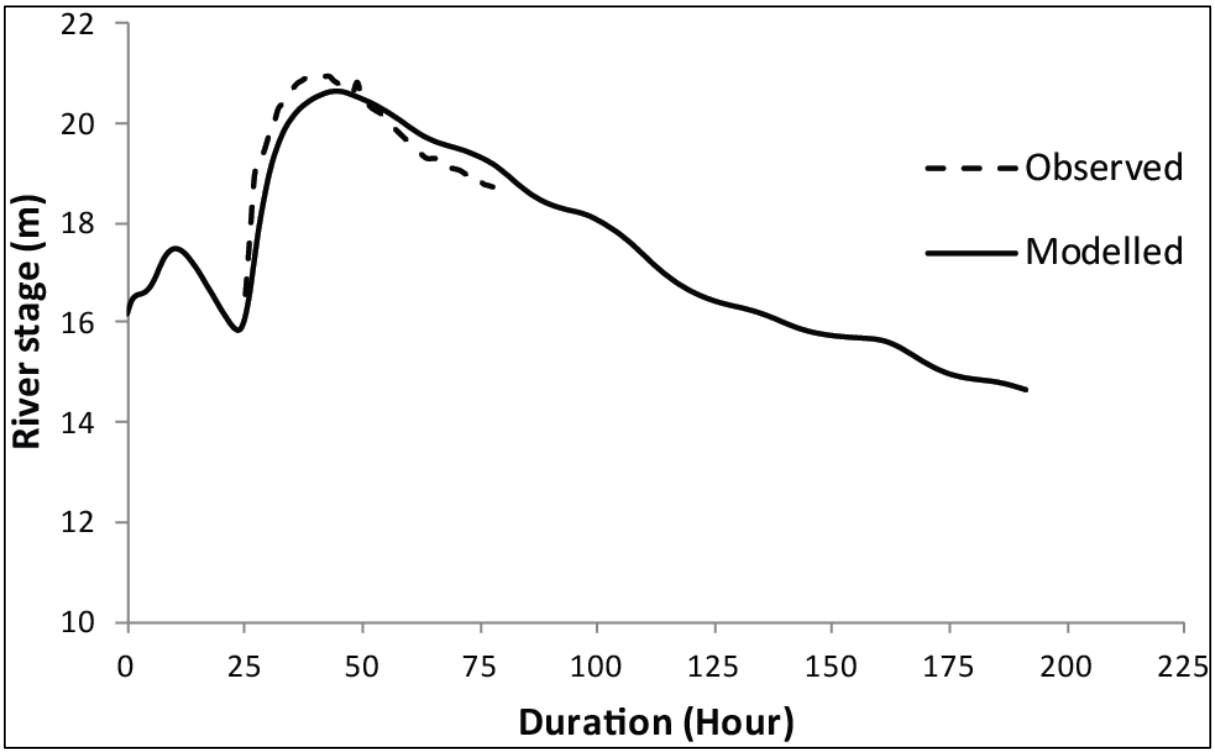

Figure 3.14 Validation of the LISFLOOD-FP model using the modelled and observed stage data at Jamalpur gauging station for the 2009 extreme flood event. The calibrated value of *n* as 0.022 was used for the channel.

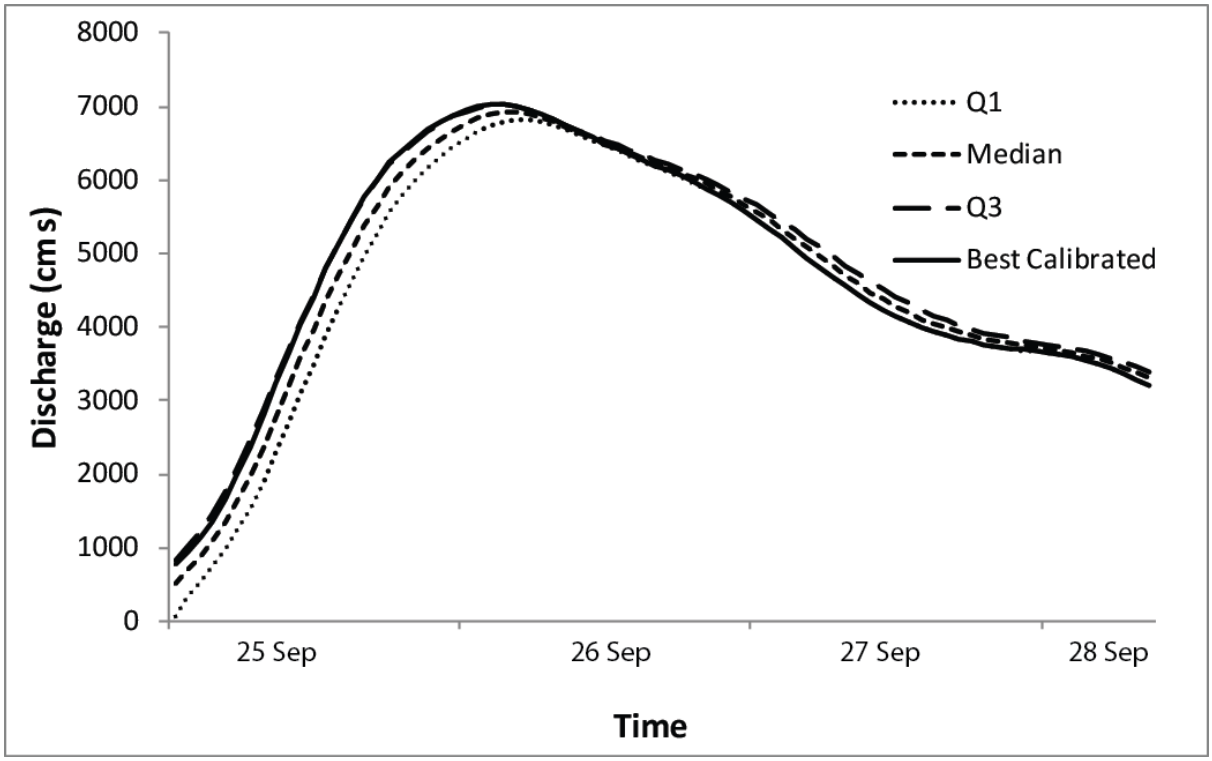

Figure 3.15 Variability of the predicted discharge hydrograph at the model downstream boundary for 3000 MonteCarlo simulation. Variability of the modelled figures at each time step is shown by 1st quartile, median and 3rd quartile figures of 3000 results. The modelled output from the best calibrated case is presented as a benchmark of accuracy.

3.5.2 Uncertainty estimates

The dotty plots in Figure 3.16 are scatter diagrams of each of the uncertain model inputs against their corresponding d values. For each individual parameter dimension the dotty plot represents a projection of sample points onto the goodness of fit response surface (Beven, 2001). Each dot represents an output of one of the Monte Carlo model runs. Figure 3.16a shows that the model was very sensitive to the channel roughness coefficient, but the variation in fixed water level at the downstream boundary has very little effect on the model performance (Figure 3.16b). Similarly, variations in channel width had no significant influence on model performance, even for sites at which the exact channel width was quite uncertain (Figure 3.16c). Similar plots constructed at various other points

where the channel width was allowed to vary for > 80 m showed comparable results and are not included here. We would also like to point out that the indices of agreement of the highest performing models are higher than what was achieved during the calibration stage. The uncertainty plot of the modelled river stages at the Jamalpur gauging station (Figure 3.17) reveals that a substantial portion of the observed flood stages are within 95% lower and upper uncertainty bounds for the 2007 event. However, Figure. 17 also illustrates the inability of LISFLOOD-FP to accurately predict the rising limb of the flood hydrograph, and there is consistent underestimation of the water level.

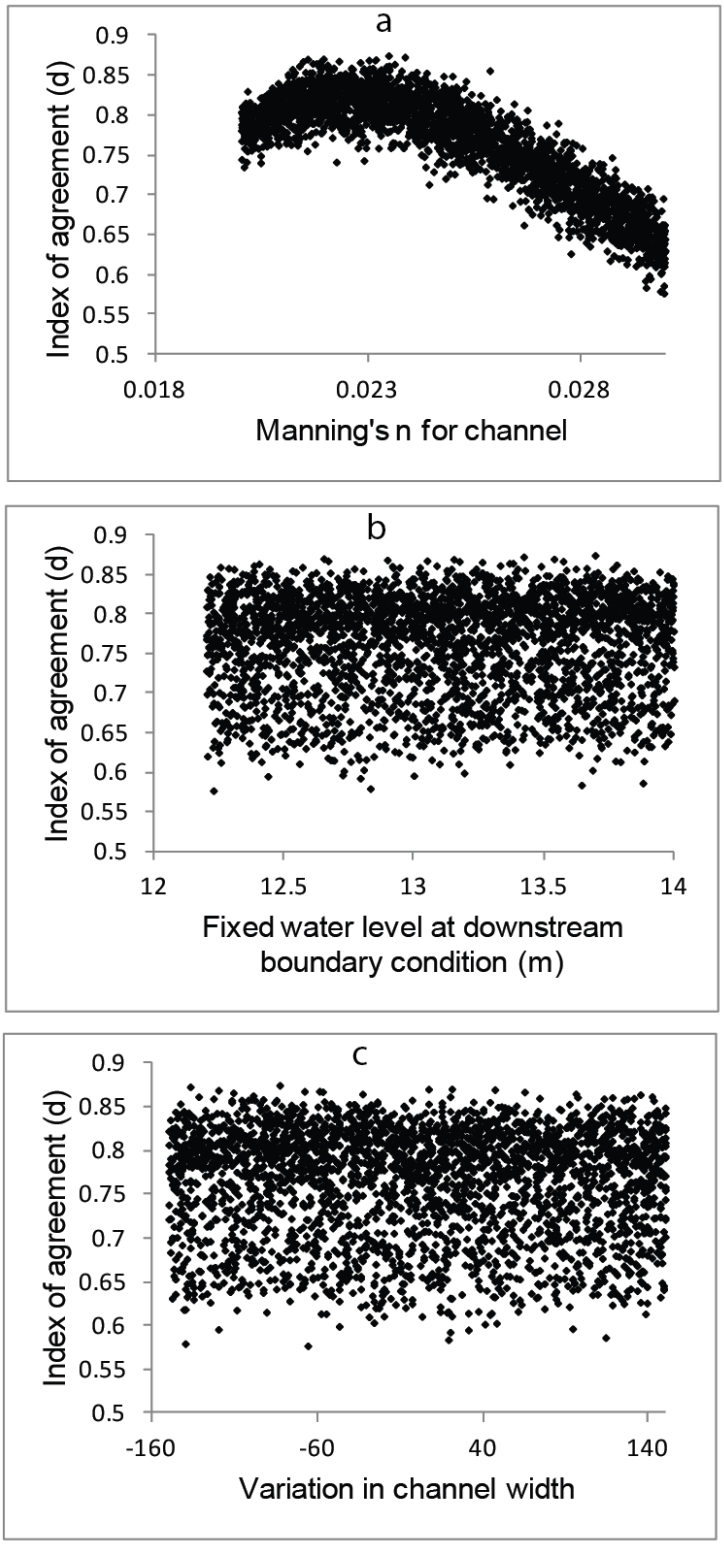

Figure 3.16 Dotty plots showing the sensitivity of the model to variations in (a) the channel roughness coefficient, (b) the imposed arbitrary water level at the downstream boundary for the 2007 flood event and (c) channel width at a particular point in the channel vector.

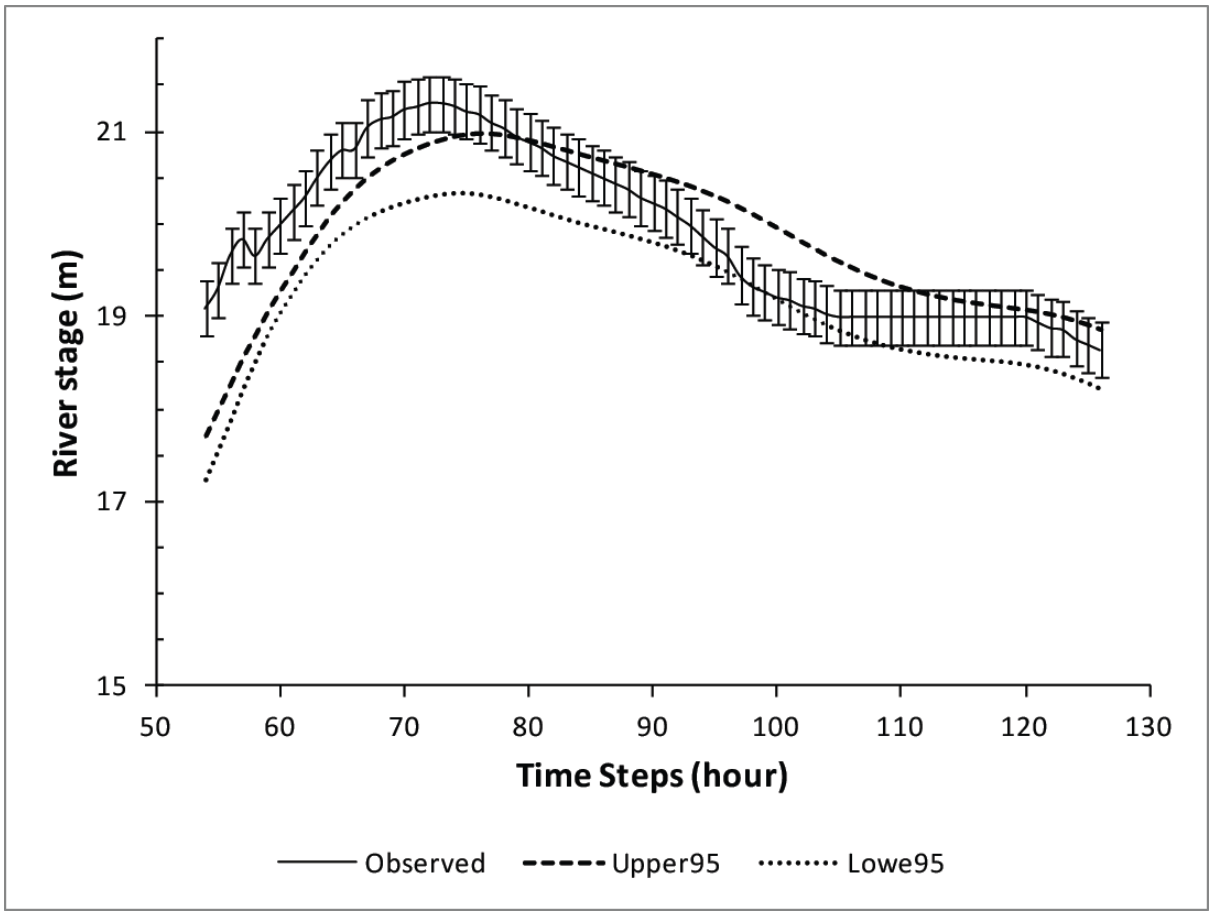

Figure 3.17 Uncertainty plot of the LISFLOOD-FP model of the 2007 flood event showing 95 percent upper and lower uncertainty bounds. Uncertainty in the observed river stages is shown by a ± 20 cm vertical error bar.

3.6 Discussion

3.6.1 The terrain data

The SRTM DEM for the channel in our study area is characterised by extensive stretches of flat terrain and steps along the longitudinal profile of the river (Figure. 3.8). In order to find out the cause of this problem, the Version 4 SRTM DEM, used in our study, was compared with the 'Unfilled Finished A' version of the data (downloaded from Global Land Cover Facility Website: http://glcf.umiacs.umd.edu), especially for the channel of the Damodar River. It was found that the two datasets are almost identical except for the existence of a very few isolated bad data pixels in the 'Unfilled Finished A' product which were probably replaced by interpolation from neighbouring pixels in Version 4. This finding confirmed that no supplementary DEM such as ASTER GDEM was used for the channel portion in the Version 4 of the SRTM DEM, because no such data were used in the creation of 'Unfilled Finished A' product. However, when the Version 4 product was compared with the 'Unfinished A' product we found that the unfinished product did not have the same flat surfaces over the channel, but instead the channel was characterised by an unrealistic noisy surface. The unfinished product thus provides a worse representation of the channel long and cross-profiles as compared to Version 4 of the data. The flat surfaces in the 'Unfilled Finished A' and subsequently in the Version 4 products were probably created during the generation of the 'Unfilled Finished A' product as Slater et al. (2006) pointed out that one of the finishing requirements for this product was to monotonically step down the elevation of rivers with more than 183 m width.

After lowering the SRTM DEM by 2 m to reduce the error we found that there was considerable mismatch between the bed slopes of the longitudinal profile derived from the SRTM DEM and those obtained by the ground survey (Figure. 8a). These factors likely contributed to the failure of our preliminary attempt with HEC-RAS that was based on cross-sections derived from the SRTM DEM. Unlike Patro et al. (2009a) we did not have access to surveyed embankment heights, because no such comprehensive record exists for

the lower Damodar Basin. The availability of accurate bank or embankment heights can be a decisive factor for maintaining model stability at extreme flow conditions in 1D hydrodynamic models, as this information is crucial for containing the water within the channel. A ground survey along the longitudinal profile of the study reach was also essential for employing LISFLOOD-FP because the channel bed elevation derived from the SRTM DEM would have yielded an inaccurate energy gradient for the river. In particular, the presence of high frequency noise in the channel portion of the SRTM DEM (Figure 8a) would interrupt the monotonic slope of the LISFLOOD-FP channel vector. The simple formulation and data requirement of the LISFLOOD-FP model enabled us to take full advantage of limited ground surveys to overcome the shortcomings of the SRTM DEM.

3.6.2 Flood routing model

The high performance of LISFLOOD-FP with very low values of Manning's *n* is consistent with the wide, deep channel in the study area. The average channel width of the study reach is ~1 km and average bankfull depth is more than 12 m, meaning that channel roughness has very limited influence over the flow pattern as only a small fraction of the flowing water is subjected to frictional drag of the channel bed and banks. The model consistently underestimated the rising limb of the observed stage hydrograph and shows some degree of error, particularly in the validation case, in simulating the receding level of flood water. Underestimation of the modelled stage hydrograph is not a serious concern because the 20 to 21 m river stage is well below the bankfull level at Jamalpur (cross-section 7 in Figure. 3.6). The error in river stage (0.5 to 1 m at the peak) is not more than 5 percent of the bankfull channel depth of approximately 24 m at Jamalpur. Slight underestimation of the rising limb may be explained by the fact that we have not considered the amount of rainfall received directly by the reach and its immediate surrounding that is directly fed into the channel of the Damodar River. Overestimation of the falling limb of a flood hydrograph is also expected as the terrain data are not

sufficiently accurate to represent smaller conduits and depressions through which the floodwater escapes after the peak flow. Slight underestimation of the supply of water in the channel also explains the slight delay in the simulated flood peak, because additional water would have increased the flood wave velocity by reducing the influence of frictional drag. Finally, we were able to obtain reasonable results despite not incorporating the inline structure and two bridges that occur in the study reach. These structures thus appear to have had a very limited influence in altering the flow pattern, probably due to the extreme nature of the modelled flow regimes. In this respect, the finding of this paper is encouraging for developing countries, as limited but reasonably accurate data appear to be sufficient for routing extreme floods using freely available and computationally less demanding models. However, such coarse inputs and simple models may not be appropriate for routing the normal or low flows of a river.

3.6.3 Uncertainty analysis

Although the overall trend in the performance of the model for the MonteCarlo runs (Figure 16a) broadly followed the sensitivity graph of the channel *n* values (Figure 12), the wide range of variation in the performance measure for each channel *n* value is probably due to the influence of DEM uncertainty, especially in terms of bank heights that determine the exchange of water between the 1D channel component and the 2D floodplain component. The variation in model performance for different stages at the downstream boundary and channel width values was probably a result of variations in other factors, particularly the channel friction and input DEMs.

Unlike Hunter et al. (2005) we have not used multiple channel roughness coefficients for different sub-reaches, as we did not have observed stage records at any intermediate points to evaluate the sensitivity of *n* for a specific sub-reach. The narrow range of the uncertainty lines in Figure. 3.17 is also encouraging for our confidence in the modelled output. As mentioned in Section 3 the difference in the vertical datum of the SOI and the EGM96

geoid based measurements leads to a certain degree of mismatch in elevation values which varies from place to place. The Jamalpur gauging station uses the SOI elevation while our model used the WGS84 and EGM96 to derive the orthometric heights which were used as an equivalent of the elevation from the mean sea level (MSL). This uncertainty in the measurements of river stages is represented by the ± 20 cm error bars in Figure. 3.17. The approximate error limit was derived by comparing the GPS-EGM96 heights at 2 points with known SOI elevations near Jamalpur. The SOI vertical datum is derived from a network of tidal gauges and there is no satisfactory geoid model available for India to accurately derive the orthometric heights from GPS (Agrawal 2005). In contrast, most freely available geospatial data such as the SRTM DEM use a global datum. Mismatch of local and global datum is quite common and the absence of robust local geoid models in many developing countries poses a challenge for using global data in applications like flood modelling where sub-metre accuracy is essential.

3.7 Conclusion

The intention of this study is to explore a low-cost methodology for predicting the dynamics of hazardous flood events. We found that a simple model (LISFLOOD-FP) combined with relatively coarse terrain and hydrologic inputs can perform this task with reasonable accuracy, with an index of agreement d of 0.77 with observed river stage time series. We have demonstrated that limited but well-designed field surveys can supplement freely-available moderate resolution DEMs for the purpose of hydraulic routing of extreme floods. We have also pointed out typical obstacles that are encountered in the developing world for hydrodynamic modelling such as the dearth of accurate terrain data, shortage of river gauging stations, absence of permanent GPS base station data in the public domain, and the lack of well-defined local geoid models, and suggested some techniques to overcome them. The limitations arising from the use of coarse hydrologic and terrain inputs may not be very significant when we are interested in routing bankfull discharge but can be quite critical for modelling normal to low flow. Our study also provides an alternative to purely cross-section based 1D hydraulic routing of floods, particularly for

river reaches where the quality of the SRTM DEM is not good enough to extract accurate cross-sections. The assessment of uncertainty that arose due to the use of sparse inputs illustrated that a significant portion of the observed records were within a narrow range of uncertainty bounds and boosts our confidence that the current setup can be employed in flood management practice in developing countries.

Chapter 4

Low-cost open access flood inundation modelling at reach scale with sparse data in the lower Damodar river basin, India.

Abstract

The the data unavailability is the main reason for limited applications of hydrodynamic models for predicting inundation in the developing world. Generation of these data sets is often cost-prohibitive in the context of the developing countries. This paper aims to generate moderately high resolution hybrid terrain data by merging height information from various sources, such as low-cost Indian Remote Sensing Satellite (IRS) Cartosat-1 stereo satellite images, freely available SRTM DEM data and limited surveyed channel cross sections for inundation modelling in a reach scale. The study reach is characterised with anabranching channels that is associated with a number of channel bifurcation, loops and river islands. We compared the performance of a simple 1D-2D coupled LISFLOOD-FP model and a complex fully 2D finite element TELEMAC2D with the hybrid terrain data. This experiment tests how a reduced complexity approach-based model like LISFLOOD-FP fares with a more physically realistic TELEMAC2D when simulating inundation in a complex fluvial environment without access to very high resolution DEMs. Results show that TELEMAC2D produced significantly improved simulated inundation with the hybrid terrain data as compared to the SRTM DEM. LISFLOOD-FP was found unsuitable to work with the hybrid DEM in a channel system with multiple flow split as it failed to efficiently divert water in the branches from the main channel.

Keywords: Inundation model, Limited Data, Developing Countries, TELEMAC2D, LISFLOOD-FP, DEM, Cartosat-1.

4.1 Introduction

The EM-DAT database maintained by the Office of US Foreign Disaster Assistance and the Centre for Research on the Epidemiology of Disasters (OFDA/CRED) reveals that more than 80 percent (3151 out of 3927) of major reported floods between 1900 and 2012 occurred in Asia, Africa and Latin America. Heavy rain, monsoon rain and tropical cyclones were reported as the causative factors for 64 %, 11 % and 6 % floods respectively between 1998 and 2008 (Adhikari et al., 2010). High incidence of these types of extreme meteorological events in the low latitudes is responsible for the higher rate of flooding incidences in the global south. In developing economies the cost of a post-flood partial or full economic recovery in relation to GDP is very high thus making the impact of these disasters more pronounced (Alcantara-Ayala, 2002). Hence, these large flood-prone regions urgently require an affordable mechanism for predicting inundation in order to devise early warning systems and design flood defences. However, the applicability of modern hydrodynamic or flood inundation models is often limited outside the industrialised nations due to lack of available data (Sanyal and Lu, 2004). Hydrodynamic models commonly in use for flood management typically require three types of data: 1) high resolution topographic data and surveyed elevations for defining the model geometry; 2) water discharge or stage data at the inlet and outlet of the reach of interest as model boundary conditions; (3) radar images for calibration and validation of model results. Digital elevation models derived from LiDAR survey are typically used as the source of terrain data (Bates et al., 2003) while differential GPS is used for accurate river cross-section survey (Wilson and Atkinson, 2005). Water discharge and stage data are generally required in high temporal resolution of 1 hour or less to feed into the models (Hunter et al., 2005). Spaceborne radar imaging platforms such as ENVISAT (Shumann et al., 2007) as well as airborne synthetic aperture radar (ASAR) (Bates et al., 2006) are commonly utilised as sources for obtaining observed flood extents.

All the data mentioned above are either scarce or non-existent in many developing countries and can only be obtained over broad areas at a high cost in resources and infrastructure. The topography of the river channel and floodplain is the most important input in any hydraulic model (Nicholas and Walling, 1997). In particular, the details

and accuracy of the representation of the channel geometry is a very significant determinant of model performance (French and Clifford 2000; Pappenberger et al, 2005). Horritt and Bates (2001a) pointed out that when predicted water surface is re-projected onto a DEM to delineate the actual wet area or the detailed shoreline, the accuracy increases steadily with the spatial resolution and vertical accuracy of the DEM. The drying process or draining of water from the floodplain with subsiding river stage is more efficient with fine resolution model although maximum inundated area is less sensitive to model grid size (Neal et al., 2011). Hence, accurate and high resolution terrain data is of utmost importance in inundation modelling. 2D hydrodynamic models require a continuous representation of the channel bed. In the majority of situations, a portion of the main channel remains under water and thus it is difficult to create a terrain model for the channel from LiDAR survey or photogrammery. Linear interpolation of the available surveyed cross-sections is not straightforward due to various facts including bends in the river, existence of channel islands not captured by a sufficient number of cross-sections and failure to capture the river thalweg (Merwade et al., 2008a). Conversion of the river coordinate system into a flow oriented coordinate system from the Cartesian one was found to increase the ability of anisotropic interpolation techniques (Merwade et al 2006). The density of the surveyed points holds the key for generating an accurate interpolation of the channel topography (Legleiter and Kyriakidis 2008). The time and cost of surveying closely packed cross-sections are considerable. Cross-section surveys become more difficult in areas with strong seasonal pattern of rainfall because the prevalence of very low flow during most of the year prevents the use of relatively inexpensive method of employing boat mounted sonar equipment for capturing the topography of the river bottom.

The SRTM DEM with a horizontal resolution of ~ 90 m is the best freely available terrain data covering the tropics where most of the developing countries are located. The SRTM DEM has been used with some success in recent years with 1D hydrodynamic codes like MIKE 11 to model flow in the Mahanadi River delta (Patro et al. 2009a; Patro et al. 2009b) and the Brahmani River basin (Pramanik et al. 2010) in India where the original DEM was modified using the spot height information derived from Survey of India topographic maps. As the X and C band radar pulses used for generating the SRTM DEM was not able to penetrate the dense canopy, the DEM contains patches of spuriously exaggerated elevation over a cluster of trees that actually

do not offer too much obstruction to flow. However, due to the coarse resolution of the SRTM DEM these features impede flow of water to a great extent in the modelling environment (Lehner et al., 2008). In order to overcome these problems, GIS-based processing of the SRTM DEM has been attempted to improve its performance in hydrodynamic modelling at regional scales. Wilson et al. (2007) degraded the SRTM DEM to 270 m resolution for an area in the Amazon Basin in order to minimize the effect of vegetation induced noise and reported a water surface RMSE of 0.99 m at high flow. Paiva et al. (2011) employed some generic rules of fluvial geomorphology in a GIS-based algorithm to derive simplified channel geometries from the SRTM DEM for 1D hydrodynamic modelling of a major tributary of the Amazon River. Yamazaki et al. (2012b) created an adjusted version of the SRTM DEM for a region of the Amazon basin by adding flow connectivity from external sources such as existing drainage maps while keeping the original elevation values almost unaltered and reported a 20 % improvement in the accuracy of predicted water extent vis-à-vis the original SRTM data. Nevertheless, the SRTM DEM has been primarily used for hydraulic modelling in the case of very large rivers such as the Amazon (da Paz et al., 2011), the Congo (Jung et al., 2010), the Niger (Neal et al., 2012a) and the Ob (Biancamaria et al., 2009). Consequently, the inaccuracies in modelled inundation extents arising from the use of a coarse DEM appear to be reasonable as a proportion of the total flooded area. Casas et al. (2006) pointed out that when using a coarse terrain input the inaccuracy in the model output decreases with increased discharge and the model becomes less sensitive to the quality of the terrain data when simulating extreme events.

The majority of the floods occurs in rivers that are much smaller in carrying capacity and peak discharge than the Amazon or its major tributaries but still affect the lives and properties of the communities seriously. Degrading the resolution of the SRTM DEM may reduce the noise, but such a coarse resolution DEM does not have much value in modelling inundation in medium size river basins with a width of < 500 m. The 90 m grid size of the SRTM DEM is not able to capture the variation in a river bed in such rivers. Narrow topographically discontinuous structures such as levees and roads that are normally not evident in the SRTM DEM (Sanders, 2007) may not make a significant impact on the accuracy of the modelled flood extent maps due to the massive scale of inundation in big rivers like the Amazon. However, for simulating

inundation in smaller rivers at the reach scale these finer topographic configurations may become important.

Recently, a few attempts have been made to model inundation at the reach scale without access to very high resolution topographic data. For example, Tarekegn et al., (2010) generated a DEM of 15 m resolution from ASTER images in the Ribb River in Ethiopia but recorded only a 30.5 % match between the simulated and observed flood extent. IRS Cartosat-1 stereo images were used by Sahardi et al (2012) to model flood extent in a mountainous region where the modelled flood extent was not very sensitive to the DEM inaccuracies. Studies that were conducted in the developing countries such as Iran (Sarhadi et al., 2012), Bangladesh (Masood and Takeuchi, 2012) or Thailand (Keokhumcheng et al., 2012) considered a designed flood event rather than an actual one and the simulation results were compared with the observed inundation maps of extreme events based on availability. This fact makes the evaluation of the performance of these models less rigorous. In addition, almost always the previous studies attempted to predict a flooding event having a continuous spatial pattern of inundation adjacent to the single channel under investigation. In these scenarios the debate is centred upon how accurately a model and the input DEM can simulate the fringe area or uncertainty zone of inundation (Merwade et al., 2008b) at a distance from the channel with certainty. However, in an anabranching channel with numerous distributaries the flood breakout zones can be in a different part of the main channel where smaller branches give rise to discrete pockets of waterlogged areas in the floodplain.

Considering the resource constraints of developing high resolution DEMs (typically available from LiDAR survey) for an entire basin, elevation data from different sources can be blended and merged for inundation modelling. Example of such endeavours were reported by Tate et al. (2002) and Shapiro and Nelson (2004) who created terrain data sets with higher density of elevation points at or near the channel and less resolution further away. Such attempts may enable us to concentrate limited resource of capturing topographic data in a manner that is suitable for hydraulic modelling.

A fully two dimensional (2D) inundation model like TELEMAC2D (Hervouet and Van Harn, 1996) is a robust tool for simulating extensive floodplain flow. Although the depth averaging mechanism of the 2D model results in lumping of some hydraulic

processes their ability to account for the variation in the hydraulic conditions within the channel and over the floodplain make them ideal in terms of the representation of hydraulic processes (Horrit, 2000). Cook and Merwade (2009) found that physically based more complex finite element codes were less sensitive to the resolution of terrain models and therefore is effective in containing the uncertainty in the model outcomes arising from the error in the terrain input. The factor of non-stationarity in the parameterisation of roughness coefficients arising from varying resistance and energy loss at different magnitudes of flow can be kept under control in fully 2D models (Horritt et al., 2007).

The issues of process representation and input data are also important with regards to the choice of the inundation model. Horritt and Bates (2001b) argued that if we lack the detailed data to parameterise a complex process representation with sufficient accuracy then it does not make sense to select a complex process which are inherently computationally demanding. Their study showed that a simple 1D-2D coupled storage cell model like the LISFLOOD-FP (Bates and DeRoo, 2000) can achieve similar high accuracy as the complex finite element fully 2D TELEMAC2D model in terms of the predicted flood extent and the authors concluded that with the increasing availability of very high resolution LiDAR DEMs the detailed representation of topography can supplement the weakness in process representation. However, the aforementioned study by Horritt and Bates (2001b) was conducted on a single reach. The low-lying alluvial plains and deltas around the world are particularly flood-prone and they are generally characterised by river bifurcation and anabranching channel pattern. It will be interesting to test whether 1D models like LISFLOOD-FP that has the advantage of the reduced complexity approach can perform equally well as the complex, fully 2D TELEMAC2D model in an intricate deltaic drainage system where no LiDAR-based high resolution terrain data is available.

In this paper we aim to address the challenges that arise due to general lack of necessary data for inundation modelling in the data-sparse developing world and present a methodology to deal with this situation in order to perform a reasonably accurate inundation modelling in a complex fluvial setting. The objectives of this paper are 1) to report a novel method for generating a hybrid terrain data from multi-source low-cost/free remotely sensed data and assess the improvement it can make over the

raw SRTM DEM in terms of the simulated inundation extent through fully 2D inundation modelling, 2) to test the ability of flood-inundation models with varying complexity: LISFLOOD-FP vs. TELEMAC2D to exploit the improved hybrid terrain data for increasing the accuracy of the simulated flood extent.

4.2 Study Area

A study area in India was selected for this paper as India is a good example of the general issue of widespread flooding (Mohapatra and Singh, 2003) and lack of data for developing prediction tools. The particular study site is located in the basin of the Mundeswari River which is one of the major distributaries of the Damodar River (Figure 4.1).

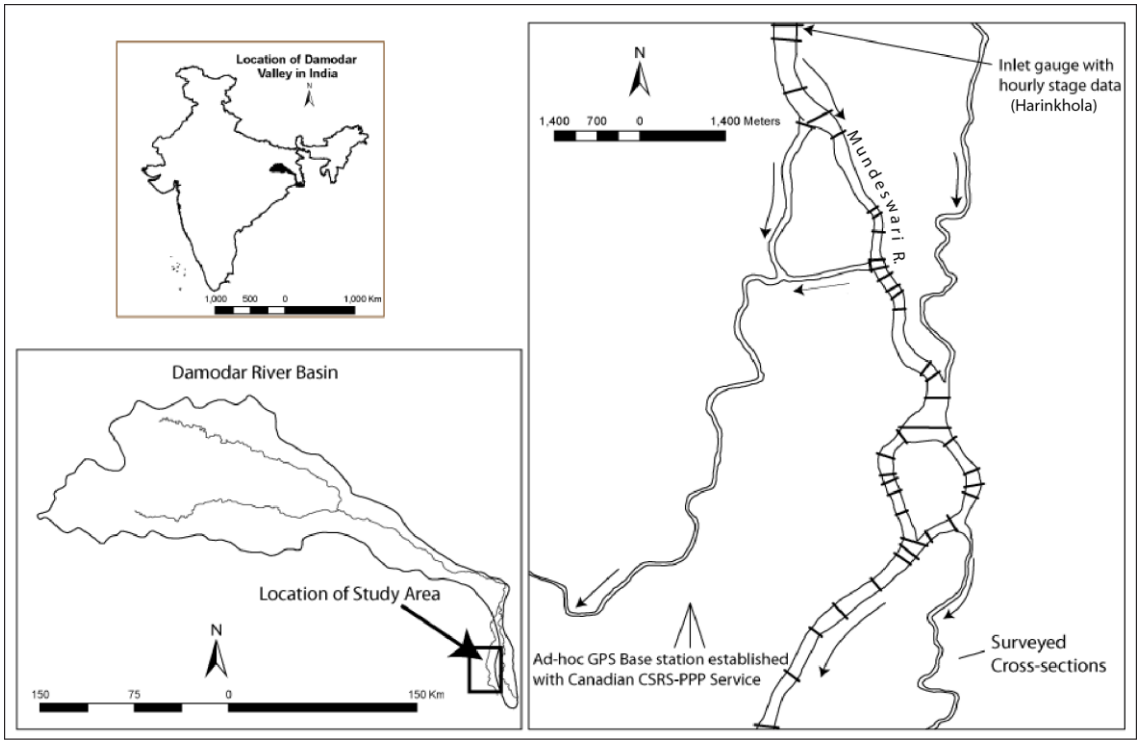

Figure 4.1 The study area; the arrows in the right panel shows the direction of flow for different channels; location of surveyed cross-sections are depicted with lines across the Mundeswari river.

The Damodar River with basin area of 24,235 km^2 is an important tributary of the Hoogly River which is one of the two branches of the Ganges. The main flow of the Damodar River started flowing through the Mundeswari River following an avulsion in the river channel during a major flood in 1914. The study area which is part of the lower Damodar Basin suffers from chronic flooding and was described by Basu (1996)

as a 'flood endemic zone' where the release of a large quantity of water from upstream reservoirs rather than heavy rainfall over the basin or its vicinity is the main cause of flooding. There were 16 major floods recorded between 1823 to 1943 (Saha, 1979) before the establishment of the Damodar Valley Corporation in 1946 that built a network of four dams and reservoirs in the upper Damodar Basin with the goal of moderating floods and provide irrigation during dry season. However, the situation has not changed much and the area was still inundated 14 times in the post-dam era between 1958 and 2000 (Chandra, 2003). More recently, this area was subjected to inundation in 2006, 2007, 2009 and 2011. The main cause of the flooding is heavy siltation of the channel, so that it cannot cope with a peak discharge of more than 2300 m^3/s (Central Technical Power Board, India, 1948).

The study area is composed of the approximate floodplain of the Mundeswari River.The channel system is anabranching and is characterised by number of smaller distributaries emanating from the main branch of the Mundeswari River and a river island. The channel bed material is mostly composed of sand and clay. Both banks of the Mundeswari River in the study area are protected by earth embankments that are 1 to 1.5 m higher than the natural river banks. The land use of the area is dominated by agriculture, mostly paddy fields, dotted with small rural hamlets. Although the study area is mostly drained by the Mundeswari River and its branches, during major floods some portion of the eastern and western boundary of this area experience influx of moderate amount of flood water from the adjacent river basins that are quite often simultaneously flooded during extreme monsoon events at the upstream area in the northwest.

4.3 Data used

The topographic data for defining the model geometry was derived from 1) Indian Remote Sensing Satellite (IRS) Cartosat-1 panchromatic stereo images with 2.5 m spatial resolution; 2) the SRTM DEM; and 3) river cross-sections that were surveyed with a combination of dGPS (for dry river bed) and portable depth sounder (wet parts of channels). Ahmed et al. (2007) extracted DEMs from Cartosat-1 stereo images and reported elevation RMSE of 4.38 m and 3.96 m for the Himalayan foothills at Dehradun and mountainous Shimla region of India respectively. Cartosat-1 stereo

images are suitable to produce DEMs of 0.3 s (approximately 8 to 9 m in lower latitude) grid size with a height accuracy of 3 to 4 in the plateau region (Srivastatava et al, 2008) while the vertical accuracy is likely to increase in flat rural areas without major forest cover. The DEMs generated from Cartosat-1 images have been found to be better in terms of both horizontal and vertical accuracy than the freely available SRTM DEM or ASTER GDEM (Rawat et al., 2012). The inflow of water at the model inlet was derived from stage data that were available at 1 hour interval at the Horinkhola gauging station (Figure 4.1) from the Irrigation and Waterways Department, Government of West Bengal, India. Due to the unavailability of discharge data or rating curve we converted the stage value into discharge using Manning's equation assuming uniform flow (Herschey, 1998) as below

$$Q = \frac{1}{n} R^a S^{0.5} \quad (1)$$

where R is the hydraulic radius (m), a is an exponent of the hydraulic radius, *n* is the Manning roughness coefficient and S is the bed slope (mm^{-1}).

The simple MS Excel-based Cross-Section Hydraulic Analyser tool (Natural Resources Conservation Service, 2012) was used for this purpose where the bed slope, hydraulic radius and cross-sectional area of the gauging site were derived from the surveyed cross-section. No stage or discharge data were available at the model outlet for specifying the downstream boundary condition.

Satellite images provided the observed extent of flood water at a particular time that was used to calibrate and validate the hydrodynamic models. The various optical satellite images used and their purpose is presented in Table 4.1. The acquisition time of two images for the 2009 flood event in relation to the inflow stage records is shown in Figure 4.2. Only freely available (MODIS and Landsat) or low-cost (IRS Resourcesat – 1 LISS-III) optical satellite images were utilised. No radar images were used because of the high cost associated with their procurement and the general unavailability of radar scenes in the archive of the major radar data providers.

Table 4.1 List of satellite images and their date of acquisition that were used for calibration and validation of the flood inundation models.

	Satellite	Sensor	Bands Used (Resolution)	Date of Acquisition	Purpose
1	MODIS Aqua	MODIS	Band 1 & band 2 (250 m)	26th September, 2006	Calibration
2	IRS P6 (Resourcesat-1)	LISS III	All bands (24 m)	12th September, 2009	Validation
3	Landsat 5	TM	Band 1 to 5 and 7 (30 m)	15th September, 2009	Validation

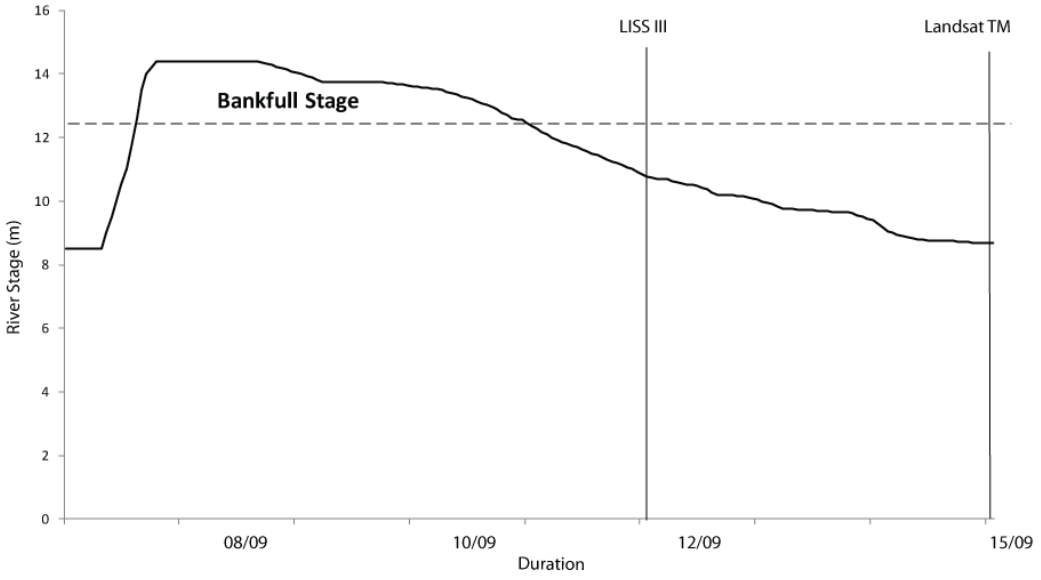

Figure 4.2 River stage (1-hour interval) at Harinkhola gauging station (Shown on Fig 1) and the timing of the two satellite overpasses that were used for validating the flood inundation models.

4.4 Methods

4.4.1 Generating the terrain data

Field survey

A field survey was conducted during November-December, 2010 at very low flow to collect necessary ground control points (GCPs) for generating the DEM from Cartosat-1 stereo images and to measure 40 channel cross-sections over the Mundeswari River in our study area. Differential GPS was used for surveying the dry river bed. Special care was taken to measure the elevation of the water surface at the time of surveying and used as an approximate representative value of channel bottom elevations for each cross-section (See Figure 4.3). A depth sounder was used from a boat to measure the depth of water while the x,y coordinates of the location of measured depths were captured with the dGPS. The sounder equipment reported depths to a precision of 10 cm. These depths are then subtracted from the water-surface elevation to obtain the bottom elevation of the wet part of the channel.

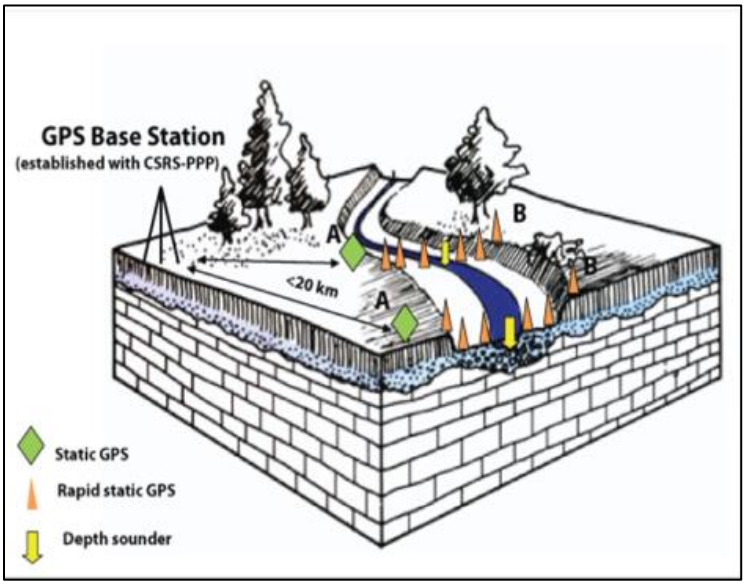

Figure 4.3 Schematic diagram of the river cross-section survey that was done with a combination of differential GPS and portable depth sounder.

The presence of a GPS base station within 20 km of the rover location is an essential prerequisite for conducting any dGPS survey with relatively inexpensive single frequency (L1) GPS receivers. No real-time observations from permanent GPS stations

are available in the public domain in India except for two IGS stations, the nearest of which is located more than 2000 km from our study area. A base station with known coordinates in the International Terrestrial Reference Frame (ITRF) / WGS84 was essential for this survey in order to make the observations consistent with the global datasets such as the SRTM DEM and Cartosat-1-generated points. Many web-based free services can correct a sufficiently long observation (more than 4 hours) of a dual frequency (L1 and L2) GPS receiver from decimetre to centimetre accuracy (Tsakiri 2008). We used the Natural Resources Canada's Precise Point Positioning (PPP) also known as CSRS-PPP which uses very precise GPS orbit or clock estimates from IGS to correct user-supplied observations. CSRS-PPP has reported that only 2 hours of continuous observation in dual frequency receivers are capable of achieving a vertical accuracy of approximately 40 mm while Ebner and Featherstone (2008) observed that more than 2 days of continuous observation reduces the vertical error down to 11.8 mm.

For setting up a base station a Leica 300 dual frequency GPS receiver took continuous observation for approximately 12 hours at a location which is within 15 km from any place in our study area (Figure 4.1). These observations were uploaded to the CSRS-PPP service and the corrected coordinates in WGS84 datum was used as the known coordinates for the base station. A single frequency PROMARK 3 GPS was used as the rover for collecting points over the channel. For surveying each cross-section we took static observations at two points by occupying the points for more than 20 minutes (Point A and B in Figure 4.3). The actual survey was done in a rapid-static mode, initialising the rover by occupying point A. After the survey was completed an additional observation was taken at point B without losing the satellite lock which was used as the measure of accuracy for the rapid-static survey. It was assumed that static points are likely to have higher accuracy than the rapid-static points and therefore can be used as the reference for measuring the accuracy of the rapid-static measurements. The rover data were post-processed in Thales GNSS software.

Seventeen well distributed GCPs were collected for the entire area covered by the overlapping portion of the Cartosat-1stereo images. These points were collected with the rover in static mode and post-processed using the base station coordinates in WGS84 obtained from the CSRS-PPP service. Employing the CSRS-PPP corrected

coordinates as the known coordinates of the base station ensured that the cross-section survey and the block model for creating the DEM from Cartosat-1 imagery remain in the same reference frame as the SRTM DEM.

Extraction of 3D points from Cartosat-1 stereo imagery by digital photogrammetry

Leica Photogrammetry Suite (LPS) was used to extract the terrain from the Cartosat-1 stereo pair. Fourteen GCPs were used to refine the block adjustment model which was initially set up using the vendor supplied rational polynomial coefficients. A total of 54 tie points were retained as satisfactory after manually checking all the tie points that were generated with the automated tie point generation tool in LPS. The triangulation process reported the control point residuals in the form of RMSE in X, Y and Z direction as 0.52 m, 0.55 m and 0.02 m respectively. The difference of intersected and measured control points were reported as 0.59 m, 0.64 m and 0.24 m as RMSE in X, Y and Z direction respectively.

Overall the triangulation process was deemed satisfactory given the pixel size of 2.5 m of the Cartosat-1 imagery. After finishing the block adjustment and areal triangulation LPS eATE module was used for extracting the terrain model in the form of a x,y,z point cloud. After giving due consideration to the pixel size and radiometric characteristics of our scenes and with several trial and error attempts we extracted the best possible set of mass points (*i.e.* an XYZ point cloud).

A 3D visualisation environment was created with the triangulated LPS block file and the eATE-extracted point cloud was superimposed over it and visualised in 3D using stereo goggles in order to facilitate terrain editing. It revealed that the overall result was not satisfactory. The automated terrain extraction particularly failed over farmlands with little contrast and the wet part of the channel. The presence of tree clusters also contributed to spurious relief in the otherwise extremely flat landscape. The main reason for partial failure of the automated terrain extraction process is the poor radiometric quality of the scenes. Cartosat-1 imagery has a 16 bit image depth and a digital number (DN) range of $2^{10} = 1024$. The histogram of the ‘aft’ image (Figure 4.4) shows that the scene has a very poor contrast where 99 % of the pixel values are confined within a narrow range of 1 to 160. Paddy fields which are the most ubiquitous

land use in our study area, in general appear dark in grayscale images. An image which is highly skewed towards lower values, the pixels composed of paddy fields as well as water body had very limited range of digital numbers. This factor made it difficult for the pattern recognition algorithm to find a correct match between both images of the stereo pair.

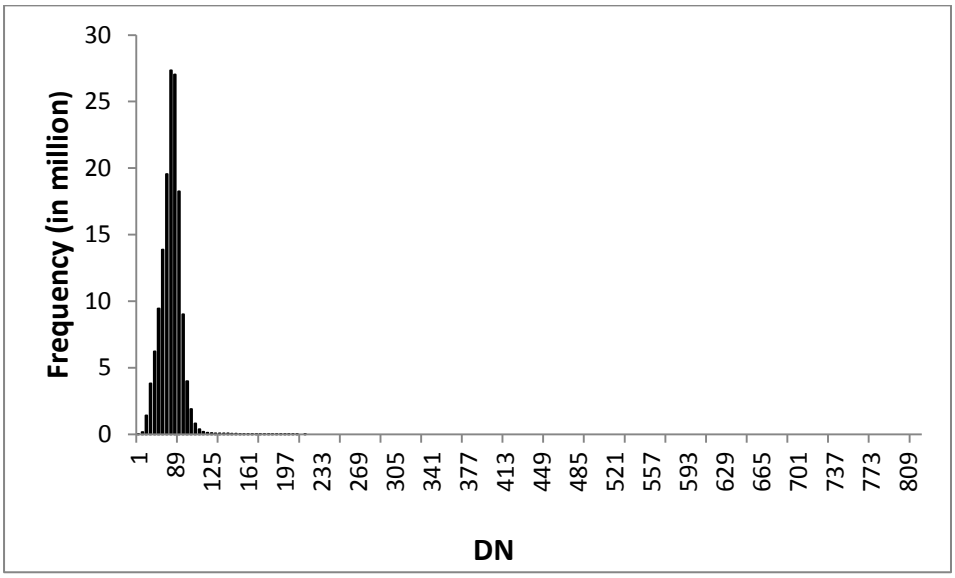

Figure 4.4 Histogram of one of the images of the Cartosat-1 stereo pair used in the present study for extracting DEM. It shows the poor radiometric quality of this particular scene with a histogram highly skewed to the lower digital numbers (DNs)

Utilising the SRTM DEM as a supplementary source of elevation

As the Cartosat-1 stereo images failed to produce an accurate terrain over the farmland we used the SRTM DEM to fill the gaps. When compared with 17 dGPS-surveyed points the original SRTM DEM showed a positive bias (systematic offset) (SRTM higher than the GPS) of 0.8 m for our study area. The surveyed points did not have any significant presence of trees in their vicinity. Hence, we assumed that the magnitude of SRTM bias is typical for more or less bare surface or paddy fields. Taking note of this bias the SRTM DEM was lowered by 0.8 m and the pixel elevations were converted into an x,y,z point cloud and imported in the same LPS block file where the Cartosat-1 generated point clouds were imported previously. The points which were found to lie at or very close to the surface were considered correct and the points floating above or below the surface were either eliminated or adjusted for vertical bias so that they rest on the surface of the 3D model. Contours were created using the point cloud in the LPS

TerrainEditor and visualised in 3D over the stereo pair to further appreciate the terrain generated by the automated terrain extraction mechanism. LPS performed well over roads, dry canals, small rural settlements and dry sandy river beds which are characteristically bright and have high contrast with the surrounding vegetation covered dark surface. The images being highly skewed towards the low values performed comparatively well for land covers with a lighter tone. For the landscape features with smaller dimensions the Cartosat-1 derived mass points were retained. The points were adjusted for vertical elevation bias and smoothed wherever necessary by using the underlying stereo block as the reference. The bias-adjusted SRTM DEM derived x,y,z coordinates were further treated for tree induced localised bias and merged with the Cartosat-1-derived points to create a seamless terrain data for the floodplain. These terrain data are characterised by low density of points over the farmlands and high density in the location of narrow features.

Creating a detailed channel

Creating a detailed channel was considered important for this study particularly due the existence of a number of river bifurcations and river islands in our study area. The channel of the Mundeswari River was created in high resolution by combining the surveyed channel cross-section information and the point cloud extracted from Cartosat-1 images. The surveyed points and Cartosat-1 derived mass points were imported into LPS Terrain Editor and edited within 3D visualization environment. The surveyed points were considered as the reference while the mass points were used to augment the details in channel geometry. The surveyed points were the only source of information in the wet portion of the channel where the automated terrain extraction procedure completely failed due to very poor contrast in the stereo images. The narrow embankments which are frequently covered with trees were difficult to derive accurately from photogrammetric output. Here, the surveyed points significantly contributed to generate this hydraulically significant feature. Figure 4.5 demonstrates how the channel would be captured if only the surveyed cross-sections were linearly interpolated (The purple lines bounded by the red lines) and how incorporating the photogrammetric outputs helped in capturing the actual configuration of the river.

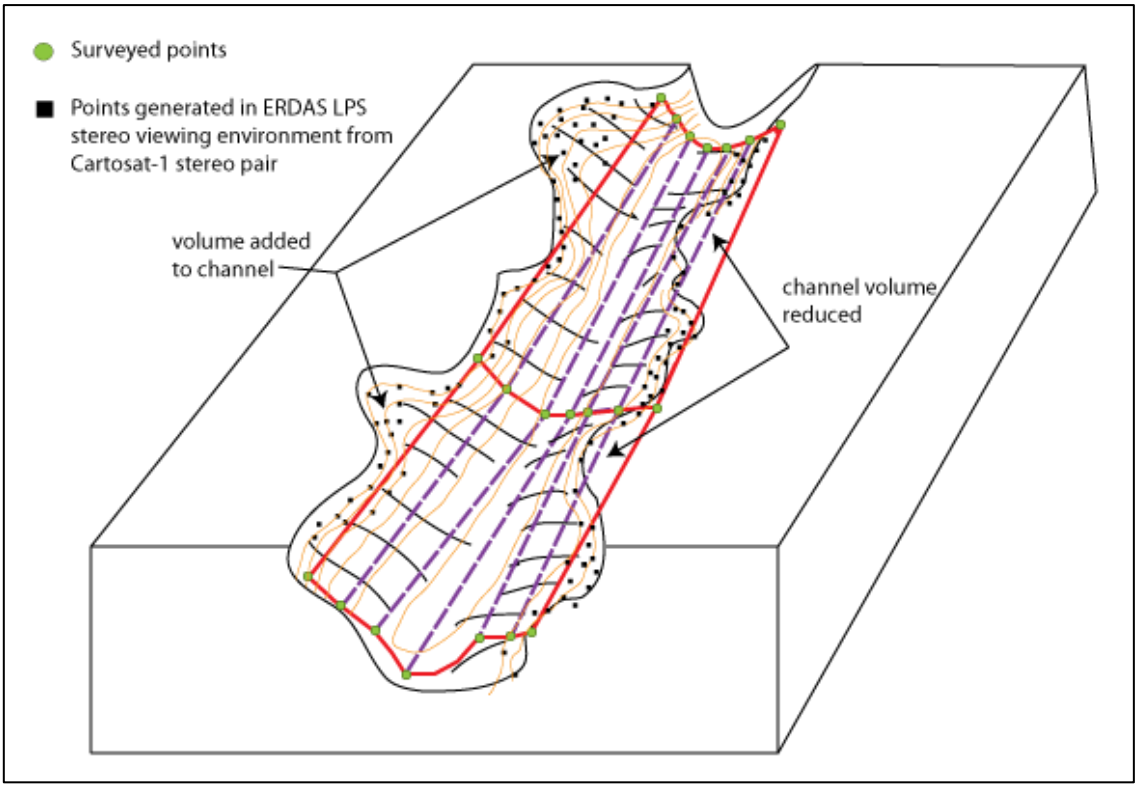

Figure 4.5 Schematic diagram showing how the channel topography was created in greater detail by supplementing the surveyed cross-sections with elevation mass points generated from digital photogrammetric outputs from Cartosat-1 stereo imagery.

Finally all edited elevation data were merged into one file and saved as xyz point as well as rasterised into 8 m grid cells to create a hybrid bare earth terrain data. A resolution of 8 m was chosen because the density of points in the channel and the linear discontinuous structures over the flood plain was approximately 8 m. Over the farmlands the raster was merely resampled into 8 m grid as the original point density was 90 m (derived from SRTM DEM).

4.4.2 Flood-inundation modelling

Two open source hydrodynamic models were selected for testing the performance of the improved hybrid terrain data. TELEMAC2D (Hervouet and Van Harn, 1996), a finite element fully 2D model with high computational cost and capability of complex hydraulic process representation was the first candidate model. The 2nd model selected was LISFLOOD-FP which is a simple raster-based 1D-2D coupled model. The virtue of this model is its simplicity and very low computational cost as compared to TELEMAC2D.

Setting up the TELEMAC2D model

TELEMAC2D model derives depth averaged free surface flow by solving the full three-dimensional Navier Stokes equations by getting the solution for the 2nd order partial differential equations in the following manner:

$$\frac{\partial v}{\partial t} + (v.\nabla)v + g\nabla(z_0 + \mathrm{h}) - \frac{(\mu+\varepsilon)}{\rho \mathrm{h}} \nabla(\mathrm{h}\nabla.\mathrm{v}) + \frac{\mathrm{F}}{\rho} = 0 \qquad (2)$$

$$\frac{\partial h}{\partial t} + \nabla(hv) = 0 \qquad (3)$$

where v is a 2D depth average velocity vector, g is the acceleration due to gravity, h is the depth of flow, μ is the molecular dynamic viscosity, ρ is the density of water, ε is the dynamic turbulent viscosity, Z_0 is the bed elevation and F is related to the bed friction. A detailed mathematical description of TELEMAC2D model can be found in Hervouet and Van Harn (1996).

TELEMAC2D model solves equations 2 and 3 over an unstructured triangular finite element mesh. Creation of an optimum configuration of the mesh is crucial for the performance of any finite element flood inundation model. Spatial resolution of the finite element mesh was found to have significant impact on TELEMAC2D output particularly in terms of the inundation extent and reported to have greater influence than calibration parameters such as friction coefficient in determining results (Hardy et al., 1999). We used Blue Kenue software (NRC Canadian Hydraulics Centre, 2012) to generate an empty mesh following the recommendations by Cobby et al. (2003) so that the mesh has approximately equilateral elements on the floodplain to minimize mass balance error, variable element size to concentrate computational resources where it is required and gradual transition between smaller and larger element size for maintaining model stability. Special sub-meshes were created at a resolution of approximately 8 m for the Mundeswari River and its distributaries as well as other hydraulically significant discontinuous topographic features like roads, canals, localised depressions for which the hybrid terrain data has a point density at approximately 8 m spacing. The density/resolution of the mesh over the farmland was kept at 90 m as the elevation data for this land use was derived from the SRTM DEM. Finally the mass points of the hybrid terrain data were triangulated and the triangulated elevation was mapped to the unstructured mesh in Blue Kenue. Varying point density in the terrain data suited the

unstructured mesh configuration and the sharp transition in element size in the triangulated terrain data from the channel to the floodplain was moderated with gradually varying composition of the finite element mesh in order to ensure stability in TELEMAC2D model runs (Figure 4.6).

In order to test the performance of TELEMAC2D with the original SRTM DEM, elevation values from the original SRTM DEM were imported onto the empty mesh except for the channel section. Since the elevation values of the channel were supplemented with the surveyed elevation values we imported and merged the channel elevations from the hybrid terrain data with the raw SRTM DEM in order to make a fair comparison between the performance of the improved hybrid DEM and the original SRTM DEM in terms of the accuracy of the modelled flood extent.

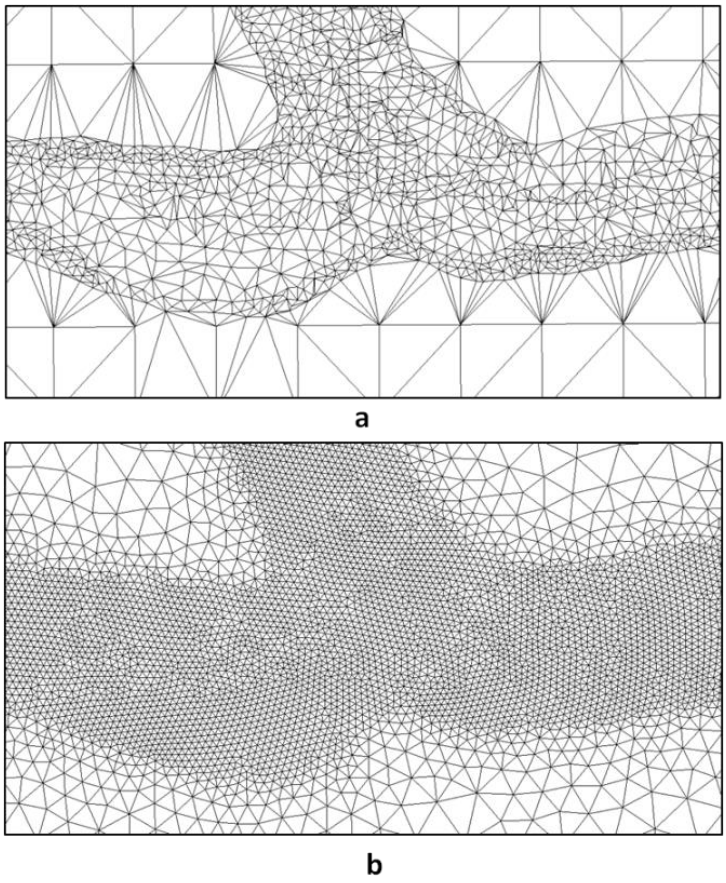

Figure 4.6 Construction of finite element mesh for the TELEMAC2D model; a: The delaunay triangulation of the elevation data derived from the hybrid mass points. b: Configuration of the empth finite element mesh characterised by smooth transition between smaller element size of the channel and larger element size of the floodplain.

Setting up the LISFLOOD-FP model

LISFLOOD-FP handles the channel flow using either a kinematic or a diffusive wave solution and once the water leaves the channel a 2D raster-based storage cell model is used to simulate floodplain flow. An approximate solution of the 1D Saint-Venant equation is used for the unsteady open channel flow. It is essentially a 1D-2D coupled hydrodynamic model and popular for its low computational cost and ease of parameterization (Horritt and Bates, 2001b). The input data requirement of the LISFLOOD-FP model is quite simple especially for the channel which is represented by a series of points, each having one value for the bed elevation and another for the channel width. The channel is assumed to be rectangular for computational efficiency. Since we need a single value for the bed elevation at each point of the 1D channel vector instead of a series of points captured by the cross-sections the water surface elevation obtained during the field survey was used for it (See Section 2.1.1). The channel width was obtained from the surveyed cross-sections as well as the Cartosat-1 image. The LISFLOOD-FP model was reported to be very sensitive to the resolution of the DEM (De Roo et al., 2007). This fact has a significant bearing on the model outputs. Because in our study area the flow of water from the main channel splits in a number of places through branching and some of the branches meet again to the main river through the loop (Fig 1). In LISFLOOD-FP any water leaving the main channel whether through purely shallow floodplain flow or branch channels is handled by a raster-based 2D storage cell mechanism and the efficiency of such routing depends significantly on both the resolution and accuracy of the DEM.

Preparing the observed data, calibration and validation

Band 1 and 2 of the MODIS images with a spatial resolution of 250 m for the 2006 flood event (See Table 3.1) was used for extracting the flooded area. The spectral characteristic of the band 2 data (841 - 876 nm) is very helpful in water classification. Brakenridge and Anderson (2006) proposed a method where MODIS images were used to calculate NDVI images (band 2 - band 1 / band 2 + band 1) for typical and flooded conditions and the difference image of the two NDVI images were utilised for detecting flooded area. Following the same technique we used a cloud free MODIS scene

acquired on 26th September, 2006 during the peak of the flood for deriving the NDVI image during the flooded condition and another MODIS image acquired on 2nd June 2006 for deriving the NDVI values for the typical condition. Finally the flooded area was derived by thresholding the difference image of the flooded and typical conditions.

The IRS Resourcesat-1 LISSIII and the Landsat-5 TM images acquired during the flood of 2009 were classified using number of methods such as supervised and unsupervised classification, NDVI thresholding and the results were compared with the false colour composite (FCC) of the original image. Finally the unsupervised classification product derived with the K-Means classifier using ENVI image processing software was found most accurate and retained as one of the validation dataset for 12th September, 2009. During the unsupervised classification process the IRS Resourcesat-1 LISS-III image was classified into 20 arbitrary spectral classes from which 5 classes were identified as representing flooded area by comparing them with the FCC image. These classes were combined to obtain the inundated area. The result of supervised classification was found to be most accurate for the Landsat TM image and retained as the validation data for 15th September 2009 (See Table 4.1).

One global Manning's roughness coefficient value for the channel and another for the floodplain were taken as the calibration parameter for the flood inundation models. The performance of model output in terms of the flooded extent was calculated using the formula proposed by Bates and DeRoo (2000) and presented as

$$F = (O_w \cap M_w / O_w \cup M_w) \times 100 \quad (4)$$

where O_w is the number of observed wet pixel and M_w is a modelled wet pixel. After consulting the published typical Manning's n values from Chow (1959) for sandy channels and floodplains with standing crops the calibration was run for 0.024 - 0.038 for the channel and 0.030 - 0.038 for the floodplain. The TELEMAC2D performed best with the *n* value of 0.037 for the channel and 0.038 for the floodplain with an F value of 48.25 % (Figure 4.7). The LISFLOOD-FP model did not show much sensitivity to the n values in the context of improving accuracy with reference to the observed flood extent. It was decided to use the chosen roughness values for the TELEMAC2D calibration runs in the validation stage for both models.

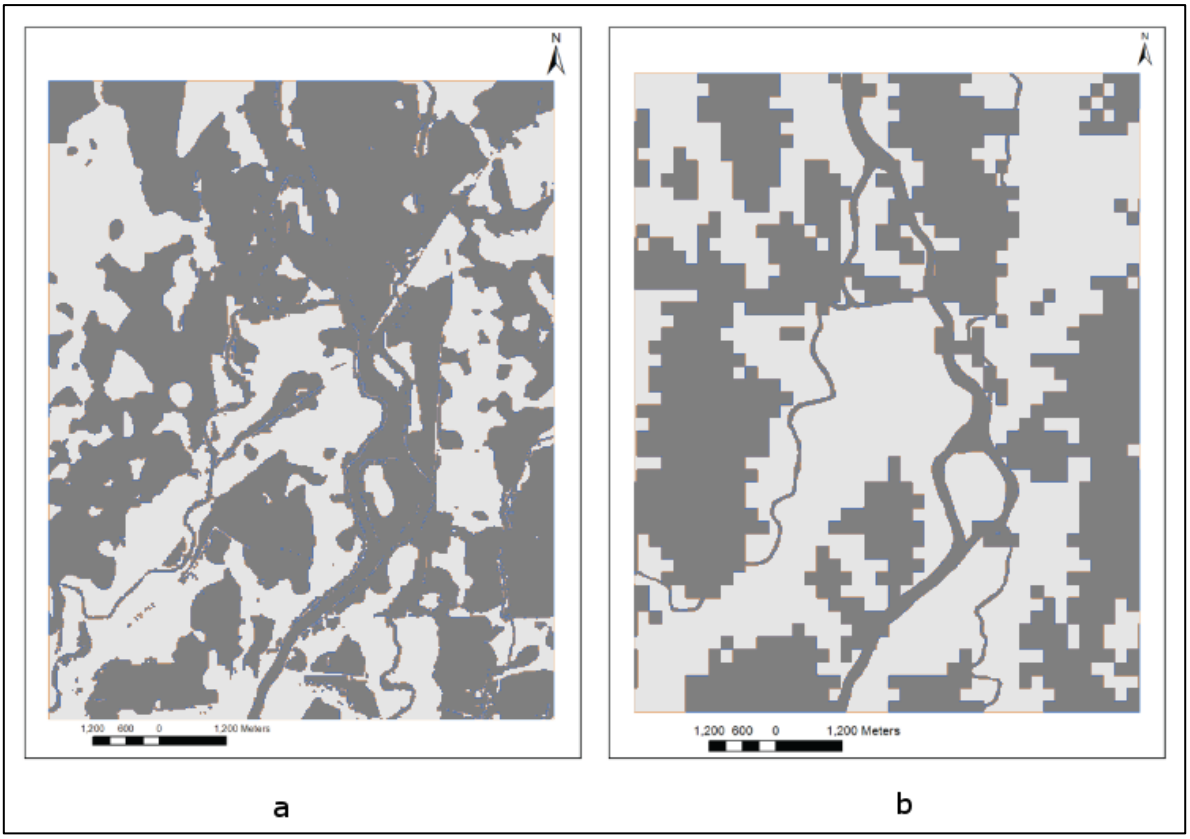

Figure 4.7 Best calibrated output of the TELEMAC2D model on 26th September, 2012, flooded areas are shown in dark shade. a: The modelled wet area. b: The observed wet area classified from the MODIS Image (Spatial resolution 240 m)

4.5 Results

Following the aforementioned methods for creating the hybrid terrain data great improvement was observed over the original SRTM DEM. Significant difference was made in the detail of the channel of the Mundeswari River, narrow but hydraulically significant features like embankments and roads (Figure 4.8), depiction of smaller branch channels and reducing noise in the original SRTM DEM (Figure 4.9). The RMSE value of the original SRTM DEM was 2.4 m when compared with 23 spot heights obtained from Survey of India topographic maps at 1:63360 scale. This figure improved to 1.1 m for the hybrid DEM.

In the validation stage, when the TELEMAC2D and LISFLOOD-FP model were run for the October, 2009 flood event, for which the actual flood extent was derived from the IRS Resourcesat -1 LISS-III images, TELEMAC2D model performed far better than the LISFLOOD-FP model in reproducing the actual flood extent (Figure 4.10). It

is evident from Figure 4.10a that LISFLOOD-FP in general failed to simulate the observed flooding pattern away from the main channel and grossly overestimated the inundation area adjacent to the channel. The F index for the TELEMAC2D output was computed as 41.45 %. The performance of the TELEMAC2D model at the further receding stage on 15th September diminishes to a F value of 28.89 % (Figure 4.11).

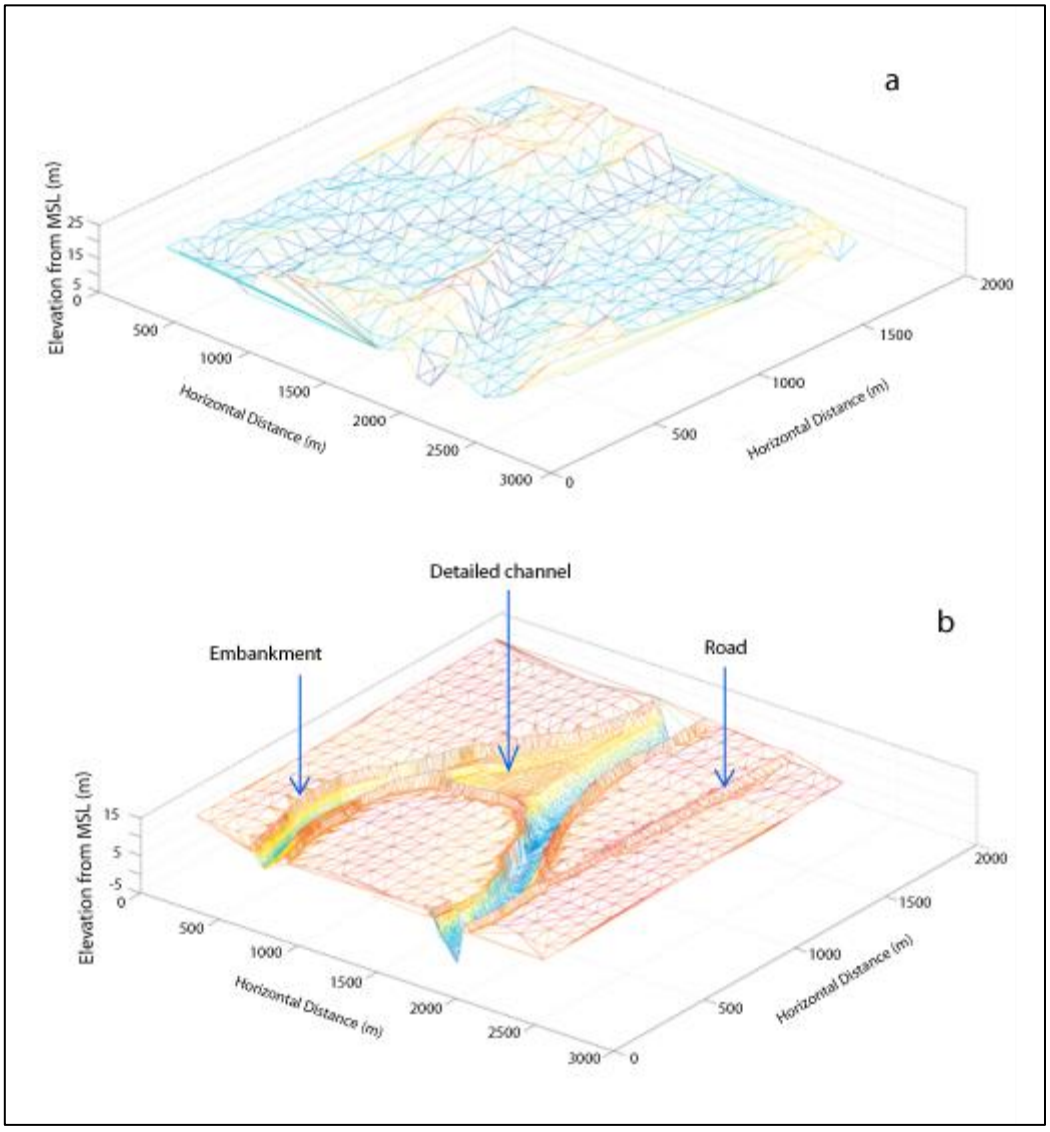

Figure 4.8 Comparison between the SRTM DEM elevation points (a) and the hybrid terrain data (b) with 3D visualization at the bifurcation of the Mundeswari River near the river island. The main channel is barely visible in (a) as compared to detail river bed in (b). The roads and narrow levee of the channel is also not captured in (a).

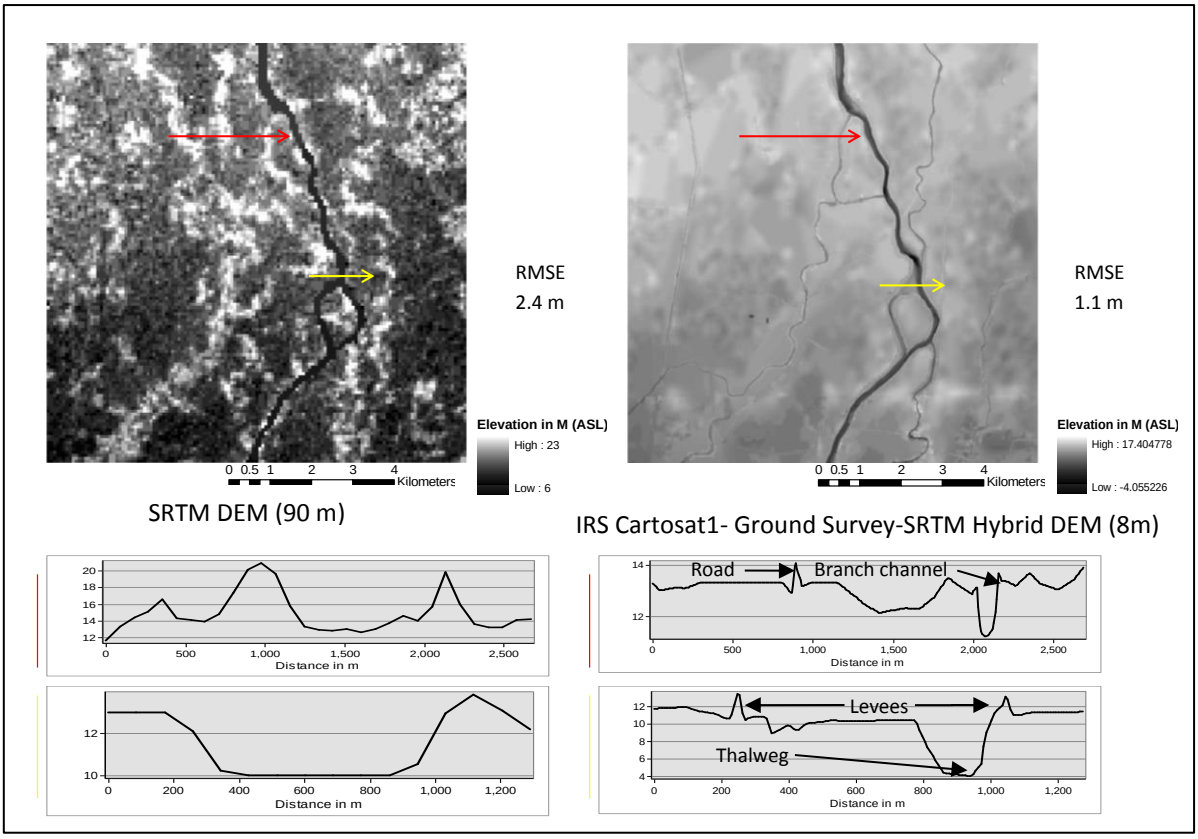

Figure 4.9 Overall improvement of the hybrid DEM over the SRTM DEM. The transect in red shows how the general noise of the SRTM DEM was reduced in the hybrid DEM and smaller channels which were not captured by the SRTM DEM is described in the hybrid DEM.

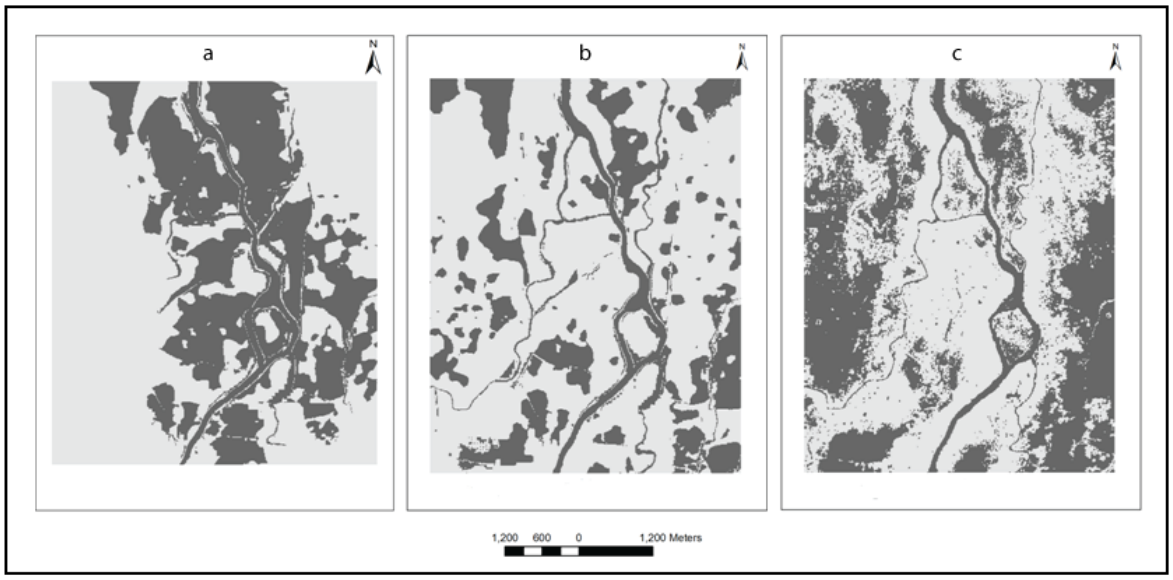

Figure 4.10 Comparison in the validation performance of the LISFLOOD-FP (a) and the TELEMAC2D (b) models at the particular time step (12th October, 10:00 Indian Standard Time) with reference to the observed flood extent (c) derived from the IRS Resourcesat-1 LISS-III image (24 m spatial resolution).

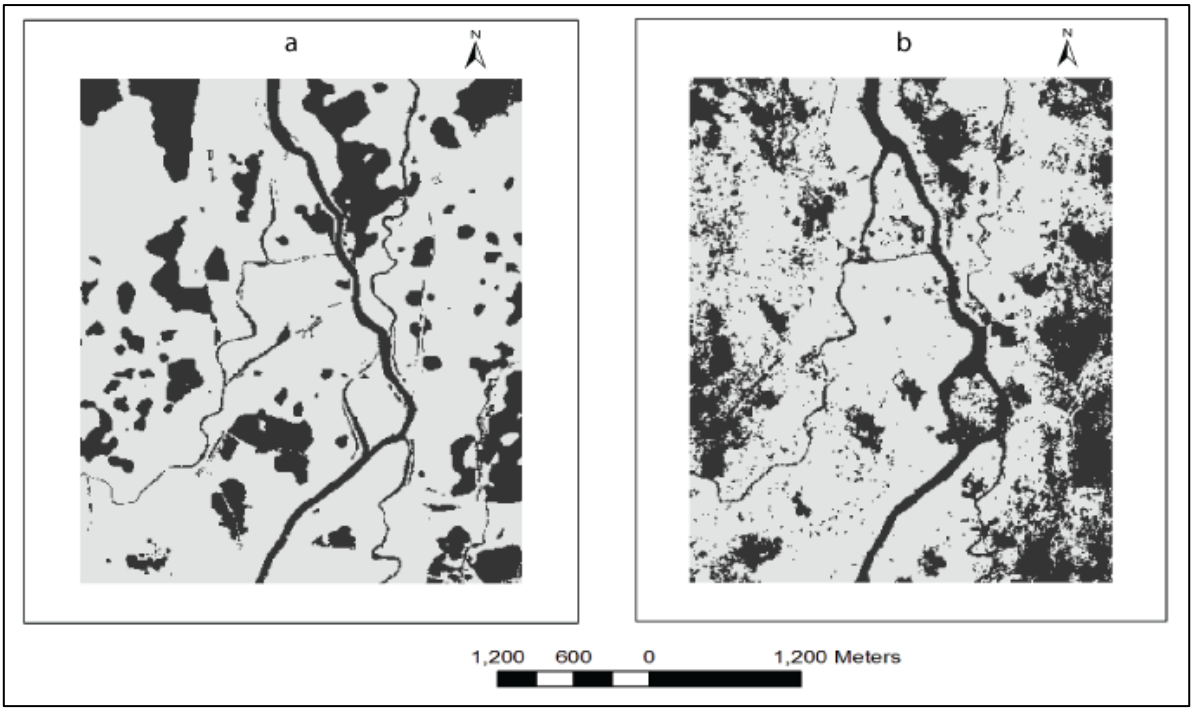

Figure 4.11 Comparison in the validation performance of the TELEMAC2D (a) model at the particular time step (15th October, 10:00 Indian Standard Time) with reference to the observed flood extent (b) derived from the Landsat-5 TM image (30 m spatial resolution).

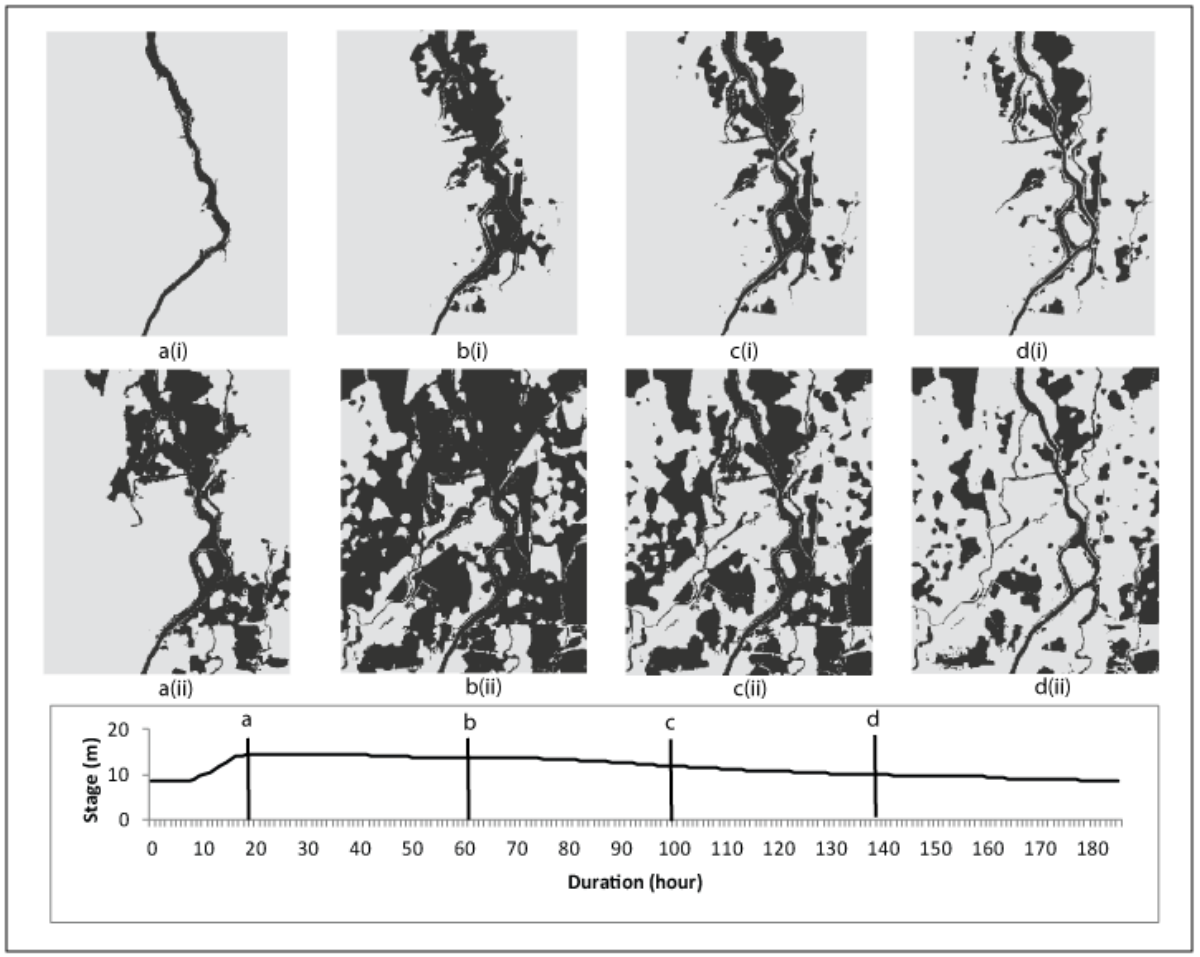

Figure 4.12 Visualization of the modelled flood extent of the LISFLOOD-FP (figures at the top row) with the TELEMAC2D (figures in the bottom row) at four stages (a, b, c and d) of the inflow hydrograph represented by river stage at 1 hour interval. The LISFLOOD-FP output remarkably failed to divert the flow in the distributaries and the flooded area remained confined to the channel of the Mundeswari River.

Although the comparison between the accuracy of the model outputs of TELEMAC2D and LISFLOOD-FP can be made at the time step of the two available satellite overpasses we realised that the visualization of the simulated flood extent by the two contending models at different stages of the flood (Figure 4.12) may help to reveal when (i.e. at which stage of the flood) and why LISFLOOD-FP failed to simulate the actual dynamics of flooding.

The contribution of the improved hybrid terrain data in producing a better result as compared to the original SRTM DEM becomes evident if we compare the simulated flood extent at the IRS Resoursesat-1 LISS III overpass (Figure 4.13) with Figure 4.10. It shows that in spite of having the detailed channel configuration of the Mundeswari river (refer to section 2.2.1) TELEMAC2D performed poorly when using the SRTM DEM raw elevation for the distributaries and floodplain.

Figure 4.13 Modelled flood extent of the TELEMAC2D using the SRTM DEM at the time step coinciding with the IRS Resourcesat-1 satellite overpass (Figure 4.10 c).

4.6 Discussion

Our results show that with the addition of survey grade cross-sections low-cost and freely available DEMs can be upgraded into products suitable for flood inundation modelling at reach scale in data-sparse environments. The typical obstacles of performing flood inundation modelling in the data-sparse developing countries are highlighted in this study and each of these challenges were dealt with a low cost yet effective alternative. The SRTM DEM supplemented with few reference channel cross-sections were found suitable to accurately predict river stage for high magnitude events with LISFLOOD-FP in a situation where the flow is mostly confined to the channel and the study reach of interest does not have flow split though distributaries (Sanyal et al., 2013). However, this study showed that when floodplain flow is widespread and the study area has numerous distributaries a more physically realistic model like TELEMAC2D is also incapable of simulating the actual inundation pattern with the SRTM DEM and a more accurate higher resolution terrain data is required.

We have reported a novel approach of combining the elevation data from different free / low cost sources to create a high resolution topography that can be used in hydrodynamic modelling for simulating extensive floodplain inundation in an anabranching channel system. The method of editing elevation in a 3D stereo environment is labour intensive and to some extent depends on the skill of the photogrammetric analyst. Although the overall accuracy of our TELEMAC2D model output may seem low in terms of the calculated F values it is important to note that the model was able to simulate the overall actual pattern of flooding (Figure 4.7). All major pockets of flood water in the observed data were modelled as wet. The modelled performed better (in terms of F index) in the calibration stage (F index 48.25 %) than the validation (F index 41.45% and 28.89 %) because the cloud free MODIS satellite overpass occurred just a few hours after the peak of the flood. The F index which is used for measuring the model performance tends to favour underprediction and may not be very appropriate for risk assessment where overprediction is preferable (Aronica et al., 2002). A more simple performance measure index (D) represented as

$$D = (A \cup B) / C \times 100 \quad (5)$$

where A is the number of pixels correctly modelled as wet, B is the number of pixels correctly modelled as dry and C is the total number of pixel in the model domain reveals a model accuracy of 68.3 % for the validation time step captured by the IRS Resourcesat-1 LISS III satellite data. Aronica et al (2002) argued that the D index may give over optimistic result in situations where there is a large higher ground in the model domain which can be very easily modelled as dry. However, in our study area the total elevation range is mostly within 2 to 3 m over the floodplain (see the profiles for the hybrid DEM in Figure 4.9) and existence of such elevated ground is not widespread. Considering this fact the model performance, at least close to the flood peak, (12th September, 2009) appear reasonably accurate. The F measure was selected for this study because it was found more sensitive to the roughness values and we wanted to test the model through a more stringent performance measure.

The moderate accuracy and resolution of the topography is the main reason for declining F value of the model output with receding flood water. Usually during the descending limb of the flood hydrograph the flood water escapes through innumerable small ditches and depressions which are difficult to capture without very high resolution images or LiDAR-generated DEMs. During the overpass of the Landsat 5 (Figure 4.2) the river stage reached almost the pre-flood level. Clearly, the drying mechanism of TELEMAC2D model could not perform well at this stage due to the limitation imposed by the input topography. However, the primary utility of a flood-inundation model is to identify the areas that are exposed to flood risk at a flood of certain return period. Hence, identifying the maximum extent of flooding is of primary interest and the TELEMAC2D model with its all input constraints performed well in our case in achieving this goal.

Figure 4.12 depicts that a major portion of the water flows through the right hand distributary of the Mundesweri River which bifurcated at the upstream end of our study area (refer to Figure 3.1 for the river network). This water is the main cause of the flooding in the west and southwest portion of the model domain. However, LISFLOOD-FP fails to divert the flows into the branch channels swiftly. As the 1D river component in LISFLOOD-FP does not have a provision for handling flow splits, the distributaries are just considered depressions over the floodplain and handled by the simple storage cell model. LISFLOOD-FP, a model with a storage cell mechanism for floodplain flow routing, was designed for shallow low velocity flows. The storage cell mechanism could not deal well with deep and fast flowing water in

the channels and failed to divert it efficiently from the main river to the distributaries. The relatively moderate resolution of the hybrid DEM used in this study probably also played a part in it. The limited ability of the raster-based floodplain component of LISFLOOD-FP to account for the eddies and turbulence at the channel bifurcation was probably another reason for its poor performance. Consequently the floodwater remained confined to the floodplain adjacent to the Mundeswari River (Figure 4.12).

Comparison of the relative performance of TELEMAC2D and LISFLOOD-FP revealed that the former was better placed to exploit the varying detail of terrain as supplied by the hybrid terrain data due to its unstructured finite element mesh. TELEMAC2D was found useful in making good use of the data with varying density of elevation information across the model domain. The unstructured finite element mesh in TELEMAC2D was found an appropriate technique for describing discontinuity in the terrain like the roads, levees in our study area as also reported by Di Baldassarre et al. (2009a) and for that reason it was selected as the appropriate model for analysing the effect of levee heightening on flood propagation in the Po river basin in Italy (Di Baldassarre et al., 2009b). TELEMAC2D is more suitable than conceptually simple LISFLOOD-FP model for simulating extensive floodplain inundation in data-sparse environment, especially in anabranching channels because it depends on very high quality topographic input not typically available outside the industrialised countries. Our finding is to the contrary of the observation of Horritt and Bates (2001b) and Alho and Aaltonen (2008) which found that the LISFLOOD-FP model performed equally well as the TELEMAC2D model. It is worth noting that the river reaches investigated in these studies do not feature any distributary or river islands which probably made the difference in the model outputs in our study.

It is not surprising that the original SRTM DEM performed poorly with the TELEMAC2D model despite having the same detailed channel configuration as the hybrid DEM (Figure 4.13). As mentioned earlier the shortcomings of the original SRTM DEM in terms of its 90 m grid size, spurious vegetation induced elevation and general noise of more than 2 m amplitude makes it unsuitable for flood inundation modelling in its raw form. However, the SRTM DEM is the most high quality DEM that is freely available and if modified skilfully, can be used to fill the gaps where local high resolution DEMs fail to produce good results.

Finally we would like to highlight that the model results are subject to a number of uncertainties arising from the coarse quality of the inputs. Conversion of river stages to

discharge without a rating curve is the most significant source of uncertainty as it affected the volume of water flowing in the model domain. The stage to discharge conversion process adopted in this study assumes uniform flow which is not the actual case during flooding. Apart from this uncertainty, observed flood extents as derived from the satellite overpasses may also vary depending on the digital image processing technique applied for extracting flooded surface. Chapter 5 will address the issues of uncertainties in detail for this experimental setting. As mentioned earlier that the contribution of water from adjacent river basins during extreme floods contribute to some of the observed flood water. This factor is particularly responsible for consistent underprediction of the models in our study, particularly at the western portion of the study area.

4.7 Conclusion

This study proposes a methodology for flood-inundation modelling in data-sparse environments that are typically present in the vast flood prone river basins outside the developed world. We demonstrated how our conventional techniques can be adapted to create low-cost terrain data that is suitable for flood inundation modelling in extremely flat floodplains at reach scale. This study also showed how open source hydrodynamic codes can be put to use in order to exploit the full potential of the improved terrain data and low cost / freely available optical remote sensing products can be utilised as the validation data. Our results also pointed out that in a complex fluvial system where river bifurcations, loops and river islands are found frequently, the fully two dimensional TELEMAC2D model is a better candidate than the 1D-2D coupled LISFLOOD-FP to simulate floods. The success in simulating spatially non-adjacent inundation pattern caused by overbank flow at the main channel as well as the smaller distributaries at different parts of the model domain shows the strength of TELEMAC2D. We also found that the choice of the model should depend on the nature of the fluvial system to be modelled and the nature of input terrain data. Finally we would like to point out that the methodology described in this study is labour intensive and appropriate to adopt for high flood risk zones with complicated river networks and paucity of data.

Chapter 5

2D finite element inundation modelling in anabranching channels with sparse data: examination of uncertainties

Abstract

Flood inundation modelling in developing countries is severely limited by the lack of high resolution terrain data and the poor availability of radar imagery which can image flood extents through clouds. This study assesses predictive uncertainty of simulated flood extent generated from TELEMAC2D model using low-cost, sparse input data of the sort that are commonly available in developing countries. The study was undertaken in a river reach characterised by anabranching channels and river islands in eastern India. We analysed the effect of incorporating the possibility of error in the satellite-derived flood extent maps on the computation of uncertainty when the input terrain data is not very accurate and the fluvial setting is complex. Generalised Likelihood Uncertainty Estimation (GLUE)-based published methodologies were adopted to generate the uncertainty maps. The results show that the model performance was quite sensitive to the uncertainty in inflow hydrograph particularly when it was examined close to the flood peak. Comparison between the flood inundation probability map, conditioned upon deterministic and probabilistic observed flood extents reveals that the effect of using probabilistic observed data is only evident for portions of the model domain where the model output is free from consistent bias (over or under prediction) created by the imperfect terrain data.

Keywords: Uncertainty, finite element inundation model, sparse data, TELEMAC2D, GLUE, high performance computing

5.1 Introduction

Flooding is one of the most serious natural hazards and it disproportionately affects the global south due to frequent occurrence of extreme precipitation events associated with tropical cyclones and monsoons burst (Adhikari et al., 2010). Topography is the most important element for building the domain of an inundation model while gauged river stage and discharge records provide upstream and downstream boundary conditions. In addition, gauged water level as well as inundation extents derived from satellite data are also used for model calibration and validation. Most of the required data mentioned above are either non-existent in many developing countries or they are limited in their spatial and temporal resolution (Patro et al., 2009a). Hence, coarse inputs are unavoidable for modelling river flooding in data-sparse regions and there is considerable uncertainty associated with the deterministic inundation maps produced with such inputs. Generally, the main sources of uncertainties in inundation maps are (1) estimated discharge at the model inlet from stage-discharge relationship; (2) topography; (3) assumed state in the model (e.g. steady versus unsteady); (4) boundary roughness parameterization; (5) calibration and validation data; (6) choice of model (1D versus 2D) (Jung and Merwade, 2012; Bales and Wagner, 2009). The uncertainty arising from model structure (i.e. different combinations of internal parameters and the way they are linked) is an issue affecting the developed and developing world alike. However, the uncertainties emanating from quality of inputs are much more pronounced in data-poor regions due to the coarse quality of available data.

Uncertainties in topographic elevation values affect the modelled water surface elevation (Wilson and Atkinson, 2005). Considering the resource constraints on developing high resolution DEMs (e.g. from LiDAR surveys) for an entire basin, elevation data from different sources can be blended and merged for inundation modelling. Chapter 4 illustrates a methodology for creating a composite dataset of this type by merging channel cross-sections derived from differential GPS and depth sounder equipment, elevation data extracted from stereo satellite imagery, and a modified form of the SRTM DEM, applied it to a fully 2D inundation model (TELEMAC2D) and reported considerable improvement in model outputs as compared to the SRTM DEM in its original form.

The inaccuracy in the inflow hydrograph of a model is the most significant source of uncertainty (Pappenberger et al., 2006). In most cases discharge figures are derived from water levels with rating curves. Published works on stage-discharge relationships either use a power law (Herschey, 1995) or Manning's equation (Herschey, 1998) to convert stage data into discharge for deriving the inflow hydrograph at the model inlet. The existence of uncertainty in deriving flow discharge from stage data is well reported in the literature (Di Baldassarre and Claps, 2011; Di Baldassarre and Montanari, 2009). Domeneghetti et al. (2012) pointed out how rating curve uncertainties may sometimes lead to unrealistic values of calibrated Manning's n in hydraulic models. Observed data in the form of downstream gauged water level (Pappenberger et al., 2005) or observed flood extents derived from remotely sensed data (Horritt, 2000) are commonly used for calibration and validation of the inundation models. Recognizing the error in the observed flood maps derived from satellite images using variety of image processing techniques, Schumann et al. (2009) proposed 'possibility of inundation' maps rather than commonly used deterministic binary flood maps for calibrating and validating inundation models.

The effect of uncertainty in a particular input data such as the inflow hydrograph is often neutralised by the uncertainty in other parameters. The overall uncertainty in flood risk estimation emanates from superimposition of number of sources of uncertainty (Merz et al., 2008). The findings of Jung and Merwade (2012) highlighted this fact where the effect of uncertainty in the topographic data was found to be responsible for making the model outputs less sensitive to uncertainties in the inflow hydrograph.

Generalised Likelihood Uncertainty Estimation (GLUE) by Beven and Binley (1992) is the most widely used framework of uncertainty assessment in hydrology and hydraulic sciences (Montanari, 2006). The GLUE procedure is a replacement for the traditional strategy that searches for optimal parameter sets, searching instead for sets of parameter values that would give reasonably accurate model outputs for a range of model inputs. This method does not require the modeller to maximize any objective performance measure for the model. Instead, it derives the performance of sets of parameters from

some index of likelihood or goodness-of-fit that broadly resembles the concept of probability.

With a steady increase in the availability of remotely sensed data for capturing the extent of inundation during flooding events, binary flood maps have been used to quantify distributed uncertainty of the inundation models under the GLUE approach (Aronica et al., 2002). Di Baldassarre et al. (2009c) incorporated the element of error in the observed flood extent in the form of possibility of inundation map (as proposed by Schumann et al., 2009) for calibrating model outputs and proposed a method for generating GLUE-based 'flood uncertain inundation maps'. Stephens et al. (2012) found that the selection of the uncertain observed data from different areas of the model domain can result in considerable differences in the consequent assessment of the overall uncertainties in the inundation modelling outcomes.

Although 1D hydrodynamic models such as HEC-RAS and simple and computationally efficient 1D-2D coupled models like LISFLOOD-FP have been used in the past in order to assess predictive uncertainty, application of fully 2D models for this purpose is rare in the scientific literature. The high computational cost of running a fully 2D model for a considerable number of iterations using Monte Carlo techniques (Merz et al., 2008) and the easy availability of very high resolution LiDAR data that favoured the use of simple and computationally efficient models (Bates, 2012) are possible causes for selecting LISFLOOD-FP or HEC-RAS for uncertainty assessment experiments. When attempts were made to use fully 2D hydrodynamic models the experiments were undertaken at a coarse resolution and at very small scale, possibly to keep the computation time small. For example, Aronica et al. (1998) reported a similar experiment covering only 22 km^2 with 1690 nodes. Recently, there have been some efforts to use emerging technologies, such as the use of graphic processing unit (GPU)-based method to overcome the constraints of computational cost of Monte Carlo analysis in 2D finite element models (Kalyanapu et al., 2012).

Fully 2D finite element flood inundation models such as TELEMAC2D are physically realistic and have certain advantages. They are suitable for terrain data with varying detail in the representation of topography (Di Baldassarre et al., 2010), less sensitive to

uncertainties in the terrain data (Cook and Merwade, 2009) and therefore suitable for applications in developing countries which lacks access to LiDAR generated DEMs. In addition, TELEMAC2D was found to be less sensitive to the roughness parameterisation (Horritt, 2000) and shows slower drop off in performance than its raster-based counterparts with increasing difference from the calibrated 'optimum' parameters (Di Baldassarre et al., 2010). The use of a complex model becomes more appropriate when the study reach is characterised with anabranching channels, loops and number of distributaries. This kind of fluvial environment is quite abundant and frequently flood-prone in the lower course of relatively large rivers, particularly in monsoon Asia. Chapter 4 reported that a fully 2D hydrodynamic model like TELEMAC2D is better placed in simulating widespread floodplain inundation in this kind of complex hydraulic situation than its more computationally efficient 1D-2D counterparts, particularly when the input data is of coarse quality. However, the uncertainty in this type of experimental setup has not been examined.

Therefore, the objectives of this study are 1) to evaluate the uncertainty in the simulated flood extent in a computationally demanding fully 2D model (TELEMAC2D) that uses coarse quality model inputs in anabranching channels, and 2) to assess the effect of incorporating elements of error in the observed flood extent maps on the spatial distribution of predicted uncertainty when employing coarse model inputs.

5.2 Study Area

The study area was the lower Damodar River basin in eastern India (Figure 5.1). The Damodar River is an important tributary of the Hoogly River which is one of the branches of the Ganges that flows through the Indian state of West Bengal to the Bay of Bengal. This area is typical of many rivers in the global South, in that it suffers from frequent flooding during the monsoon season and has very limited availability of the datasets that are normally required for inundation modelling. The Mundeswari River, one of the main branches of the lower Damodar River, is the primary channel in this area. The fluvial setting is characterised number of anabranching channels associated with numerous channel bifurcations, loops, and a major river island. The area is extremely flat with a relative relief of only 10 to 12 m. Channel beds are mostly

composed of sand and clay while paddy field is the dominant land use in the floodplain. This type of fluvial setting is found quite frequently near the lower course or delta of large rivers particularly in monsoon Asia. The area is entirely rural with farmlands dotted with small hamlets. Although the study area is mostly drained by the Mundeswari River and its branches, during major floods some portion of the eastern and western boundary of this area experience influx of moderate amounts of flood water from adjacent river basins.

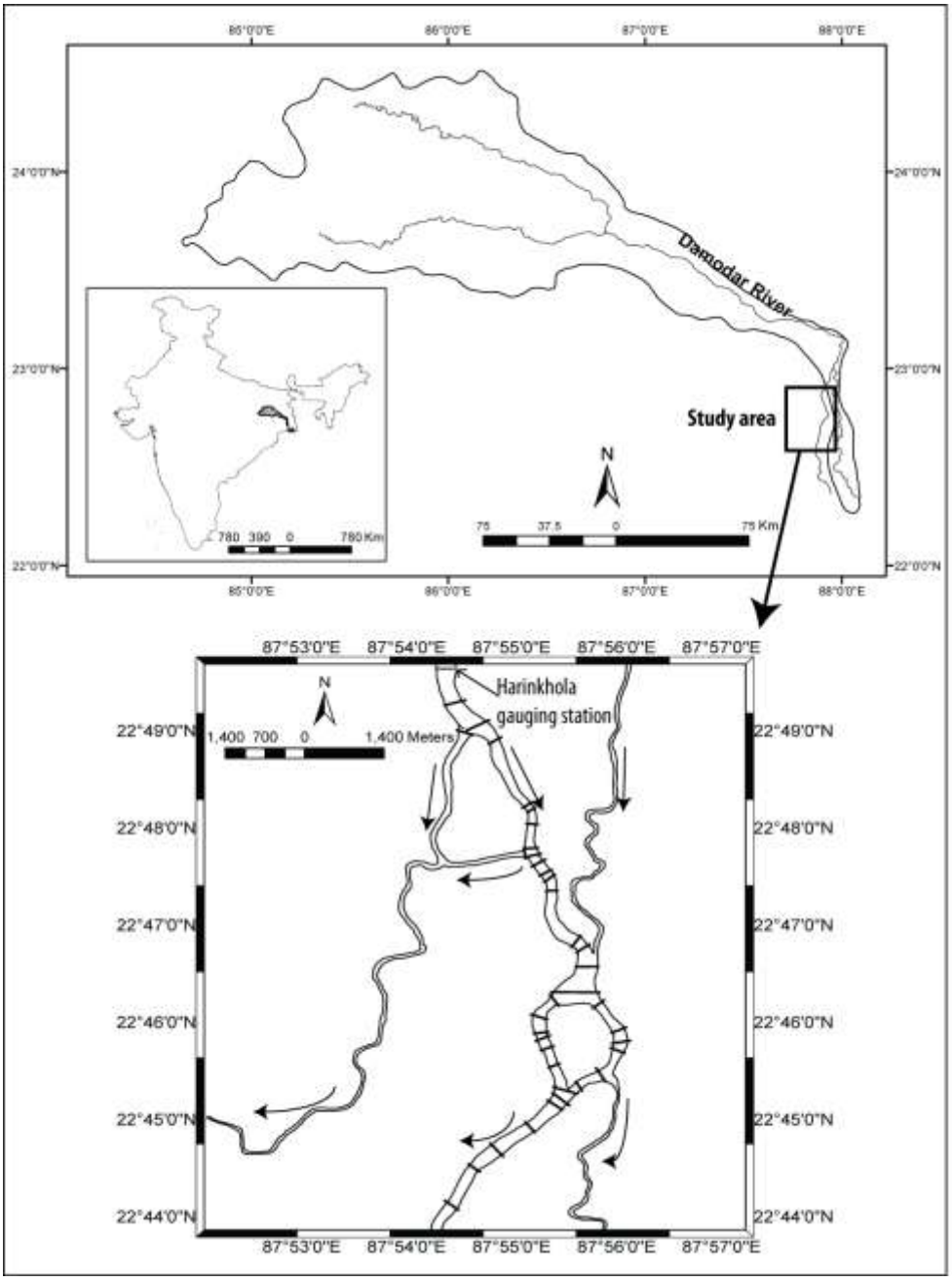

Figure 5.1 Study area. Inset in the top panel shows the location of the Damodar Basin in India. The complex fluvial setting of the area is evident with many river bifurcations, loops and a river island. Locations of the surveyed cross-sections on the main channel are shown.

5.3 Data and Methods

5.3.1 Terrain data

With complete unavailability of LiDAR data and very high resolution areal photographs in our study area we used low-cost IRS Cartosat-1 panchromatic stereo images (2.5 m spatial resolution) to create the terrain data. A detailed description of generating this terrain data can be found in Chapter 4. The ERSAD LPS software was used in conjunction with 14 ground control points to extract xyz coordinates or mass points from the Cartosat-1 stereo images by means of digital photogrammetric techniques. Channel cross-sections surveyed with differential GPS and portable depth sounders were used to create a detailed river terrain model including the adjacent levees and embankments. The SRTM DEM was compared with the surveyed ground data and adjusted for vertical bias. The modified SRTM data were used to fill the gaps over low contrast homogeneous paddy fields where the digital photogrammetry failed to produce accurate terrain. The elevation data from three sources (Cartosat-1, differential GPS and SRTM DEM) were merged and edited under 3D visualisation using the block model created with Cartosat-1 stereo images. The final product was characterised by higher details for the channels, roads, canals and other narrow but hydraulically significant features with progressively low resolution towards the floodplain where paddy cultivation is the dominant land use.

5.3.2 Hydrologic inputs

The hydrological data at the upstream boundary of the model were available as river stages at one hour intervals but without any rating curve. Following the Manning's equation the stage data were converted into discharge (Herschey, 1998) using

$$Q = \frac{1}{n} R^a S^{0.5} \qquad (1)$$

where R is the hydraulic radius (m), a is an exponent of the hydraulic radius, n is the manning roughness coefficient and S is the bed slope (mm^{-1}). The hydraulic radius and bed slope were derived from a cross-section that we surveyed at the gauging station. The uncertainty in the discharge figures derived with this method stems from the

tentative nature of the Manning's *n* values for the channel and floodplain at the gauging site.

5.3.3 Preparing the distributed calibration and validation data

A flood event on 8-15 September, 2009 was selected to perform the uncertainty assessment exercise. With no availability of radar images we had to use two cloud free optical satellite images from IRS Resourcesat-1 LISS-III (24 m spatial resolution multispectral image) and Landsat 5 TM for 12th and 15th September, 2009 respectively. The satellite overpass times with respect to the inflow hydrograph are presented in Figure 5.2. The performance of the flood-inundation model at these two specific times will be referred as model state 1 and 2 respectively henceforth in this chapter. The near infrared area of the electromagnetic spectrum is particularly useful for delineating water bodies. In order to exploit this property of water the Normalized Difference Vegetation Index (NDVI) has been commonly used for differentiating flooded area from dry surface (Jain et al., 2006). The Normalized Difference Water Index (NDWI), developed by McFeeters (1996) in line with the NDVI was applied by Jain et al., (2005) using Landsat TM and IRS LISS-III images for flooded area demarcation.

We used 1) supervised classification 2) unsupervised classification 3) NDVI and 4) NDWI techniques for creating binary wet/dry flood extent maps using ENVI software. A false colour composite of the IRS Resourcesat-1 LISS III image (Figure 5.3) shows the main sources of uncertainty in demarcating flooded and non-flooded areas. In particular, the existence of wet soil, which should be considered as non-flooded for modelling purposes, and very shallow standing water make it difficult to produce a deterministic flood extent map from multispectral images.

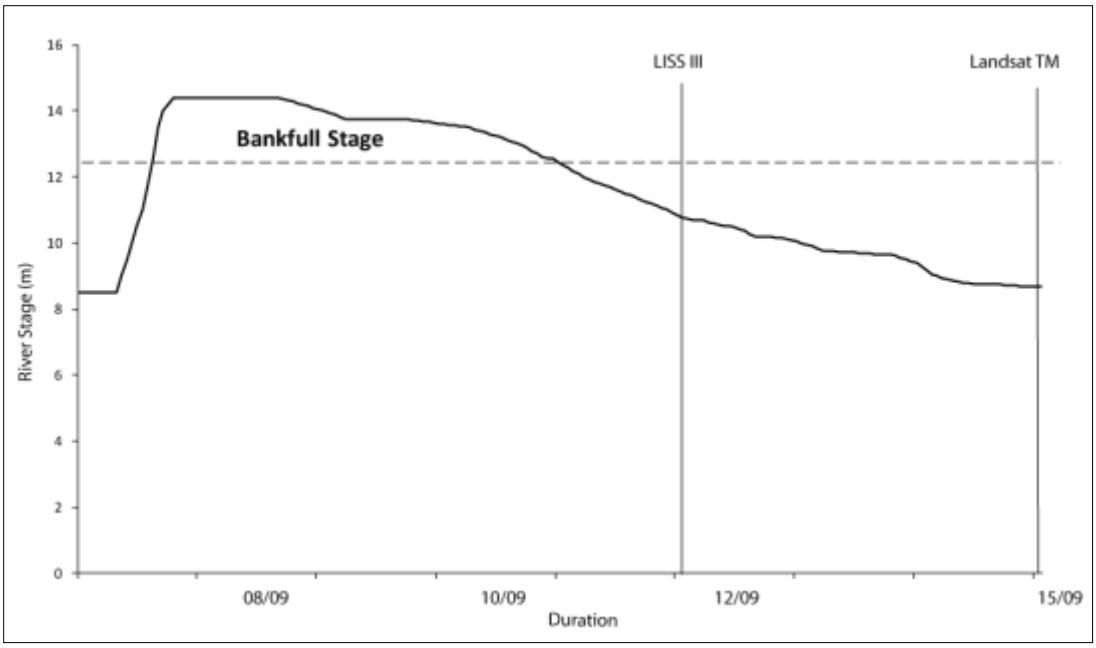

Figure 5.2 The hydrograph of river stage at Harinkhola gauging station (September, 2009) at the model inlet and the acquisition times of two satellite images that were used to derive the actual inundated areas on ground.

In order to include the element of error or uncertainty arising from the choice of image processing technique in the flood maps, we followed the general principle of the so called possibility of inundation maps as proposed by Schumann et al. (2009). However, unlike that study we did not have access to multiple images that were acquired at the same time, and so we did not follow the methodology for creating the possibility of inundation map. We also note that such data are extremely difficult to obtain over developing countries due to rare data acquisition requests for radar satellites and the low probability of overpass of two optical satellites in post-flood cloud-free conditions. As the differences in digital image processing techniques are the main reason for variation in the output binary flood maps, we added all four binary maps produced by different methods pixel-by-pixel and divided the summed map by 4 to produce a simple possibility of inundation map (Figure 5.4) where the pixels represent discrete probabilities (Table 5.1)

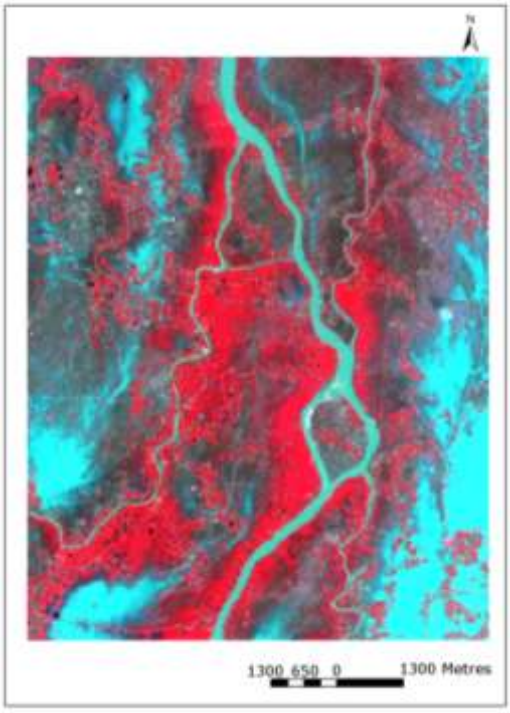

Figure 5.3 A false colour composite of the IRS Resourcesat-1 LISS-III Image. The sky blue colour represents deep flood water while the dark tone represents very shallow water as well as areas of wet soil.

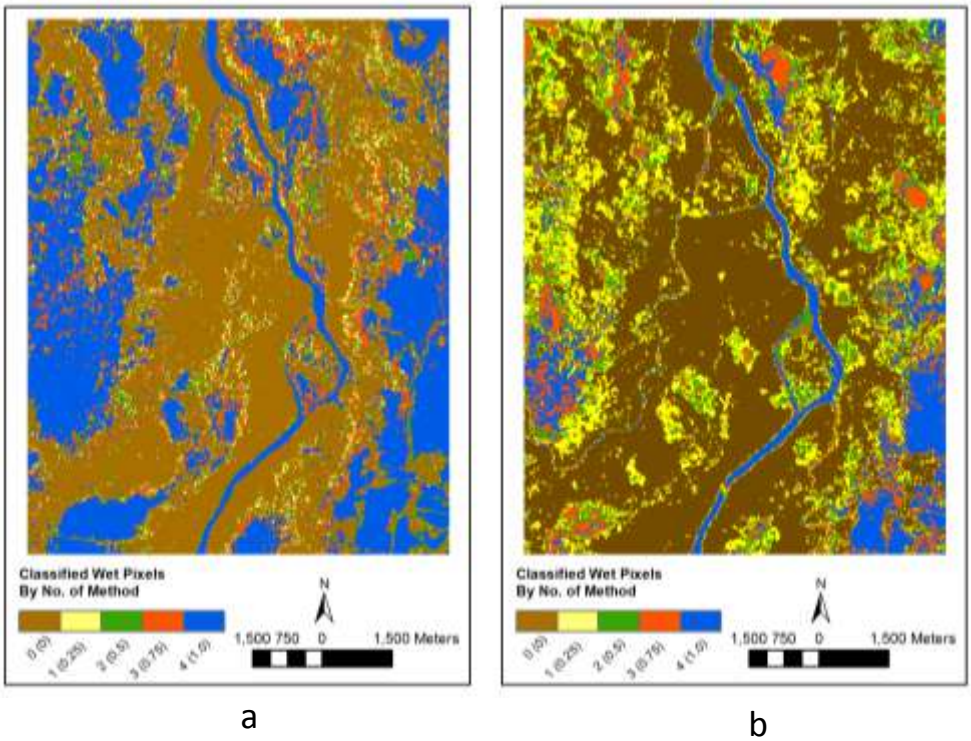

a b

Figure 5.4 Possibility of inundation maps derived from (a) the IRS Resourcesat-1 LISS-III image on 12th September, 2009 and (b) the Landsat 5 TM image on 15th September, 2009.

Table 5.1 The pixel values and their actual meanings in the possibility of inundation maps.

Pixel Value	Characteristics
0	Pixels not classified as flooded by any of the four methods
0.25	Pixels classified as wet by one of the four methods
0.50	Pixels classified as wet by two of the four methods
0.75	Pixels classified as wet by three of the four methods
1	Pixels classified as wet by all four methods

This pragmatic methodology assumes that all methods have equal ability for extracting the wet surface from the dry one. The inundation maps derived by unsupervised classification from the IRS Resourcesat-1 LISS III (12th September, 2009) and supervised classification from the Landsat 5 TM (15th September, 2009) were used as the deterministic binary inundation maps (Figure 5.5).

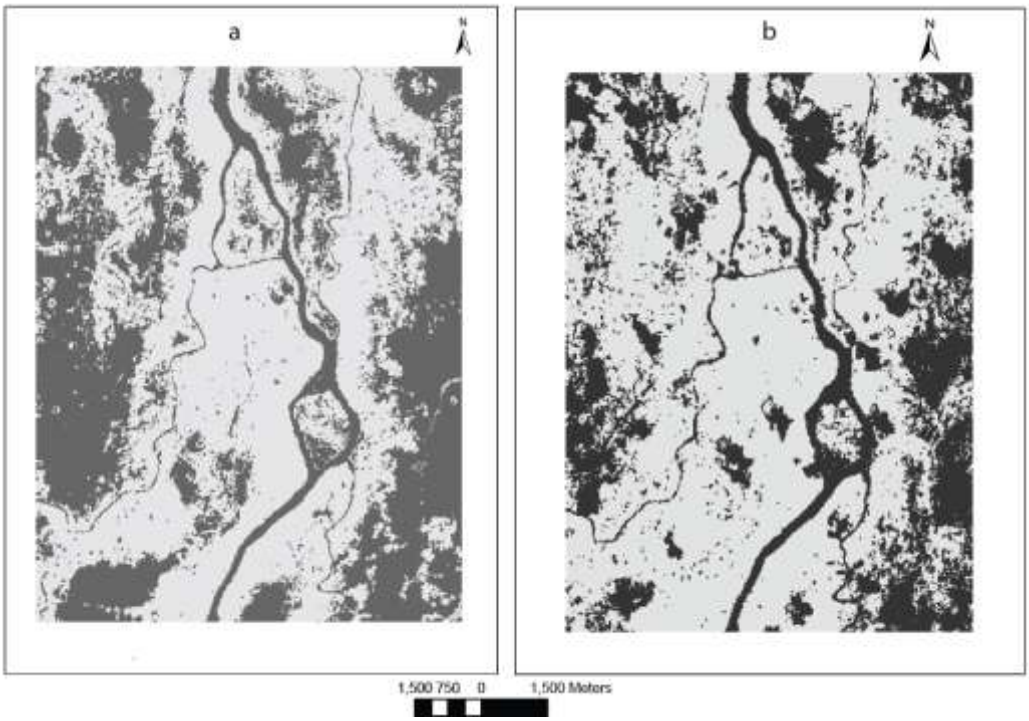

Fig 5.5 Deterministic binary inundation maps derived by (a) unsupervised classification of the IRS Resourcesat-1 LISS-III image on 12th September, 2009 and (b) supervised classification of the Landsat 5 TM image on 15th September, 2009.

5.3.4 Setting up the inundation model

TELEMAC2D (Hervouet and Van Harn, 1996), a fully 2D finite element inundation model was selected for this study as it showed good performance in our study area to simulate a few high magnitude floods (Sanyal et al., In Prep). This model has been applied to simulate inundation for number of rivers (Hervouet and Petitjean, 1999; Di Baldassarre et al., 2009b) and the results have been validated with observed hydrograph at it external boundaries (Besnard and Goutal, 2011) as well as using inundation maps derived from satellite images (Bates et al., 1997). TELEMAC2D solves second-order partial differential equations for calculating free surface hydraulics. The equations are depth averaged free surface flow equations that are derived from the three-dimensional Navier-Stokes equations. A full description of the equations can be found in Hervouet and Van Harn (1996).

The unstructured finite element mesh was created using Blue Kenue software (NRC Canadian Hydraulics Centre, 2013). We ensured that the mesh had approximately equilateral elements on the floodplain to minimize mass balance error, variable element size to enable concentration of computational resources as necessary. Smooth transition between smaller element sizes over channel and other narrow features to larger element sizes over paddy fields in the floodplain was ensured to increase model stability. The node spacing in the finite element mesh roughly followed the density of mass points (xyz point cloud) in the hybrid terrain data that was created by merging elevation information derived from Cartosat-1 stereo images, the SRTM DEM and surveyed cross-sections for the main channel.

5.3.5 Setting up the GLUE-based uncertainty assessment experiment

The model was composed of 674901 nodes and 1349048 elements and took 50 hours to complete one simulation run for the 186 hour (approximately 8 day) flood event using a PC with an Intel i7 8-core processor and 16 GB RAM. Clearly, standard workstations are not capable of performing numerous Monte Carlo type simulations for this kind of models. One of the main reasons for selecting TELEMAC2D for this uncertainty assessment study is its easy adaptability to parallel computing architecture that is

typically used in high performance computing (HPC) hardware. Moulinec et al. (2011) reported the performance of TELEMAC2D model with meshes ranging from 2 to 12 million elements using variety of HPC hardware. Their investigation observed that the CPU time for computation reduced steeply from 1 to 1024 cores and adding more cores had a diminishing effect on the rate of reducing computing time primarily due to the excessive time of pre-processing that is required for domain decomposition in parallel computing.

We used the HPC facility housed in the Computing and Information Service (CIS) of Durham University for performing our Monte Carlo simulations. This HPC system is a HP Linux cluster (known as the Hamilton Cluster) with 1824 cores having a clock-speed of 2.26 GHz (CIS, 2012). 40 cores were used for running each simulation. Five parameters were identified as the primary source of uncertainty: 1) Manning's n for the channel at the gauging site (InQnch) for converting stage into discharge, 2) Manning's *n* for the floodplain at the gauging site (InQnfp) for converting stage into discharge, 3) a global Manning's *n* for the channel during computation (nch), 4) a global Manning's *n* for the floodplain during computation (nfp), 5) the solver used for the system of equations. Parameters 1 and 2 were directly related to the amount of water entering the model domain, with higher roughness resulting in lower discharge for same stage. Parameter 3 and 4 are very conventional sources of uncertainty and have been analysed by number of studies. Parameter 5 which deals with the nature of the solver used for finding the solutions of the partial differential equations and has impact on both the computational time and the model solution. The effect of solvers on the model output was discussed in detail by Bates et al.(1995). We used four out of seven available solvers in TELEMAC2D in the Monte Carlo realisations in order to keep the total number of possible parameter combinations limited. The four solvers used were 1: conjugate gradient method (CG); 2: conjugate residual method (CR); 3: normal equation method (NE) and 4: squared conjugate gradient method (SCG). The range of the five uncertain parameters is presented in Table 5.2.

Table 5.2 Range of variation of the uncertain parameters applied in the Monte Carlo simulation.

Sl no.	Parameter	Range	Increment	No. of possible choice
1	InQnch	0.026-0.038	0.001	13
2	InQnfp	0.030, 0.035, 0.038	N/A	3
3	nch	0.024-0.038	0.001	15
4	nfp	0.030, 0.035, 0.038	N/A	3
5	Solver	CG, CR, NE, SCG		4

Random samples were drawn assuming uniform distributions for all parameters and a total of 1000 simulations were run on the Hamilton Cluster. *514* simulations did not converge and the model crashed before the completing the entire simulation. Only 1 simulation was successful with the 'normal equation' solver (Solver 3) out of 403, whereas the failure rate for other solvers is more or less the same. After discounting the simulations that were run with the normal equation solver, it was found that percentage of model failure (Figure 5.6) was approximately 4 times higher (up to ~ 80 %) for the lower channel roughness value of 0.024 compared to the standard values of 0.029 to 0.035 recommended in Chow (1959) for straight rivers with primarily sandy beds.

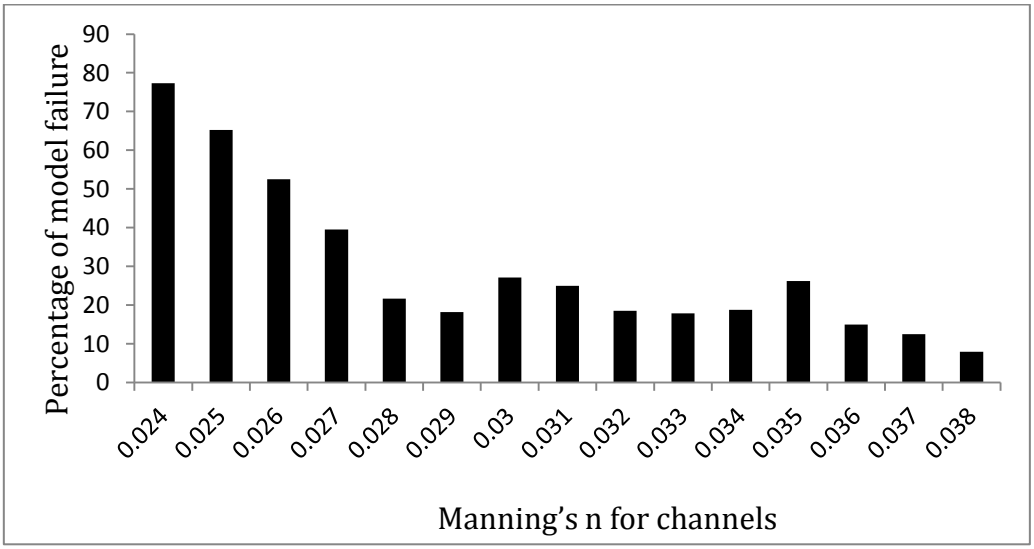

Figure 5.6 Percentage of cases where the TELEMAC2D model solution failed to converge is shown in relation to the used Manning's roughness coefficients for channels. All simulations that used Solver 3 were kept out of this analysis as all but one such cases failed to converge.

The computing time for each simulation run depended mostly on the solver used (Figure 5.7). The modelled water depth was taken as the output for comparing against observed flood extent. A MATLAB routine was developed that works in conjunction with the MATLAB program Telemac Tools (Benson, 2012) to extract the water depth from the native TELEMAC2D output files (selafin format) and save them in XYZ format where X and Y are the planimetric coordinates of the node in UTM coordinates and Z is the simulated water depth. These depths were then interpolated using the natural neighbour method in ArcGIS to create output rasters of water depth. The pixels having a water depth of more than 20 cm were classified as flooded, as shallower water is not likely to be identified as flooded from the satellite imageries. The use of a threshold depth for identifying a flooded pixel involves some elements of subjectivity and the decision of selecting a threshold depth of 20 was selected on the basis of the study conducted by Bates and DeRoo (2000).

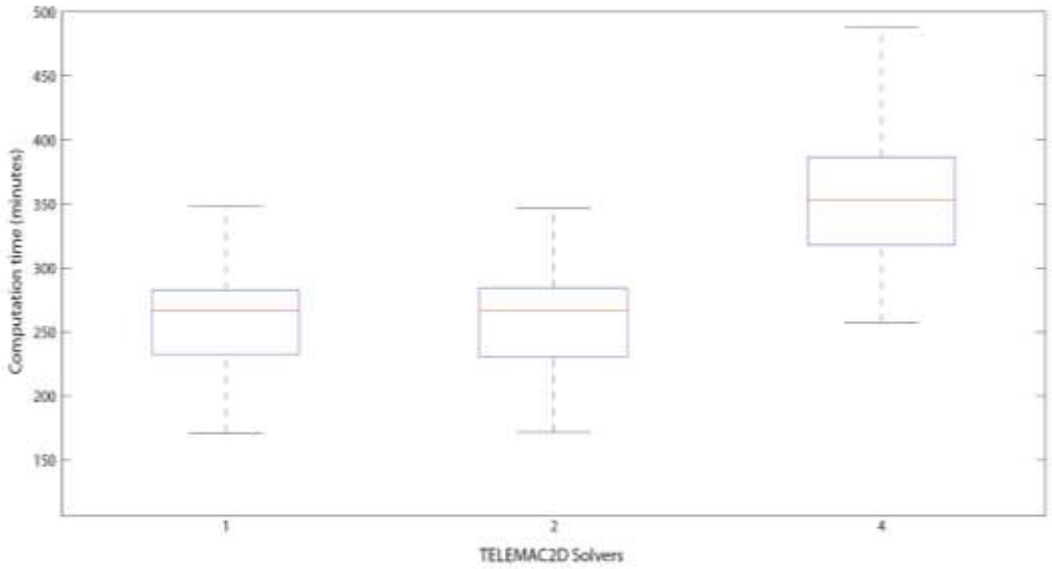

Figure 5.7 Box plot showing the distribution of computation time of TELEMAC2D Monte Carlo simulations with reference to the solvers. The median, upper and lower quartiles are represented by the red line and the upper and lower bounding line of each box respectively.

We used GLUE-based framework to quantify the predictive uncertainty in TELEMAC2D outputs by employing two types of binary pattern observed inundation maps for conditioning the likelihood weights. First, satellite-derived deterministic flood maps (Figure 5.5) were used following the method proposed by Aronica et al. (2002). In the second case, possibility of inundation maps (Figure 5.4) were used for

incorporating the uncertainty in satellite observation of flood extents in the uncertainty analysis following the methodology suggested by Di Baldassarre et al. (2009c). As both approaches lead to generation of probability maps of predicted inundation we intend to examine the spatial pattern of their difference from each other.

First, the performance of TELEMAC2D model was measured against the with the objective function given by Horritt and Bates (2001) as

$$F = (O_w \cap M_w / O_w \cup M_w) \times 100 \quad (2)$$

where O_w is the number of observed wet pixels and M_w is the number of modelled wet pixel. Following the principle of GLUE a likelihood weight L_i was assigned to each successful Monte Carlo simulation i, where

$$L_i = F_i - \text{Min}(F) / \text{Max}(F) - \text{Min}(F) \quad (3)$$

In Equation 3, F_i is the performance score of the i th simulation, Max(F) and Min(F) are the maximum and minimum figures of performance found through the ensemble.

The weighted average flood state (X_j) for the jth computational cell was derived as

$$X_j = \Sigma L_i m_{ij} / \Sigma L_i \quad (4)$$

where m_{ij} is the model output for the jth computational cell which takes a value of 1 for wet and 0 for dry. The likelihood values (L_i) for the successful runs (the cases where the solution converged) were stored in a vector. Each cell of each of the simulated inundation outputs (cell values were either 1 or 0) was multiplied with the corresponding likelihood value of that simulation run, then the matrices were added and each cell of the summed up matrix was divided by ΣL_i to produce the probability of predicted inundation map. The entire process was automated using MATLAB.

The second approach entails slightly more complex treatment of the raw model outputs. As proposed in Di Baldassarre et al. (2009c), we used the principle of a reliability diagram (Horritt, 2006), where for each output i the observed possibility of inundation map (Figure 5.4) was classified into regions of similar probability (i.e. 0, 0.25, 0.50

etc.) and the number of simulated wet cells falling in each of the probability regions was counted. It is assumed that in a fully accurate model the proportion of modelled wet cells (model proportion) for each of the probability regions would match the possibility of inundation value. For example, in a perfectly accurate model, 25 % pixels in the possibility of inundation map with a probability value of 0.25 is simulated as wet. Horritt (2006) argued that the reliability diagram of a perfectly accurate model would result in a 1:1 line relationship between the probability (in our case the figures in the possibility of inundation map) and model proportion and the accuracy of any given simulation run can be measured by calculating the RMSE deviation from the 1:1 line. For each simulation, the model proportion for the probability regions (p_j) of 0, 0.25, 0.50, 0.75 and 1 were calculated. Then, we derived the RMSE as the deviation from the ideal relationship between the possibility of inundation and model proportion. A MATLAB routine was developed to perform this task for all the successful Monte Carlo simulation runs. The RMSE for each simulation was weighted by the number of cells in that class, ignoring the dry area where $p_j = 0$. The purpose of computing the RMSE was to bring out the discrepancy between the possibility of inundation and model proportion. Figure 5.8 exhibits a schematic diagram of the graphical representation of the calculation of the RMSE that signifies the deviation from the ideal 1:1 relationship between the model proportion and the possibility of inundation.

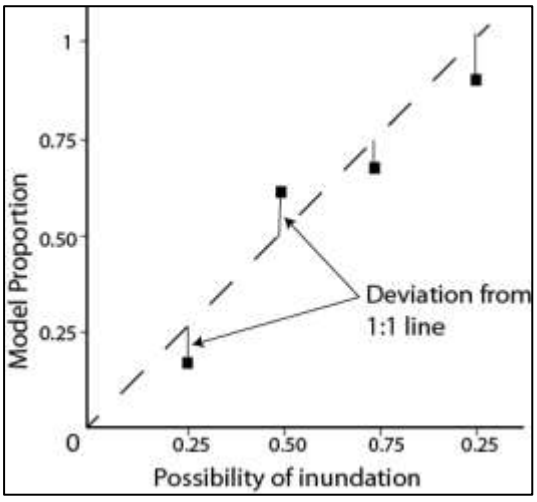

Figure 5.8 Scatter diagram of model proportion and possibility of inundation for each of the successful Monte Carlo simulation. Only four points are realised for each simulation as we used four image processing techniques to obtain the values of the possibility of inundation map. The 1 :1 line representing a perfect model is shown with the dashed line.

The likelihood value (L_i) for each simulation was derived from the RMSE values as

$$L_i = \text{Max(RMSE)} - \text{RMSE}_i \,/\, \text{Max(RMSE)} - \text{Min(RMSE)} \quad (5)$$

where Max(RMSE) and Min(RMSE) are the maximum and minimum RMSE values for all successful Monte Carlo simulation runs. The weighted average flood state for the jth computational cell was calculated using the same way as Equation 4 and the raster containing the average flood state values was presented as the flood uncertain inundation map which illustrates the predictive uncertainty in the modelled inundation map incorporating the element of error in deriving an observed flood extent map.

In line with the study published by Di Baldassarre et al. (2009c) we computed a quantity D_j for the model state 1 in order to investigate the amount of difference between the possibility of inundation map and the flood uncertain inundation map. For the jth computational cell the quantity D_j was computed as the flood uncertain inundation figure minus the possibility of inundation figure. However, unlike Di Baldassarre et al. (2009c) we did not consider all cells in the model domain for computing D_j as there were many cells that were dry (cell value = 0) in both flood uncertain inundation map and possibility of inundation map. Hence, a direct subtraction would result in large number of spurious 0 values that would falsely indicate a condition of little bias. In order to resolve this problem we ignored all cells that had a value of 0 in the possibility of inundation and flood uncertain inundation maps. Therefore, the 0 values that appeared in the subsequent computed values of D_j correctly depicted a scenario of perfect non-bias. A histogram of the D_j values was created to analyse the nature of the bias.

5.4 Results

The outputs of the Monte Carlo simulation runs corresponding to model state 1 and 2 were compared against the respective deterministic inundation maps and the goodness-of-fit was measured with the F index (Equation 2). Figure 5.9 and Figure 5.10 indicate

the performance of the Monte Carlo simulations in relation to the four uncertain parameters in dotty plots. Considerable equifinality for all the uncertain parameters was noticed, indicating that similar accuracy in the predicted output was achieved using a range of values within each parameter. Despite this overall trend, Figure 5.9a illustrates that a lower roughness coefficient for the channel (0.026 to 0.030) for deriving the discharge from stage (InQnch) generally had less cases with poor model performance and none of the cases that used higher roughness coefficients (0.035 - 0.038) attained a goodness-of-fit of more than 0.36. However, this definite trend is not found for InQnch at model state 2, when the river level was down to almost the pre-flood level (Figure 5.2). Later at this stage the performance of the model was quite poor and the highest goodness-of-fit figure attained was a modest 0.28, but the model showed less equifinality and the advantage of using a smaller InQnch value is evident (Figure 5.10a).

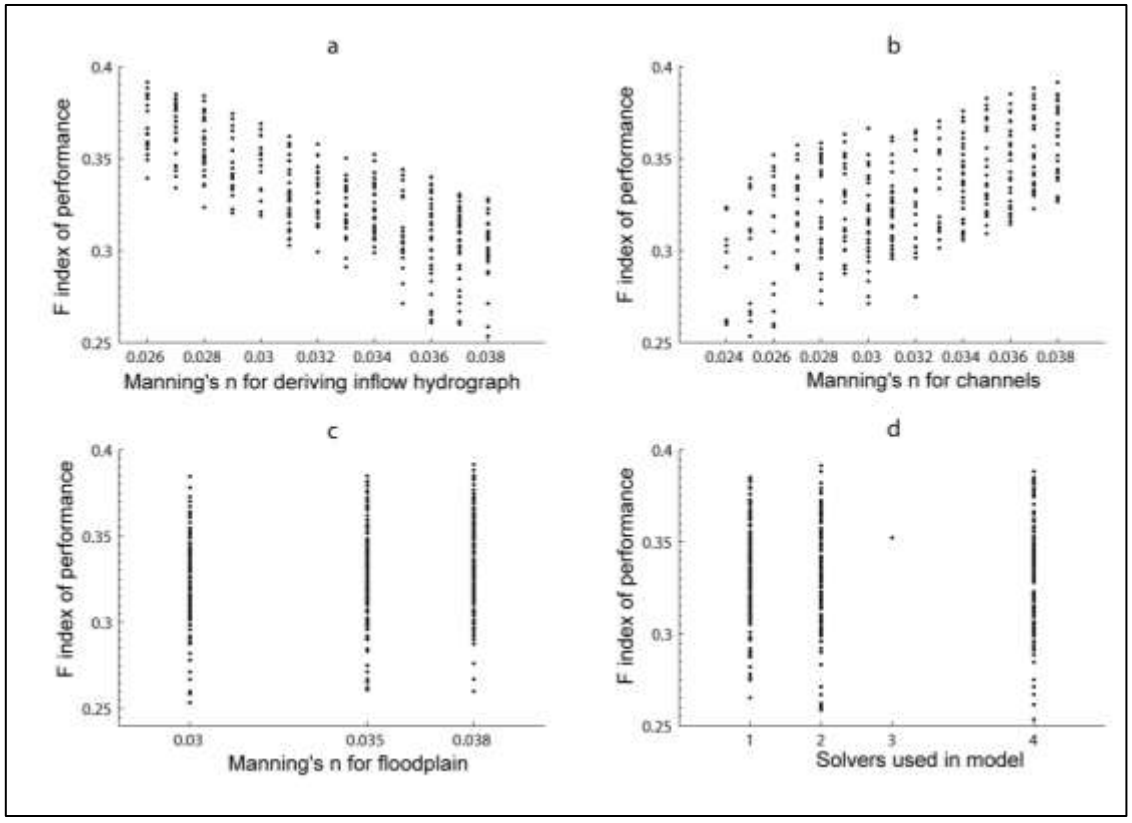

Figure 5.9 Dotty plots showing the performance (F index) of the TELEMAC2D model to simulate inundation extent at model state 1 in relation to (a) Manning's n for deriving the inflow hydrograph from stage data (InQnch), (b) Manning's n for the channels (nch), (c) Manning's n for the floodplain (nfp), and (d) the solver used for solving the system of equations

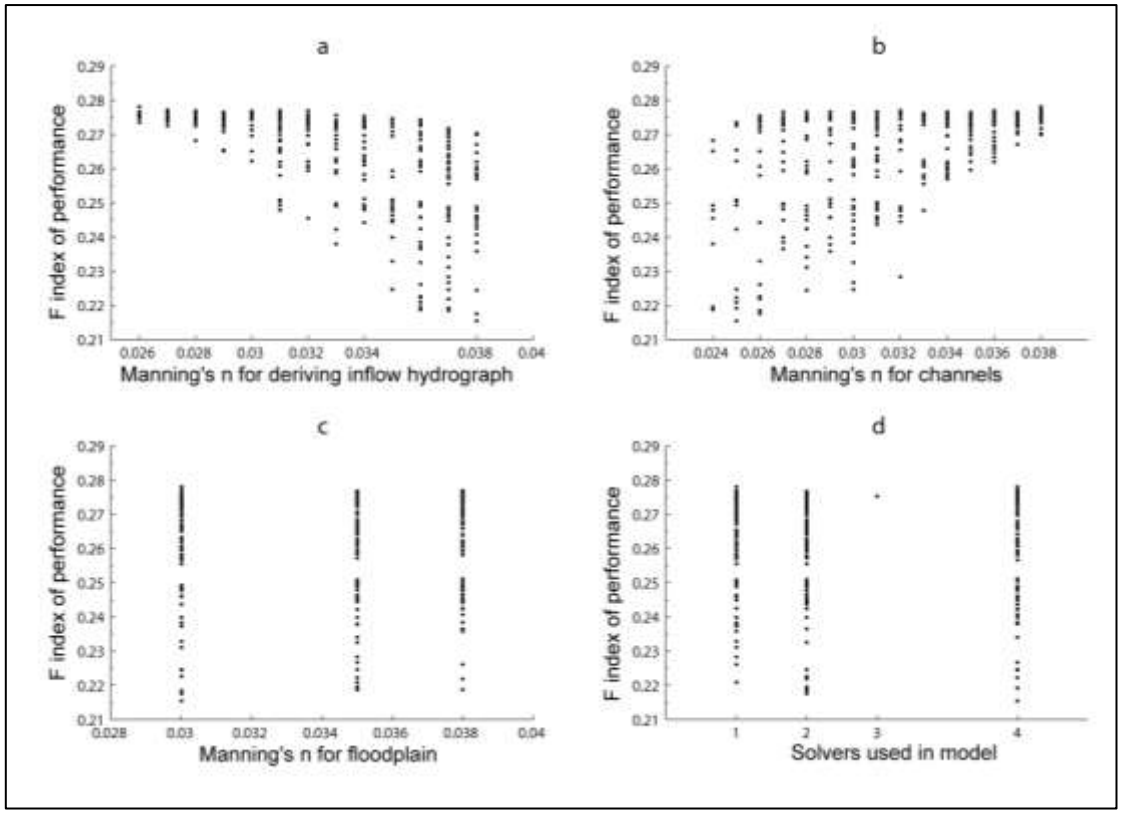

Figure 5.10 Dotty plots showing the performance (F index) of the TELEMAC2D model to simulate inundation extent at model state 2 in relation to (a) Manning's n for deriving the inflow hydrograph from stage data (InQnch), (b) Manning's n for the channels (nch), (c) Manning's n for the floodplain (nfp), (d) The solver used for solving the system of equations.

The Manning's roughness coefficient for the channels (nch) shows an overall trend of equifinality for just after the flood-peak (model state 1) with similar levels of goodness-of-fit attained using wide range of nch values. However, a trend of achieving higher goodness-of-fit against a deterministic observed inundation maps with higher nch values is evident (Figure 5.9b). A clear trend of higher relative accuracy with increasing value of nch emerges at the model state 2 (Figure 5.10b) but occasionally the model performed equally well with low nch values.The model outputs were found to be completely insensitive to Manning's roughness coefficient for the floodplain and the choice of the solver in TELEMAC2D at the two stages of the flood under consideration (Figure 5.9c, 5.9d and Figure 5.10c, 5.10d). The effect of the Manning's n values used for the floodplain in order to deriving the inflow hydrograph (InQnfp) also had little influence over model performance and hence was not included in the dotty plots.

The probability of inundation maps (Figure 5.11) show that both at model state 1 and 2 the occurrence of the inundated surface is patchy and not necessarily found adjacent to the channels. A substantial portion of the total area under flooding has been modelled as inundated in majority of the Monte Carlo realisations. These areas have a very high likelihood of inundation (0.9 - 1) in Figure 5.11 and are depicted in black. Lower probability of inundation (shades of grey) is observed at the periphery of the high probability areas.

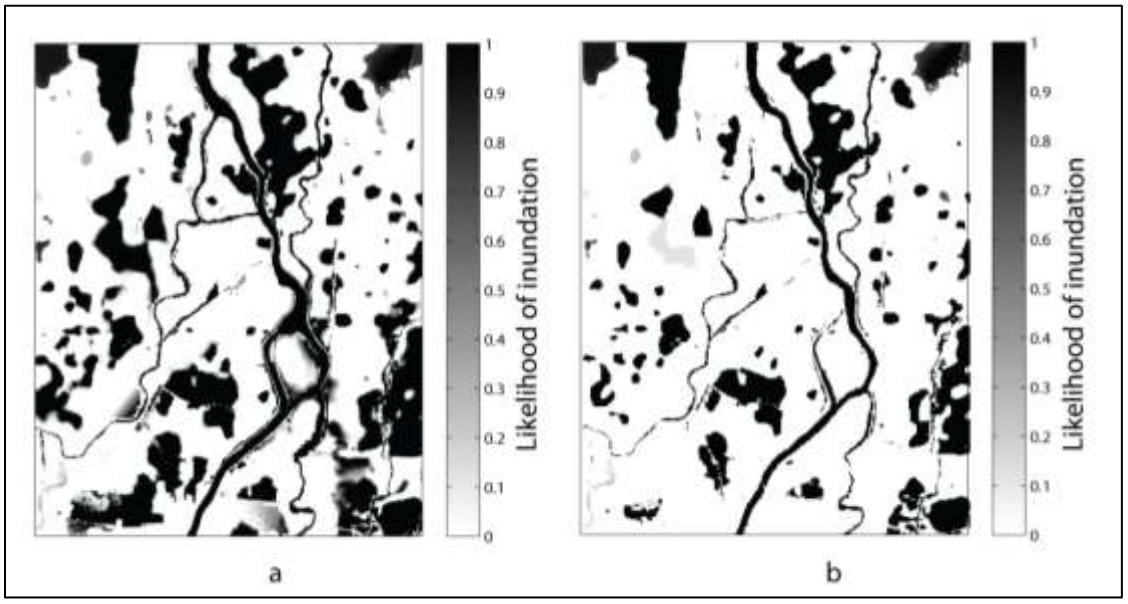

Figure 5.11 Probability of inundation maps derived from the deterministic binary inundation maps showing the likelihood of the model predicted inundation area on (a) model state 1 and (b) model state 2.

The flood uncertain inundation map (Figure 5.12) created by incorporating the uncertainty of satellite derived inundation map into the probability of inundation map shows a quite similar pattern as the probability of inundation map (Figure 5.11). However, if we consider the pixel values of Figure 5.11 and Figure 5.12 as a measure of likelihood of flooding we notice certain subtle differences in the spatial distribution of these figures. In order to examine the nature and causes of these differences the probability of inundation map for the model state 1 (Figure 5.11a) was subtracted from the flood uncertain inundation map (Figure 5.12a) of the same model state on a pixel-by-pixel basis to produce Figure 5.13. It shows that the difference is pronounced at three type places: 1) at the periphery of the areas that have a very high likelihood of being modelled as flooded, 2) the areas where complex hydraulic processes take place

such as the river island at the centre, 3) areas in the extreme south near the left bank of the Mundeswari River and the northeast corner of the model domain where the possibility of inundation map (Figure 5.4) indicates lower level of confidence on the observed inundation data. In general, the areas that fall outside the highly likely modelled inundation zones, and are having uncertainty in the observed inundation data (Figure 5.4a) are the places where the probability figures in Figure 5.11 and Figure 5.12 tend to differ.

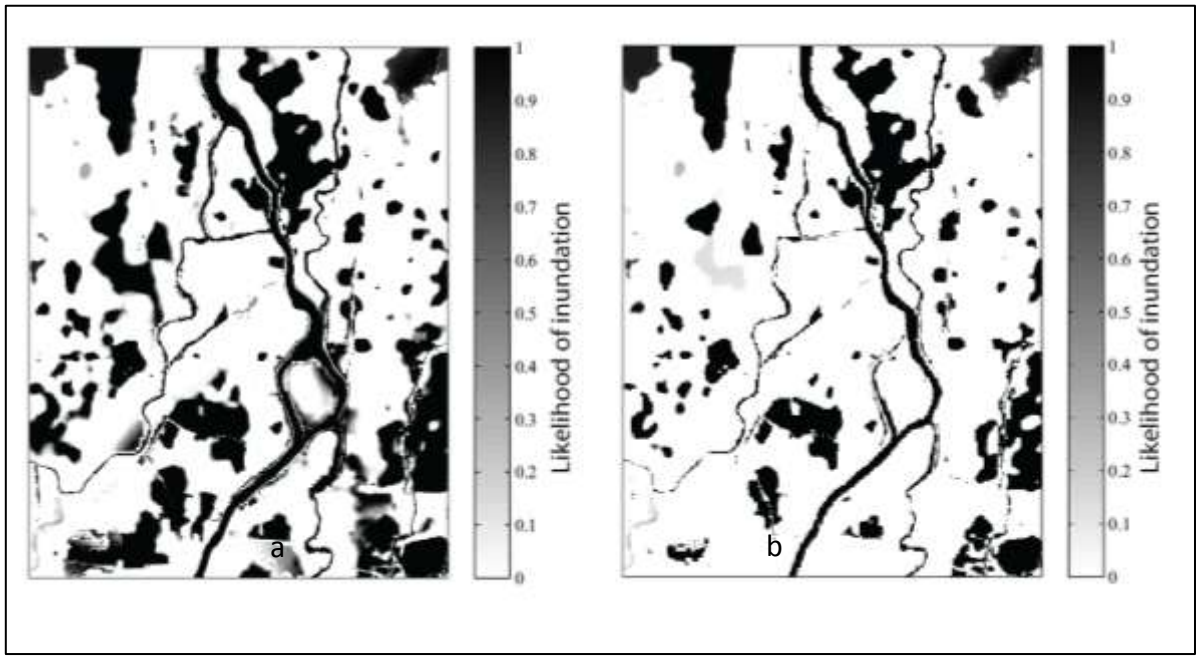

Figure 5.12 Flood uncertainty inundation maps on (a) model state 1 and (b) model state 2.

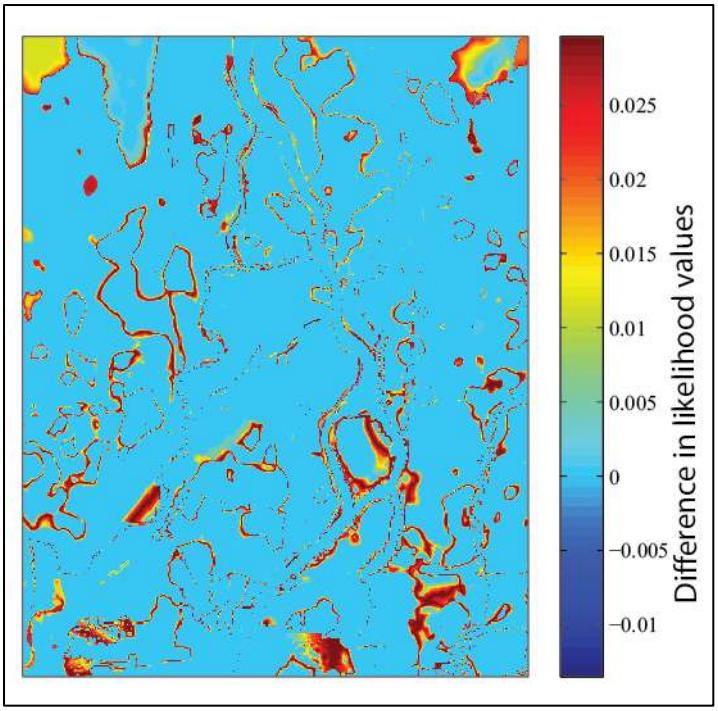

Figure 5.13 Difference in probabilities derived by subtracting probability of inundation from flood uncertain inundation for the model state on 10 AM, 12th September, 2009. The pixels with warm colours show the area where flood uncertain inundation is higher than probability of inundation.

The histogram of the D_j values (Figure 5.14) was created to test the tendency of bias in the model output for the model state 1. It shows a bimodal distribution with one peak around 0 and another around -1. The peak around 0 is a sign of little or no bias between the modelled and observed probability of inundation. The other peak of -1 is an indication that a substantial portion of the observed flooded area was simulated as dry by the model (underestimation). Since the quantity D_j was calculated as flood uncertainty inundation *minus* possibility of inundation, the value of -1 indicates the cells that were 0 in modelled output but 1 in the possibility of inundation map. Here the value 0 signifies that none of the successful Monte Carlo simulation predicted those cells as wet and 1 represents the cells that were classified as flooded by all four digital image processing methods.

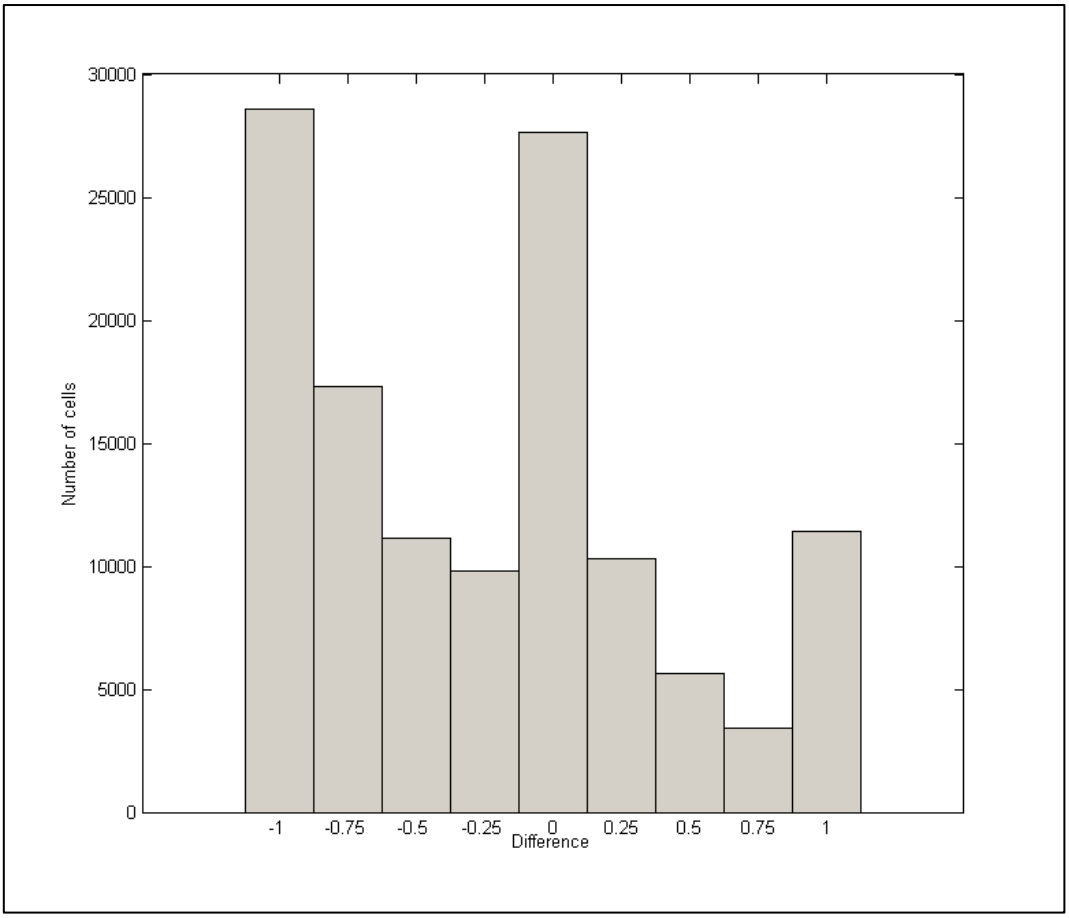

Figure 5.14 Histogram of Dj values. The peak around 0 shows a lack of bias in the flood uncertain probability map but the peak around -1 illustrates that a substantial portion of the observed flooded area is underpredicted by the model.

5.5 Discussion

The parameter InQnch, the Manning's n values for the channel in order to derive discharge data from river level observations at the model inlet, affected the performance of TELEMAC2D in a different fashion at two flood states under consideration. An increase in the value of InQnch results in less discharge for a given river stage and vise versa. The overall accuracy of predictions for the model state 1decreased steadily with a reduction in the inflow of water in the model domain (Figure 5.9a). At a later stage of the flood (model state 2), however, the model was found to be less sensitive to the variation of inflow discharge and performed with equal accuracy for a range of inflow hydrographs resulted from random variation in InQnch values during the Monte Carlo runs (Figure 5.10a). There are two possible reasons for this model behaviour. First, at a very high river stage on the model state 1, slight

differences in the channel roughness coefficient led to considerable increase in the computed discharge values. A decrease in the supply of water at the inlet possibly amplified the problem of underprediction, particularly in the western section of the model domain, resulting in decline in the model performance score. Secondly, during the model state 2 when the river level is well below its bankfull depth, the change in discharge values had little impact on the modelled flood extent maps. At this stage the model efficiency mostly depends on the strength of its wetting and drying algorithm which is also very much dependent on the resolution and accuracy of the input terrain data.

The areas represented in very dark tones in the probability of inundation maps (Figure 5.11) or the flood uncertain inundation maps (Figure 5.12) do not imply a very high actual probability of inundation, are instead highly likely to be modelled as inundated by the existing inundation modelling setup. A comparison of Fig 5.11 with Fig 5.5 reveals that the drying process of the model could not fully reproduce the actual pattern of drying between the two stages (from 12th September to 15th September, 2009) of this flooding event. The model showed little sensitivity to the reducing inflow from 12th to 15th September when simulating inundation at the extreme upper portion of the image. This was probably due to the coarse quality of the terrain data, especially over the farmlands which was mostly derived from the SRTM DEM. The existence of large flat areas with small variations in relief was probably responsible for the poor performance of TELEMAC2D in terms of draining shallow water from parts of the floodplain. This overestimation of the flooded area is also manifested in Figure 5.13. It shows a considerable number of pixels with a D_j value of 1 indicating the pixels that were modelled as wet but not classified as inundated using any of the image processing techniques. The issue of underestimation of the model as represented by the mode around -1 in Figure 5.13 was mainly attributed to the existence of two rivers at the edge of our study area which concurrently experienced flooding with the Mundeswari River. The flood water in the central west of the study area (Figure 5.4) was partly contributed by another river which was not considered for this study. The existence of such widespread inundated patches at the western edge of the study area (Figure 5.4) at such distance from the main channel is unusual and further supports our general inference

that the underestimation in our model is partly attributed to some external factors that were not within the scope of the present experiment.

Running numerous Monte Carlo simulations in TELEMAC2D is a very computationally intensive task, and therefore it is beneficial to avoid unstable model runs that may use considerable amount of computational resource before the numerical instability exceeds the tolerance level. We found that the low channel roughness values had a high incidence of instability (Figure 5.6) and that their use did not lead to best model performance, at least near the peak of the flood (Figure 5.9b). Likewise, use of the squared conjugate gradient method (Solver 4) did not result in general improvement of the model performance (Figure 5.9d and Figure 5.10d) but took much more computation time than the other solvers (Figure 5.7). We acknowledge that model stability depends on the complex interplay between the chosen parameter space, model inputs and the physical characteristics of the model domain. Due to these factors every inundation modelling experiment will have a unique pattern of model stability. However, a small but representative subset of the entire range of parameters may be used to perform some pilot runs to understand the incidence of instability with reference to the choice of parameter space.

5.6 Conclusion

The present study is an effort to quantify the predictive uncertainty in inundation modelling with sparse data in a complex fluvial system. We undertook a GLUE-based uncertainty assessment of the simulated flood extent at two stages of the descending limb of a flood hydrograph using TELEMAC2D model. The uniqueness of this study lies in adapting the existing techniques of uncertainty assessment for data-poor regions. Our study highlighted that the spatial distribution of uncertainties in an area with anabranching channels depends on 1) the ability of the model to simulate the actual hydraulic processes, 2) the state of the flood under consideration in relation to the occurrence of the flood peak, and 3) the amount of consistent bias in the model output arising from sparse nature of the model inputs (e.g. terrain). We observed that the portions of the modelled flood-extent maps were less sensitive to change in important

inputs, such as the inflow hydrograph. This type of model behaviour can be attributed to the lack of detailed floodplain topography for portions of the model domain.

Incorporation of varying confidence levels in the spatially distributed observed data, as opposed to the deterministic flood maps, is not likely to make much difference in the uncertainty computation unless the model inputs are of high resolution. In this situation it is hard to justify the additional computation procedure to incorporate the probabilistic observed data in examining the uncertainty. Therefore we recommend the use of deterministic flood-extent maps in data-sparse study sites for uncertainty assessment. The uncertainty assessment of a fully 2D finite element model has never been attempted with sparse inputs in areas of multiple channel bifurcations. Hence, the findings of this paper will be helpful in judging the limitations of a similar modelling task where ideal model inputs and validation data sets do not exist.

Chapter 6

Analysing the effect of land-use/cover changes at sub-catchment levels on the downstream flood peak: a semi-distributed modelling approach with sparse data

Abstract

This paper aims to evaluate how varying degrees of land use/cover (LULC) changes across sub-catchments affects the flood peak at the catchment outlet. The Konar catchment, a part of the upper Damodar Basin in eastern India, was the study site. A HEC-HMS model was set up to simulate rainfall-runoff processes for two LULC scenarios three decades apart. Because of sparse data at the study site, we used the Natural Resource Conservation Service (NRCS) Curve Number (CN) approach to account for the effect of LULC and soil on the hydrologic response. Although a weak ($r = 0.53$) but statistically significant positive linear correlation was found between sub-catchment wise LULC changes and the magnitude of flood peak at the catchment outlet, a number of sub-catchments showed marked deviations from this trend. The varying timing of flow convergence at different stream orders due to the localised LULC changes makes it difficult to upscale the conventional land use and runoff relationship, evident at the plot scale, to a large basin. However, a simple modelling framework is provided based on easily accessible input data and a freely available and widely use hydrological model (HEC-HMS) to check the possible effect of undertaking remedial land use planning at a particular sub-catchment on the hydrograph at the basin outlet.

Keywords: Land use/cover, peak discharge, NRCS CN, HEC-HMS, Sub-catchment, Flow Convergence Timing.

6.1 Introduction

Soil, topography and land cover are the most important factors that control rainfall-runoff processes at the scale of single flood events for river basins. As alterations in soil and topography are insignificant in the short term, changes in land cover are considered to be the key element in modifying rainfall-runoff processes (Miller et al., 2002). Land-use/land-cover (LULC) change and any consequent hydrological response have been prominent topics of research in recent years (Chen et al., 2009; Amini et al., 2011; Fox et al., 2012). With changing climate and the increasing frequency of flooding events across the world (Collins 2009; Hurkmans et al. 2009; Xu et al. 2009), the effects of LULC changes on extreme runoff events are likely to draw more attention.

Wan and Yang (2007) concluded that anthropogenic land use change is one of the major drivers of an increased frequency of flooding incidents. At small spatial scales (< 2 km^2) deforestation was reported to have strong correlation with increase in flooding (Bosch and Hewlett, 1982). However, the picture is less clear for larger catchments, where a number of studies have reported no significant change in flooding pattern with deforestation (Beschta et al., 2000; Andréassian, 2004) while others have observed even a negative trend in flood occurrence with reductions in forest cover (Troendle and King, 1985; Hornbeck et al., 1997). Wei et al. (2008) linked deforestation with reduction in peak flow. Van Dijk et al. (2009) came to the conclusion that the empirical evidence and theoretical arguments for increased flood intensity with removal of forest are not very convincing. Shi et al. (2007) reported that high antecedent moisture conditions reduce the effect of increased urbanization on runoff in a small 56 km^2 catchment in Shenzhen, China. Sriwongsitanon and Taesombat (2011) observed a non-linear relationship between the runoff coefficient and flood peaks and further reported a negative correlation between runoff coefficient and increase in forest cover for smaller flood events (< 2 year return period).

A number of studies have attempted to analyse the impact of land-use change on storm runoff at the event scale (Chen et al., 2009; Ali et al., 2011; O'Donnell et al., 2011). LULC scenario-based studies have used past and present LULC states or radical LULC change scenarios in event-scale hydrological models to assess the hydrological

response of catchments (Camorani et al., 2005; Olang and Furst, 2011). Chen et al. (2009) coupled a LULC scenario-generation model with a hydrological model and concluded that increasing urban areas led to increase in the total runoff volume and peak discharge of storm runoff events. Ali et al. (2011) conducted an event-scale experiment in a predominantly urbanised catchment containing the city of Islamabad in Pakistan and had similar findings. It is noted that this type of study is generally restricted to small urban catchments and it is not surprising that their findings coincide with the conventional wisdom that reduction in forest or increase in paved surface leads directly to increased runoff. An over-emphasis on the effect of afforestation and urbanization and lack of interest in examining the LULC changes in river basins with diverse LULC types have been the characteristics of recent research on the effect of land-cover change in flooding (Wan and Yang, 2007).

The contribution of streamflow from a specific land use is not uniformly proportional to the area of that land use and depends greatly on the location of that land use within the basin (Warburton et al., 2012). This study further showed that the streamflow response at the basin outlet is influenced by the spatial distribution of various land uses present in the entire catchment and the balancing or cancelling effect of those land uses. For example, where urbanization takes place in the upper sub-catchments, it leads to a disproportionately larger increase in the flood peak downstream (Amini et al. 2011). Fox et al. (2012) found that the additional surface runoff generated by expanding urban area or reducing forests are counterbalanced in a positive way by augmentation of channel capacity resulting from improved channel management, particularly at the vicinity of major urban areas.

The primary application of findings from investigations dealing with LULC change and its effect on downstream flood peaks is in watershed management. Watershed management strategies often aim to identify the source area that generates a significant contribution to the downstream flood peak and implement remedial land use practices to reduce the runoff coefficient from this flood source area. As with the effects of LULC change on catchment hydrology, the effects of land management have been convincingly documented by studies involving small catchments (Bloschl et al., 2007; O'Connell et al., 2007). Implementation of land-use management practice is only worth pursuing if we can identify the sub-catchments that are responsible for exaggerating the

downstream flood peak in terms of magnitude and timing of the flow convergence (Pattison et al., 2008). Pattison and Lane (2012) reviewed this topic of possible relation between land-use change and possible downstream flood risk and pointed out that it is not uncommon to find an association between land-use change and streamflow behaviour at field and plot scales but it is quite challenging to upscale this effect to show similar hydrological responses for large catchments. Analysis and identification of the flood source area and its contribution at the cumulative basin outlet has been carried out with hydrologic modelling using the HEC-HMS model (Saghafian and Khosroshahi 2005; Roughani et al., 2007; Saghafian et al. 2008) and with statistical approaches involving rainfall and runoff data at the sub-catchment level (Pattison et al., 2008). Recently, Ewen et al. (2012) attempted to model the causal link between LULC changes at small scale to the flood hydrograph at the basin outlet by using reverse algorithmic differentiation and showed the sources of imact at the scale of small tiles that were used to decompose the model domain.

The statistical approach by Pattison et al. (2008) and the modelling approach described by Ewen et al. (2012) are heavily dependent on a dense network of automatic rain and river gauging stations and are not possible to follow in a data scarce environment, which is typical in developing countries. Although a variety of hydrological models are available it is difficult to use them in data scarce environment such as India due to their requirement in terms of soil moisture and channel topography related data. The US Natural Resources Conservation Service (NRCS) curve number (CN) approach for runoff estimation is particularly suitable for applying in data scarce situations and has been widely used to estimate surface runoff in an accurate manner with limited data (Bhaduri et al, 2000; Mishra et al, 2003). The CN is an empirically derived dimensionless number that accounts for the complex relationship of land cover and soil and can be computed with widely available datasets such as satellite-derived LULC maps and small scale soil maps. Easy integration of remotely sensed LULC information has made the NRCS CN a popular choice among the scientific community for runoff estimation from the early days of remote sensing (Jackson et al., 1977; Slack and Welch 1980; Stuebe and Johnston 1990). For a typical data-poor, developing country such as India there are numerous case studies that used remote sensing for deriving CN in order to estimate runoff at catchment scale (*e.g.* Tiwari et al., 1991; Sharma and Singh, 1992; Amutha and Porchelvan, 2009). However, the strong seasonal pattern of

land-use in monsoon climates has not been highlighted when comparing the hydrologic response of two land use scenarios observed over a period of few decades. Changing canopy cover and the proportion of cultivated land and other land covers may exert considerable control over rainfall-runoff processes.

The investigations to date have mostly dealt with the issue of LULC change across the catchment as a whole. However, as pointed out by Pattison et al. (2008), remedial land management practices are conceived and implemented at the sub-catchment scale. Although the modelling-based approach by Saghafian et al., (2008) and Roughani et al. (2007) attempted to identify the sub-catchments that have serious impact over the flood peak (flood source area) at the main catchment outlet, they did not assess how changes in LULC across the sub-catchment may change the location of the flood source area. There is a need for a systematic evaluation of sub-catchment wise LULC change and resultant changes in priority areas for implementing remedial land-use measures. LULC can change significantly in short periods, and the occurrence of LULC change in different parts of the catchment is likely to affect the flood peak at the catchment outlet in a complex manner.

This study is part of a broad investigation that deals with developing an adequate system for routing flood waves in the lower Damodar River in eastern India with freely available data and minimum ground survey (Chapter 4) and modelling widespread floodplain inundation at a frequently flooded reach further downstream using low-cost high resolution terrain data (Chapter 5).

The objective of this study is to investigate (1) the effect of LULC change at sub-catchment level over the peak discharge at the catchment outlet during storm events, and (2) the interplay between sub-catchment position, LULC change and runoff. The findings of this paper have a direct bearing on land-use management practices that are undertaken to reduce the peak inflow to reservoirs during storm events. The uniqueness of this investigation lies in the establishment of a direct link between sub-catchment scale LULC changes and their changing contribution to the flood peak at the basin outlet through semi-distributed rainfall-runoff modelling. In addition, this study also points out the typical challenges of modelling rainfall-runoff processes in data scarce environments and the required adaptations in methods to deal with this constraint.

6.2 Study Area

The Konar Reservoir is impounded by one of the four major dams in the upper catchment of the Damodar River in eastern India (Figure 6.1). The catchment upstream of the reservoir is a typical example of physiographic, drainage and LULC conditions in the upper Damodar basin. A number of previous authors (e.g. Choudhury, 2011; Ghosh, 2011; Bhattacharyya, 1973) have argued that deforestation in the upper hilly and forested catchments in the upper Damodar basin has increased both the runoff coefficient and flood peak, and has reduced the capacity of the four reservoirs to moderate flood waves downstream. The catchment also exemplifies the scarcity of required data for hydrological modelling, which is a typical scenario in the developing countries. The catchment is drained by the Konar and Siwane Rivers and is 998 km^2 in size. The topography is characterised by a dissected plateau region with occasional hills. Elevation ranges from 402 to 934 m asl. The upland areas in the catchment are mostly under forest cover while paddy cultivation during the monsoon season is the dominant land use in the lower reaches. Rainfall has a strong seasonal pattern which is heavily influenced by the southwest Indian monsoon. Torrential rain for a few hours per day during the monsoon season (mid June to mid October) often leads to high magnitude river discharge in this part of the Damodar Basin.

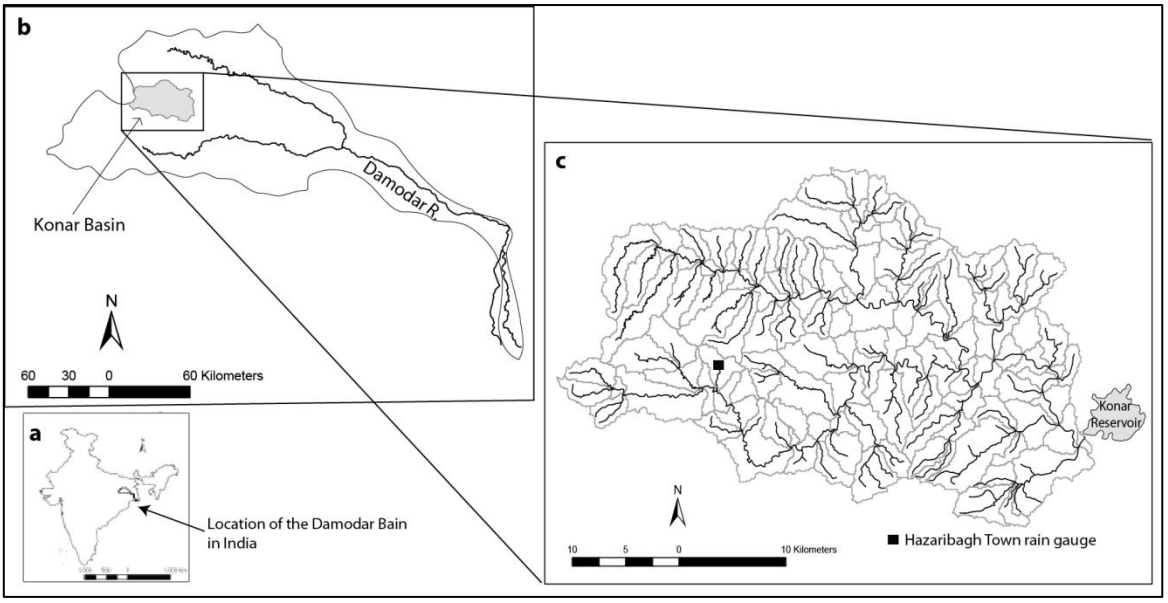

Figure 6.1 The Study area; a: Location of the Damodar Basin In India, b: Location of the Konar River catchment in the Upper Damodar River Basin, c: The sub-catchments of the Konar River derived from the SRTM DEM with dark lines showing the streams vectorised from topographic maps. Automatically extracted drainage networks (derived from the SRTM DEM with a threshold contributing area of 5 km^2) that approximately correspond with the 2nd order streams from the topographic maps were used to delineate the 124 sub-catchments.

6.3 Materials and Methods

6.3.1 Generating curve numbers for two LULC scenarios

The NRCS CN model is appropriate for use in data-sparse situations because the primary model inputs are LULC and soil types that are easy to obtain from remote sensing and widely available soil maps. The NRCS method of estimating runoff due to rainfall (NRCS, 1972) is expressed in the following equations:

$$Q = 0 \qquad P \leq 0.2\,S \qquad (1)$$

$$Q = (P - 0.2\,S)^2/(P+0.8S) \qquad P \geq 0.2S \qquad (2)$$

where Q is the direct runoff, P is the storm rainfall, and S in the potential maximum retention. S is related to a dimensionless curve number, CN by:

$$S = (254000/CN) - 254 \qquad (3)$$

In this method soil types are classified into four hydrological soil groups (A, B, C, and D) with increasing potential for generating runoff. Hydrological soil groups of any area can be identified by analysing soil texture. The method also considers the antecedent soil moisture condition by providing modified value for dry (AMCI) and wet (AMCIII) condition based on the preceding 5 days' daily rainfall.

In order to assess the impact of different land-cover scenarios on the peak flood discharge at the entry of the Konar Reservoir, two land-cover maps were generated from satellite imagery. A Landsat MSS image (79 m spatial resolution) from 27th October, 1976 and a Landsat TM image (30 m spatial resolution) from 2nd November, 2004 were used for generating two LULC maps. These two dates were chosen as this is the largest possible timespan that was possible to capture with due considerations to the availability of cloud-free images at the final stage of the southwest monsoon season when the flood events considered took place.

Unsupervised classification was used to classify each image into 30 arbitrary spectral classes. In the next step, the spectral classes were compared with a high resolution panchromatic Corona satellite image from 21st November, 1973 and a topographic map (1:50,000 scale) from the Survey of India (Map No. 73 E/5) which was surveyed in 1978-79. Similar classes were combined appropriately to create a land-cover map for 1976. High resolution imagery available in GoogleEarth for 15th November, 2004 was utilised for the same purpose in order to classify the Landsat TM image of 2004. Finally we generated two LULC maps with following classes: 1) water body, 2) rocky waste, 3) urban area, 4) paddy field, 5) shrub, 6) open forest, and 7) dense forest. There is a potential problem in comparing LULC changes from pixel to pixel between the two time periods because of the use of different sensors for acquiring the two images. However, Landsat MSS and TM data have been successfully used with unsupervised classification for identifying changes of broad land cover categories in Africa (Brink and Eva, 2009). The spectral resolution of Landsat MSS and TM for Band 1, 2 3 and 4 are quite close and we only attempted to identify the broad land cover classes that are identifiable in the coarse resolution Landsat MSS images. Post-classification comparison of the LULC maps for the two time period is likely to eliminate most of the discrepancies arising from the use of different sensors and spatial resolution. Due to the limitation of the spatial and spectral resolution of the available satellite imagery,

identifying land-cover classes for which a CN value is available in standard lookup tables was not always possible and an adjustment of the CN table was necessary to get optimal runoff estimates using the NRCS-CN approach (Kumar et al., 1991). We used the CN lookup table compiled by Tripathi et al. (2002) for land-use and soil texture classes in the Nagwan sub-catchment, a part of the Konar Reservoir catchment, except that the CN value for paddy fields was taken from Shi et al. (2007); the table in Tripathi et al. (2002) classified the paddy fields as upland and lowland paddy, but it was not possible to distinguish these in our land-cover classification. Hydrologic soil groups of the study area were determined by consulting the composition and texture of the soil types obtained from the soil maps of National Bureau of Soil Survey and Land Use Planning, India (NBSS&LUP). The land-cover maps and hydrologic soil groups map were combined using the lookup table in GIS to create CN maps for 1976 and 2004.

6.3.2 Setting up the rainfall-runoff model

The HEC-HMS modelling suite was chosen for simulating the rainfall-runoff process, as this model has a host of modelling options for computing the runoff hydrograph for each sub-basin and routing it through river reaches at the basin outlet (Beighley and Moglen, 2003). HEC-HMS has the option of using the NRCS CN method for computing direct runoff volume for a given rainfall event, which is a popular modelling choice for application in the data scarce environment (Olang and Furst, 2011; Candela et al., 2012; Du et al., 2012; Jia and Wan, 2011; Amini et al., 2011). The model has a GIS pre-processor known as HEC-GeoHMS which was used for extracting and integrating GIS data such as DEM, LULC and soil maps into the hydrological model.

A total of 124 sub-catchments were delineated from the SRTM DEM in the Konar catchment during the pre-processing stage in HEC-GeoHMS. The streams were vectorised from the topographic maps of the study area for use as a reference for guiding the automated sub-catchment delineation from the SRTM DEM. Das et al. (1992) used Strahler's stream ordering technique to identify the optimal basin size for NRCS-CN-based estimation of runoff volume for part of the upper Damodar River basin and this principle was used in our study. After filling the sinks a threshold contributing area of 5 km^2 was found suitable to delineate the streams that in general match the 2nd-order streams in the topographic maps. Due to the coarse nature of the

SRTM DEM we could not automatically extract the 1st order streams as found in the topographic maps.

Sub-daily rainfall is an essential input for simulating storm runoff, particularly in tropical region where high intensity rainfall for a few hours often leads to flooding. We obtained rainfall figures at 1 hour intervals for a storm event lasting from 11 to 12 October, 1973 from a autographic rain gauge located in Hazaribagh Town (Figure 6.1). The data are supplied by the Indian Meteorological Department (IMD). In order to validate the accuracy of the model for the 2004 land cover scenario we used a storm rainfall event from 8-10 October, 2003, which was estimated by the 3B42 V6 product of the Tropical Rainfall Measuring Mission (Huffman et al., 2007). No gauged sub-daily rainfall data was available after 1976 as the autographic rainfall station has been defunct since then. The October, 2003 event was deemed most appropriate as the CN values for 2004 derived from a Landat TM image acquired on 2nd November reflected a land cover that is very similar to the prevailing LULC situation when the storm event of 2003 took place. It has been reported that TRMM data frequently do not match with *in situ* observations. For this reason, the area averaged 3-hourly 3B42 V6 TRMM data for the Konar catchment were summed into daily totals and compared with the daily rainfall product of the Indian Meteorological Department (Rajeevan and Bhate, 2008) which is derived from rain gauges and supplied in 0.5 degree gridded format. We found that the TRMM records for the 3 days (8-10 October, 2004) was only 3.7% higher than the IMD figures. After considering the preceding rainfall of last 5 days for the 1973 and 2003 events from the daily rainfall products of IMD we decided that the antecedent moisture condition was normal (AMCII) (35-53 mm) for the 1973 event but it was dry (AMCI) (> 35 mm) for the 2003 event. Hence, the normal CN values for the 2004 land cover scenario were converted to AMCI using the formula proposed by Mishra et al. (2008):

$$CN_I = CN_{II}/(2.2754 - 0.012754\, CN_{II}) \quad (4)$$

As four TRMM tiles cut across the Konar catchment, we downloaded and stacked 3-hourly gridded TRMM data for those four tiles for the storm period and extracted the pixel data into a time series. In the next step, four artificial rain gauges were created in HEC-HMS for the NW, NE, SW and SE portions of the Konar catchment and the

gauges were populated with the extracted pixel values of the corresponding TRMM grid. In this way we managed to use quasi-distributed rainfall data into HEC-HMS for simulating the 2003 storm event.

The NRSC unit hydrograph lag method was used for computing the basin lag which is necessary for transforming the excess rainfall (or direct runoff volume) into runoff into the channels. Finally, the Muskinghum-Cunge flow routing model was employed to route the flow through the channels to the outlet. Initially the model was run with the hourly rainfall of 11-12 October, 1973 and the CN values (AMCII) derived from the 1976 land cover map and the results were compared with the available daily runoff volume at the entry point of the Konar Reservoir (basin outlet). We attempted to calibrate this HEC-HMS model with the Manning's roughness coefficients of the reaches. Initially the roughness coefficients for each reach were decided with the method described in Arcement and Schneider (1989) by combining information on channel properties like bed materials, morphology, presence of obstructions and extents of meandering in an approximate manner as apparent from the topographic maps and the high resolution images in GoogleEarth.

The model was calibrated against observed total daily runoff volume (in hectare m/day) records at the outlet of the Konar basin which was supplied by the Damodar Valley Corporation (DVC). No sub-daily measurement in m^3/s was available. During the calibration runs the coefficients were increased and decreased by 10 and 20% of the initial estimate. The model showed very little sensitivity to the roughness coefficients in terms of the improved performance against the observed daily runoff data. Hence, we decided to use the initial estimates for the subsequent runs. In the next step, the model was run with the 3-hourly TRMM rainfall of 8-10 October, 2003 with the CN values (AMCI) of 2004 and the hydrograph in terms of daily runoff volume was compared with the observed data. Following Knebl et al. (2005) and McColl and Agget (2007) it was anticipated that evapotranspiration losses would be negligible as the interest of this study is in high intensity monsoon storms that lead to flooding. Since our model only simulated the direct runoff, we derived the base flow component from the observed data graphically by joining the point of infections of the rising and falling limb of the hydrograph and eliminated this flow component in order to make the observed and modelled figures comparable.

The relationship between changing LULC patterns in the sub-catchments of the Konar catchment and the peak rate of discharge at the reservoir inlet was assessed by computing the unit flood response (Saghafian and Khosroshahi, 2005) of each of the 124 sub-catchments for the LULC scenarios of 1976 and 2004. The unit flood response approach can be used to standardise the contributions of sub-catchments to the peak flow. With changing land use, the unit flood response of various sub-catchments within a catchment is likely to change. The storm event of 11-12 October, 1973 was used as the meteorological input in both scenarios. The unit flood response approach ranks each sub-catchment on the basis of their contribution to the flood generation at the basin outlet and is expressed by

$$f = \Delta Q_p / A \qquad (2)$$

where f ($m^3/s/km^2$) is unit area flood index, ΔQ_p is the amount of decrease in peak discharge at the basin outlet due to elimination of a particular sub-catchment (m^3/s), and A is the sub-catchment area (km^2). A version of the HEC-HMS model containing all basin components was saved. In order to compute f for each sub-catchment, the HEC-HMS model was placed in a working directory and only that particular sub-catchment was deleted from the basin component keeping the connectivity intact for the entire model. Consequently, the f value was calculated by subtracting the flood peak produced by all but the sub-catchment under consideration from the flood peak considering all sub-catchments.

6.4 Results

The changes in LULC for the entire Konar catchment from 1976 to 2004 (Figure 6.2) show considerable increase in rocky waste and decreases in the areas under paddy cultivation and open forest (Table 6.1).

Table 6.1 Percentage coverage of different LULC categories for 1976 and 2004 and the changes between the two time periods.

	LULC Classes	**Percentage Cover 1976**	**Percentage Cover 2004**	**Difference in Percentage Cover (2004 - 1976)**
1.	Water body	5.4	5.9	0.5
2.	Rocky wasteland	9.7	24.2	14.5
3.	Urban	0.1	8.2	8.1
4.	Paddy Field	42.3	20.9	-21.4
5.	Shrub	9.6	23.2	13.6
6.	Open Forest	26.5	14.5	-12
7.	Dense Forest	11.3	8.2	-3.1

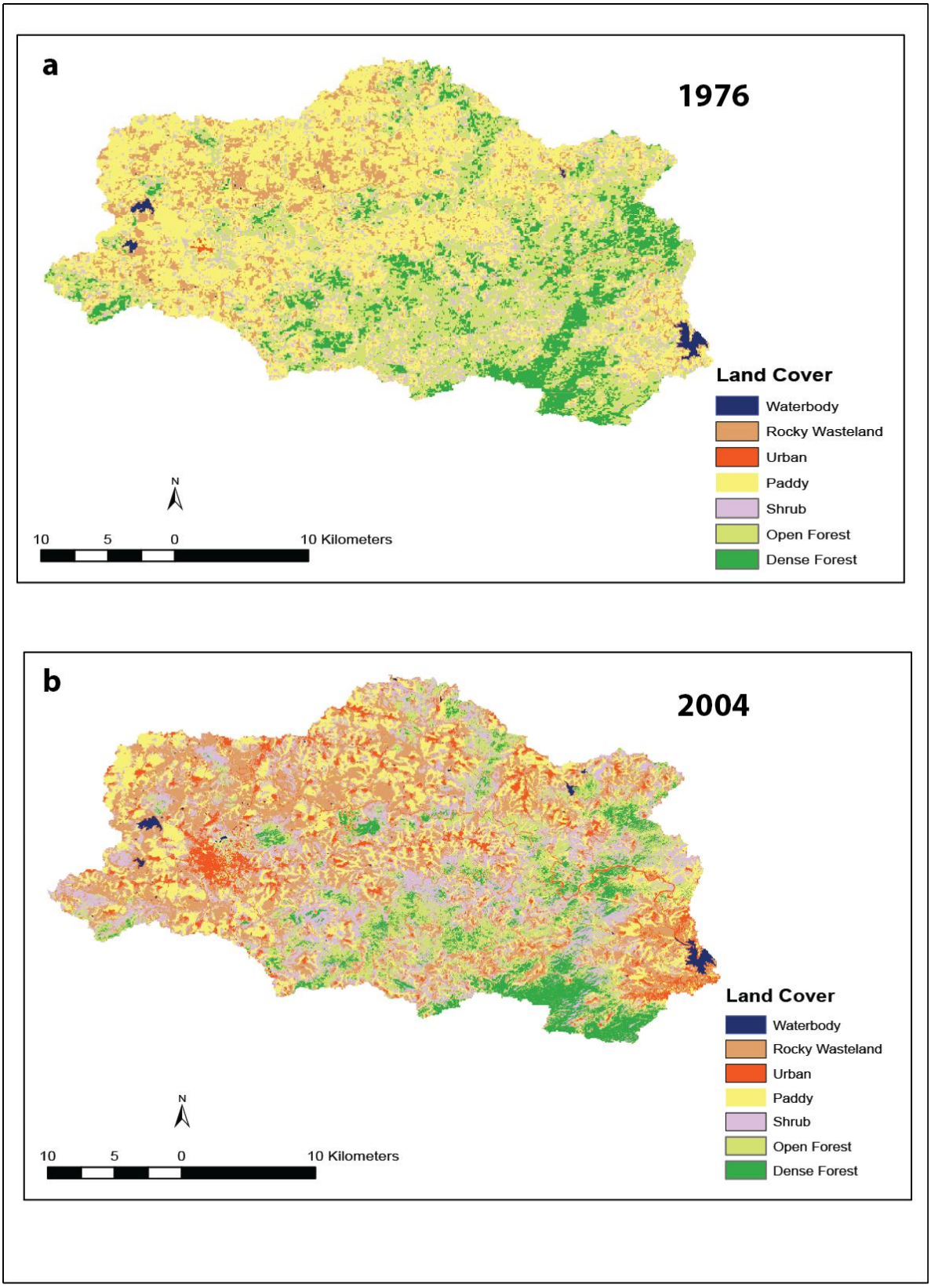

Figure 6.2 Land cover classification of (a) 1976 and (b) 2004. Maps were derived from Landsat MSS (a) and Landsat TM (b) in the early post-monsoon season in late October to early November.

Between 1976 and 2004 a substantial percentage of the total area in the Konar catchment changed in LULC from paddy to rocky waste, paddy to shrub, open forest to shrub and paddy to urban (Figure 6.3). The comparison of the simulated rainfall runoff event of October 1973 with the LULC situation prevailing in 1976 (Fig 6.4) reveals a good match between the observed and simulated daily streamflow volume. The association between the modelled and observed daily surface runoff figures for the 2004 LULC situation using the 2003 TRMM rainfall estimates (Figure 6.5) and the calibrated Manning's roughness values from the previous experiment also shows a good match.

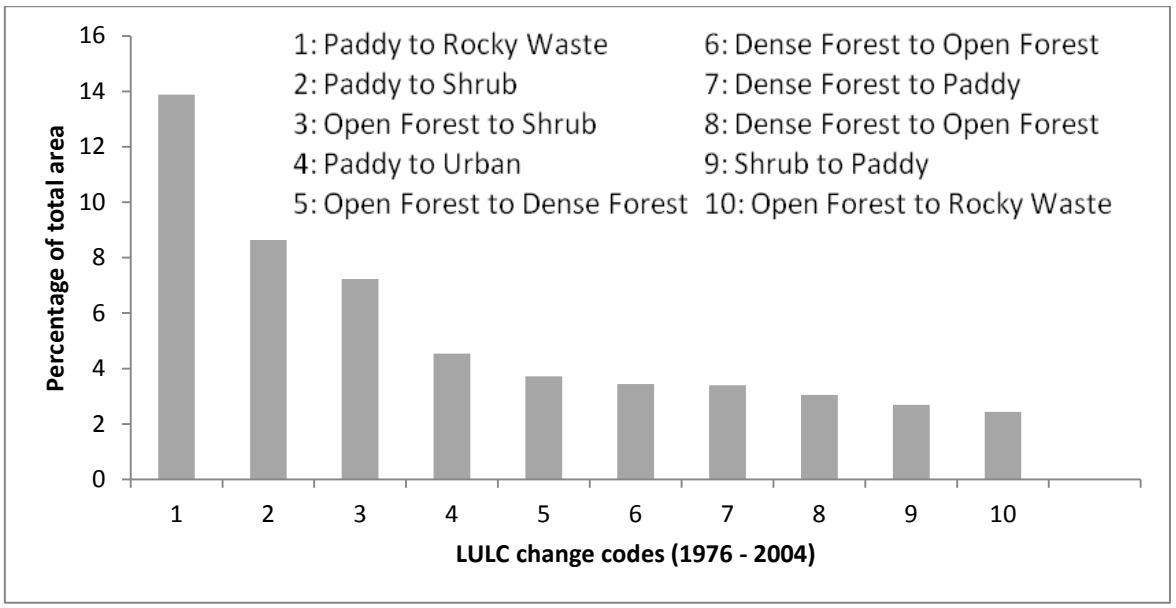

Figure 6.3 Percentage of land in the Konar basin that had undergone substantial transformation from one LULC category to another between 1976 to 2004. These LULC scenarios are valid for the early post-monsoon season in late October to early November.

When considering the effect of LULC change in the entire Konar catchment on the peak discharge for the 1973 storm event at the reservoir inlet we found that, for the 1976 LULC scenario the peak discharge was 1023.3 m^3/s occurring on 12th October at 20:10, while for the 2004 LULC scenario the peak discharge increased to 1194.7 m^3/s and the time to peak was decreased by 1 hour and 10 minutes. After ranking the sub-catchments according to the unit flood response computed with the rainfall event of 1973 and LULC scenarios of 1976 and 2004 (Figure 6.6), we found that in spite of significant LULC change between 1976 and 2004 (Figure 6.2) there was little change in the ranking.

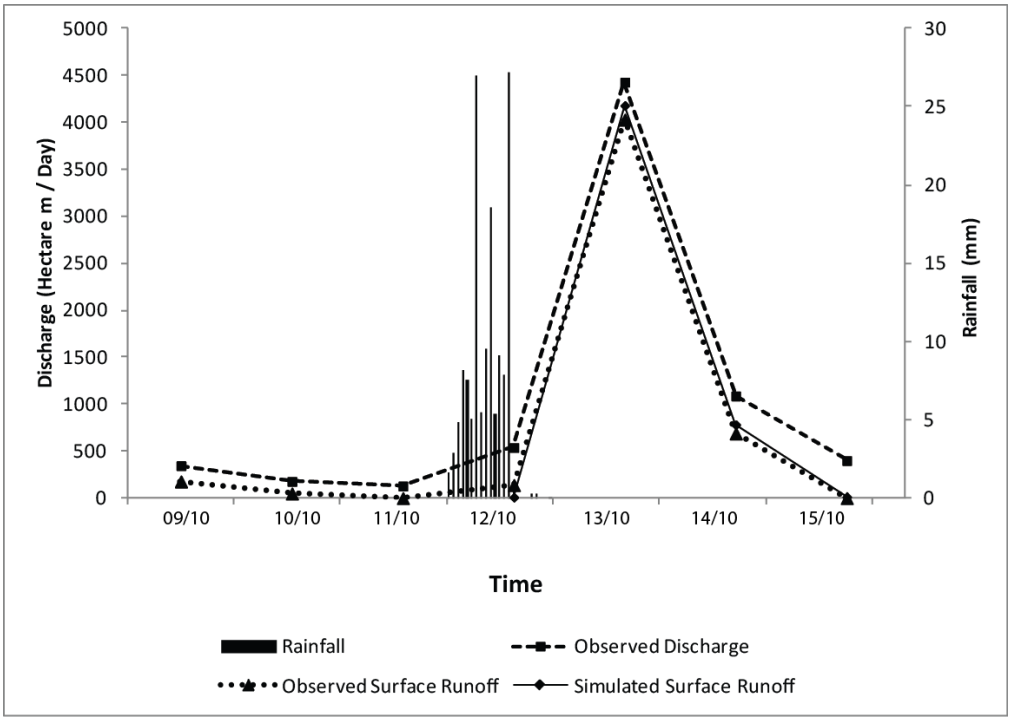

Figure 6.4 Simulated surface runoff with gauged hourly rainfall input of October 1973 and land cover of 27th October, 1976. The observed surface runoff (depicted as dotted line) was derived from the observed discharge figure by means of base flow separation.

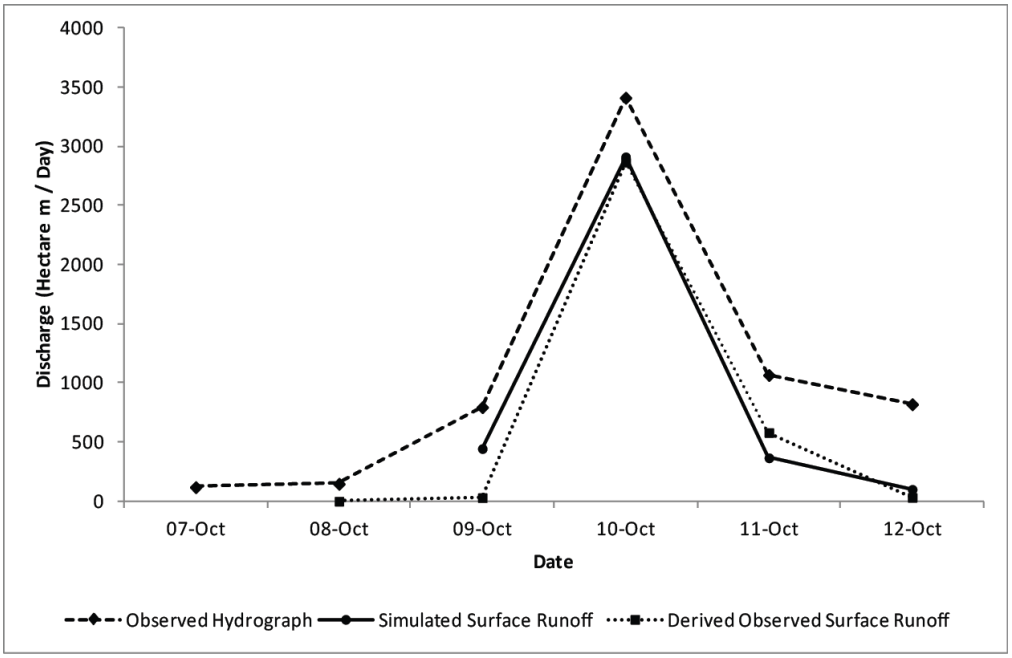

Figure 6.5 Simulated surface runoff with TRMM 3-hourly rainfall input of October, 2003 and land cover of 2nd November, 2004.

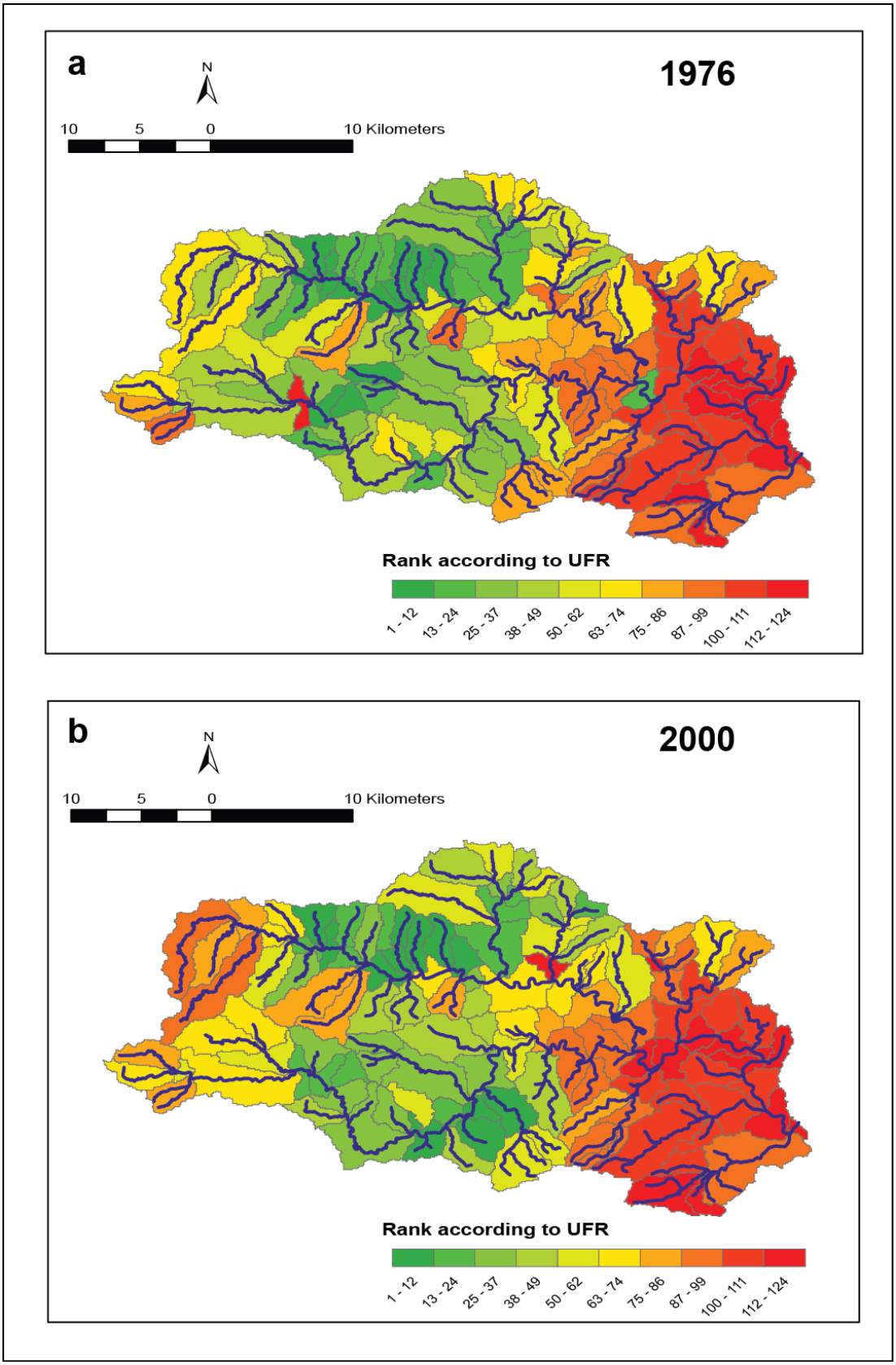

Figure 6.6 Rank of the sub-catchments according to the unit flood response (UFR) values derived with the land cover of 1976 (a) and 2004 (b). The gauged hourly storm rainfall event of October, 1973 was used as the meteorological input in both models.

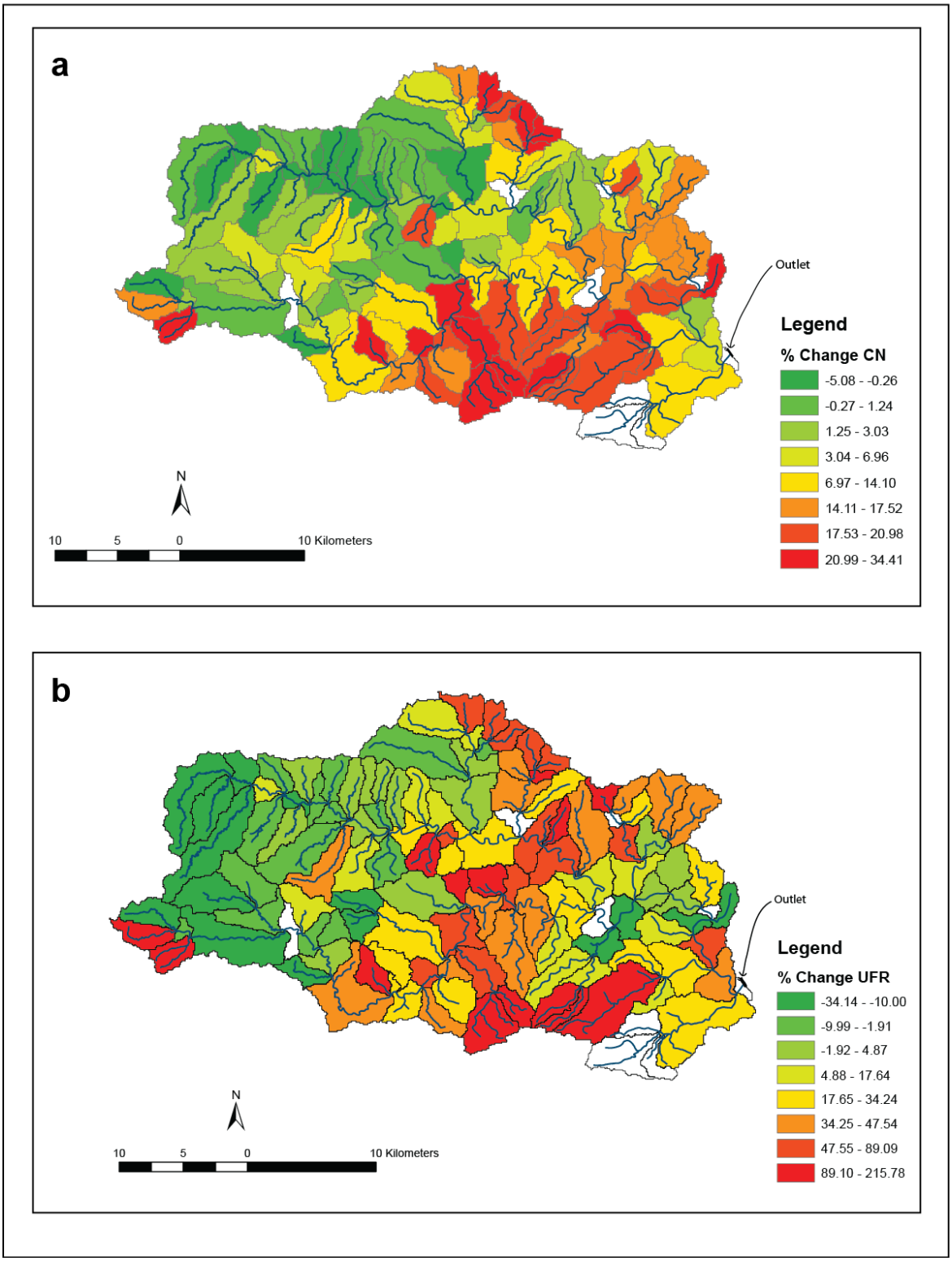

Figure 6.7 a, percentage change in NRCS Curve Number (CN) values (1976 - 2004); b, percentage change in unit flood response (UFR) values (1976 land cover to 2004 land cover). In both panels, negative values indicate that the CN or UFR was higher in 1976 than 2004, and positive values show the opposite. The sub-catchments shown in white experienced negligible change.

The spatial patterns of the percentage change in the CN values (Figure 6.7a), a proxy for the change in the combined effect of the soil and LULC, and the unit flood response between 1976 and 2004 LULC scenario (Figure 6.7b) did show some degree of agreement; sub-catchments showing a higher percentage change in CN values (i.e. change in LULC) in the predominately forested area in the south and near the main stream of the Konar River tend to show a increase in their unit flood response values between the 1976 and 2004 LULC scenarios. The location of the LULC change in terms of the distance from the outlet may have an negative impact over the intensity of the consequent percentage change in unit flood response. In order to test this, an attempt was made to assess if the distance from the sub-catchment centroid to the outlet, measured along the connecting stream network, had a statistically significant negative relationship with percentage change in unit flood response. However, no statistically significant relationship could be established.

Finally, a weak positive linear correlation was found (Pearson's correlation coefficient (r) of 0.53 ($p < 0.01$) between the sub-catchment percentage change in unit flood response (1976 - 2004) and curve number (CN) values (Figure 6.8a). Three clusters of sub-catchments showed marked deviations from the overall positive trend between the two variables. Cluster 1 consists of sub-catchments with a large increase in CN values from 1976 to 2004 and a disproportionately large increase in the unit flood response. Cluster 2 consists of sub-catchments with a moderately high percentage increase in the CN values but a negative change in unit flood response values. Cluster 3 includes sub-catchments with small increases in CN values but large increases in unit flood response. In order to reveal any apparent geomorphological reason for these deviations from the overall trend we mapped the sub-catchments falling in the three aforementioned clusters which did not reveal an overall relationship between the location of LULC changes and proximity to higher order streams or the basin outlet (Figure 6.8b).

As we could not establish a relationship between the proximity of LULC change to the outlet or a higher order trunk stream and the peak discharge at the catchment outlet due to paucity of data, we tested the influence of timing effect of flow convergence at the sub-catchment level following the general argument of Pattison et al. (2008). In HEC-HMS, a single sub-catchment (with identifier W2080) and junction (identifier J425) were selected as an example of a disproportionate rise in unit flood response (UFR)

caused by moderate increase in CN value (LULC change towards more runoff producing LULC). (Figure 6.8a). On the other hand, sub-catchment W2510 and Junction J328 were chosen as an example of the general positive linear correlation between unit flood response and CN change between 1976 and 2004 LULC conditions (Figure 6.8a). The location of these sub-catchments can be found in Figure 6.9.

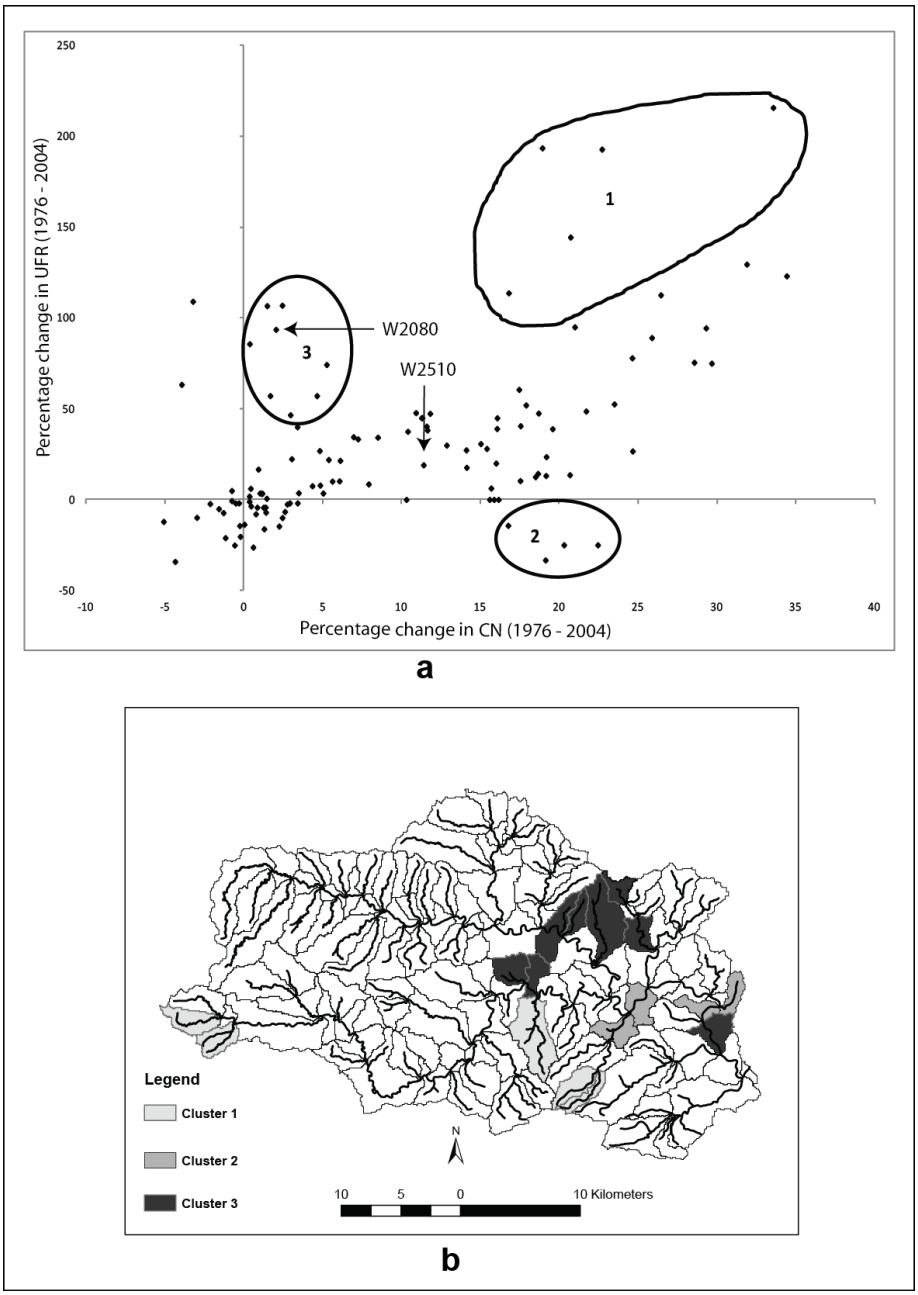

Figure 6.8 a, Scatter diagram of the sub-catchment wise percentage changes in the unit flood response (1976 - 2004) and curve number (CN) values. Sub-catchments that did not fit into the overall linear positive correlation pattern were separated into 3 clusters. Sub-catchments W2080 and W2510 were selected as representative of extreme and typical cases, respectively, of UFR change in relation to changing LULC conditions. b, Location of the sub-catchments identified as 3 clusters in panel a.

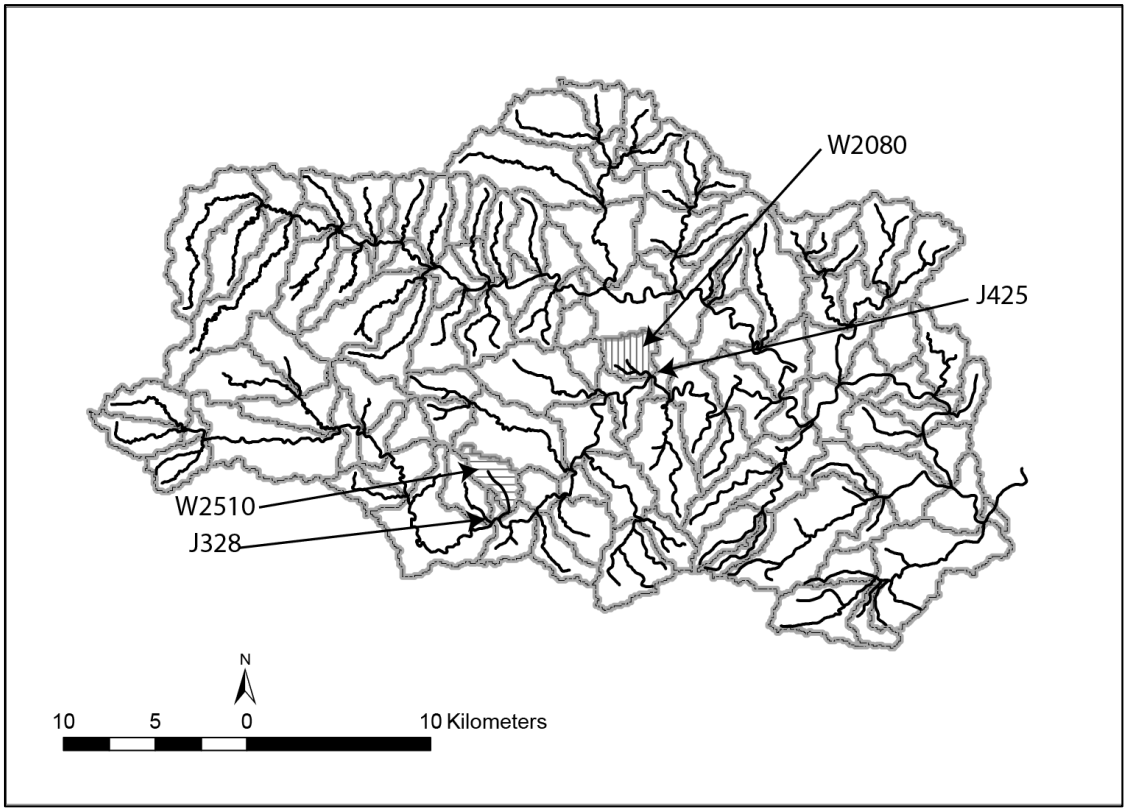

Figure 6.9 Location of the sub-catchments and flow junctions that were selected for testing the influence of timing effects of flow convergence on the relationship of local LULC changes and downstream flood peak.

W2080 demonstrated a 93 percent change in the unit flood response for only 2.03 percent change in the CN values from 1976 to 2004. The simulated hydrographs for W2080 showed little difference in the direct runoff pattern for the LULC conditions of 1976 and 2004 alone (Fig. 10). Under the LULC conditions of 2004, Junction J425, the confluence of runoff generated from W2080 and the Konar River, experienced a peak discharge of 484.3 m^3/s at 15:35 on 12 October. At that time, the discharge from W2080 was 4.40 m^3/s which was 22.9 % of its peak discharge (19.2 m^3/s) (Figure 6.10). The contribution of W2080 to the combined discharge at 15:35 on 12th October was thus 0.90 %. Using the LULC conditions of 1976, when the discharge from W2080 merged with the Konar River during the peak outflow at J425 on 12 October, 16:35 (1 hour later than the 2004 LULC scenario) the combined discharge at J425 was 383.8 m^3/s and the contribution from W2080 was 2.1 m^3/s (0.55% of the total) which was only 11.5% of its peak discharge of 18.3 m^3/s (Figure 6.10). This example illustrates that with only a 2.3 percent increase in the CN value from 1976 to 2004, the contribution of the sub-catchment W2080 to the combined flow of a vast contributing area almost doubled (0.55% to 0.90%).

Sub-catchment W2510 revealed a different picture at Junction J328, where the runoff from the sub-catchment converged with the Konar River. Under the 2004 LULC conditions J328 experienced a combined peak discharge of 280.7 m^3/s at 15:15 on 12th October. At that time the discharge from W2510 was 7.8 m^3/s, which was 2.77% of the combined discharge and 65.54 % of the peak discharge of W2510 (11.9 m^3/s) (Figure 6.11). For the LULC conditions of 1976, the runoff from W2510 merged with the peak discharge at J328 on 15:45 (30 minutes later than 2004 LULC case) at a rate of 6.1 m^3/s, which was 2.42 % of the combined peak flow of 251.7 m^3/s. The runoff from W2510 at that time was 70.11% of its peak discharge (8.7 m^3/s) (Figure 6.11). This test case illustrated that for a moderate 11% increase in the CN value from 1976 to 2004 LULC conditions the contribution of W2510 during the peak flow at Junction J328 increased from only 2.42% to 2.77%, which is in line with the overall trend in Figure 6.8.

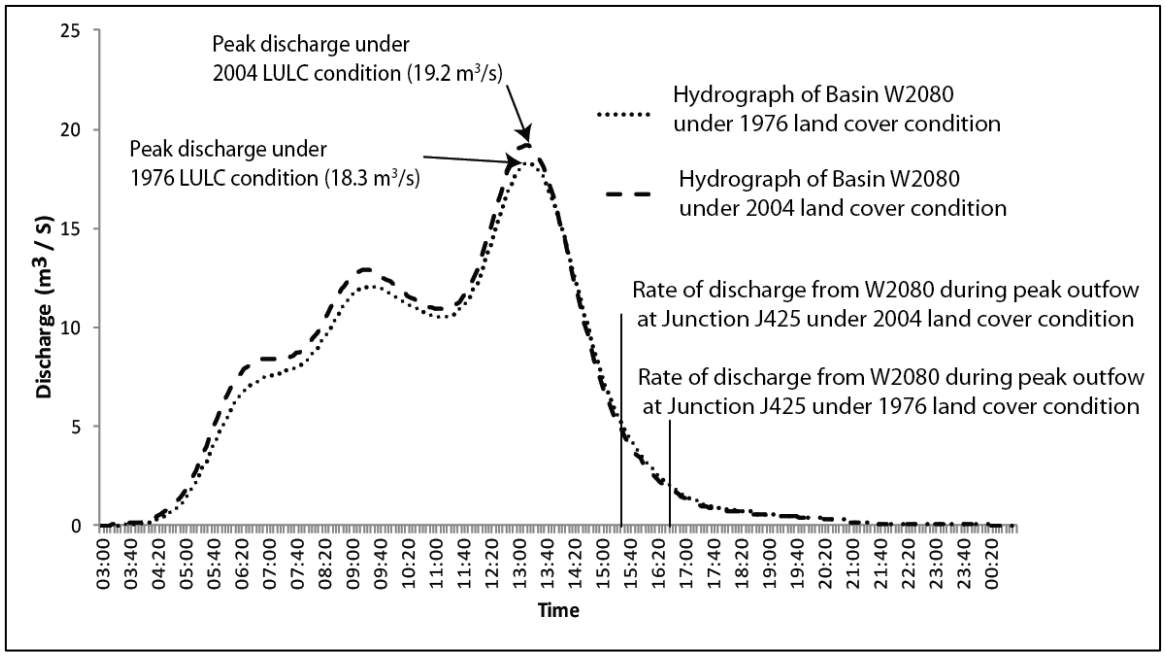

Figure 6.10 Hydrographs of sub-catchment W2080 for 1976 and 2004 LULC scenarios. Vertical lines show the timing of the combined peak flow at J425 for the 1976 and 2004 LULC.

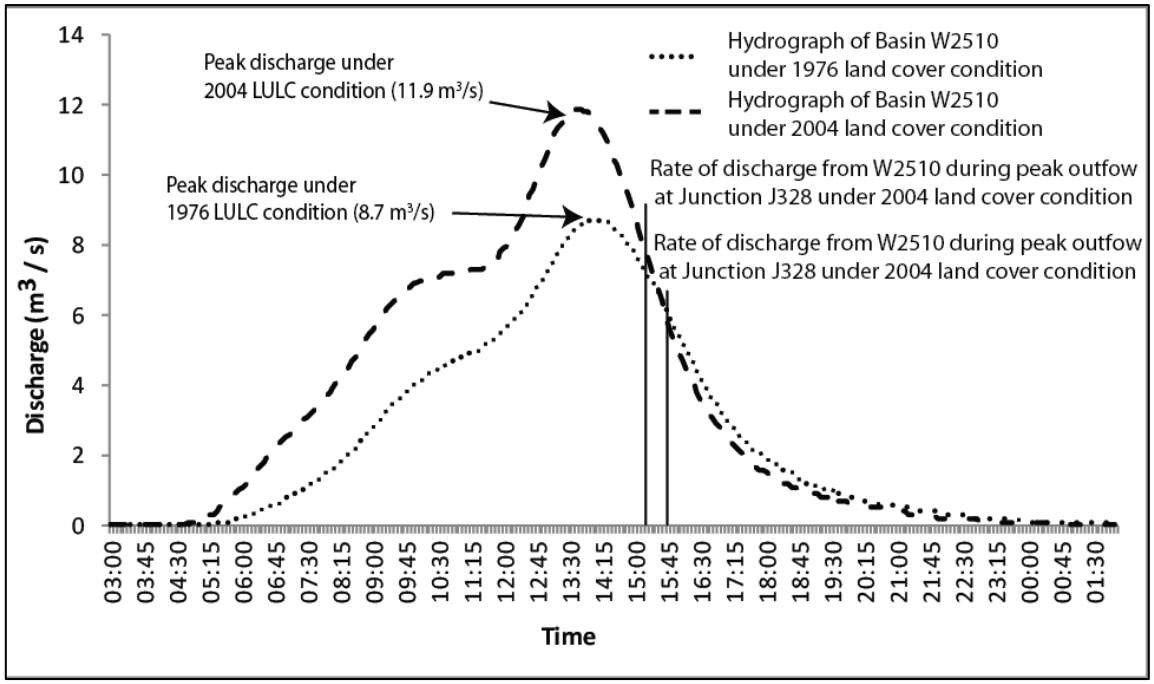

Figure 6.11 Hydrographs of sub-catchment W2510 for 1976 and 2004 LULC scenario, Vertical lines show the timing of the combined peak flow at J328 for the 1976 and 2004 LULC.

6.5 Discussion

If we consider the effect of overall LULC changes in the Konar catchment to the flood peak at the catchment outlet, it becomes evident that a general increase in the higher runoff producing LULC classes resulted in higher peak discharge and shortened the time to peak. However, when investigating the sub-catchment-wise local LULC change and its influence over the peak discharge at the catchment outlet a complex relationship began to emerge. When the location of the sub-catchments showing marked deviation from the overall trend was mapped (Figure 6.8) we could not find a convincing reason for their unusual hydrologic response, For example, two of the predominantly deforested sub-catchments in cluster 1 (see Figure 6.2 and 6.8b) were found to be near the trunk stream, which may explain their rapid reaction in terms of increase in percentage unit flood response; however, the other two sub-catchments in the same cluster that are located at the farthest point from the outlet did not have any apparent physical explanation based on the distance from the outlet or proximity to a stream of very high stream order. Nothing could be established about the negative reaction of the sub-catchments in cluster 2 to their contribution to the peak discharge at the outlet. The sub-catchments in cluster 3 were found to be adjacent to each other and located at a consistent position near the main stream (Figure 6.8) which may partially explain the

spike in their percentage increase in the unit flood response caused by moderate positive percentage change in CN values.

Although an overall statistically significant positive relationship was found between the changes in LULC at the sub-catchment scale and their impact on the basin flood peak, the pattern was altered by other factors. Increments of 2.03% and 11% in the CN values of sub-catchment W2080 and W2510 between 1976 and 2004 resulted in expected changes in their surface runoff hydrographs (Figures 6.10 and 6.11). However, during the peak discharge at the junctions where the runoff from these two sub-catchments flows into the Konar River, their contribution to the combined flow differed markedly. Pattison and Lane (2012) highlighted the important role played by the timing of extreme rainfall events at different parts of the catchment and the consequent hydrological response. In addition, they also pointed out that the structure of the basin also determines the convergence of hillslope and channel flow which changes with distance and influences the magnitude and timing of the flood peak downstream. For example, W2080 has little difference in the shape of hydrograph (not surprising because of small change in CN) for the two LULC conditions, but its apparent change in UFR is very high because the time of the peak at its outlet is very different (big spread between the vertical lines in Figure 6.10). On the other hand, W2510 has a very different hydrograph, but because the peak at the outlet comes on the falling limb, and because there's a fairly small change in the time of the peak, the change in UFR is modest. Thus the effect of time matters more than the effect of changes in CN.

The characteristics of individual sub-catchments such as shape and slope may also play a vital role in the causal relationship between sub-catchment wise LULC changes and the flood peak at the basin outlet. These factors may partially explain why similar amounts of LULC change in different sub-catchments have varying impacts on the flood peak at the catchment outlets. It is likely that more than one of these factors are simultaneously playing a role in influencing the peak discharge at the catchment outlet. Thus, correcting the land use practice in one of the priority flood generating sub-catchments may not always result in reducing the flood peak. Hence, it is not surprising that this study did not find any pattern similar to one reported by Roughani et al. (2007), in which the sub-catchments located at the centroid of the catchment were

found to be more likely to exert an influence to the peak discharge at the catchment outlet.

In order to implement remedial land management practices for controlling the flood peak at the reservoir inlet and reducing soil erosion, authorities like the DVC generally try to identify the sub-catchments that require urgent attention. If only a single LULC condition is of interest then the unit flood response approach (Saghafian and Khosroshahi, 2005) can be considered as an ideal solution to identify the priority target area for land-use planning. However, LULC conditions across sub-catchments change with time and the nature of this transformation from one LULC class to other LULC classes varies considerably from one sub-catchment to another. This factor tends to have a complex influence on the hydrologic response of the entire catchment over the years. Hence, the relevance of this study comes from testing whether local changes in LULC, at which scale the remedial measures are likely to be implemented, actually have a straight forward mitigating effect on the flood peak at the basin outlet. Pattison and Lane (2012) recommended that any empirical association found between local LULC change and downstream flood peak is valid only for that particular catchment and storm event. We suggest that, after identifying the major flood source areas for an average storm event, further simulations should be carried out to evaluate the effect of possible remedial land-use planning in those sub-catchments over the flood peak at the cumulative basin outlet of interest. Undertaking remedial land-use measures in a few sub-catchments, especially in the upper catchment, may alter the tributary flow convergence timing in an adverse manner, nullifying the effects of corrective land management measures at the local scale.

Our study has emphasised the challenges faced in data scarce areas such as developing countries for modelling the impact of LULC changes on basin hydrology. The LULC maps were derived from freely available satellite data that varied in spatial and spectral resolution. In our study area, we had severe constraints in the availability of high-frequency (~hourly) rainfall data and historic ground truth data in terms of topographic maps, as well as low-cost, high resolution imagery such as Corona or GoogleEarth images. The reasonable match between the simulated and observed daily hydrographs for varying rainfall events and LULC conditions demonstrated that the HEC-HMS model in conjunction with the NRSC CN method is capable of accurately reproducing

rainfall-runoff processes with broad LULC classes and moderate resolution topography. Figures 6.4 and 6.5 illustrated that the HEC-HMS model setup in our study can accurately reproduce rainfall-runoff processes under two LULC conditions resulting from two different storm events. It established that the model can perform well independently of the nature of the storm event and LULC scenarios, and this provided an element of confidence when we applied the same storm event of 1973 for the LULC situations of 1976 and 2004 to address the core purpose of this research. Lower-frequency discharge data at the inlet of the Konar Reservoir might have hidden some mismatch between the observed and simulated surface runoff patterns. Availability of a more disaggregated observed streamflow record would have revealed some element of inaccuracies in the simulated hydrograph, possibly arising from the low resolution of Landat MSS image (in terms of LULC and CN) or the SRTM DEM (in terms of delineation of channels, sub-catchments and channel configuration parameters for routing). However, we argue that availability of more data would not make much difference in the findings related to the influence of LULC on the hydrological response, as Wang and Kalin (2011) reported that the selection of model parameters (derived from coarse quality inputs) had little influence on modelling the impact of changing LULC scenario on surface runoff with the NRSC CN method.

6.6 Conclusion

We have illustrated a systematic approach of analysing the effect of LULC changes in the sub-catchment level and their varying impact on the flood peak at the catchment outlet. An overall positive linear relationship was found between the two factors. However, our findings indicated that varying timing of flow convergence between hillslope and streams at the sub-catchments caused by localised LULC changes is the key factor behind the frequent deviation from this overall trend. While unit flood response (Saghafian and Khosroshahi, 2005) is an innovative means of identifying the sub-catchments that need urgent attention in terms of land management to reduce flood peak, we argue that the complex interaction between changing LULC in sub-catchments, especially in large basins with heterogeneous LULC, is likely to be dependent on other factors which are not within the scope of this study. These factors may include soil types and nature and duration of the precipitation event. This study

also demonstrated ways of utilising free or low-cost spatial and meteorological data, typically available in developing countries, to set up a widely used hydrological model that is capable of reproducing event scale rainfall-runoff processes with reasonable accuracy. The described methodology and the key findings will be beneficial for mitigating flooding through non-structural measures, particularly in the developing world.

Chapter 7

Overall Discussions

The goal of this chapter is to highlight the important findings of this thesis and discuss their significance with respect to flood management. This chapter also re-examines the key scientific questions addressed in this thesis by tackling different aspects of flood predictions and management with severe constraints of available data. Different parts of the Damodar River Basin in Eastern India has been used as the study sites for addressing the overall picture of the challenges in flood predictions at varied scales.

7.1 Considerations for sources of terrain data in developing countries

This thesis reveals a few important facts regarding the creation of suitable terrain data for hydraulic modelling in data-sparse regions. For large scale applications in a single, wide, reach, where the intended model output is the stage hydrograph at a downstream point, freely available DEMs such as the SRTM DEM can be effectively used to simulate high magnitude streamflow. However, the DEM needs to be modified with reference to the existing map-based height information to minimise the vertical bias. There is apparently no relation between the general elevation of the terrain and the vertical inaccuracies in the SRTM data, at least where the overall terrain is gently sloping plain land. The local noise in elevations caused by the ineffectiveness of the C-band radar to penetrate the dense foliage can only be removed manually with reference to the land-use information. This kind of modified SRTM DEM is suitable for flow routing only when the stream flow is predominantly confined within its bankfull level. The channel-bed information is difficult to obtain from the SRTM directly and some surveyed cross-sections are absolutely necessary to establish a smooth longitudinal profile of the reach in order to capture an accurate stream energy gradient. When the landform is gently sloping without any abrupt change of slope, measured cross-sections can be located at a considerable distance from each other. When the details of the channel bed morphology and the slope of the banks are likely to exert more influence on the flow pattern, it is acknowledged that this kind of input geometry for the channel may not be effective for simulating low flows. On the other hand, in reach-scale application (< 20 km) where extensive floodplain inundation is common, globally available DEMs are of limited use in flood inundation modelling. Low-cost stereo satellite images such as IRS Cartosat-1 are not capable of producing a high resolution terrain data of uniform quality across all types of land-uses and terrain. Due to its imperfect radiometric quality and relatively coarse resolution of 2.5 m, a few

supplementary sources of elevation are necessary to produce a terrain data of acceptable standard. The use of Cartosat-1 images made it possible to create the narrow branch channels, embankments and roads, which were not present in the coarse resolution SRTM data. This factor led to an impressive improvement in the model performance.

7.2 Choice of hydrodynamic models with reference to scale and channel morphology and available input data

The findings of this thesis indicate that the suitability of a particular hydrodynamic model depends on the scale of the study, the nature of the model output of interest (e.g. stage, flood extent) and the physical characteristics of the study reach (e.g. single reach versus rivers with distributaries). The simple input requirements and computational efficiency of LISFLOOD-FP was found to work well for a single river reach with no significant flow bifurcation. However, when LISFLOOD-FP was used for modelling floodplain inundation in anabranching channels it failed to produce a simulated flood-extent map that matched well with the observed flood extents derived from the satellite overpasses. The complex nature of the channel networks and widespread overtopping of levees, sometimes in the branch channels at a distance from the main flow, called for a more robust model with regards to its ability to account for the hydraulic processes. The raster-based floodplain flow routing component of LISFLOOD-FP was unable to cope with the flow split at different parts of the main channel due to the high velocity of the water at the channel with a considerable depth. Simple conceptualisation of the flow hydraulics in LISFLOOD-FP is compensated with the use of a high resolution DEM. The resolution and accuracy of the hybrid terrain data created for the lower course are not comparable with the LiDAR derived ones (typically 1 m grid size with a vertical accuracy of 25 cm). This factor might have been responsible for not being able to exploit the full potential of LISFLOOD-FP in modelling the floodplain inundation in the lower course.

TELEMAC2D, a fully two dimensional hydrodynamic model, was found suitable for simulating inundation events with a low-cost adapted terrain data in a complex fluvial setting. As the model domain is decomposed into an unstructured finite element mesh in TELEMAC2D, it is able to concentrate the computational resources where it is

needed most. The hybrid terrain data for the lower course has varying point density and was created with a similar intention of representing the hydraulically significant part of the model domain in greater detail than the other parts where high density elevation information was not available. Thus, TELEMAC2D was well equipped to take advantage of the hybrid terrain data. The ability of TELEMAC2D to model the turbulence at the channel bifurcations was also a key factor for its better performance vis-a-vis LISFLOOD-FP in the lower course. This finding is one of the key results of this thesis as the previous comparative studies between fully a 2D finite element model (such as TELEMAC2D), 1D models (such as HEC-RAS) and 1D-2D coupled system (such as LISFLOOD-FP) did not report a marked disparity between the accuracies of the predicted inundation extents. The role of the drainage pattern in conjunction with the suitability of a type of code for a type of terrain input is highlighted in this thesis. Notwithstanding the issue of higher computing cost and complex model setup, fully 2D finite element models were found to be still relevant in inundation modelling. Where the channels and topographically discontinuous features can be represented in finer details this kind of model can produce quality results. Although TELEMAC2D performed well in the small scale application, it is computationally demanding and requires a detailed configuration of the channel bed in order to produce accurate water surface elevation and inundation extent. Hence, employing this type of model for simulating flood waves for a reach length of more than 50 km was unrealistic from the point of view of computational cost and accuracy of the available DEM.

The experimental design for the middle course of the Damodar River provides certain new outlooks regarding flood routing at large scale with very limited availability of data. In a gently sloping river, a characteristic fairly common for large rivers, the unavailability of the downstream boundary condition information is not a major concern. The uncertainty analysis clearly indicates that (Figure 3.16b) the performance of LISFLOOD-FP is not sensitive to this information. Similarly, for a wide river with more than 1 km of average width, the small inaccuracies in measuring channel width was not found to influence the model performance in a significant manner. Channel widths measured from freely available high resolution images available in GoogleEarth™ were found to be of sufficient accuracy for this purpose. Where the flow is mostly confined within the bankfull level, uncertainty in the terrain data for the floodplain may still affect the model performance to a specific extent. This is primarily

caused by the uncertainty in computing the bankfull depth from inaccurate bank elevations. However, it is beyond doubt that the roughness parameterisation of the channel is the key factor governing the accuracy of the modelled water-surface elevation. Where the channel portion of the freely available DEMs are either noisy or stepped down monotonically, the river cross-sections derived from these products are not likely to be within the acceptable limit of error. Unknown embankment heights are also a major obstacle to maintain stability while simulating an extreme event with an 1D hydrodynamic code. The 1-2D hybrid nature of LISFLOOD-FP makes it less sensitive to the bank/embankment heights. Its simple rectangular conceptualisation of the channel geometry also reduces the dependency on very accurate channel cross-section data at each cross-section. These features make LISFLOOD-FP an ideal candidate for flow routing in large rivers where accurate topographic data are scarce.

7.3 Uncertainty

In terms of estimating the widespread floodplain inundation and the associated uncertainties, particularly in the rivers with multiple bifurcations, this thesis illustrates a challenging scenario on flood inundation modelling. Unlike majority of published case studies in this topic the present investigation does not deal with a continuous nature of flooding where the depth of the flood water progressively diminishes away from the main channel. In the common scenario, the main debate about the model uncertainty is confined to a narrow zone at the fringe of the inundated area. The efficiency of a particular model setup is measured by means of its effectiveness in correctly predicting the shoreline of flood water in this so called zone of uncertainty (Figure 7.1)

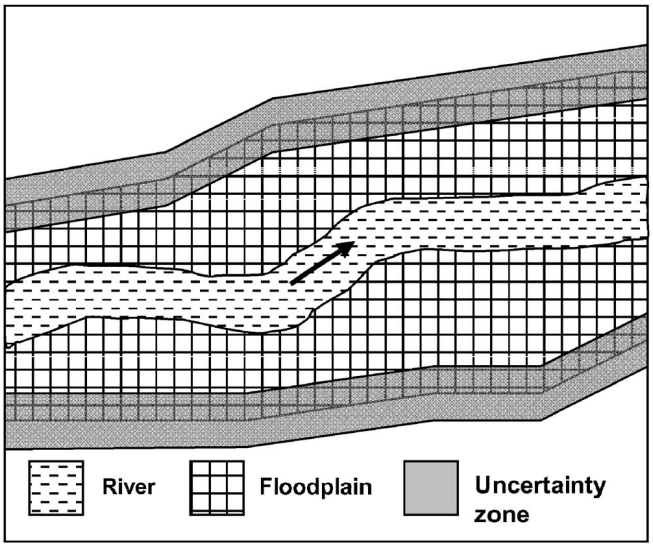

Figure 7.1 Flood inundation map with uncertainty zone (After Merwade et al., 2008b)

Due to the complex nature of flooding in the lower course of the Damodar River floodwater accumulates or at least persists in patches, sometimes at considerable distance from the main channel. The visualization of uncertainties in the predicted inundation-extent maps (Figure 5.11) did not conform to the common picture of concentration of uncertain zones at the boundary of the spatial clusters of the predicted flooded area. Instead, a complex pattern emerged where the zone of uncertainty could be found right at the middle of a predicted patch (e.g. in the SE corner in Figure 5.11). This kind of pattern is a result of the complex interplay between the limited resolution of the terrain data over the farmlands, uncertain inflow discharge at the model inlet and the inefficiency of the model itself to reproduce parts of the actual hydraulic processes. It is acknowledged that some of the observed pattern is spurious and a fall out of the error in the terrain data and discussed in detail below.

The most important source of uncertainty in the model output comes from the uncertainty in the inflow hydrograph as evident from the reach scale study presented in Chapter 5. As the outflow discharge figures are available from Durgapur Barrage this factor has not been taken into the uncertainty analysis in Chapter 3. The fully 2D finite element models are not very sensitive to the roughness parameterisation. Unlike Chapter 3, the model performance was not clearly controlled by the channel roughness factor in the case of the lower Damodar River. The combined effect of less sensitivity to the roughness parameterisation and the uncertainty in the inflow figures resulted in a

trend of equifinality in the relationship between channel roughness and model performance. This trend became more evident towards the receding stage of the flood hydrograph (Figure 5.10b) than near the flood peak (Figure 5.9b).

This research has pointed out the issue of input induced biases in the modelled outputs at different scales. Although Chapter 3 and Chapter 4 deal with water-surface elevations and modelled flood extents respectively both studies showed consistent under or over estimations in the modelled output. The systematic bias is readily identified in the Monte Carlo-based visualization of uncertainties (Figure 3.17 and Figure 5.11). It is interesting to note that the systematic biases are evident in both temporal and spatial dimensions. Part of the rising limb of the observed hydrograph at Jamalpur gauging station was not within the upper and lower uncertainty bound of the Monte Carlo simulations. The model consistently underestimated the rising limb and shows a slight delay attaining the peak when compared with the gauged river stage data. Many factors, including inaccuracy in the DEM, bed elevation for the channel and no consideration of minor influx of water in the main channel from the adjacent areas might have caused it. Similarly, the spatial dimension of the consistent model bias was illustrated by a comparison between the distributed predictive uncertainties (Figure 5.11) with the deterministic flood extent maps (Figure 5.5). The overprediction was due to the low density of elevation data over agricultural fields that created flat surfaces in some portions of the hybrid terrain data. Limited influx of flood water from adjoining river basins that were not considered in the model was mainly responsible for the underestimation of modelled inundation extent at the western portion of the model domain.

Chapter 5 further illustrates that incorporating the level of confidence in the observed records in an uncertainty analysis as opposed to considering the observed information in a deterministic way makes a difference in the assessment of uncertainty. This difference has been found to be more pronounced in portions of the model domain that are not affected by the input induced model bias. Considering the amount of effort required for taking into account the uncertainty in observed data in the computation of predictive uncertainty it is hard to justify in places where the available model inputs are not of ideal standard. It is evident that the use of the 'possibility of inundation maps' as

oppose to deterministic flood extent maps is not likely to make much difference in the uncertainty assessment in such a scenario.

7.4 The issue of roughness paramiterisation

Straatsma (2009) identified roughness of the terrain as the most important parameter after topography in influencing the flow in natural channels and overland inundation. Manning's roughness coefficient (*n*) is the most common form of roughness parameter used in modelling hydrological/hydraulic studies. This parameter is part of the empirically derived formula put forward by Manning (1889) to calculate uniform flow rates in open channels as functions of flow velocity, flow area and channel slope. With the assumption of uniform flow it has also been assumed that 1) the cross-sectional area in the channel does not vary within a reach, and 2) the bottom slope of a channel is equivalent to the energy gradient of the water-surface. Although *n* is primarily used to account for the energy loss due to friction at the boundary of the flowing water and terrain surfaces, it is often used to compensate for the physical processes that are not considered by the governing equations of a hydraulic model (Morvan et al., 2008).

By rearranging Manning's equation *n* can be represented as

$$n = R^{2/3} S^{1/2} / V \quad (1)$$

where, S is the slope of the plane surface (mm^{-1}), R is the hydraulic radius (m) and V is the velocity of water (ms^{-1}).

Different values of Manning's *n* in the published literature were mostly derived from runoff plot data collected from different natural and agricultural surfaces applying constant rainfall rates produced by rainfall simulators (Arcement and Schneider, 1989). Engman (1985) pointed out that the roughness values computed in this manner are essentially 'effective' roughness and also include the effect of raindrop impacts, agricultural practice (e.g. nature of tillage), obstructions to flows and also the energy loss due to the erosion and transportation of sediments. The retardation of velocity of water due to interaction with the surface also depends on the particle size of the materials on the streambed, bank irregularities, channel bed configurations and sediment load (Limerinos, 1970). Efforts have also been made to measure channel roughness on the basis of the amount of biomass present (De Doncker et al., 2009) and as a function of microtopography (Strelkoff et al., 2000).

Various modified forms of Manning's equation for estimating *n* have also been reported in the literature including special forms for steep channels with stable bed and banks (Jarrett, 1984), alluvial channels (Limerinos, 1970) as well as floodplains (Acrement and Schneider, 1989). Wohl (1998) performed a sensitivity analysis of simulated flow rates using these formulae as well as different channel conditions and reported that 1) the change in the discharge due to variation in *n* is inversely proportional to the stream

gradient and width/depth ratio, and 2) the variation in discharge due to the use of computed *n* values using different formulae is modest, especially in channels with a low gradient and smooth surface.

Various studies have also used measured flow velocity, depth and cross-sectional area to determine bottom friction with numerical modelling (Stephen and Gutknecht, 2002; Mailapalli et al., 2008; Arico et al., 2009). In most of these studies terrains were used as inputs, measured flow data as boundary conditions and values of *n* are calibrated to achieve best-fits to measured water-surface data.

The extent to which a hydrodynamic model is sensitive to roughness and geometry uncertainties partially depends on the dimensionality of the model structure, as this factor represents the geometry in different manners (Lane et al., 1999). However, Lane (2005) argued that roughness is strictly a component of topography and better parameterizations of topography would ultimately reduce the sensitivity of hydrodynamic models to *n* values. This view has been further supported by Medeiros et al. (2012) who concluded that parameterising floodplain roughness on the basis of detailed terrain configurations and the presence of obstructions would be more effective than relying on remotely sensed LULC information for inundation modelling. We often change the description of roughness with changes in scales to compensate for the effect of topography on the processes influencing interaction between the surface and the terrain, hence implicitly recognising that roughness is scale dependant (Lane, 2005). As the published sources for recommended values of *n* were commonly derived from plot scale experimental set-ups or small controlled experimental catchments, use of these values sometimes become unreliable for numerical modelling involving large rivers.

In order to reduce the uncertainty involved in using recommended *n* values from published sources for diverse flow and terrain conditions, the effect of topography needs to be addressed in a more explicit manner. The numerical porosity approach, proposed by Lane et al. (2004) is one of the most promising ways of retaining the original effect of the terrain on the flow process. In this approach a landscape has a porosity of zero when fully blocked and a porosity of unity when water is flowing freely. For all the intermediate flow conditions, which are often the case in the nature, the porosity remains between zero and one. For similar grid sizes, use of this method resulted in a significant improvement in the efficiency of a model to predict inundation extents over the use of calibrated *n* values (Yu and Lane, 2006a, 2006b).

Nevertheless, these recent developments in reducing the reliance on uncertain and calibrated roughness coefficients, sometimes without an appropriate physical meaning, essentially depends on very detailed terrain inputs in the model, which have limited global availability. For this reason, the practice of using a recommended range of *n* values from published tables as a calibration parameter is likely to continue in the field of inundation modelling for data-sparse regions in near future.

7.5 Non-structural mitigation strategy for the flood source areas

The current research highlights that even for large basins with heterogeneous topography and land cover types, the changing land-use/cover has an overall significant effect towards the flood peak at the basin outlet. When the matter was investigated at the implementation scale of remedial land management (i.e. sub-catchments) a weak but statistically significant correlation was noted. The systematic evaluation of the causal link between sub-catchment-wise LULC changes and the flood hydrograph at the basin outlet provided us some important insights. It is found that in some instances the location of a sub-catchment with relation to the topology of the drainage network act as an important factor in exerting disproportionate influence over the downstream flood peak. However, no general, significant, relationship between the location of the land-use change in relation to the proximity to a higher order stream or the basin outlet and its high sensitivity of the flood hydrograph was found. It is the specific nature of the rainfall event and an existing state of LULC across all the sub-catchments that are responsible for making the flood hydrograph hypersensitive to the LULC changes in certain locations. This finding implies that remedial land-use management practices in the prioritised sub-catchments may not have a mitigating effect on the flood peak at the basin outlet. I agree with the view of Pattison and Lane (2012) that any relation between the local LULC change and downstream flood risk is difficult to generalise and transfer from one basin or flood event to another.

7.6 Impact on flood management in the developing world

This study demonstrated simple but effective ways of utilising freely available DEMs for large scale river routing problems in data sparse countries and pointed out the minimum required supplementary information. This methodology will enable the flood managers in the developing counties to develop flow routing system in order to provide early warning for the downstream flood-prone areas. This kind of capability will be particularly beneficial for communities that live downstream of large dams in monsoon-dominated Asia. In addition, the ability to predict water surface elevation at a distant downstream point from major dams will also help in computing design floods of specific return periods for planning mitigation strategies.

Successful implementation of a flood-inundation model in an anabranching river in a developing country is a unique achievement of the current research. The novel method of creating appropriate terrain data from variety of low-cost/free sources will make it possible to assess detail flood risk at an individual settlement/community level in the developing world. The utilisation of freely available satellite images like MODIS, and Landsat 5 as a source of distributed calibration and validation data were keys for rigorous performance testing of the model outputs. This factor, along with the comprehensive uncertainty assessment of the modelled flood extents paints a detailed picture of merits and limitations of the proposed methodology.

Flood managers in the data-sparse regions will be able to take advantage of the experimental design and findings presented in Chapter 6 for carrying out planning non-structural flood mitigation strategies. Use of widely available model inputs and validation datasets as well as user friendly freely available modelling tools will be attractive to the scientists and other practitioners in the relevant discipline, particularly in the developing countries. It will not only enable them to prioritise the sub-catchments for implementing remedial land-use management measures but also make it possible to judge the effect of such measures at individual sub-catchments on the downstream flood risk in advance. It is acknowledged that the simulation results are difficult to generalise for other rivers basins. Nevertheless, design rainfall events of specific return periods can be used as inputs to view the entire prediction process from a probabilistic point of view.

7.7 Limitations

Having highlighted all the merits of the methods adopted in the thesis I would like to acknowledge the limitations of my findings. The majority of the limitations mainly stem from unavailability of data for model inputs and validation. For example, having a few more gauging stations between Durgapur Barrage and Jamalpur would put the performance of LISFLOOD-FP to a more stringent test in the middle course of the Damodar River. A river gauging station in the lower course would enable us to evaluate the performance of TELEMAC2D for the entire duration of the events under investigation rather than for two discrete time steps. As mentioned in Chapter 6, the availability of few more rain gauges in the Konar Basin and streamflow records at a

more disaggregated form at the basin outlet would enable us to judge the performance of HEC-HMS model in more detail. Similarly, a moderate resolution MODIS image (240 m cell size) was the only source for delineating a flood extent map for the calibration event in 2006 (Chapter 4). The model outputs, although available at a much finer scale had to be resampled into 240 m resolution for the calibration. A more detailed observed flood extent map might reveal more sensitivity of the simulated flood extent with relation to the roughness coefficient that was used as the calibration parameter in Chapter 4. The consistent bias in the model predictions arising from lack of details in the hybrid terrain data over part of the floodplain also made it difficult to understand the effect of uncertainty in inflow hydrographs and roughness coefficients on the simulated flood extent in part of the model domain considered in Chapter 5. Better radiometric quality of the satellite stereo pairs used for terrain extraction in Chapter 4 may have made it possible to represent more part of the floodplain in finer detail. This would help in reducing the area affected by terrain induced consistent bias in the uncertainty assessment experiment in the lower course of the Damodar Basin.

7.8 Summary

By addressing the aspect of flood mitigation through rainfall-runoff modelling this thesis has presented a holistic perspective to flood management in all major physiographic sub-divisions of a large flood-prone river basin with sparse data. The overall message from this thesis is that when our general goal is to predict dynamics of high magnitude stream flow in data sparse regions, we should pay particular attention to the choice of the model in relation to the available data and hydraulic characteristics of the event. Adaptations are necessary to create inputs for the models that have been primarily designed for areas with better availability of data. Freely available geospatial information of moderate resolution can often meet the minimum data requirements of hydrological and hydrodynamic models if they are supplemented carefully with limited surveyed/measured information. The amount of uncertainty in these types of prediction setups for extreme streamflow events was not found so great that it would discourage scientific community from using them under severe data constraint.

Chapter 8

Conclusion

This thesis has highlighted the typical challenges in modelling flood inundation and the rainfall-runoff process in the developing countries arising from lack of data. I have modelled the passage of extreme streamflow events through different courses of a river. The nature and manifestation of high magnitude flows in different part of a river tend to vary. Consequently, the type of flood hazard and the necessary prediction capability change from upper course of the river basin to its middle and lower course. It is important to understand the dynamics of flow at all physiographic sections of the river valley. However, due to severe constraints of available data, both in model inputs and for the validation of model performance, it is essential to set priorities within the hydrological variables that are significant for flood management at different portion of the river valley. In the Damodar River Basin the rainfall-runoff process in relation to the changing land cover is important in the upper catchment as it can increase the magnitude and reduce the lag time of high magnitude flows entering the reservoirs, making them less effective in controlling floods downstream. The travel time and discharge/water level of the flow through the middle course towards the flood-prone lower basin is of primary significance. Finally, the extent of inundation caused by different magnitude of flood water coming from the middle course is of major interest for natural hazard mitigation planning. Widespred flooding in complicated channel networks is fairly common, particularly in monsoon-dominated Asia where seasonal high magnitude rainfall patterns are prevalent.

During the course of this study it has been demonstrated that models of different levels of complexities in terms of physical process representations are appropriate for accurate prediction of important hydraulic variables at different parts of a river basin. The necessary level of processing of the existing freely available terrain data also varies depending on the modelled hydraulic variable of importance and the physical characteristics of the channels. The bare minimum requirement of surveyed information also varies depending on the scale of the study. When only predicting water surface elevations at a particular distant downstream point of a single channel is of concern, the SRTM DEM and few surveyed channel cross-sections are sufficient to perform well without much uncertainties with a simple model like LISFLOOD-FP. However, for simulating extensive floodplain inundation in anabranching channels at reach scale, much more effort in terms of the improving the quality of the input terrain is required.

The benefit of hybrid terrain data can only be exploited fully if a physically more realistic 2D finite element model such as TELEMAC2D is employed.

Chapter 5 discussed various aspects of uncertainties in model outcomes pertaining to the TELEMAC2D-based modelling experiment presented in Chapter 4. However, it is also necessary to point out that the comparison between the performances of LISFLOOD-FP and TELEMAC2D, as presented in Chapter 4, is also subject to modelling uncertainties. The output of the LISFLOOD-FP model is particularly susceptible to uncertainties in the *n* values used for the channel section. This property of LISFLOOD-FP was noted in Section 3.5.2. In addition, the effect of uncertainty in the topographic data on the model outcome has not been taken into account in Chapter 4. As LISFLOOD-FP is known to be very sensitive to the accuracy and resolution of the input topography, this factor is also a potential source of uncertainty for the results presented in Chapter 4. The inability of the LISFLOOD-FP to divert fast flowing water into the smaller branches has been considered as the most important factor responsible for the poor performance of LISFLOOD-FP in anabranching channels. The influence of other factors in influencing the model outcome has been considered negligible. Nevertheless, when evaluating the comparative performance of LISFLOOD-FP and TELEMAC2D in a complicated channel system, the effects of these unmeasured uncertainties are required to be kept under consideration.

Outcomes of the rainfall-runoff modelling experiments described in Chapter 6 have a number of limitations, which stem mainly from limited availability of model inputs and observed records for validation. The most important source of uncertainty comes from the use of only one rain gauge for a basin of approximately 1000 km^2. The use of TRMM rainfall estimates of 3 hour interval for the 2004 LULC scenario also contributed to more uncertainty in the model results. However, these data sources were the only source of sub-daily rainfall information found in the Konar River Basin, which is likely to be a typical scenario in other river basins in developing countries.

Lack of sub-daily observations of measured discharge at the main basin outlet also masked inter-day variation in the discharge. Had this type of data been available, it would have been possible to validate the simulated discharge at a finer temporal scale, adding confidence to the model outcomes. Due to the absence of river gauges at sub-catchment levels in the Konar Basin, it was not possible to validate the simulation results pertaining to the effect of tributary sequencing and flow convergence times on the flood hydrograph at the main basin outlet. This factor added to considerable uncertainty in the model results and the derived conclusion in Chapter 6.

Additional sources of uncertainties also arise from the use of small scale soil maps, relatively coarse resolution satellite images for generating LULC maps and averaging out CN values from published tables to derive CN values for more broad LULC classes that could be identified from the moderate resolution satellite products. The errors in all inputs are likely to propagate through different components of the modelling process in a complex manner which are difficult to isolate and quantify.

Incorporating the uncertainties in the observed flood extent map involves complex processing of the model outputs and it can be only justified if the input, particularly the terrain, induced biases in the model output is restricted in a small portion of the modelled flood inundation. It is acknowledged in this thesis that due to the use of coarse quality terrain as well as validation data it is rather difficult to isolate the sources of uncertainties in the model prediction. This drawback is perhaps more pronounced at the reach scale. Nevertheless, the probabilistic approach towards distributed flood inundation prediction is of vital importance when working with sparse inputs and validation data. Uncertainty assessment is the key to probabilistic flood hazard assessment and it helps to assess the level of confidence one can have when employing model inputs that are not of ideal resolution and accuracy.

Land-use planning in the flood source areas at the steep hillslopes of upper catchments of a river basin is an important non-structural strategy to dampen the energy in the fast flowing flood water. This thesis has addressed the issue of flood mitigation in the

Damodar Basin by systematically evaluating the effect of land use changes at the sub-catchment level on the flood hydrograph at the basin outlet. The outcome of this analysis indicates that with the current constraints of rain and river gauging stations in the developing countries there is no conclusive way of establishing a clear relationship between local land use changes and the global hydrological response in a basin. However, this study recommends that before undertaking remedial land use planning at a particular sub-catchment it is helpful to simulate its effect on the hydrograph at the basin outlet. This study provided a simple modelling framework based on easily accessible input data and a freely available, widely used, hydrological model to perform this kind of simulation.

Due to the easily accessible data sources and open source models used in this study it will be of interest to a wide community of researchers and flood managers, particularly in the data-sparse regions for modelling flood inundation. Key methodological innovations of this study are the 1) channel cross-section survey without access to permanent GPS base stations, 2) merging digital photogrammetic outputs with other sources of elevation data, 3) modelling widespread inundation in anabranching channels without high resolution terrain data, 4) uncertainty assessment of a computationally demanding finite element inundation model for a relatively large flood-prone area in high resolution and 5) the use of easily available data and modelling tools to evaluate the impact of local land-use change on the downstream flood risk.

In this thesis, I have presented a holistic approach to developing essential flood prediction capabilities in data sparse situations and in different reaches of a river basin. River flooding was viewed from the point of view of natural hazards which requires more accuracy in model performance than studies dealing with understanding seasonal water cycles in the continental rivers. The conclusion of this thesis is that depending on the scale of the phenomenon and physical characteristics of the channels different type of inputs and hydrodynamic codes can provide optimal solutions. The existing data available in the public domain or that can be obtained at low-cost in the developing

countries can be put to use for flood prediction and mitigation planning with careful adjustments.

References

Acrement GJ and Schneider VR (1989) Guide for selecting Manning's roughness coefficients for natural channels and floodplains. US Government Printing Office.

Adhikari P, Hong Y, Dauglas KR, Kirschbaum DB, Gourley J, Adler R, Brakenridge GR (2010) A digitized global flood inventory (1998-2008): compilation and preliminary results. Natural Hazards 55: 405-422.

Agrawal NK (2005) Geodetic infrastructure in India. Coordinates 1(7) http://mycoordinates.org/geodetic-infrastructure-in-india/ Accessed online on 30th January, 2012

Ahmed N, Mahtab A, Agrawal R, Jayaprasad P, Pathan SK, Ajai, Singh DK, Singh AK (2007) Extraction and validation of Cartosat-1 DEM. Journal of the Indian Society of Remote Sensing 35: 121-127.

Alcántara-Ayala I (2002) Geomorphology, natural hazards, vulnerability and prevention of natural disasters in developing countries. Geomorphology 47:107-124.

Alho, P and Aaltonen, J (2008) Comparing a 1D hydraulic model with a 2D hydraulic model for the simulation of extreme glacial outburst floods. Hydrological Processes 22: 1537-1547.

Ali M, Khan SJ, Aslam I, Khan Z (2011) Simulation of the impacts of land-use change on surface runoff of Lai Nullah Basin in Islamabad, Pakistan. Landscape and Urban Planning 102(4): 271-279.

Allenby B and Fink J (2005) Toward inherently secure and resilient societies. Science 309: 034-1036.

Amini A, Ali T, Ghazali A, Aziz A, Akib S (2011) Impacts of land-use change on streamflows in the Damansara watershed, Malaysia. Arabian Journal for Science and Engineering 36(5): 713-720.

Amutha R and Porchelvan P (2009) Estimation of surface runoff in Malattar sub-watershed using SCS-CN method. Journal of the Indian Society of Remote Sensing 37(2): 291-304.

Andréassian V (2004) Waters and forests: from historical controversy to scientific debate. Journal of Hydrology 291(1–2): 1-27.

Arcement GJ and Schneider VR (1989) Guide for selecting Manning's roughness coefficients for natural channels and floodplains. United States Geological Survey Water-Supply Paper 2339: 1–38.

Aricò C, Nasello C, Tucciarelli T (2009) Using unsteady-state water level data to estimate channel roughness and discharge hydrograph. Advances in Water Resources 32(8): 1223-1240.

Aronica G, Bates PD, Horritt MS (2002) Assessing the uncertainty in distributed model predictions using observed binary pattern information within GLUE. Hydrological Processes 16: 2001–2016.

Bales JD and Wagner CR (2009) Sources of uncertainty in flood inundation maps. Journal of Flood Risk Management 2:139-147.

Basu S (1996) An evaluation of DVC project as flood moderator. Social and Economic Development in India. Tripathi RS, Singh Parmer SB. (eds). Ashis Publishing House, New Delhi; 143-157.

Bates PD, Anderson MG, Hervouet J.-M (1995) An initial comparison of two 2-dimensional finite element codes for river flood simulation. Proc. Inst. Civ. Engrs., Water: Maritime and Energy 112: 238–248.

Bates PD, Horritt MS, Smith CN, Mason D (1997) Integrating remote sensing observations of flood hydrology and hydraulic modelling. Hydrological Processes 11: 1777–1795.

Bates PD, DeRoo APJ (2000) A simple raster-based model for flood inundation simulation. Journal of Hydrology 236:54-77.

Bates PD, Marks KJ, Horritt MS (2003) Optimal use of high-resolution topographic data in flood inundation models. Hydrological Processes 17: 537–557.

Bates PD, Horritt MS, Aronica G, Beven K (2004) Bayesian updating of flood inundation likelihoods conditioned on flood extent data. Hydrological Processes 18: 3347-3370.

Bates PD, Wilson MD, Horritt MS, Mason D, Holden N, Currie A (2006) Reach scale floodplain inundation dynamics observed using airborne synthetic aperture radar imagery: Data analysis and modelling. Journal of Hydrology 328:306–318.

Bates PD, Horritt MS, Fewtrell TJ (2010) A simple inertial formulation of the shallow water equations for efficient two-dimensional flood inundation modelling. Journal of Hydrology 387:33-45.

Bates PD (2012) Integrating remote sensing data with flood inundation models: how far have we got? Hydrological Processes 26: 2515-2521.

Beighley RE and Moglen GE (2003) Adjusting measured peak discharges from an urbanizing watershed to reflect a stationary land use signal. Water Resources Research 39(4): 1093.

Benson T (2012) Telemac Tools.
(http://www.mathworks.com/matlabcentral/fileexchange/25021-telemac-tools.
Accessed 30 November, 2012)

Beschta RL, Pyles MR, Skaugset AE, Surfleet CG (2000) Peakflow responses to forest practices in the western Cascades of Oregon, USA. Journal of Hydrology 233: 102–120.

Besnard A and Goutal N (2011) Comparison between 1D and 2D models for hydraulic modeling of a floodplain: case of Garonne river. Houille Blanche-Revue Internationale De Leau 3: 42-47.

Beven KJ and Binley AM (1992) The future of distributed models: model calibration and uncertainty prediction. Hydrological Processes 6:279–298.

Beven KJ (2001) Rainfall-runoff modelling-The primer. John Wiley and Sons, Chichester, p-235.

Beven K (2006) A manifesto for the equifinality thesis. Journal of Hydrology 320: 18-36.

Beven K (2010) Environmental modelling: An uncertain future? An introduction to techniques for uncertainty estimation in environmental prediction. Routledge, pp 121

Bhaduri B, Harbor J, Engel B, Grove M (2000) Assessing watershed-scale, long term hydrologic impacts of land use change using a GIS-NPS model. Environmental Management 26(6): 643-658.

Bhang KJ, Schwartz FW, Braun A (2007) Verification of the vertical error in C-band SRTM DEM using ICESat and Landsat-7, Otter Tail County, MN. Geoscience and Remote Sensing, IEEE Transactions on 45(1): 36-44.

Bhattacharya AK (1973) Flood control in the Damodar Valley. Geographical Review of India 35(2): 134-146.

Biancamaria S, Bates PD, Boone A, Mognard NM (2009) Large-scale coupled hydrologic and hydraulic modelling of the Ob river in Siberia. Journal of Hydrology 379(1-2): 136-150.

Bloschl G, Ardoin-Bardin S, Bonell M, Dorninger M, Goodrich D, Gutknecht D, Matamoros D, Merz B, Shand P, Szolgay J (2007) At what scale do climate variability and land cover change impact on flooding and low flows? Hydrological Processes 21: 1241-1247.

Bosch JM and Hewlett JD (1982) A review of catchment experiments to determine the effect of vegetation changes on water yield and evapotranspiration. Journal of Hydrology 55: 3–23.

Brakenridge GR, Nghiem SV, Anderson E, Chien S (2005) Space-based measurement of river runoff. EOS: Transactions of the American Geophysical Union 86(19): 185–192.

Brakenridge R. and Anderson E (2006) MODIS-based flood detection, mapping and measurement: The potential for operational hydrological applications. Transboundary Floods: Reducing Risks Through Flood Management. Marsalek J, Stancalie G, Balint G (eds). (NATO Science Series: IV: Earth and Environmental Sciences); 1-12.

Brink AB and Eva HD (2009) Monitoring 25 years of land cover change dynamics in Africa: A sample based remote sensing approach. Applied Geography 29(4): 501-512.

Bronstert A, Neihoff D, Burger G (2002) Effects of climate and land-use change on storm runoff generation: present knowledge and modelling capibilities. Hydrological Processes 16: 509-529.

Callede J, Kosuth P, Guyot J-L, Guimaraes V S (2000) Discharge Determination by Acoustic Doppler Current Profilers (ADCP): A Moving Bottom Error Correction Method and Its Applications on the River Amazon at Obidos. Hydrological Sciences 45 (6): 911–924.

Camorani G, Castellarin A, Brath A (2005) Effects of land use changes on the hydrologic response of reclamation systems. Physics and Chemistry of the Earth 30: 561-574.

Candela L, Tamoh K, Olivares G, Gomez M (2012) Modelling impacts of climate change on water resources in ungauged and data-scarce watersheds. Application to the Siurana catchment (NE Spain). Science of the Total Environment 440: 253-260.

Casas A, Benito G, Thorndycraft V, Rico M (2006) The topographic data source of digital terrain models as a key element in the accuracy of hydraulic flood modelling. Earth Surface Processes and Landforms 31: 444–456.

Central Technical Power Board, Preliminary memorandum on the development of the Damodar River, (1948) Government of India Press, Kolkata.

Chandra S (2003) India: Flood management-Damodar River Basin, World Meteorological Organization.
www.apfm.info/pdf/case_studies/cs_india.pdf. Accessed 29th March 2012

Chen Y, Xu Y, Yin Y (2009) Impacts of land use change scenarios on storm-runoff generation in Xitiaoxi basin, China. Quaternary International 208: 121-128.

Choudhury S (2011) Damodar Valley Corporation, the missed opportunity. Journal of Infrastructure Development 3(2): 117-126.

Chow VT (1959) Open channel hydraulics. McGraw-Hill, New York.

Cobby DM, Mason DC, Horritt MS, Bates PD (2003) Two-dimensional hydraulic flood modelling using a finite-element mesh decomposed according to vegetation and topographic features derived from airborne scanning laser altimetry. Hydrological Processes 17: 1979-2000.

Collins MJ (2009) Evidence for changing flood risk in New England since the late 20th century. J. Am. Water Resour. Assoc. 45(2): 279–290.

Computing and Information Service (CIS) (2012) Durham University website: https://www.dur.ac.uk/cis/local/hpc/hamilton/technical_spec/ (Last accessed, 30th July, 2012)

Cook A and Merwade V (2009) Effect of topographic data, geometric configuration and modelling approach on flood inundation mapping. Journal of Hydrology 377: 131-142.

da Paz AR, Collischonn W, Tucci CEM, Padovani CR (2011) Large-scale modelling of channel flow and floodplain inundation dynamics and its application to the Pantanal (Brazil). Hydrological Processes 25(9): 1498-1516.

Das SN, Narula KK, Laurin R (1992) Run-off potential indices of watersheds in Tilaya catchment, Bihar (India) through remote sensing and implementation of GIS. Journal of Indian Society of Remote Sensing 20(4): 207-221.

De Roo A, Barredo JI, Lavalle C, Bodis K, Bonk R (2007) Potential flood hazard and risk mapping at pan-European scale. Digital terrain modelling: Development and applications in a policy support environment. Peckham R, Jordan G (eds). Series: Lecture Notes in Geoinformation and Cartography. Springer-Verlag Berlin.

Di Baldsssarre G and Montanari A (2009) Uncertainty in river discharge observations: a quantitative analysis. Hydrology and Earth System Sciences 13: 913-921.

Di Baldassarre G, Castellarin A, Montanari A, Brath A (2009a) Probability weighted hazard maps for comparing different flood risk management strategies: a case study. Natural Hazards 50: 479–496.

Di Baldassarre G, Castellarin A, Brath, A (2009b) Analysis of the effects of levee heightening on flood propagation: example of the River Po, Italy. Hydrological Sciences Journal, 54: 1007-1017.

Di Baldassarre G, Schumann G, Bates PD (2009c) A technique for the calibration of hydraulic models using uncertain satellite observation of flood extents. Journal of Hydrology 367: 276-282.

Di Baldassarre G, Schumann G, Bates PD, Freer JE and Beven KJ (2010) Flood-plain mapping: a critical discussion of deterministic and probabilistic approaches. Hydrology Science Journal 55(3): 364-376.

Di Baldsssarre G and Claps P (2011) A hydraulic study on the applicability of rating curves. Hydrology Research 42:10-19.

Di Baldassarre G, Laio F, Montanari A. (2012) Effect of observation errors on the uncertainty of design floods. Physics and Chemistry of the Earth 42-44: 85-90.

Domeneghetti A, Castellarin A, Brath A (2012) Assessing rating curve uncertainty and its effects on hydraulic model calibration. Hydrology and Earth System Sciences 16: 1191-1202.

Du J, Qian L, Rui H, Zuo T, Zheng D, Xu Y, Xu C-Y (2012) Assessing the effects of urbanization on annual runoff and flood events using an integrated hydrological modelling system for Qinhuai River basin, China. Journal of Hydrology 464-465: 127-139.

Ebner R, Featherstone WE (2008) How well can online GPS PPP post-processing services be used to establish geodetic survey control networks. J of Applied Geodesy 2:149-157.

El-Mowafy A (2011) Analysis of web-based GNSS post-processing services for static and kinematic positioning using short data spans. Survey Review 43:535-549.

Engman ET (1985) Roughness coefficients for routing surface runoff. Journal of Irrigation and Drainage Engineering 112 (1): 39-53.

Ewen J, O'Donnell G, Bulygina N, Ballard C, O'Connell E (2012) Towards understanding links between rural land management and the catchment flood hydrograph. Quarterly Journal of the Royal Meteorological Society doi: 10.1002/qj.2026

Farr TG, Rosen PA, Caro E, Crippen R, Duren R, Hensley S, Kobrick M, Paller M, Rodriguez E, Roth L, Seal D, Shaffer S, Shimada J, Umland J, Werner M, Oskin M, Burbank, D, Alsdorf D (2007) The shuttle radar topography mission. Reviews of Geophysics 45, RG2004, 1-33.

Fewtrell TJ, Duncan A, Sampson SC, Neal JC, Bates PD (2001) Benchmarking urban flood models of varying complexity and scale using high resolution terrestrial LiDAR data. Physics and Chemistry of the Earth 36: 281-291.

Fewtrell TJ, Bates PD, Horritt MS, Hunter NM (2008) Evaluating the effect of scale in flood inundation modelling in urban environments. Hydrological Processes, 22: 5107–5118.

Fox DM, Witz E, Blanc V, Soulié C, Penalver-Navarro M, Dervieux A (2012) A case study of land cover change (1950–2003) and runoff in a Mediterranean catchment. Applied Geography 32(2): 810-821.

French JR, Clifford NJ (2000) Hydrodynamic modelling as a basis for explaining estuarine environmental dynamics: Some computational and methodological issues. Hydrological Processes, 14(11-12): 2089-2108.

Garbrecht J and Brunner G. (1991) Hydrologic Channel-Flow Routing for Compound Sections. J. Hydraul. Eng. 117(5): 629–642.

Ghosh S (2011) Hydrological changes and their impact on fluvial environment of the lower damodar basin over a period of fifty years of damming The Mighty Damodar River in Eastern India. Procedia - Social and Behavioral Sciences 19: 511-519. doi: 10.1016/j.sbspro.2011.05.163.

Gorokhovich Y and Voustianiouk A (2006) Accuracy assessment of the processed SRTM-based elevation data by CGIAR using field data from USA and Thailand and its relation to the terrain characteristics. Remote Sensing of Environment 104:409-415.

Gupta SNP (2004) Geomorphology of Damodar Basin. Rajesh Publications, New Delhi.

Hall JW, Tarantola S, Bates PD, Horritt, MS (2005) Distributed Sensitivity Analysis of Flood Inundation Model Calibration. Journal of Hydraulic Engineering 131:117-126.

Hall AC, Schumann GJ-P, Bamber JL and Bates PD (2011) Tracking water level changes of the Amazon Basin with active spaceborne remote sensing and integration with large scale hydrodynamic modelling: A review, Physics and Chemistry of the Earth 36: 223-231.

Hall AC, Schumann GJ-P, Bamber JL , Bates PD, Trigg MA (2012) Geodatic corrections to Amazon River water level gauges using ICESat altimetry. Water Resources Research 48: W06602.

Hardy RJ, Bates PD, Anderson MG (1999) The importance of spatial resolution in hydraulic models for floodplain environments. Journal of Hydrology 216: 124-136.

Herschey RW (1995) Streamflow measurement. E&FN Spoon, London.

Herschey RW (1998) Flow measurement. Hydrometry: principles and practices. Herschey RW (eds.). Wiley, Chichester, 9–83.

Hervouet J-M and Van Haren L (1996) Recent advances in numerical methods for fluid flows. Floodplain Processes. Anderson MG, Walling DE, Bates PD (eds). Wiley: Chichester, 183 – 214.

Hofton M, Dubayah R, Blair JB, Rabine D (2006) Validation of SRTM elevations over vegetated and non-vegetated terrain using medium flootprint lidar. Photogrammetric Engineering and Remote Sensing 72: 279-285.

Hornbeck JW, Martin CW, Eagar C (1997) Summary of water yield experiments at Hubbard Brook Experimental Forest, New Hampshire. Canadian Journal of Forest Research 27: 2043-2052.

Horritt MS (2000) Calibration of a two-dimensional finite element flood flow model using satellite radar imagery. Water Resources Research 36: 3279-3291.

Horritt MS and Bates PD (2001a) Predicting floodplain inundation: raster-based modelling versus the finite-element approach. Hydrological Processes 15: 825–842.

Horritt MS and Bates PD (2001b) Predicting floodplain inundation: raster-based modelling versus the finite element approach. Hydrological Processes 15: 825-842.

Horritt MS and Bates PD (2002) Evaluation of 1D and 2D numerical models for predicting river flood inundation. Journal of Hydrology 268:87-99.

Horritt MS, Di Baldassarre G, Bates PD, Brath A (2007) Comparing the performance of a 2-D finite element and a 2-D finite volume model of floodplain inundation using airborne SAR imagery. Hydrological Processes 21: 2745–2759.

Huffman GJ, Adler RF, Bolvin DT, Gu G, Nelkin EJ, Bowman KP, Hong Y, Stocker EF, Wolff DB (2007) The TRMM multi-satellite precipitation analysis: Quasi-global, multi-year, combined-sensor precipitation estimates at fine scale. Journal of Hydrometeorology 8: 38-55.

Hunter NM, Bates PD, Horritt MS, De Roo APJ, Werner MGF (2005) Utility of different data types for calibrating flood inundation models within a GLUE framework. Hydrology and Earth System Sciences 9: 412-430.

Hunter NM, Bates PD, Horritt MS, De Roo APJ, Werner MGF (2005) Utility of different data types for calibrating flood inundation models within a GLUE framework. Hydrology and Earth System Sciences 9:412-430.

Hunter NM, Bates PD, Horritt MS, Wilson MD (2007) Simple spatially-distributed models for predicting flood inundation: A review. Geomorphology 90: 208-225.

Hunter NM, Bates PD, Neelz S, Pender G, Villanueva I, Wright NG, Liang D, Falconer RA, Lin B, Waller S, Crossley AJ, Mason DC (2008) Benchmarking 2D hydraulic models for urban flooding. Proceedings of the ICE - Water Management 161 (1): 13-30.

Hurkmans RTWL, Terink W, Uijlenhoet R, Moors EJ, Troch PA, Verburg PH (2009) Effects of land use changes on streamflow generation in the Rhine basin. Water Resources Research 45(6): W06405.

Ip F, Dohm JM, Baker VR, Doggett T, Davies AG, Castano B, Chien S, Cichy B, Greeley R, Sherwood R (2006) Flood detection and monitoring with the Autonomous Sciencecraft Experiment onboard EO-1. Remote Sensing of Environment 101(4): 463–481.

Jackson TJ, Ragan RM, Fitch WN (1977) Test of Landsat-based urban hydrologic modeling. J. Water. Resour. Plann. Manag. 103(1): 141–158.

Jain SK, Sing RD, Jain MK, Lohani AK (2005) Delineation of flood prone areas using remote sensing techniques. Water Resource Management 19: 333-347.

Jain S, Saraf A, Goswami A, Ahmad T (2006) Flood inundation mapping using NOAA AVHRR data. Water Resources Management 20(6): 949-959.

Jarvis A, Reuter HI, Nelson A, Guevara E (2008) Hole-filled SRTM for the globe Version 4, available from the CGIAR-CSI SRTM 90m Database (http://srtm.csi.cgiar.org).

Jia HJ and Wan RR (2011) Simulating the impacts of land use/cover change on storm-runoff for a mesoscale watershed in east China. Advanced Materials Research 347-353: 3856-3862.

Jonkman SN (2005) Global perspectives on loss of human life caused by floods. Natural Hazards 34: 51-175.

Jung HC, Hamski J, Durand M, Alsdorf D, Hossain F, Lee H, Hossain AKMA, Hasan K, Khan AS, and Hoque AKMZ (2010) Characterization of complex fluvial systems using remote sensing of spatial and temporal water level variations in the Amazon, Congo and Brahamaputra Rivers. Earth Surface Processes and Landforms 35(3): 294-304.

Jung Y and Merwade V (2012) Uncertainty quantification in flood inundation mapping using generalised likelihood uncertainty estimation and sensitivity analysis. Journal of Hydrologic Engineering 17(4): 507-520.

Kale VS (2002) Fluvial geomorphology of Indian rivers-an overview. Progress in Physical Geography 26: 400-433.

Kale VS (2003) Geomorphic effects of monsoon floods on Indian rivers. Natural Hazard 28: 65-84.

Kale V (2012) On the link between extreme floods and excess monsoon epochs in South Asia. Climate Dynamics 39: 1107-1122.

Kalyanapu AJ, Judi DR, McPherson TN, Burian SJ (2012) Monte Carlo-based flood modelling framework for estimating probability weighted flood risk. Journal of Flood Risk Management 5: 37–48.

Kaur S and Das AK (2011) Catastrophic flood in Kosi catchment during August 2008 Mausam 62(1): 21-26.

Keokhumcheng Y, Tingsanchali T, Clemente RS (2012) Flood risk assessment in the region surrounding the Bangkok Suvarnabhumi Airport. Water International 37(3): 201-217.

Knebl MR, Yang ZL, Hutchinson K, Maidment DR (2005) Regional scale flood modeling using NEXRAD rainfall, GIS, and HEC–HMS/RAS: a case study for the San Antonio River Basin Summer 2002 storm event. Journal of Environmental Management 75: 325–336.

Kumar P, Tiwari KN, Pal DK (1991) Establishing SCS runoff curve number from IRS digital database. Journal of the Indian Society of Remote Sensing 19(4): 245-251.

Lane SN, Bradbrook KF, Richards KS, Biron PA, Roy AG (1999) The application of computational fluid dynamics to natural river channels: three-dimensional versus two-dimensional approaches. Geomorphology 29(1): 1-20.

Lane SN and Hardy RJ (2002) Porous rivers: a new way of conceptualising and modelling river floodplain flows. Transport Phenomena in Porous media II. Ingham DP, Pop I. (eds). Pergamon Press, Oxford, 425-449.

Lane SN, Hardy RJ, Ingham DB, Elliott DB (2004) Numerical modelling of flow processes over gravelly-surfaces using structured grids and a numerical porosity treatment. Water Resources Research 40: W01302

Lane SN (2005) Roughness–time for a re-evaluation? Earth Surface Processes and Landforms 30(2): 251-253.

Lane SN, Morris J, O'Connell PE, and Quinn PF (2007) Managing the rural landscape. In: Thorne CR, EvansEP, and Penning-Rowsell EC (Eds) Future Flooding and Coastal Erosion Risks. London: Thomas Telford, 297–319.

Legates DR and McCabe Jr GJ (1999) Evaluating the use of "goodness-of-fit" measures in hydrologic and hydroclimatic model validation. Water Resour. Res. 35: 233–241.

Legleiter CJ and Kyriakidis PC (2008) Spatial prediction of river channel topography by kriging. Earth Surface Processes and Landforms 33: 841-867.

Lehner B and Verdin K (2008) New global hydrography derived from spaceborne elevation data. EOS. Transactions American Geophysical Union 89: 93.

Lemoine FG, Smith DE, Kunz L, Smith R, Pavlis EC, Pavlis NK, Klosko SM, Chinn DS, Torrence MH, Williamson RG, Cox CM, Rachlin KE, Wang YM (1996) The development of the NASA GSFC and NIMA joint geopotential model. Proc. for the International Symposium on Gravity, Gravity, Geoid, and Marine Geodesy, (GRAGEOMAR 1996), The University of Tokyo, Tokyo, Japan, September 30 to October 5, 1996.

Limerinos JT (1970) Determination of the Manning coefficient from measured bed roughness in natural channels. US Government Printing Office.

Mailapalli DR, Raghuwanshi NS, Singh R, Schmitz GH, Lennartz F (2008) Spatial and temporal variation of Manning's roughness coefficient in furrow irrigation. Journal of Irrigation and Drainage Engineering 134(2): 185-192.

Manfreda S, Di Leo M, Sole A (2011) Detection of flood-prone areas using digital elevation models. Journal of Hydrologic Engineering 16(10): 781-790.

Manning R (1891) On the flow of water in open channels and pipes, Ireland, Inst. Civil Engineers Trans. 20: 161-207.

Mason DC, Bates PD, Dall' Amico JT (2009) Calibration of uncertain flood inundation models using remotely sensed water level. Journal of Hydrology 368(1-4): 224-236.

Mason DC, Speck R, Schumann GJ-P, Neal JC, Bates PD (2010a) Flood detection in urban areas using TerraSAR-X. IEEE Transactions on Geoscience and remote Sensing 48(2): 882-894.

Mason DC, Schumann G, Bates PD (2010b) Data Utilization in Flood Inundation Modelling, in Flood Risk Science and Management, Pender G and Faulkner H (Eds), Wiley-Blackwell, Oxford, UK.

Masood M and Takeuchi K (2012) Assessment of flood hazard, vulnerability and risk of mid-eastern Dhaka using DEM and 1D hydrodynamic model. Natural Hazards, 61: 757-770.

McColl C and Agget G (2007) Land use forecasting and hydrologic model integration for improved land use decision support. Journal of Environmental Management 84: 494-512.

McFeeters SK (1996) The use of Normalised Difference Water Index (NDWI) in the delineation of open water features. Int. J. Remote Sens. 17(7): 1425–1432.

Medeiros SC, Hagen SC, Weishampel JF (2012) Comparison of floodplain surface roughness parameters derived from land cover data and field measurements. Journal of Hydrology 452-453: 139-149.

Merwade VM, Maidment DR, and Goff JA (2006) Anisotropic considerations while interpolating river channel bathymetry. Journal of Hydrology 331: 731-741.

Merwade V, Cook A, and Coonrod J (2008a) GIS techniques for creating river terrain models for hydrodynamic modelling and flood inundation mapping. Environmental Modelling and Software 23: 1300-1311.

Merwade V, Olivera F, Arbi M, and Scott E (2008b) uncertainty in flood inundation mapping: Current issues and future directions. Journal of Hydrologic Engineering 13(7): 608-620.

Merwade V (2009) Effect of spatial trends on interpolation of river bathymetry. Journal of Hydrology 37: 169-181.

Merz B, Kreibich H, Apel H (2008) Flood risk analysis: uncertainties and validation. Österreichische Wasser- und Abfallwirtschaft 60(5): 89-94.

Miller W P (2002) Integrating landscape assessment and hydrologic modeling for land cover change analysis. J American Water Resour Assoc. 38(4): 915–929.

Mishra SK and Singh VP (2003) Soil Conservation Service Curve Number Methodology. Kluwer Academic Publishers, Dordrecht, The Netherlands.

Mishra SK, Pandey RP, Jain MK, Singh VP (2008) A rain duration and modified AMC dependant SCS-CN procedure for long duration rainfall-runoff events. Water Resources Management 22: 861-876.

Mohapatra PK and Singh RD (2003) Flood management in India. Natural Hazards 28: 131-143.

Montanari A (2006) What do we mean by uncertainty? The need for a consistent wording about uncertainty assessment in hydrology. Hydrological Processes 21: 841-845.

Morvan H, Knight D, Wright N, Tang X, Crossley A (2008) The concept of roughness in fluvial hydraulics and its formulation in 1D, 2D and 3D numerical simulation models. Journal of Hydraulic Research 46(2): 191-208.

Moulinec C, Denis C, Pham C-T, Rougé D, Hervouet J-M, Razafindrakoto E, Barber RW, Emerson D R, Gu X-J (2011) TELEMAC: An efficient hydrodynamics suite for massively parallel architectures. Computers & Fluids 51(1): 30-34.

Natural Resources Conservation Service, USA (2012) Cross-Section Hydraulic Analyser (http://go.usa.gov/0Eo, last accessed on 15th May, 2012)

Natural Resources Conservation Service (NRCS). (1972) National Engineering Handbook. Section 4, Hydrology, U.S. Government Printing Office.

Neal JC, Fewtrell TJ, Bates PD, Wright NG (2010) A comparison of three parallelisation methods for 2D flood inundation models. Environmental Modelling and Software. 25(4): 398-411.

Neal J, Schumann G, Fewtrell T, Budimir M, Bates P, Mason D (2011) Evaluating a new LISFLOOD-FP formulation with data from the summer 2007 floods in Tewkesbury, UK. Journal of Flood Risk Management, 4: 88–95.

Neal J, Schumann G and Bates P (2012a), A subgrid channel model for simulating river hydraulics and floodplain inundation over large and data sparse areas. Water Resources Research 48: W11506.

Neal J, Villanueva I, Wright N, Willis T, Fewtrell T, Bates P. (2012b) How much physical complexity is needed to model flood inundation? Hydrological Processes 26: 2264-2282.

Nicholas AP and Walliang DE (19970 Modelling flood hydraulics and overbank deposition on river floodplains. Earth Surface Processes and Landforms 19: 349-368.

NRC Canadian Hydraulics Centre (2012)
http://www.nrc-cnrc.gc.ca/eng/ibp/chc/software/kenue/blue-kenue.html Last accessed on 10th July, 2012.

O'Connell E, Ewan J, O'Donnell G, Quinn P (2007) Is there a link between agricultural land use management and flood risk? Hydrology and Earth System Sciences 11: 96-107.

O'Donnell G, Ewen J, O'Connell PE 92011) Sensitivity maps for impacts of land management on an extreme flood in the Hodder catchment, UK. Physics and Chemistry of the Earth, Parts A/B/C. 36(13): 630-637.

Olang LO and Furst J (2011) Effects of land cover change on flood peak discharges and runoff volumes: model estimates for the Nyando River Basin, Kenya. Hydrological Processes. 25: 80-89.

Paiva RCD, Collischonn W, Tucci CEM (2011) Large scale hydrologic and hydrodynamic modeling using limited data and a GIS based approach. Journal of Hydrology 406:170-181.

Panchawagh NV and Vaidya SS (2011) Link between break/active phases of summer monsoon over India and China. Current Science 100: 1-8.

Pappenberger F, Beven K, Horritt M, Blazkova S (2005) Uncertainty in the calibration of effective roughness parameters in HEC-RAS using inundation and downstream level observations. Journal of Hydrology 302(1–4): 46-69.

Pappenberger F, Matgen P, Beven, KJ, Henry J-B, Pfister L, Fraipont de P (2006) Influence of uncertain boundary conditions and model structure on flood inundation predictions. Advances in Water Resources 29: 1430-1449.

Patro S, Chatterjee C, Singh R, Raghuwanshi NS (2009a) Hydrodynamic modelling of a large flood-prone river system in India with limited data. Hydrological Processes 23:2774-2791.

Patro S, Chatterjee C, Singh R, Raghuwanshi NS (2009b) Flood inundation modeling using MIKE FLOOD and remote sensing data. J Indian Soc Remote Sens 37:107-118.

Pattison, I., Lane S. N, Hardy, R. J., Reaney, S., 2008. Sub-catchment peak flow magnitude and timing effects on downstream flood risk. Paper presented at 10th National hydrology symposium, 15–17 September 2008 Exeter. http://www.hydrology.org.uk/Publications/exeter/44.pdf Accessed on 30th January 2013.

Pattison I and Lane SN (2012) The link between land-use management and fluvial flood risk: A chaotic conception? Progress in Physical Geography 36(1): 72-92.

Petersen G and Fohrer N (2010) Two-dimensional numerical assessment of the hydrodynamics of the Nile swamps in southern Sudan. Hydrology Sciences Journal 55:17–26.

Pramanik N, Panda RK, Sen D (2010) One dimensional hydrodynamic modelling of river flow using DEM extracted river cross-sections. Water Resources Management 24:835-852.

Quast J, Messal H, Ehlert V, Sbjeschni A, Schmidt W (2012) Model-based assessment of land use impacts on runoff and inundation caused by flood events. Irrigation and Drainage 61: 155-167.

Rajeevan M and Bhate J (2008) A high resolution daily gridded rainfall data set (1971-2005) for mesoscale meteorological studies. National Climate Centre Research Report No: 9/2008. National Climate Centre, Indian Meteorological Department, Pune, India. http://www.imdpune.gov.in/ncc_rept/RESEARCH%20REPORT%209.pdf Accessed 30th January, 2013

Rawat KS, Mishra AK, Sehgal VK, Ahmed N, Tripathi VK (2012) Comparative evaluation of horizontal accuracy of elevations of selected ground control points from ASTER and SRTM DEM with respect to CARTOSAT-1 DEM: a case study of Shahjahanpur district, Uttar Pradesh, India. Geocarto International doi: 10.1080/10106049.2012.724453

Reuter H, Nelson A, Strobl P, Mehl W, Jarvis A (2009) A first assessment of Aster GDEM tiles for absolute accuracy, relative accuracy and terrain parameters. Proc. Geoscience and Remote Sensing Symposium, IGARSS 2009 IEEE International. pp. 240-243.

Rodríguez E, Morris CS, Belz JE. (2006) A global assessment of the SRTM performance. Photogrammeric Engineering and Remote Sensing 72(3): 249-260.

Romanowicz R and Beven K (2003) Estimation of flood inundation probabilities as conditioned on event inundation maps. Water Resources Research 39(3): 1073.

Roughani M, Ghafouri M, Tabatabaei M (2007) An innovative methodology for the prioritisation of sub-catchments for flood control. International Journal of Applied Earth Observation and Geoinformation 9: 79-87.

Saghafian B and Khosroshahi M (20050 Unit response approach for priority determination of flood source area. Journal of Hydrologic Engineering 10(4): 270-277.

Saghafian B, Farazjoo H, Bozorgy B, Yazdandoost F (2008) Flood intensification due to change in land use. Water Resources Management 22: 1051-1067.

Saha SK (1979) River-Basin planning in the Damodar Valley of India. Geographical Review 69: 273-287.

Sampson CC, Fewtrell TJ, Duncan A, Shaad K, Horritt MS, Bates PD (2012) Use of terrestrial laser scanning data to drive decimetric resolution urban inundation models. Advances in Water Resources 41: 1-17.

Sanders R, Shaw F, Mackay H, Galy H, Foote M (2005) National flood modeling for insurance purposes: using IFSAR for flood risk estimation in Europe. Hydrology and Earth System Sciences 9: 449-456.

Sanders BF (2007) Evaluation of on-line DEMs for flood inundation modeling. Advances in Water Resources 30:1831-1843.

Sanyal J and Lu XX (2004) Application of remote sensing in flood management with special reference to monsoon Asia: a review. Natural Hazards 33:283–301.

Sanyal J and Lu XX (2005) Remote sensing and GIS-based flood vulnerability assessment of human settlements: a case study of Gangetic West Bengal, India. Hydrological Processes 19(18): 3699–3716.

Sanyal J, Carbonneau P, Densmore AL (2013) Hydraulic routing of extreme floods in a large ungauged river and the estimation of associated uncertainties: A case study of the Damodar River, India. Natural Hazards, 66(2), 1153-1177.

Sarhadi A, Soltani S, Modarres R (2012) Probabilistic flood inundation mapping of ungauged rivers: Linking GIS techniques and frequency analysis. Journal of Hydrology 458-459: 68-86.

Schumann G, Matgen P,Hoffmann L, Hostache R, Pappenberger F, Pfister L (2007) Deriving distributed roughness values from satellite radar data for flood inundation modelling. Journal of Hydrology 344: 96-111.

Schumann G, Di Baldassarre G, Bates PD (2009) The utility of spaceborne radar to render flood inundation maps based on multialgorithm ensembles. IEEE Transactions on Geosciences and Remote Sensing 47(8): 2801–2807.

Sefe FTK (1996) A study of the stage-discharge relationship of the Okavaiigo River at Mohembo, Botswana. Hydrological Sciences Journal 41(1): 97-116.

Shapiro MG and Nelson EJ (2004) Digital terrain model processing of integrated hydraulic analysis and floodplain mapping. Sehlke G, Hayes DF, Stevens DK (eds). World Water Congress 2004. Salt Lake City, Utah.

Sharma KD and Singh H (1992) Runoff estimation using Landsat Thematic Mapper data and SCS model. Hydrological Sciences Journal 37(1): 39-52.

Shi PJ, Yuan Y, Zheng J, Wang JA, Gi Y, Qiu GY (2007) The effect of land use/cover change on surface runoff in Shenzhen region, China. Catena 69(1): 31-35.

Sinha R (2009) The great avulsion of Kosi on 18 August 2008 Current Science 97(3): 429-433.

Slack RB and Welch R (1980) SCS runoff curve number estimates from Landsat data. Water. Resour. Bull. 16(5): 887–893.

Slater JA, Garvey G, Johnston C, Haase J, Heady B, Kroenung G, Little J (2006) The SRTM data "finishing" process and products. Photogrammetric Engineering and Remote Sensing 72(0): 237-247.

Slater JA, Heady B, Kroenung G, Curtis W, Haase J, Hoegemann D, Shockley C , Tracy K (2011) Global Assessment of the New ASTER Global Digital Elevation Model. Photogrammetric Engineering and Remote Sensing 77(4): 335-339.

Smith K, Ward R (1998) Floods: physical processes and human impacts. Wiley, New York.

Smith K (2001) Environmental hazards assessing risk and reducing disaster, Third ed. Routledge, London.

Srivastava PK, Srinivasan TP, Gupta A, Singh S, Nain JS, Amitabh, Prakash S, Kartikeyan B, Krishna BG (2008) Advanced studies in strip pair processing of Cartosat-1 data. The Photogrammetric Records 23: 290-304.

Sriwongsitanon N and Taesombat W (2011) Effects of land cover over runoff coefficient. Journal of Hydrology 410: 226-238.

Stephens EM, Bates PD, Freer J, Mason D (2012) Calibration of flood inundation models using uncertain satellite observed water levels. Journal of Hydrology.
doi: 10.1016/j.jhydrol.2011.10.040

Straatsma M (2009) 3D float tracking: in situ floodplain roughness estimation. Hydrological Processes 23: 201-212.

Stephan U and Gutknecht D (2002) Hydraulic resistance of submerged flexible vegetation. Journal of Hydrology 269(1): 27-43.

Stuebe MM and Johnston DM (1990) Runoff volume estimation using GIS technique. Water. Resour. Bull. 26(4): 611–620.

Suwandana E, Kawamura K, Sakuno Y, Kustiyanto E, Raharjo B (2012) Evaluation of ASTER GDEM2 in comparison with GDEM1, SRTM DEM and topographic-map-derived DEM using inundation area analysis and RTK-dGPS data. Remote Sensing 4: 2419-2431.

Tarekegn TH, Haile AT, Rientjes T, Reggiani P, Alkema D (2010) Assessment of an ASTER-generated DEM for 2D hydrodynamic flood modelling. International Journal of Applied Earth Observation and Geoinformation 12: 457-465.

Tarekegn TH, Haile AT, Rientjes T, Reggiani P, Alkema D (2010) Assessment of an ASTER-generated DEM for 2D hydrodynamic flood modelling, International Journal of Applied Earth Observation and Geoinformation, 12, 457-465.

Tate EC, Maidment DR, Olivera F, and Anderson DJ (2002) Creating a terrain model for floodplain mapping. Journal of Hydrologic Engineering 792: 100-108.

Tiwari KN, Kumar P, Sebastian M, Pal DK (1991) Hydrologic modelling for runoff determination. International Journal of Water Resources Development 7(3): 178-184.

Trigg MA, Wilson MD, Bates PD, Horritt MS, Alsdorf DE, Forsberg BR, Vega MC (2009) Amazon flood wave hydraulics. Journal of Hydrology, 374(1-2), 92-105.

Tripathi MP, Panda RK, Pradhan S, Sudhakar S (2002) Runoff modelling of a small watershed using satellite data and remote sensing. Journal of the Indian Society of Remote Sensing 30: 39-52.

Troendle CA and King RM (1985) The effect of timber harvest on the Fool Creek watershed, 30 years later. Water Resources Research 21(12): 1915–1922.

Tsakiri M (2008) GPS processing using online services. J of Surveying Eng 134:115-125.

Van Dijk AIJM, Van Noordwijk M, Calder IR, Bruijnzeel LA, Schellekens J, Chappell NA (2009) Forest–flood relation still tenuous–comment on 'Global evidence that deforestation amplifies flood risk and severity in the developing world', Bradshaw CJA, Sodi NS, Peh KS.-H, Brook BW(eds.). Global Change Biol. (15): 110–115.

Wan R and Yang G (2007) Influence of Land use/cover change on storm runoff-A case study of Xitiaoxi River Basin in upstream of Taihu Lake watershed. Chinese Geographical Science 17(4): 349-356.

Wang R and Kalin L (2011) Modelling effects of land use/cover changes under limited data. Ecohydrology 4: 265-276.

Wang Y, Colby JD, Mulcahu KA (2002) An efficient method for mapping flood extent in coastal flood plain using Landsat TM and DEM data. International Journal of Remote Sensing 23(18): 3681-3696.

Wang W, Yang X, Yao T (2012) Evaluation of ASTER GDEM and SRTM and their suitability in hydraulic modelling of a glacial lake outburst flood in southeast Tibet. Hydrological Processes 26: 213-225.

Warburton ML, Schulze RE, Jewitt GPW (2012) Hydrological impacts of land use change in three diverse South African catchments. Journal of Hydrology 414–415: 118-135.

Wei X, Sun G, Liu S, Jiang H, Zhou G, Dai L (2008) The forest-streamflow relationship in China: a 40-year retrospect. J. Am. Water Resour. Assoc. 44 (5): 1076–1085.

Weichel T, Pappenberger F, Schulz K. (2007) Sensitivity and uncertainty in flood inundation modelling-concept of an analysis framework. Advances in Geosciences 11: 31-36.

Willmot CJ (1984) On the evaluation of model performance in physical geography. Spatial Statistics and Models. Gaile GL, Willmot CJ, Reidel D (eds). Dordrecht, pp 443–460.

Wilson MD and Atkinson PM. (2005a) The use of elevation data in flood inundation modelling: a comparison of ERS interferometric SAR and combined contour and differential GPS data. International Journal of River Basin Management 3: 3–20.

Wilson MD and Atkinson PM. (2005b) Prediction uncertainty in elevation and its effect on flood inundation modelling. GeoDynamics. Atkinson PM, Foody GM, Darby S, Wu F (eds.). Wiley, Chichester, 185–202.

Wilson M, Bates P, Alsdorf D, Forsberg B, Horritt M, Melack J, Frappart F, Famiglietti J (2007) Modeling large-scale inundation of Amazonian seasonally flooded wetlands. Geophysical Research Letters 34:L15404.

Wilson MD (2012) readstage.m (available under GNU General Public Licence) http://www.mdwilson.org/research-background/useful-code Accessed 30th January 2012.

Wohl EE (1998) Uncertainty in flood estimates associated with roughness coefficient. Journal of Hydraulic Engineering 124.2: 219-223.

Xu Y, Xu C, Gao X, Luo Y (2009) Projected changes in temperature and precipitation extremes over the Yangtze River Basin of China in the 21st century. Quat. Int. 208(1–2): 44–52.

Yamazaki D, Lee H, Alsdorf DE, Dutra E, Kim H, Kanae S, and Oki T (2012a) Analysis of the water level dynamics simulated by a global river model: A case study in the Amazon River. Water Resources Research 48: W09508 doi:10.1029/2012WR011869

Yamazaki D, Baugh CA Bates PD, Kanae S, Alsdorf DE, Oki T. (2012b) Adjustment of a spaceborne DEM for use in floodplain hydrodynamic modelling. Journal of Hydrology 436–437: 81-91.

Yamazaki D, Kanae S, Kim H , Oki T (2011) A physically based description of floodplain inundation dynamics in a global river routing model. Water resources Research 47: W04501. doi: 10.1029/2010Wr009726.

Yu D and Lane SN (2006a) Urban fluvial flood modelling using a two-dimensional diffusion-wave treatment, part 1: mesh resolution effects. Hydrological Processes 20(7): 1541-1565.

Yu D and Lane SN (2006b) Urban fluvial flood modelling using a two-dimensional diffusion-wave treatment, part 2: development of a sub-grid-scale treatment. Hydrological Processes, 20(7): 1567-158.

Zahera SS, Di Baldassarre G, Balekelay CN (2011) Modelling seasonally flooded wetlands in the semi-arid Sahelian Zone. Nile Basin Water Science and Engineering Journal 4(2): 83-93.